A Search for Novel Synergistic Combinations Against Prevalent Fungal Phytopathogens

Taran Alexander Young

Thesis submitted to the University of Nottingham (UK)
for the degree of Doctor of Philosophy

School of Life Sciences

2022

ABSTRACT

With the global population rising, the emergence of new types or variants of crop pathogens (phytopathogens), and the increasing resistance of these organisms to current crop treatments, there is an urgent need to improve global food security. Each year, fungi destroy crops that could feed up to 600 million people annually. Wheat, the most widely grown crop worldwide, has the second highest yield of all crops, with a global production of 778.5 million metric tonnes in 2021/2022. *Zymoseptoria tritici*, a major pathogen of wheat, causes Septoria Tritici Blotch (STB). This organism is responsible for around 70% of annual fungicide usage in the EU and up to 20% of annual yield losses in the UK. Novel treatments involving synergistic combinations of inhibitory compounds could improve efficacy while decreasing cost and toxicity to both non-target organisms and the wider environment. In this thesis, novel synergistic combinations of agents, primarily targeting *Z. tritici*, were sought. The initial focus was on protein translation as a target. Specifically, it was hypothesised that pairs of agents disrupting the fidelity of protein translation could be effective at synergistically inhibiting phytopathogenic fungi. To examine this, rational combinations of compounds were tested against fungi of interest.

Several synergies against *Botrytis cinerea* and *Z. tritici* were found among compounds of interest. A series of different combinations involving the dual targeting of aminoacylation (attachment of an amino acid to a tRNA), with one compound inhibiting a tRNA synthetase, and a second compound targeting the biosynthesis of the corresponding amino acid, yielded several synergies. One such synergy was between tavaborole, an inhibitor of the leucyl-tRNA synthetase, and chlorimuron ethyl, an inhibitor of the non-cognate branched-chain amino acids. This synergy decreased the minimum inhibitory concentrations (MIC) for each compound by four-

fold when in combination, compared to individual application. This proof of principle for dual targeting – inhibiting both biosynthesis and aminoacyl tRNA synthetase function for particular amino acids – opens up the possibility for dozens of potential synergistic combinations targeting the availability of different amino acids for protein translation, and hence growth, of undesirable fungi. For fungi pathogenic to humans, one or both targets should be the availability of essential amino acids to decrease cytotoxicity risks.

Furthermore, a powerful synergy against *Z. tritici* was discovered. This synergy decreased the MICs of the two compounds involved, cyprodinil and diphenyleneiodonium, by 16- and 32-fold when in combination, compared to individual application. However, this synergy was less potent in *B. cinerea* and *Saccharomyces cerevisiae*. The mechanism behind this synergy was investigated, initially testing for synergistic mechanisms based around the NADH kinase Pos5p and the electron transport chain, as these were reported as potential targets for the compounds. Experiments suggested that the mechanism most likely involves the synergistic increase of oxidative damage within mitochondria, although some experiments contradict this. Diphenyleneiodonium, an inhibitor of NAD(P)H oxidases, was evidenced to confer increased sensitivity to the pro-oxidant H_2O_2. The specific action of cyprodinil in the synergy remains unclear while characteristics of increased oxidative stress were seen.

Finally, two synergies of interest were tested on live wheat plants to determine if they could protect crops from *Z. tritici* infection. Experiments showed that at the concentrations used, these synergistic combinations were unable to effectively inhibit the pathogenicity of *Z. tritici*. Nevertheless, this poor reproduction of laboratory

findings in real infections highlights one difficulty with the discovery of novel treatments against fungal phytopathogens, viable for real-world applications.

Despite the poor success in preventing *Z. tritici* infection in the small trial with wheat at the end of this study, the potency of inhibitory-agents acting synergistically, demonstrated in the laboratory here, remains a strategy of high potential. The synergies discovered in this research could be tested against other undesirable fungi with the possibility of successfully controlling infection, and the mechanisms of synergistic action proposed here may provide a foundation to inform future combinatorial testing.

ACKNOWLEDGEMENTS

I would like to express my sincerest gratitude to my supervisor, Professor Simon Avery, for his guidance and patience throughout this PhD research. I am also extremely grateful to my industrial supervisor, Dr Andy Corran, for his insightful comments and suggestions. In addition, I would like to especially thank Dr Cindy Vallières for her ideas and endless patience with my never-ending questions.

To B44 and the fungal group, thank you for being a great source of support and friendship over the last four and a half years. Harry, Franziska, Cathy, Liam, Joe, Kamil, Zee, Alex, and Matt, I couldn't have asked for a better working environment to help me through. To Saskia, I will always be grateful for your support throughout some of my most stressful times. To the D&D gang, thank you for the all the laughs and escapism to different worlds away from the laboratory – thank you for your patience and let's get rolling once more! To my flatmate and fellow PhD candidate Derek, who has endured as I have, thank you for your continued friendship and support. You have made the last four years significantly easier, and I have thoroughly enjoyed the constant presence of another Scotsman, even if I do have a dodgy accent.

Finally, thank you to my (other) loved ones. To my parents and family in Aberdeen, thank you for your unwavering support throughout my life. Coming home to see you is always the highlight of my year and the fuel I needed to keep me going. Lastly, thank you Georgia for making my write-up as stress-free as possible and I look forward to returning the favour.

CONTENTS

LIST OF FIGURES

LIST OF TABLES

APPENDIX FIGURES AND TABLES

Chapter 1 - General Introduction

1.1. Fungi and global food security

Phytopathogenic fungi are a major threat to human food security. Globally, 20-40% of agricultural productivity losses are due to pests, with fungi making up a large proportion of this (Savary *et al*., 2012). Alone, phytopathogenic fungi destroy enough crops to feed up to 600 million people annually, around 8% of the global population (Calderone *et al*., 2014; United Nations, 2019) with more than 70% of all major crop diseases being caused by fungi (Agrios, 2005). Due to inadequate transportation and storage facilities, as well as improper handling methods, developing countries experience greater yield losses than developed countries (Pathak, 1997). It is estimated that the current global food production is enough to feed the predicted 2050 human population of 9.7 billion, provided significant socio-economic changes are made (e.g., a decrease in meat-heavy diets; not using human-edible crops as animal feed). If these changes are not made, humankind will need to increase production of edible crops by 119% by 2050, unless the threat of fungal phytopathogens can be significantly reduced (Berners-Lee *et al*. 2018). In addition to the detrimental effects of the climate crisis, such as more irregular seasons, global warming is enabling fungal phytopathogens to spread poleward, contributing novel threats to countries that previously did not have to deal with specific species. It has been estimated that there is an average poleward shift of fungal phytopathogens of 2.7±0.8 km yr^{-1} since 1960 when comparing hundreds of pests and pathogens of crops (Bebber *et al*., 2013). Interestingly, fungi host-ranges are the most broad of any other pathogen taxa (Fisher *et al*., 2012).In the past 150 years, major disease outbreaks caused by fungal phytopathogens have had significant impact on economies and cultures. The fungus-like oomycete pathogen *Phytophthora infestans* was the proximate cause of the Irish

potato famine in which around 1 million people died, and a further 1.5 million emigrated, while the rice-pathogenic fungus *Cochliobolus miyabeanus* (formerly *Helminthosporium oryzae*) was partly responsible for the Bengal famine of 1943, which resulted in 2.1-3.8 million deaths (Padmanabhan, 1973; Strange *et al*., 2005). In Sri Lanka during the second half of the 19th century, *Hemileia vastatrix* devastated the country's coffee industry, and is thought by some historians to explain why the British became tea drinkers (van Esse *et al*., 2019). It is clear that without adequate prevention or control, fungal phytopathogens can have devastating impacts with the potential to cause widespread famine, especially with predominant reliance on monocultures.

1.1.1. Fungal diseases of crops

Blotch, such as septoria tritici blotch (STB), caused by *Zymoseptoria tritici*, is a term used to describe diseases that are intermediate between blights, where the entire leaf or shoot dies, and leaf spots, where the necrotic lesions are clearly delimited. Blotches are irregular indefinite necrotic areas on leaves or fruit (Horst, 2013). Other blotch-causing fungi include *Parastagonospora nodorum* and *Pyrenophora tritici-repentis*, both of which also infect wheat. These organisms are notably problematic in Australia, costing the industry a combined AU$ 300,000,000 per annum (Murray and Brennan, 2009; Figueroa *et al*., 2018).

Rust diseases are caused by highly specialised obligate fungal parasites, primarily those of the taxonomical order Pucciniales. Species such as *Puccinia graminis* and *Puccinia striiformis* f. sp. *tritici* lead to an estimated global annual loss of US$ 4.3 to 5.0 billion. Fusarium head blight disease, caused by *Fusarium graminearum*, resulted in yield losses in the US between the early 1990s and 2008 equating to around US$ 3 billion. While this PhD research focuses mostly on the wheat pathogen *Zymoseptoria*

tritici, it is important to remember that there are hundreds of fungal phytopathogens causing extensive economic damage, threatening local and global food security.

Only around 150,000 species of fungi have been described to date, well below the estimated 2.2-3.8 million species thought to exist (Hawksworth and Lücking 2017). With around 2,000 novel species described annually, at the current rate it could take >1,800 years to describe all uncatalogued species, many of which are likely to be plant pathogens (Cheek *et al*., 2020; Pedro *et al*., 2021).

1.2. Important fungal phytopathogens

Several different fungal phytopathogens are relevant to large-scale agriculture; some are very specific in their target crop, while others can infect a broad range of plant hosts. Dean *et al* (2012) created a list detailing the top ten fungal phytopathogens that were voted by authors, reviewers, editors, and senior editors of Molecular Plant Pathology. On this list, the fungus receiving most votes was the phytopathogen *Magnaporthe oryzae*, causing disease in rice, a crop that over one half of the world's population relies on as their main source of calories (Dean *et al*., 2012). *M. oryzae* is capable of overcoming host resistance quickly, with resistant rice cultivars becoming ineffective within 2-3 years (Ou, 1980; Zeigler *et al*., 1994). In addition, yield losses on afflicted fields can be as much as 100% (Musiime *et al*., 2005).

1.2.1. *Botrytis cinerea*

On the aforementioned list of fungal phytopathogens *Botrytis cinerea* was listed as number two and is one of the most widely studied fungal phytopathogens. *B. cinerea* infects over 500 species of plant host causing the disease *grey mould* (Hua *et al*., 2018). The phytopathogen is considered a 'necrotroph' – the organism co-opts programmed cell death pathways to achieve infection. Necrotrophs are reported to be more

economically damaging than their opposites, biotrophs, which require living host tissue to survive (Newman and Derbyshire, 2020).

One of the main issues regarding the pathogenesis of *B. cinerea* infection is the large time periods that the organism can remain quiescent before beginning to rot plant tissue. Infestation can occur from the seedling stage of hosts all the way to ripening. The infected produce may only show symptoms well after harvest leading to spoilage during storage, transport, or display at retailers, further compounding financial losses. Because of the broad host range, the overall economic costs of *B. cinerea* infections are extremely high, with estimates placed in the range of US$ 10-100 billion worldwide annually (Hua *et al*., 2018). It has previously been estimated that fungicides specifically targeting *B. cinerea* make up 10% of the world fungicide market (UIPP, 2002). Despite this, one redeeming quality of *B. cinerea* infection is that it can be beneficial in the wine industry, causing 'noble rot' under the right conditions. If the weather stays wet after infection, the damaging grey rot can destroy crops of grapes; but if infected grapes are exposed to drier conditions to the point of partial 'raisining', this noble rot can lead to fine and concentrated sweet wines (Negri *et al*., 2017). The fact remains that this organism is a serious threat to global food production.

1.2.2. *Zymoseptoria tritici*

Zymoseptoria tritici (previously *Mycosphaerella graminicola*) is well known for causing STB (Arraiano and Brown, 2016). This disease devastates wheat fields, in some cases causing up to 50% loss of crops (Fones and Gurr, 2015). Wheat is the most widely cultivated crop worldwide and has the second highest yield of all crops annually (behind rice). Global wheat harvests reached 705 million metric tonnes in 2013 and 2014, with wheat the number one most cultivated crop in the European Union. *Z. tritici* infection is such a prevalent problem for European farmers that it accounts for around

70% of annual fungicide usage in the EU (Fones and Gurr, 2015). Depending on the cultivars of wheat that are used, annual losses in the UK can be up to 20%, with "resistant" varieties of wheat still suffering from losses of 5-10%. *Z. tritici* is a genetically diverse species, largely due to its heterothallic sexual reproduction (enabling genetic recombination between genetically distinct parents) to produce ascospores. The genome of *Z. tritici* is comprised of 21 chromosomes, eight of which are dispensable with regards to plant pathogenesis. The rate at which this organism diversifies is so great that as much as 90% of the global genetic variation has been seen in a single wheat field (Zhan *et al*., 2003). It is *Z. tritici* that has been the primary phytopathogen of focus of this PhD research.

Zymoseptoria tritici growth and pathology is complex (Figure 1.1), but due to the organism's importance, is relatively well studied. Vegetative growth of *Z. tritici* includes three different forms: single-celled yeasts, multi-cellular and tip growing hyphae, and asexual and sexual spores (Steinberg, 2015). In laboratory conditions, and so throughout this PhD project (with the exception of the live plant trials), the most common cell form of *Z. tritici* is typically the "yeast-like" macropycnidiospore, eventually germinating to form thin hyphae. Macropycnidiospores are multi-cellular structures consisting of 4-8 elongate cells (Steinberg, 2015). On leaves, the pycnidia, asexual fruiting bodies, appear as dark spots, which develop beneath the stomata on the underside of the wheat leaves. Pycnidiospores are generally dispersed locally through the splashing of rain, whereas sexual ascospores, formed in perithecia (Wiese, 1987), are distributed by air and can travel extensive distances.

As discussed by Steinberg (2015), from a cell biological point of view, the infection cycle of *Z. tritici* can be divided into three phases, beginning with the pathogen's entry

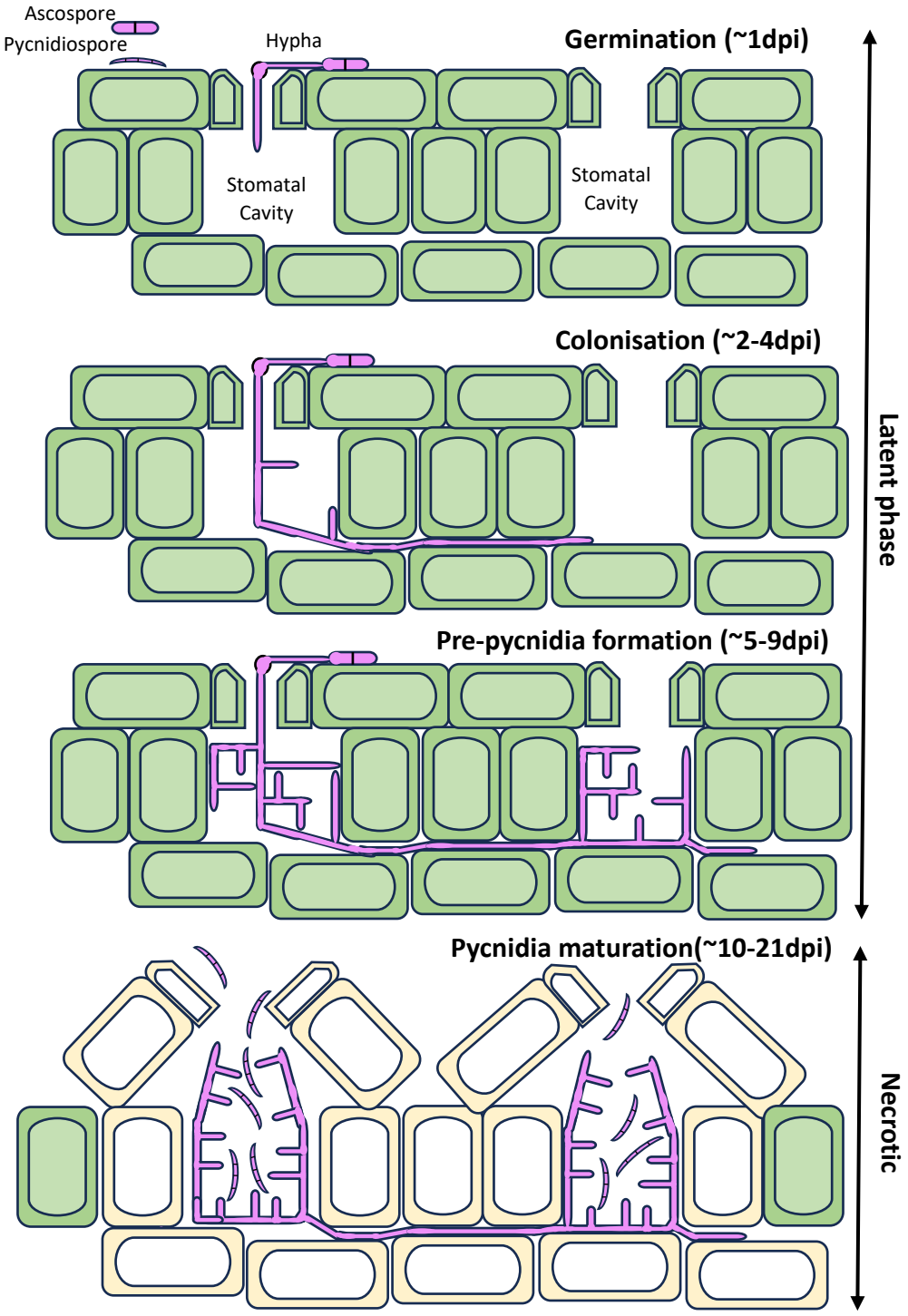

Figure 1.1. **Infection cycle of *Zymoseptoria tritici***. Figure adapted from Steinberg (2015). Summary of plant infection stages of *Z. tritici*. Asexual pycnidiospores or sexual ascospores land on wheat leaf epidermis where they germinate. Hyphae penetrate the leaf tissue via the stomata and begin colonisation of the stomatal cavity. Hyphae then invades the apoplast of the surrounding tissue. Pre-pycnidia formation begins in colonised cavities, leading to the transition of *Z. tritici* from a latent phase to a necrotrophic phase. During this phase, plant cells undergo programmed cell death leading to a release of nutrients that encourages rapid fungal growth. Pre-pycnidia then mature into pycnidia, which produce multicellular pycnidiospores. These infectious spores are released by water splash. Pseudothecia and formation of sexual ascospores not shown.

into the plant. Both pycnidiospores and ascospores are pathogenic and switch to hyphal growth upon contact with the leaf. *Z. tritici* hyphae then enter the host tissue via substomatal openings, potentially responding to an unknown signal (Duncan and Howard, 2000). *Z. tritici* then colonises and grows in the intracellular spaces between wheat mesophyll cells for a period of 9-11 days (Yang *et al*., 2013). During this period, *Z. tritici* competes for nutrients with other microbes in the phyllosphere, adapting to the apoplast environment (Karlsson *et al*., 2014). However, acquisition of nutrients by *Z. tritici* is an unknown process and no feeding structures, such as haustoria, are developed. In addition, there appears to be no changes in host metabolism or in the composition of apoplastic fluid. Some evidence of altered host physiology does exist, however, in the movement of chloroplasts towards the cell wall during infection (Kema *et al*., 1996).

During this asymptomatic growth phase, *Z. tritici* may utilise reserves that were stored in the germinating spore, as well as nutrients already found within the apoplast. These are released via β-oxidation of fatty acids and lipids and the activity of hydrolytic enzymes such as plant cell wall degrading enzymes (PCWDEs) and peptidases (Sánchez-Vallet *et al*., 2015). The expression of cellulases, peptidases, hemicellulases, and xylansases during the asymptomatic phase suggests that degradation of the plant host cell wall releasing nutrients is a source of food for the pathogen. In the necrotic phase, these nutrients may then be imported by sugar and amino acid transporters, which are highly expressed 9-10 days after infection (Keon *et al*., 2007).

The necrotic phase of *Z. tritici* onsets suddenly and is likely induced through several mechanisms (Sánchez-Vallet *et al*., 2015). This phase is seen by the appearance of chlorotic and necrotic lesions on the plant leaf surface. It is within these lesions that *Z. tritici* will ultimately sporulate. These symptoms may arise from a toxin produced by

the fungus (Kema *et al*., 1996) which could induce programmed cell death (PCD). Hypersensitive response (HR) is a form of PCD commonly associated with resistance response by plants to pathogens. It is an extremely rapid and localised autophagic form of PCD that aids to prevent the spread of pathogens (Liu *et al*., 2005). As disease symptoms develop in infected leaves, levels of reactive oxygen species (ROS) increase (Keon *et al*., 2007). This includes H_2O_2 during early symptomatic phases, and later superoxide once infection is more developed. Interestingly, it is undetermined whether these ROS originate from the host, *Z. tritici*, or both (Keon *et al*., 2005). Plant PCD is also associated with the release of cytochrome c from the mitochondria into the cytoplasm of the dying cells. Despite these possible attempts at host defence, it appears that wheat PCD is ineffective at containing *Z. tritici* infection and may in fact increase the growth rate and transition towards sporulation (Keon *et al*., 2007).

It has been shown that during infection, *Z. tritici* increases the expression level of genes encoding ROS-scavenging proteins including peroxidases, Cu^{2+}/Zn^{2+} superoxide dismutases, glutathione S-transferases, hydroperoxide reductases, thioredoxins, and peroxiredoxins (Yang *et al*., 2013). ROS production in fungi can also cause the accumulation of aldehydes and alcohols (Asiimwe *et al*., 2012), and so *Z. tritici* may protect itself through the increased expression of aldehyde dehydrogenase and alcohol dehydrogenase (Yang *et al*., 2013).

H_2O_2 produced as part of defence mechanisms by plants is reported to inhibit biotrophic pathogens but favour necrotrophic pathogens. In the hemibiotroph, or "latent necrotroph" (Sánchez-Vallet *et al*., 2015), *Z. tritici*, it has been shown that H_2O_2 is an effective defence mechanism in the early phases of plant infection, but that during the necrotrophic phase of growth, accumulation of H_2O_2 is also harmful, contradicting the responses of other necrotrophic fungi (Shetty *et al*., 2007).

1.3. Methods of fungal phytopathogen control

1.3.1. Resistant Cultivars

The two main methods of coping with fungal phytopathogens are the development of resistant cultivars and the application of fungicides. An ideal solution would be for all crops to be bred or genetically modified (GM) to become more robust and resistant to fungal phytopathogens, negating the need for potentially toxic and environmentally harmful fungicides. However, the process of developing resistant cultivars is difficult and traditional hybrid breeding takes between 8-10 years. Despite new technology such as Clustered Regularly Interspaced Palindromic Repeats (CRISPR) reducing this to 4-6 years (Chen *et al*., 2019), it is possible for resistance to be overcome by the fungi relatively quickly, outpacing resistance breeding (Wani, 2010). In addition to this, where genetic modification is used, the perception of GM crops by non-scientists is still generally negative, impacting the potential of genetic modification for crop resistance to fungal phytopathogens (Cui and Shoemaker, 2018; McPhetres *et al*., 2019). Fungicides or other methods are therefore a current and future necessity to help protect the vulnerable crop monocultures from disease. This is reflected in the value of the global fungicide market, estimated at USD$ 13.4 billion dollars in 2018, a number which is only predicted to rise every year (Garside, 2019).

1.3.2. Fungicides

As with overcoming resistant cultivars, fungi are capable of developing resistance to fungicides. *B. cinerea* is commonly treated with quinone outside inhibitors (QoI), succinate dehydrogenase inhibitors (SDHI), anilinopyrimidines, phenylpyrroles, and hydroxyanilides (Rupp *et al*., 2017) with reports of resistance to all major classes (Leroux *et al*., 2002). *Z. tritici* is commonly treated with SDHI fungicides as these have been effective to date. However, it has been shown that *Z. tritici* can gain resistance

to SDHI fungicides by single nucleotide polymorphisms (SNP) in the gene for succinate dehydrogenase (Scalliet *et al*., 2012), the target enzyme complex that participates in both the electron transport chain and the citric acid cycle (Oyedotun and Lemire, 2004). *Z. tritici* populations have acquired field resistance to both methyl benzimidazole carbamates (Hawkins and Fraaije, 2016), which inhibit tubulin polymerisation (FRAC, 2022), and QoI fungicides (Esstep *et al*., 2014; Cheval *et al*., 2017), which act at the quinol outer binding site of the cytochrome bc1 complex (FRAC, 2022). *Z. tritici* is also known to have a large number of efflux pumps, with the organism reported to have a total of 44 putative ATP-binding cassette (ABC) transporter genes and 229 putative major facilitator superfamily (MFS) transporter genes (Goodwin *et al*., 2011; Omrane *et al*., 2015). It has been shown that multidrug resistance (MDR) of *Z. tritici* relies mainly on the increased expression of the major facilitator superfamily (MFS) transporter, MFS1 (Omrane *et al*., 2015), which has been shown to be directly correlated to the resistance of *Z. tritici* to the fungicide boscalid (Fouché *et al*., 2022). ATP-binding cassette (ABC) transporters are also implicated in MDR of *Z. tritici* to fungicidal treatments. MFS transporters utilise energy from the proton-motive force, while ABC transporters utilise energy from ATP-hydrolysis (Omrane *et al*., 2015).

Between different fungal species, the inherent ability to generate resistance occurs at different rates, with some known to gain resistance to novel fungicides after a single season of application (Avenot and Michailides, 2019; Baibakova *et al*., 2019). There are four main mechanisms by which phytopathogenic fungi gain fungicide resistance: overexpression of the fungicide target, improved detoxification/metabolism of the fungicide, increased ability to expel intracellular fungicides, and modification of the target site (Lucas *et al*., 2015). The latter is the most common route, as a large proportion of fungicides used are single target. As stated with regards to *Z. tritici*, it

has been seen that a SNP, otherwise known as a point mutation, is enough to confer complete resistance to previously effective fungicides (Ma and Uddin, 2009; Mosbach *et al*., 2017; Sierotzki and Gisi, 2000).

Two main strategies are used to try to combat the development of fungicide resistance: rotational fungicide programmes and fungicide mixtures. The Fungicide Resistance Action Committee (FRAC), a global body dedicated to fighting the increasing emergence of fungicide resistance, strongly recommends that growers of crops alternate the fungicides applied seasonally (FRAC, 2007). In doing this, there is a decreased selection pressure against specific fungicides in the long term, which is proven to slow the spread of resistance. Secondly, it is recommended that different fungicides be used in combinatorial mixtures (FRAC, 2007). While this theoretically has little effect on the selection pressure exerted by individual fungicides, if a fungal phytopathogen were to develop resistance to one fungicide, a second fungicide (with a separate mode of action) remains to act on "resistant" individuals. Evidence supports that this is an effective method to slow the spread of resistance, reducing selection against "high-risk" fungicides (Hobbelen *et al*., 2014). To employ both mixtures and rotational programmes at once a number of effective fungicides are needed, ideally belonging to different fungicide classes with differing modes of action. Applying fungicides of different classes is important as resistance (e.g., SNP-mediated) to one fungicide can also protect the phytopathogen against closely related compounds. This is known as cross resistance (FAO, 2013; FRAC, 2007). Triazole fungicides, belonging to the group of fungicides known as demethylation inhibitors (DMI), are subject to cross-resistance with clinical triazoles, accelerating the already desperate need for new clinical fungicides (Dalhoff, 2018; Snelders *et al*., 2012). This cross resistance is possible as azoles all have the same molecular target: lanosterol 14α –demethylase, which converts lanosterol into ergosterol.

The targeting of ergosterol biosynthesis has been one major weapon against fungal phytopathogens for several decades. Ergosterol, serving many of the same functions as cholesterol in animal cells, is a molecule essential to most fungi and protozoa (Sheehan *et al*., 1999). As ergosterol does not exist in animal and plant cells, there is a reduced chance of drugs specifically targeting ergosterol to be toxic to these taxonomic kingdoms – a problem often encountered when looking for drugs to target eukaryotes such as fungi. Due to the success of ergosterol as a fungicide target, the majority of known fungicides interfere with this molecule in one way or another (Sangamwar *et al*., 2008). While several other fungicide classes exist, such as echinocandins which also target fungal cell wall synthesis (Denning, 2002), the diverse nature of fungi means that many fungicides only successfully inhibit, and may only be approved for use on, specific fungal phytopathogen species. This can lead to difficulties in designing successful fungicide mixtures and rotational programmes, as there is not enough variety among available treatments. While a number of broad-spectrum fungicides do exist, they are much less common. The widely used broad-spectrum multisite fungicide, chlorothalonil, was recently banned (March 2019) in the European Union. As a side effect of increasingly tightening fungicide regulations, development of novel fungicides is becoming more constrained. This is a particular problem given that toxicity/environmental concerns are motivating bans against chlorothalonil and other fungicides, while their effectiveness is lost due to development of resistance. Another example of a banned fungicide is the ethylene-bis-dithiocarbamate (EBDC), mancozeb (Saha *et al*., 2022; EU, 2020). Mancozeb (like other EBDCs) has multiple modes of action. However, due to evidence of mancozeb being an endocrine disruptor, it was deemed unsafe for agricultural use within the EU.

Newly developed fungicides and their by-products should be of very limited toxicity to non-target organisms, and highly specific to the target phytopathogen(s).

In order to help slow the development of resistance, multisite fungicides are preferred. As mentioned, SNPs are a common way through which fungicide resistance is developed. Multisite fungicides alleviate this as multiple concurrent mutations would be needed to overcome the different mechanisms of action. Although novel fungicides with a broad spectrum (in terms of different fungal phytopathogens) could benefit a wider range of crops, there are concerns about negative impacts of broad range (particularly systemic) fungicides, or fungicides applied to soil, on the beneficial mycorrhizal fungi present at the roots of plants and within the soil. This could lead to non-optimal plant growth, requiring extended growing periods or reduced crop yields (Channabasava *et al*., 2015). Therefore, ideally novel fungicides (particularly any with a broad-spectrum) should not have significant detrimental effects to the beneficial non-target fungi or other biota.

1.3.3. Biocontrol

As the global population becomes more concerned about the environmental impact of pesticides, there is a need to explore safer and more eco-friendly pest control measures. Biological control (biocontrol) has received increased attention as a strategy in the fight against fungal phytopathogens. Biocontrol with crops involves the use of biological processes, or of naturally occurring or introduced antagonists, to combat plant diseases (Baker, 1987; Stirling and Stirling, 1997) and has been theorised as a method of control since as early as 1921 (Hartley, 1921). Microbial biocontrol agents, most often bacterial or fungal strains isolated from the phyllosphere (aerial region of plants colonised by microbes), the endosphere (microbiome inside the plant), or the rhizosphere (area of root microbiome), can prevent infection of the host plant naturally through mechanisms such as antibiosis, mycoparasitism, induced resistance, or growth enhancement (Thambugala *et al*., 2020). Reports of successful examples include the use of *Trichoderma*, a fungal symbiont of plants, and

biopesticides based on *Bacillus thuringiensis* (Menzler-Hokkanen, 2006). Drawbacks of biocontrol include variable performances under different environmental conditions, including poor environmental longevity of many proposed biocontrol organisms, and poor host specificity (Thambugala *et al*., 2020). Additional constraints of biocontrol agent development or application include: the often lower activity of microbial antagonists when compared to that of synthetic pesticides, the scarcity of information available due to industrial secrecy, and complex registration and patent procedures in place in some countries (Palmieri *et al*., 2022).

1.4. Drug-drug interactions

1.4.1. Synergies

As discussed above, fungicide mixtures are an important strategy for helping to control fungal phytopathogens. Such mixtures, however, are typically formulated on the basis that the compounds included have unique modes of action. Therefore, the individual fungicides (and their respective mechanisms of action) are not necessarily expected to have any interaction or association with one another. Different types of compound-compound interactions are possible though, including synergy.

Synergy can be described as where the combined effect of two compounds is greater than that predicted by their individual potencies (Tallarida, 2011). Such synergies are important in medicine as they can improve therapeutic outcomes. They commonly arise where two agents target a common process or pathway, albeit at different specific targets. One well-known synergy is that of amoxicillin and clavulanic acid. This combination treatment is on the World Health Organisation's List of Essential Medicines (twelve different azoles also make the list) (WHO, 2013). Amoxicillin, a drug used to treat bacterial infections, has a four-atom ring known as a beta-lactam ring, like that of other penicillin derivatives. Bacterial resistance commonly arises through

the production of beta-lactamases, which break down the beta-lactam ring via hydrolysis (Drawz *et al*., 2010). However, *Streptomyces clavuligerus*, a filamentous bacterium that produces antibiotics naturally, inhibits the action of beta-lactamases by producing clavulanic acid. Clavulanic acid works by competitively binding to beta-lactamases to alleviate their effect on beta-lactam antibiotics (Drawz et al, 2010). Consequently, in combination with amoxicillin (co-amoxyclav), and other beta-lactam antibiotics, clavulanic acid provides a synergistic action through which these drugs can more effectively kill bacteria. This particular example is one of *syncretic* synergy, in which one component has an essential cellular target, while the other has a non-essential target.

As well as syncretic synergies, *congruous* and *coalistic* synergies are possible (Tyres and Wright, 2019). Coalistic synergies involve two compounds that each have non-essential cellular targets individually, but when used in combination, synthetic lethality is achieved. In *Saccharomyces cerevisiae* (*S. cerevisiae*), only about 20% of genes are essential (Zhang and Ren, 2015). The remaining 80% of gene products have therefore been seen as weak candidates as potential antibiotic targets (Rancati *et al*., 2018). A gene deletion library of *S. cerevisiae* found more than 500,000 binary combinations of non-essential gene deletions resulted in negative interactions, with ~10,000 of these synthetic lethality. Despite this knowledge of a possible 500,000 coalistic interactions (in *S. cerevisiae*), it is less likely that current compounds exist (or have these targets identified) to directly test these possibilities, as most of the antimicrobial discovery (in medical or agricultural settings) searches for compounds targeting essential genes. High-throughput approaches such as the screenings of large chemical libraries may be a simpler way to identify coalistic synergies. Synthetic lethality from higher order combinations is also possible with recent evidence suggesting that ternary interactions are 100-fold more prevalent than the standard

two-combination interactions (Kuzmin *et al*., 2018). However, due to strict regulations on the number of chemicals applied in the EU (and elsewhere), addition of further agents may be disadvantageous.

Congruous synergies include two compounds, each with an essential molecular target. Several different congruous combinations have been successfully exploited (albeit against human pathogens) including those under the trade names of Neosporin, Septra and Synercid (Tyres and Wright, 2019). Congruous combinations may be more readily testable than coalistic combinations due to the large variety of existing antimicrobials with known actions at essential targets (and compounds with unknown MoA but which are still inhibitory). The work described in this thesis primarily focuses on congruous synergies.

Drug synergies have certain key advantages. Due to the increased potency of the compounds when in combination, lower doses can be used while still achieving inhibition. Lower dosage means lower costs, reduced potential environmental impact, and reduced potential toxicity to non-target organisms including pathogen hosts. A good example of reduced dosage possibilities can be seen with the drug caspofungin, an inhibitor of β(1,3)-d-glucan synthesis needed for fungal cell wall development (Letscher-Bru and Herbrecht, 2003). With the addition of the relatively cheap drug chloroquine, the minimum inhibitory concentration (MIC) of caspofungin was decreased by up to five-fold against the important pathogen of humans, *Candida albicans* (Islahudin *et al*., 2013). Synergies can also be an effective way of repurposing old drugs. High throughput screens testing for synergies between known compounds is proposed as a fast-track way to discover new treatments (Zheng *et al*., 2018). Several studies have attempted large-scale screens, with varying degrees of success (Ramón-García *et al*., 2011; Kim *et al*., 2016; Margue *et al*., 2019;). Taking this further, some

groups have developed computational algorithms and machine learning approaches to try and predict compound synergies based on known modes of action, the likelihood of affected proteins/pathways having a possible link, compound structures, and knowledge of previously discovered synergies (Ianevski *et al*., 2019; Yang *et al*., 2020,). It is also possible that two existing compounds, already approved for applications (whether it be on humans, plants, etc) could produce synergy through previously unknown mechanisms.

Synergistic combinations also have possible disadvantages, however. One is the inclusion of more than one active agent, which has potential regulatory and environmental implications. Secondly, the target organism in principle needs to develop resistance to only one of the agents to be resistant to the synergy, so the usual advantage of conventional combinations (i.e., inclusion of a back-up agent) may be undermined when the second agent is supplied at a lower than normal concentration as would be the case where there is synergy. It has been reported that application of synergies can in fact lead to a faster evolution of resistance than if their constituent parts were applied individually (Hegreness *et al*., 2008). With fungicides in mind, this potential hastening of resistance could be decelerated by the incorporation of synergies into rotational programmes. It is envisaged that an ideal combination might contain two multisite inhibitors, with (at least) two synergistic mechanisms. However, such combinations, while theoretically possible, may be uncommon and/or difficult to identify.

1.4.2. Antagonisms

Considered the opposite of synergies, drug antagonisms are also of importance. Antagonisms occur when the interaction of two or more drugs causes an overall decreased effect, e.g., promoting the survival of an organism. This could arise from the

compounds physically/chemically interfering with one another, or when one compound inhibits the cell death mechanism of the other. While characterising such antagonisms may not typically be so applicable for inhibiting growth, they can give insight to unknown resistance mechanisms that may undermine otherwise inhibitory drugs, including for predicting how future resistances might develop (Yeh *et al*., 2009).

Drug antagonisms have an additional use: selecting against drug resistance (Chait *et al*., 2007). In a population of cells resistant to a particular drug, a known antagonist can be applied in combination to help select against this resistance. This selection can lead to subsequent generations re-acquiring vulnerability to the original drug. This occurs because the antagonistic interaction selects against the developed mechanism(s) of resistance (Chait *et al*., 2007). While a main goal of this project was the search for combinatorial synergies, evidence of antagonisms was not overlooked.

1.4.3. The search for synergies

There are four primary methods commonly used to test for synergies (Doern, 2014). These include multiple-combination bactericidal antimicrobial testing (MCBT), Etest (gradient diffusion), and time-kill curve assays. However, perhaps the most common validation technique in the search for synergies is the checkerboard (or chequerboard) assay (Odds, 2003). In the checkerboard assay, drug combinations are applied to the organism of interest over a range of the individual-drug concentrations. An example checkerboard assay showing synergy is shown in Figure 1.2.

Checkerboard results allow calculation of the fractional inhibitory concentration index (FICI). The FIC index indicates the nature and strength of any drug interactions

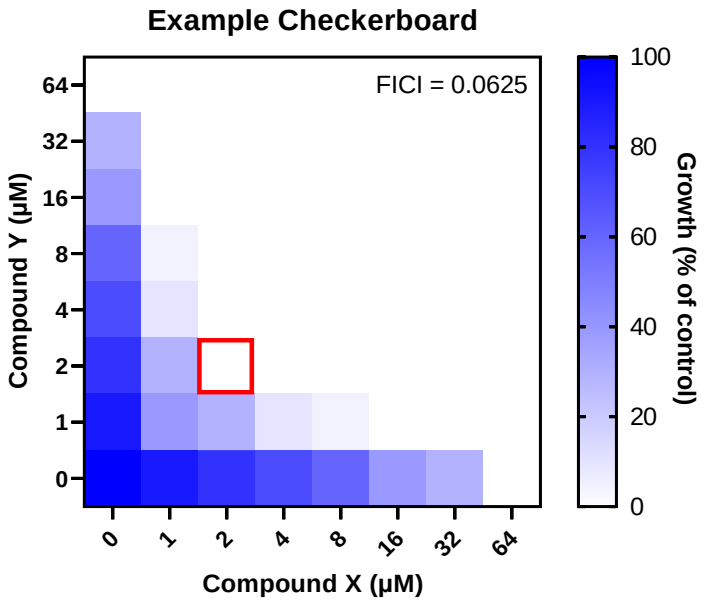

Figure 1.2. **Example analysis of a checkerboard experiment showing synergy**. Each square represents one well of a 96-well plate. One compound increases in concentration along the x-axis while the other increases in concentration along the y-axis. Colour scale shows the percentage final growth compared to the bottom-left control well. Red square indicates which well was used for calculating the FIC (). The calculated FICI is shown as an inset in the top-right of the checkerboard.

(Meletiadis *et al*., 2009) versus additive effects. The FIC index also indicates any antagonisms, and is calculated as follows:

$$FICI = \frac{Drug\ X\ MIC\ in\ combination}{Drug\ X\ MIC\ alone} + \frac{Drug\ Y\ MIC\ in\ combination}{Drug\ Y\ MIC\ alone}$$

Figure 1.3. **Calculation of Fractional Inhibitory Concentration Index (FICI)**. Equation used for determining synergism or antagonism between two compounds in a checkerboard format.

In theory, an FICI of <1 indicates a synergistic interaction, as this is a stronger effect than that predicted by their individual potencies. However, checkerboards have been criticised due to reproducibility concerns (Odds, 2003). Variation in a single result can place the observed MIC in a three-dilution range. In the equation above, a small change such as this can have large consequences on the FIC output. To address this, it is generally accepted that an FICI ≤ 0.5 is required to interpret any results as synergistic, with 0.5 < FICI < 1 considered additive. On the other hand, the cited cut-

off for antagonism is more varied. Some sources state that an FICI of ≥ 1.5 is required to interpret results as an antagonistic, while others indicate FICI > 4. Alternative methods of determining synergy and antagonism do exist and are commonly used within the field of virology (Chou *et al*., 1984; Prichard *et al*., 1993). However, due to the relative simplicity of the checkerboard and its interpretation, this was the primary measure for synergy employed in this thesis. In the example checkerboard shown in Figure 1.2, it is easily seen that each compound individually inhibits the unnamed organism at 64 µM. In combination, the concentration required by each compound to inhibit the organism is 2 µM, a 32-fold decrease.

Discovering compound synergies is a rare event (Cokol *et al*., 2011) but as suggested earlier, it can be possible to anticipate rationally. For this, ideally the mode of action of both drugs should be known, or at least predicted. A simple example is the rational prediction of a synergy between one drug that creates sufficient pores in the cell membrane to allow a second drug increased entry into the organism. This synergistic mechanism could underlie the interactions of azoles or amphotericin B with flucytosine (Johnson *et al*., 2004). The current fungicidal mixtures on the market, as recommended by FRAC, generally contain two fungicides with distinctive modes of action that are not known to interact with one another (BAYER; Syngenta). This further illustrates how synergies are an untapped strategy in the fight against fungal phytopathogens.

Just as in the search for novel fungicide targets, any newly discovered synergies are likely to be most valuable where their synergistic mechanism is novel. It has previously been reported that fungicide combinations targeting the process of protein translation/translation fidelity could offer such a novel target. It was shown that the toxic metal chromium, when combined with the antibacterial aminoglycoside

paromomycin, synergistically inhibited *S. cerevisiae*, potentially via a mechanism based on synergistically increased mistranslation of mRNA (translation error) (Holland *et al*., 2007). Subsequently, Moreno-Martinez *et al*. (2015) tested different aminoglycoside antibiotics in combination with a number of agents which, like chromate, inhibit the sulphate transport that is necessary for the synthesis of sulphur-containing amino acids cysteine and methionine. Several combinations synergistically inhibited several different fungi, including the human pathogens *Candida albicans* and *Cryptococcus neoformans*, the food spoilage yeast *Zygosaccharomyces bailii*, and the fungal phytopathogens *Rhizoctonia solani* and *Zymoseptoria tritici*. The compounds' respective MICs were decreased by ≥8-fold and tested combinations increased the mistranslation rate by up to 10-fold in yeast (Moreno-Martinez *et al*., 2015). Crucially, these combinations were not synergistic against tested bacterial or mammalian cells. Furthermore, Vallières *et al*. (2018) rationally identified 48 combinations that inhibited different fungi synergistically, using compounds that targeted the availability of functional amino acids in different ways. Again, key combinations were not synergistic against mammalian, bacterial, or plant cells. This body of work supported targeting of the fidelity of protein synthesis in fungi as a potential new target for control of problematic fungi.

There are additional molecular targets that could potentially be exploited in the search for fungicidal synergies with regard to protein synthesis fidelity: the different enzymes involved in the biosynthesis of each amino acid, the proteins involved in supply of required protein-biosynthesis materials (e.g., akin to sulphur transport/uptake for methionine and cysteine biosynthesis described above), the components of ribosome function and ribosome attachment to mRNA or inhibition of aminoacyl tRNA synthetases, the molecules necessary for 'charging' amino acids to the correct tRNA.

Compounds that interfere with different stages of tRNA processing also exist, although not necessarily with activity against fungi (Chopra and Reader, 2015).

1.5. The yeast *Saccharomyces cerevisiae* as a model organism

The brewer's or baker's yeast *S. cerevisiae* has been a crucial tool for biologists for several decades now. The organism's eukaryotic nature means that it shares many gene orthologs and cellular processes with humans and as such it can be used to gain insights relevant to human cell biology, genetics and human disease. It is thought that at least 20% of human genes known to have a role in disease have counterparts in yeast, spanning one in ten yeast genes (Forslund *et al*., 2011; Mohammadi *et al*., 2015). Moreover, genetic modification of yeast is easy and cheap when compared with other eukaryotic model organisms such as mice and zebrafish or the vast majority of other fungi. *S. cerevisiae* is also hardy, grows on inexpensive substrates, and is easy to cultivate on both rich and defined media, allowing for greater control over experiments. The organism has short generation times meaning that research can be carried out relatively quickly, with the potential to then further explore key results of interest in main organisms of interest. *S. cerevisiae* also offers an outstanding toolbox of genetic/genomic tools, resources and databanks. For example, complete yeast gene deletant and gene overexpression libraries were used during this PhD. Tools such as the *Saccharomyces* Genetic Database (SGD) contain easily accessible functional information on the entire yeast genome including detailed descriptions and data for thousands of genes and proteins. Yeast therefore can also present a useful model organism for research of other fungal species (such as the fungal phytopathogens of interest here) for which genetic manipulation is more laborious.

As mentioned, *S. cerevisiae* acts as a model organism for a wide range of purposes. However, there are limitations in how well results obtained from experiments with

this species translates to usable information in other organisms. For example, *S. cerevisiae* prefers to utilise fermentation for growth, whereas *Z. tritici* solely utilises aerobic respiration. As such, experiments involving these processes in one organism may not directly translated to the other. In addition, *S. cerevisiae* lacks complex I of the electron transport chain (Friedrich *et al*. 1995) where it is present in almost all other fungi (Joseph-Horne *et al*., 2001). Furthermore, the mitochondria in fungal pathogens can play different and/or more important roles than in the non-pathogenic *S. cerevisiae* (Black *et al*., 2018; Mendoza *et al*., 2020). One example of this is the role of mitochondria in iron homeostasis. In pathogens, competition for iron with the host can be an important aspect of disease, and links between iron and virulence have been shown (Hood and Skaar, 2012). Mitochondria also play a role in the response and adaptation of fungal pathogens to stress conditions in the host. In mammalian fungal pathogens, mitochondria were implemented in responses to oxygen and nutrient limitation, variability in pH, elevated temperature, as well as oxidative stresses (Verma *et al*., 2018).

1.6. Overall thesis aims

As outlined, there is an imperative to increase the arsenal available in the fight against fungal phytopathogens. While developing new fungicides is an important option, repurposing existing compounds is an attractive prospect. Discovery and application of fungicidal synergies is a promising approach for combatting fungal diseases of crops, with the potential of decreasing both cost and toxicity to non-target organisms.

Below are the aims and objectives of this PhD research.

- Discover novel synergies targeting major phytopathogenic fungi, with a primary focus on protein synthesis and translational fidelity
- Determine the modes of action of any synergies found
- Determine the industrial relevance of any synergies found (e.g., toxicity, viability)

Chapter 2 - Materials and Methods

2.1. Materials

2.1.1. Chemicals, Media, and Solutions

Table 2.1. **Chemicals used in this study**.

Chemical	Solvent	Supplier
Amphotericin B	DMSO	Sigma
Amodiaquine	H_2O	Sigma
Chlorimuron Ethyl	Acetone	Sigma
Cumene Hydroperoxide	DMSO	Sigma
Cyprodinil	DMSO	Sigma
Diamide	Acetone	Sigma
DHR 123	H_2O	ThermoFisher
Diphenyleneiodonium chloride	DMSO	Sigma
EPG	100% Ethanol	Glentham
H_2DCF-DA	H_2O	ThermoFisher
Glyphosate	H_2O	Sigma
L-cyclopropylalanine	H_2O	Sigma
Mefloquine	H_2O	Sigma
Menadione	H_2O	Sigma
Methotrexate Hydrate	0.1 M NaOH	Glentham
Mupirocin C	DMSO	Glentham
Paraquat	70% Ethanol	Sigma
Primaquine	70% Ethanol	Sigma
REP3123	DMSO	Axon Chemicals
Rhodamine 123	H_2O	Sigma
Sodium Bicarbonate	H_2O	Sigma
Sodium Orthovanadate	H_2O	Sigma
Sodium Probenecid	H_2O	Sigma
Tavaborole	DMSO	Sigma
t-BOOH	H_2O	Sigma
Tetramethylrhodamine	H_2O	ThermoFisher

Table 2.2. **Cultivation media and solutions used in this study**.

Media/Solutions	Composition
Aspergillus minimal medium (AMM)	Contains per litre ddH_2O: 20x salts, 50 ml; trace elements solution, 4 ml; glucose, 10 g.
20x Salt solution (AMM)	Contains per litre ddH_2O: $NaNO_3$, 1.4 M; KCl, 140 mM KCl; KH_2PO_4, 224 mM; $MgSO_4$, 42 mM.
Trace elements (AMM)	Contains per litre ddH_2O: $FeSO_4$, 1 g; $ZnSO_4$, 8.8 g; $CuSO_4$, 0.4 g; $MnSO_4$, 0.15 g; $Na_2B_4O_7$, 0.1 g; $(NH_4)_6Mo_7O_{24}$.
DNA carrier	10 mg mL^{-1} (stored at -20˚C) boiled for 20 min (100˚C), transferred on ice, and diluted to 2 mg mL^{-1} in ddH_2O.
Induction medium (IM) for *Agrobacterium*-mediated transformation of *Zymoseptoria tritici*	Contains per litre ddH_2O: stock solution A, 50 ml; stock solution B, 50 ml; stock solution C, 50 ml; $FeSO_4$, 50 µM; MES, 40 mM; glucose, 10 mM; glycerol, 0.5%. pH adjusted to 5.6 using 1 M NaOH before made up to final volume with ddH_2O. (20 g L^{-1} Bacto agar added for making IM plates). Autoclaved and 100 µg ml^{-1} spectinomycin added while cooled to 40-50^oC.
Stock solution A (IM)	Contains per litre ddH_2O: K_2HPO_4, 200 mM; KH_2PO_4, 200 mM; NaCl, 50 mM.
Stock solution B (IM)	Contains per litre ddH_2O: $MgSO_4$, 40 mM; $(NH_4)_2SO_4$, 80 mM.
Stock solution C (IM)	Contains per litre ddH_2O: $CaCl_2$, 15 mM.
Lysogeny Broth (LB) medium	Contains per litre ddH_2O: Peptone, 10 g; Yeast Extract, 5 g; sodium chloride, 5 g.
Modified Coursen and Sisler Medium (MCS)	Contains per litre ddH_2O : glucose, 10 g; KH_2PO_4, 2 g; K_2HPO_4, 1.5 g; $(NH_4)_2SO_4$, 1 g; yeast extract, 1 g; NaCl, 0.5 g, $MgSO_4$, 0.5 g. Sterile filtered.
MES buffer	10 mM MES hydrate in ddH_2O, pH 6. pH adjusted with HCl/NaOH.
MMZT medium	Contains per litre: glucose, 20 g; $NaNO_3$, 2g; KH_2PO_4, 1.5 g; K_2HPO_4, 1 g; $MgSO_4$, 0.5 g; KCl, 0.5 g; $CaCl_2$; 0.01% thiamine, 1 ml; trace element solution, 1 ml; vitamin solution, 1 ml. Autoclaved.
Trace elements (MMZT)	Contains per litre ddH_2O: $ZnSO_4$, 22 g; $B(OH)_3$, 11 g; $MnCl_2$, 0.5 g; $FeSO_4$. 0.5; $CoCl_2$, 0.17 g; $CuSO_4$, 0.16 g; Na_2MoO_4, 0.15 g; tetrasodium EDTA, 5 g.
TE buffer	EDTA, 0.1 mM; Tris-HCl, 10mM.
Vitamin stock (MMZT)	Contains per litre: biotin, 0.01 g; pyridoxine, 0.01 g; thiamine, 0.01 g; riboflavin, 0.01 g; *p*-aminobenzoic acid, 0.01 g; nicotinic acid, 0.01 g. Sterile filtered.

Potato dextrose agar (PDA)	39 g L^{-1} PDA (Sigma) in ddH_2O.
Potato dextrose broth (PDB)	24 g L^{-1} PDB (Sigma) in ddH_2O.
Potassium phosphate buffer (0.5 M)	0.25 M KH_2PO_4, 0.25 M K_2HPO_4 in ddH_2O, pH 7.4.
Salt solution	Contains per litre ddH_2O: KCl, 26 g, $MgSO_4.7H_2O$, 26 g L^{-1}, KH_2PO_4 76 g L^{-1}.
Triphenyl tetrazolium chloride (TTC) agar	Contains per litre ddH_2O: Agarose, 15 g; sodium phosphate buffer (pH 7), 1 L; TTC, 1 g.
Sodium phosphate buffer (TTC)	$Na_2HPO_4.7H_2O$, 12.39 g; $NaH_2PO_4.H_2O$, 4.661 g; ddH_2O, 700 ml. Adjusted to pH 7 using HCl and NaOH. Distilled water was added to make a final volume of 1 L.
Vitamin stock (MCSD)	Per 100 ml: Thiamine HCl, 200 µg; Pantothenic Acid, 200 µg; Nicotinic Acid, 200 µg; Biotin, 10 µg; Myo-inositol, 2 mg. Sterile filtered.
Vogel's Minimal Medium (50x) (VMM)	Contains per litre ddH_2O: Trisodium citrate, 125 g; KH_2PO_4, 250 g; NH_4NO_3, 100 g; $MgSO_4.7H_2O$, 10 g; $CaCl_2.2H_2O$, 5 g; biotin solution, 2.5 ml; trace elements, 5 ml, $CHCl_3$, 2-3 ml.
VMM (1x)	Contains per litre ddH_2O: VMM 50x, 20 ml; Na_2HPO_4, 3.54 g; NaH_2PO_4, 3.44 g; sucrose, 20 g. Sterile filtered.
Biotin solution (VMM)	1.5 mg in 15 ml ddH_2O.
Trace elements (VMM)	Contains per 100 ml: Citric acid.H_2O, 5 g; $ZnSO_4.7H_2O$, 5 g; ; Ferrous ammonium sulphate.$6H_2O$, 1 g; $CuSO_4.5H_2O$, 0.25 g; $MnSO_4.4H_2O$, 0.05 g; H_3BO_3, 0.05; $Na_2MoO_4.2H_2O$, 0.05 g; $CHCl_3$, 1 ml.
YEPD medium	Contains per litre ddH_2O: peptone (bacteriological, Sigma), 20 g; yeast extract (Sigma), 10 g, glucose, 20 g.
YNB medium	Contains per litre ddH_2O; 6.9 g YNB without amino acids (Formedium). Unless stated otherwise, glucose was used as carbon course (2% w/v).

2.1.2. Fungal strains used in this study

Table 2.3. **Fungal strains used in this study**. Does not include extensive list of *S. cerevisiae* overexpression or deletion strains. These are named in legends of appropriate figures in the Results section.

Species/Strain/	Information
Agrobacterium tumefaciens EHA105	electrocompetent cells with rifampicin resistance marker.
Botrytis cinerea SAR109940	Field Isolate (Matthew Dickinson).
Microdochium nivale 217	Field Isolate (Matthew Dickinson).
Rhizoctonia solani AG2-1 1939	Field Isolate (Matthew Dickinson).
Saccharomyces cerevisiae BY4741	*MATa his3Δ1 leu2Δ0 met15Δ0 ura3Δ0* (Euroscarf, Y00000).
Saccharomyces cerevisiae BY4741 pcm190-CFD1-HA	Strain transformed with pCM190-CFD1-HA. doi: 10.1016/j.chembiol.2017.08.005.
Saccharomyces cerevisiae BY4741 pcm190-ISU1-HA	Strain transformed with pCM190-ISU1-HA. doi: 10.1016/j.chembiol.2017.08.005.
Saccharomyces cerevisiae BY4741 pcm190-NAR1-HA	Strain transformed with pCM190-NAR1-HA. doi: 10.1016/j.chembiol.2017.08.005.
Saccharomyces cerevisiae BY4741 pcm190-RLI1-HA	Strain transformed with pCM190-RLI1-HA. doi: 10.1016/j.chembiol.2017.08.005. and doi: 10.1128/AAC.00459-17.
Saccharomyces cerevisiae BY4741 pcm190-YAH1-HA	Strain transformed with pCM190-YAH1-HA. doi: 10.1016/j.chembiol.2017.08.005.
Saccharomyces cerevisiae BY4741 pcm190-YFH1-HA	Strain transformed with pCM190-YFH1-HA. doi: 10.1016/j.chembiol.2017.08.005.
Saccharomyces cerevisiae BY4743	MATa: his3Δ1 leu2Δ0 ura3Δ0 (Euroscarf, Y20000)
Saccharomyces cerevisiae BY4743 with 'GFP^{Leu}' dual fluorescence construct	Ura+ plasmid containing RFP and GFP which are transcribed together. Threonine at position 65 essential for fluorescence replaced with leucine.
Saccharomyces cerevisiae BY4743 with 'GFP^{Ser}' dual fluorescence construct	Ura+ plasmid containing RFP and GFP which are transcribed together. Threonine at position 65 essential for fluorescence replaced with serine (still fluoresces)
Saccharomyces cerevisiae BY4743 with 'GFP^{Thr}' dual fluorescence construct	Ura+ plasmid containing RFP and GFP which are transcribed together. Threonine at position 65 essential for fluorescence retained.
Saccharomyces cerevisiae BY4741 with 'TAAT' dual luciferase construct (DL^{TAAT})	Ura+ plasmid containing firefly and *Renilla* luciferase, separated by an in-frame stop codon (TAA). Plasmid source: David Bedwell.

Saccharomyces cerevisiae BY4741 with R868H dual luciferase construct (DL^{868})	Ura+ plasmid containing firefly and *Renilla* luciferase. Histidine at position 868 essential for firefly fluorescence replaced with arginine.
Saccharomyces cerevisiae Leu2	Leu2 insertion complementing leucine auxotrophy. BY4743 background. MATa: his3Δ1 ura3Δ0 (Created by Kamil Szepe).
Saccharomyces cerevisiae L1494	Has a stable deletion of the chromosomal rDNA locus and carries multicopy plasmid with the rDNA locus on. *MATα ade1−14*(UGA) *his7−1*(UAA) *lys2-L864*(UAG) *leu2−3*, *112 trp1Δ1ura3−52RDNΔ* pRDN-wt (TRP1 LEU2-d rDNA).
Saccharomyces cerevisiae L1583	Has a stable deletion of the chromosomal rDNA locus and carries multicopy plasmid with the rDNA locus on. Locus has a C1054A mutation associated with error-prone mistranslation. *MATα ade1−14*(UGA) *his7−1*(UAA) *lys2-L864*(UAG) *leu2−3*, 112 *trp1Δ1ura3−52RDNΔ* pRDN-1A (TRP1 LEU2-d rDNA).
Saccharomyces cerevisiae L1597	Has a stable deletion of the chromosomal rDNA locus and carries multicopy plasmid with the rDNA locus on. Locus has a C1054U mutation associated with low translational fidelity. *MATα ade1−14*(UGA) *his7−1*(UAA) *lys2-L864*(UAG) *leu2−3*, *112 trp1Δ1ura3−52RDNΔ* pRDN-1T (TRP1 LEU2-d rDNA).
Saccharomyces cerevisiae overexpression library	AB320 genomic library in YEp13 *Escherichia coli*. https://www.atcc.org/products/37323
Saccharomyces cerevisiae pos5Δ	Deletion strain for the *POS5* gene in the BY4743 background. ORF: YHR008C. Source: Horizon Discovery.
Saccharomyces cerevisiae pos5Δ strains	A *pos5Δ* deletion strain (from above) was transformed with pCM190 plasmids carrying *POS5* genes cloned either from *S. cerevisiae*, *B. cinerea*, or *Z. tritici*. Sequences from ATG start codon to TAA stop codon. Sequences were codon optimised for *S. cerevisiae*. Plasmids synthesised by Genewiz.
Saccharomyces cerevisiae sod2Δ	Deletion strain for the *SOD2* gene in the BY4741 background. ORF: YHR008C. Source: Euroscarf.
Saccharomyces cerevisiae yap1Δ	Deletion strain for the *YAP1* gene in the BY4741 background. ORF: YML007W. Source: Euroscarf.
Saccharomyces cerevisiae W303	*MATa ura3-1 ade2-1 trp1-1 his3-11,15 leu2-3* (source: Roland Lill, University of Marburg).
Zymoseptoria tritici IPO323	Reference strain (source: Syngenta).

Zymoseptoria tritici ROY-UN	*Z. tritici* isolated from infected wheat in Royston, Hertfordshire. Wheat was untreated. Source: Steve Rossall, University of Nottingham.
Zymoseptoria tritici ROY-PZ	*Z. tritici* isolated from infected wheat in Royston, Hertfordshire. Wheat was treated with prochloraz. Source: Steve Rossall.

2.1.3. Plasmids used in this study

Table 2.4. **Plasmids used in this study**.

Plasmid	Information
pcm190-CFD1-HA	pCM190-CFD1-HA. doi: 10.1016/j.chembiol.2017.08.005.
pcm190-ISU1-HA	pCM190-ISU1-HA. doi: 10.1016/j.chembiol.2017.08.005.
pcm190-NAR1-HA	pCM190-NAR1-HA. doi: 10.1016/j.chembiol.2017.08.005.
pcm190-RLI1-HA	pCM190-RLI1-HA. doi: 10.1016/j.chembiol.2017.08.005. and doi: 10.1128/AAC.00459-17.
pcm190-YAH1-HA	pCM190-YAH1-HA. doi: 10.1016/j.chembiol.2017.08.005.
pcm190-YFH1-HA	pCM190-YFH1-HA. doi: 10.1016/j.chembiol.2017.08.005.
'GFP^{Leu}' dual fluorescence construct	Ura+ plasmid containing RFP and GFP which are transcribed together. Threonine at position 65 essential for fluorescence replaced with leucine.
'GFP^{Ser}' dual fluorescence construct	Ura+ plasmid containing RFP and GFP which are transcribed together. Threonine at position 65 essential for fluorescence replaced with serine (still fluoresces)
'GFP^{Thr}' dual fluorescence construct	Ura+ plasmid containing RFP and GFP which are transcribed together. Threonine at position 65 essential for fluorescence retained.
'TAAT' dual luciferase construct (DL^{TAAT})	Ura+ plasmid containing firefly and *Renilla* luciferase, separated by an in-frame stop codon (TAA). Plasmid source: David Bedwell.
R868H dual luciferase construct (DL^{868})	Ura+ plasmid containing firefly and *Renilla* luciferase. Histidine at position 868 essential for firefly fluorescence replaced with arginine.

L1494	*MATα ade1−14*(UGA) *his7−1*(UAA) *lys2-L864*(UAG) *leu2−3*, *112 trp1Δ1ura3−52RDNΔ* pRDN-wt (TRP1 LEU2-d rDNA).
L1583	*MATα ade1−14*(UGA) *his7−1*(UAA) *lys2-L864*(UAG) *leu2−3*, 112 *trp1Δ1ura3−52RDNΔ* pRDN-1A (TRP1 LEU2-d rDNA).
L1597	*MATα ade1−14*(UGA) *his7−1*(UAA) *lys2-L864*(UAG) *leu2−3*, *112 trp1Δ1ura3−52RDNΔ* pRDN-1T (TRP1 LEU2-d rDNA).
Saccharomyces cerevisiae overexpression library	AB320 genomic library in YEp13 *Escherichia coli*. https://www.atcc.org/products/37323
pCM190-*POS5Bc*	pCM190 plasmids carrying *POS5* genes cloned either from *B. cinerea*. Sequences from ATG start codon to TAA stop codon. Sequences were codon optimised for *S. cerevisiae*. Plasmids synthesised by Genewiz.
pCM190-*POS5Sc*	pCM190 plasmids carrying *POS5* genes cloned either from *S. cerevisiae*. Sequences from ATG start codon to TAA stop codon. Sequences were codon optimised for *S. cerevisiae*. Plasmids synthesised by Genewiz.
pCM190-*POS5Bc*	pCM190 plasmids carrying *POS5* genes cloned either from *Z. tritici*. Sequences from ATG start codon to TAA stop codon. Sequences were codon optimised for *S. cerevisiae*. Plasmids synthesised by Genewiz.

2.1.4. Laboratory equipment used in this study

Table 2.5 . **Equipment used in this study**.

Equipment	Model	Supplier
Anaerobic chamber	Whitley DG250 Anaerobic Workstation	Don Whitley Scientific
Centrifuge	Centrifuge 5810	Eppendorf
Centrifuge (refrigerated)	Harrier 18/80 (MSE)	Sanyo
Centrifuge (tabletop)	Centrifuge 5424 R	Eppendorf
DeNovix Spectrophotometer/ Fluorimeter	DS-11 FX+	DeNovix Inc., Wilmington, USA
Flow cytometer	ID7000™ Spectral Cell Analyzer	Sony
Flow cytometer	MoFlo Astrios	Beckman Coulter
Haemocytometer	Standard Hemocytometer	Weber Scientific International Ltd, Teddington, UK
Imaging software	Harmony	Perkin Elmer
Brightfield Microscope	Prior PX043	Prior Scientific Instruments Ltd, Cambridge, UK
Fluorescence Microscope	GXML3201LED	GX Microscopes
Plasmid preparation kit	PureYield™ Plasmid Miniprep System	Promega
Multidrop robot	Freedom EVO platform	TECAN
Multiwell plate readers	EL800	BioTek
	Epoch 2	BioTek
	Powerwave XS2	BioTek
	Sunrise	TECAN
Plate reader (imaging)	Phenix plus	Perkin Elmer
Plate reader (fluorescence)	Synergy HTX	BioTek
Statistical Data Analysis	Prism 9	GraphPad Software, Inc.

Structure Drawing	ChemDraw® Professional 16.0.1.4 (77)	PerkinElmer
6-well plates	CELLSTAR® 6 well suspension culture plate: sterile, F-bottom, with lid	Greiner bio-one
96-well plates	CELLSTAR® 96 well suspension culture plate: sterile, F-bottom, with lid	Greiner bio-one
96-well plates (black, clear bottom)	CELLSTAR® µCLEAR® 96 well suspension culture plate: sterile, F-bottom, with lid	Greiner bio-one

2.2. Methods

2.2.1. *S. cerevisiae* plate stocks

S. cerevisiae strains required were briefly removed from -80°C. A scraping was taken with a sterile pipette, and cells were spread onto an agar plate and left to incubate at 30°C for 48-72 h. Plates were kept for no longer than two weeks before a new working culture was prepared. Plates were stored at 4°C until required.

2.2.2. *S. cerevisiae* precultures

For experiments involving *S. cerevisiae* in liquid medium, a single colony from an agar plate stored at 4°C was inoculated into 10 ml of the appropriate medium (see figure legends) in a 50 ml flask. This was incubated overnight at 30°C at 120 revolutions min^{-1}. OD_{600} was then measured, and cultures diluted to OD_{600} 0.5. Cultures were incubated for 4 h at 30°C at 120 rev min^{-1} until exponential phase was reached.

2.2.3. *Botrytis cinerea* and *Zymoseptoria tritici* spore stocks

Aliquots (100 µl) of 10^7 *B. cinerea* or *Z. tritici* spores originally obtained from Syngenta were pipetted and spread onto a PDA plate. Plates were left in the dark (under foil) for one week at room temperature. 2-3 ml of TWEEN was added to the plates, and spores were scraped off using a sterile plastic spreader. The suspension was then filtered through 40 µM cell strainer. The filtrate was centrifuged at 4000 rpm for three minutes. The supernatant was removed, and the pellet was resuspended in 5 ml PBS for every two plates spores were scraped from. Spore concentration was measured with a haemocytometer. Spore suspensions were diluted to ~$1.43x10^7$ spores per ml. Aliquots (700 µl) of spore suspension were added to cryovials containing 300 µl 60% glycerol. The final spore concentration in each cryovial was 10,000,000 spores per ml.

2.2.4. Yeast transformation protocol

An aliquot (5 ml) of exponential phase yeast culture at OD_{600} 2 was centrifuged at 1900 g for 2 min. Pellets were resuspended in 1 ml 0.1 M lithium acetate and incubated for 10 min at 30°C before centrifugation again at 1900 g or 2 min. Pellets were resuspended in 240 µl 50% PEG3500, 36 µl 1 M lithium acetate, 52 µl 2 mg ml^{-1} DNA carrier, between 50-1000 ng DNA to be transformed, and H_2O (sufficient to 100 µl total). Samples were incubated at 30°C for 30 min, then at 42°C for 20 min before centrifugation again at 1900 g for 2 min. Pellets were resuspended in 500 µl sterile water and plated out onto selective agar plates specific for the introduced marker.

2.2.4.1. Yeast transformation protocol for high-copy plasmid library

Aliquots (10 ml) of exponential phase yeast cultures were centrifuged at 1900 g for 2 min and pellets were resuspended in 10 ml H_2O. Samples were centrifuged again, and pellets resuspended in 1.5 ml Solution A (500 µl 2 M lithium acetate, 1 ml TE buffer, 8.5 ml H_2O). After centrifugation, pellets were resuspended in 200 µl of Solution A and incubated for 1 h at 30°C with shaking. A sample (200 µl) was added to a 2 ml microcentrifuge tube containing 50 µl 4 mg ml^{-1} DNA carrier, 4 µg DNA, and 1.2 ml Solution B (1.6 ml PEG3500, 100 µl 2M lithium acetate, 200 µl TE). Samples were mixed by inverting and incubated at 30°C for 30 min while shaking. Samples were then incubated at 42°C for 20 min and centrifuged as above. Pellets were resuspended in 4 ml YEPD and incubated for 1 h at 30°C with shaking. Samples were transferred to 2 ml microcentrifuge tubes and centrifuged as above. Pellets were resuspended in 1.5 ml YNB without a carbon source and 200 µl was spread onto plates selective for leucine prototrophy.

2.2.5. Yeast plasmid-miniprep protocol

Aliquots (1.5 ml) of overnight yeast culture were centrifuged for 1 min at 15,000 g. Supernatant was discarded and the pellet resuspended in 100 µl cold resuspension buffer (25 mM pH 8 Tris-HCl, 10 mM EDTA, 20 µg ml^{-1} RNAse). 200 µl of lysis solution (0.2 M NaOH, 1%(w/v) SDS) was added and samples were mixed by inversion 4-6 times and then incubated for no more than 5 min at room temperature. 150 µl of neutralisation solution (3 M potassium acetate, pH 5.3) was added and samples were mixed immediately by inverting 4-6 times before centrifugation for 10 min at 15,000 g. Supernatant was transferred to a new tube and centrifuged at 15,000 g for 5 min. Supernatant was transferred to a new tube and an equal volume of 100% ethanol was added before mixing by inverting 4-6 times. Samples were then centrifuged at 15,000 g for 20 min and supernatant was discarded. 500 µl of 70% ethanol was added to the microcentrifuge tubes and samples were centrifuged for a short duration at maximum speed. The ethanol was removed, and the pellet was dried at 37^{o}C for 15 min. The pellet was then resuspended in 30 µl sterile water and DNA concentration/purity was measured using a DeNovix Nanodrop by checking for A_{260}/A_{230} and A_{260}/A_{280}.

2.2.6. Plasmid Midiprep

Overnight culture (50 ml) was centrifuged for 3 min at 4000 rpm. Pellets were resuspended in 2 ml resuspension buffer (25 mM pH 8 Tris-HCl, 10 mM EDTA, 20 µg ml^{-1} RNAse). An aliquot (4 ml) of lysis solution (0.2 M NaOH, 1% SDS) was added, and samples were mixed by inversion 4-6 times and incubated at room temperature for no more than 5 min. An aliquot (2.5 ml) of neutralisation buffer (3 M potassium acetate, pH 5.3) was added and samples were mixed by inversion before centrifugation at 4000 rpm for 15 min. Supernatant was transferred to a new vessel and filtered through four layers of cheesecloth. An equal volume of isopropanol was added, and samples were

mixed by inversion before centrifugation at 4000 rpm for 15 min. Supernatant was discarded and pellets were washed with 70% ethanol. Pellets were then dried at 37°C for 15 min before resuspension in 1 ml sterile water.

2.2.7. Checkerboard assays

2.2.7.1. Standard protocol

Initial experiments were carried out to find the minimum inhibitory concentrations (MIC) and sub-inhibitory concentrations (SIC) of each drug in the desired media, to guide selection of appropriate concentrations in checkerboard assays. This was carried out by measuring OD_{600} after treatment with a series of 2-fold dilutions. For checkerboards, 25 µl of serially diluted compounds at 4x final desired concentration were added to wells of flat-bottomed 96-well plates with one increasing in concentration in one dimension, and the other increasing in concentration in the other dimension. Aliquots (50 µl) of cell suspension in the appropriate medium (see figure legends) were then added to wells at 2x desired final concentration. If other supplements (e.g., amino acids, antioxidants) were to be added, 25 µl of cell suspension at 4x concentration was added, along with 25 µl of supplement at 4x desired final concentration. Wells contained final volumes of 100 µl. Control wells always contained appropriate concentrations of any solvent(s) used in a particular experiment.

2.2.7.2. S. cerevisiae

Exponential phase yeast cells were added to a final starting OD_{600} of 0.1. Plates were incubated at 30°C except where an anaerobic chamber was used, as this was set to 24°C (2.2.7.6). Plates were incubated statically unless stated otherwise. Checkerboards were read for absorbance at OD_{600} at 0 h and either 24 h (for YEPD medium) or 48 h (YNB medium) using a multiwell plate reader.

2.2.7.3. Filamentous fungi

Spores were added to a final starting concentration of 10^4 spores ml^{-1} in appropriate medium (see figure legends). Plates were incubated statically for one week at room temperature. For *B. cinerea* and *Z. tritici*, checkerboards were read for absorbance at OD_{600} at 0 h and 168 h. For both *S. cerevisiae* and filamentous fungi, the absorbance at 0 h time point was considered background and subtracted from the final reading.

2.2.7.4. Calculating fractional inhibitory concentration index

As shown in Figure 1.3, the fractional inhibitory concentration index (FICI) was calculated as follows:

$$\frac{MIC\ Drug\ A\ in\ combination}{MIC\ of\ Drug\ A\ alone} + \frac{MIC\ Drug\ B\ in\ combination}{MIC\ of\ Drug\ B\ alone}$$

As previously described in Meletiadis *et al*. 2009, a FICI of ≤0.5 was considered synergistic, and a FICI of >1 considered antagonistic.

2.2.7.5. Checkerboard assays involving electrolysed water

The first tube contained 2 ml 20% EW (400 µl 100% EW in 1.6 ml HPLC-grade H_2O). The remaining concentrations had 1000 µl of HPLC-grade H_2O (including control) prior to start of serial dilution. These were diluted in two-fold series to obtain the concentrations desired. After the preparation of the dilutions, 100 µl was removed from each tube (dilution), ready for the addition of 100 µl of $1x10^4$ spores ml^{-1} of *Z. tritici*. The final EW concentrations were 18%, 9%, 4.5%, 2.25%, 1.13%, 0.57%, 0.28%, 0.14%, 0.72%, 0.36%, 0.018%, 0%. Spores were treated with EW in the dark for exactly 5 min, before 1 ml of YEPD was added to deactivate the EW (Wohlgemuth *et al*., 2020) and incubation at room temperature for 5 min. Samples were then each transferred to 2 ml microcentrifuge tubes and spun down at 10,000 rpm for 15 min. Supernatant was removed and spores were resuspended in 500 µl of H_2O. Spores were spun down again at 10,000 rpm for 15 min. Supernatant was removed and the spores were

resuspended in 500 µl of MCS broth. During this last centrifugation, solutions of the second agent REP3123 were prepared and pipetted to checkerboard format in a 96-well plate. After resuspension, spore concentrations of each sample were determined using a haemocytometer and aliquots each calculated to contain $2x10^4$ spores. EW-treated spores were then added in a checkerboard format to the 96-well plate containing REP3123 to a final concentration of $1x10^4$ spores ml^{-1}.

2.2.7.6. Anaerobic checkerboard experiment

All materials required for this experiment were pre-equilibrated by placing in the anaerobic chamber for >30 min and by sparging nitrogen gas through the medium 10 ml at a time for 5 min to remove as much oxygen as possible before the experiment. As the anaerobic chamber is at 24°C, the control plate incubated aerobically was at 24°C also and both test and control plates were incubated statically.

2.2.7.7. MTT assay checkerboard experiment

To test for insect cell toxicity an MTT (3-(4,5-dimethylthiazol-2-yl)-2,5-diphenyl tetrazolium bromide) assay was used. MTT is a cell permeant tetrazolium salt (yellow) that is reduced to an insoluble formazan (purple) by metabolically active cells. This can be dissolved by SDS to give an even colour, which is proportional to the number of live cells present after incubation with test chemicals.

Insect cell line Sf21 (*Spodoptera fugiperda*) cells were grown in TC100 media supplemented with 5% heat inactivated foetal calf serum. Media used also contains the antibiotic-antimycotic solution (penicillin, streptomycin, amphotericin B) obtained from Sigma. Sf21 cells were added to checkerboards to a final concentration of $1x10^4$ cells $well^{-1}$. Plates were incubated for four days at 27°C in a humidified box before addition of 50 µl 5 mg ml^{-1} MTT to each well. Plates were then incubated for a further 4 h at 27°C. 50 µl 20% SDS was then added to each well to solubilise the MTT and thus

provide even colour distribution. Plates were then incubated overnight at 27°C before reading at 570 nm using a Dynatech plate reader and Revelation software. R413516, an uncoupler, was used as a standard.

2.2.8. Copper chelation in YEPD medium

3 ml YEPD medium in 6-well plates was supplemented with $CuSO_4$ or H_2O equivalent. Neocuproine or ziram were then added to wells to final concentrations of 5 mM, with equal volume of YEPD removed prior. The final $CuSO_4$ concentration was 1 mM and the final well volume 3 ml. Wells were mixed by pipetting. Plates were then incubated at room temperature for 5 min and wells were checked for colour change.

2.2.9. Testing inhibitory effects of $CuSO_4$, neocuproine, and ziram

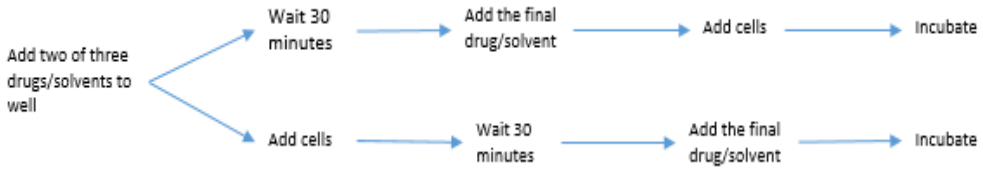

Figure 2.1. **Schematic of protocol**.

96-well plates were prepared with 25 µl containing each of two specified initial compounds and concentrations. Plates were then either incubated for 30 min at 30°C before the addition of the third compound and cells, or cells were added and incubated at 30°C along with the first two compounds for 30 min before addition of the final compound. Plates were then incubated at 30°C for 24 h in an Epoch 2 plate reader with shaking. OD_{600} was read every 30 min. Exponential phase *S. cerevisiae* BY4743 at a final starting-OD_{600} of 0.1 were used for this experiment. The $CuSO_4$ concentration was 3.42 µM with H_2O as solvent, with neocuproine at 20 µM and methanol as solvent, and ziram at 20 µM with DMSO as solvent.

2.2.10. Dual luciferase assay of mistranslation

S. cerevisiae BY4741 transformed with dual-luciferase plasmids harbouring *Renilla* (sea-pansy) and *Photinus* (firefly) luciferase coding sequences.

Samples (300 µl) of exponential phase *S. cerevisiae* transformed with 'DL^{TAAT}' or 'DL^{868}' plasmids were pipetted into wells of a 48-well plate to a final starting OD_{600} of 0.1 (overnight treatment) or OD_{600} 0.5 (4-hour treatment). Aliquots (1 µl) of appropriately-concentrated tavaborole or paromomycin stocks were added, to give the desired final concentrations. Control additions were 1 µl DMSO and H_2O, respectively. After incubation in a multiplate reader at 30°C for 16 h, cell suspensions were transferred into 1.5 ml microcentrifuge tubes and spun for 10 seconds at 10,000 rpm. The supernatant was removed, and cells were resuspended in 300 µl PBS buffer. Each sample was adjusted to OD_{600} 2. In fresh microcentrifuge tubes, 20 µl of 1x passive lysis buffer (from the Promega Dual Luciferase kit) were added to 20 µl of OD_{600} 2 cells in PBS. This was incubated at 30°C for 10 min with shaking at 120 rev min^{-1}. 40 µl of Luciferase Assay Reporter II (LARII) was added and mixed by pipetting. Firefly luminescence was then measured in the Glomax 20/20 luminometer. Once read, 40 µl of STOP-AND-GLOW solution were added and mixed by vortexing. *Renilla* luminescence was then measured. A ratio between the two readings was calculated using the *Renilla* luminescence as a background.

2.2.11. Dual fluorescence assay of mistranslation

2.2.11.1. Flow cytometry

Exponential phase GFP^{Thr}, GFP^{Ser} or GFP^{Leu} expressing cells were treated with specified compounds in 96-well plates and incubated statically at 30°C overnight. Cells were removed from plates and centrifuged at 4000 rpm for 3 min. Pellets were resuspended in 200 µl PBS and transferred to test tubes wrapped in foil. Cell fluorescence was

measured using a Beckman Coulter MoFlo Astrios cell sorter. For measuring GFP, the 488 nm laser with the 513/26 filter was used. For RFP, the 561 nm laser with the 579/16 filter was used. Analysis was carried out with Kaluza software. In specified experiments, suspensions were supplemented with leucine at 75% (572 μM) of the normal level in YNB. In specified experiments, serine was supplied at 475 μM – normally there is no serine added to the media.

2.2.11.2. Fluorescence microscopy

Samples (10 μl) of cell suspension were pipetted onto a glass microscopy slide. Cells were observed under visible light and filters to view fluorescence. Green fluorescence was viewed through a blue filter. Red fluorescence was viewed through a green filter. The GXML3201LED microscope was equipped with a GXCAM controlled by GXCapture software.

2.2.12. Visual assessment of stop codon readthrough with strains expressing *ade1-14* or *ade2-1*

2.2.12.1. Spotting and spreading

S. cerevisiae strains W303 or L1494 diluted to OD_{600} 1, 0.1, 0.01, or 0.001 were pipetted in 5 μl aliquots onto agar plates containing different concentrations of tavaborole or paromomycin, added after melted agar had cooled to ~50°C and before it set. Plates were left at 30°C for 72 h to allow large colonies to form. YNB agar plates contained different concentrations of adenine: 0 μM, 37.5 μM, and 150 μM (the latter is the standard concentration). Colour changes were assessed visually.

For spotting experiments there was the notable change that 100 μl of OD_{600} 0.001 *S. cerevisiae* W303 or L1494 cells were pipetted onto each agar plate and spread using a sterile plastic spreader.

2.2.12.2. TTC overlay

A 20 ml aliquot of triphenyl tetrazolium chloride (TTC) agar was poured gently over plates containing yeast colonies. TTC agar was allowed to set, and plates were left to incubate at 30°C for 24 h. Any colour changes of colonies from white to red were noted.

2.2.13. Screening for growth inhibition by the Prestwick Chemical Library

2.2.13.1. Main screen protocol

MCS medium containing 4% w/v DMSO or 4% w/v tavaborole stock (at 80 ng ml^{-1} final concentration) was aliquoted in 144 µl volumes to wells of 96-well plates before addition of 6 µl of Prestwick Chemical Library (PCL) compound (dissolved in DMSO), giving 40 µM of the PCL compound in 150 µl medium. 50 µl of a suspension of 20,000 spores ml^{-1} *Z. tritici* were added to each well. Final concentrations in each well were: 10 µM PCL compound (except control), 20 ng ml^{-1} tavaborole (except control), 10,000 spores ml^{-1} *Z. tritici*. Plates were sealed with electrical tape and incubated at room temperature in the dark. OD_{600} readings were taken at 0 h, 72 h, 96 h, 168 h using a multiwell plate reader. For readings, tape was removed in a class II hood and any condensation on the lid was wiped with residue briefly left to evaporate to minimise volume loss. Plates were re-incubated until the final timepoint of 168 h.

Effect Strength for each compound was calculated by subtracting the 'average % control growth when in combination with tavaborole' with the 'average % control when not in combination with tavaborole'.

2.2.13.2. Follow-up screen protocol

The protocol for the main screen was repeated with 28 compounds. These were screened against tavaborole, as well as another compound, REP3123. The final

tavaborole concentration was changed to 40 ng ml^{-1} and REP3123 was used at the sub-inhibitory concentration of 9.4 µg ml^{-1}.

2.2.14. Generation of rho^0 mutants

S. cerevisiae cells were grown to OD_{600} 4-8 in YEPD medium with 10 µg ml^{-1} ethidium bromide and plated on YEPD plates to isolate individual colonies. Colonies were selected to inoculate once more and the procedure was repeated. After three successive rounds, clones were checked for growth defects on YEP agar plates containing a nonfermentable carbon source (2% glycerol).

2.2.15. Screen for phenotype suppression by gene overexpression

2.2.15.1. Overexpression library screen

E. coli cells from the ATCC® 37323™ overexpression library, in which random segments of *S. cerevisiae* DNA (average size ≥7.5kb) had been inserted onto the YEp13 plasmid, were plated onto LB agar plates containing 100 µg ml^{-1} ampicillin. A minimum of 10,000 colonies were required for good coverage of the library. Colonies were collected using plastic spreaders and a plasmid midiprep (2.2.6) was performed to extract plasmids from the *E. coli* strains. *S. cerevisiae* W303 cells were transformed with the extracted overexpression plasmids (2.2.4.1) with selection for successful transformants on YNB minimal agar plates without leucine. Enough plates were spread to give >10,000 yeast transformants. All transformants were pooled together and stored in glycerol at -80°C until required. Transformed cells were plated from frozen onto selective medium containing either DMSO, 94 µM cyprodinil and 625 µM DPI, or 188 µM cyprodinil and 1250 µM DPI. Colonies on control plates lacking DPI or cyprodinil were counted to ensure good genome coverage. Samples were also spread to plates from which either tryptophan, histidine, or uracil were omitted. Small numbers of colonies on these plates served as corroboration of good genome

coverage as some overexpression clones should complement these *S. cerevisiae* W303 auxotrophies.

2.2.15.2. Sequencing of resistant transformants

Plasmid minipreps were carried out for transformants that proved resistant to the cyprodinil-DPI combination. Each plasmid of the ATCC® 37323™ library contains a random insert at a BamHI restriction site. The same primers (Table 2.6) can therefore be used to amplify inserts by PCR. Amplified DNA was sent to Eurofins for sequencing.

Table 2.6. **Primers used for sequencing overexpressed genes in transformants of interest from the ATCC® 37323™ yeast overexpression library**.

Restriction Site	Forward Primer	Reverse Primer
BamHI	CTCGCTTCGCTACTTGGA	GTGATGTCGGCGATATAGG

2.2.16. Yeast heterozygous deletant library screen

Heterozygous deletion strains (in the *S. cerevisiae* BY4743 background (Winzeler *et al*., 1999)) stored in 96-well plates were thawed from -80°C. 80 µl of YEPD containing 200 µg ml^{-1} geneticin was added to each well of the thawed plates. Plates were covered with a gas-permeable plastic seal and incubated overnight at 30°C, 200 rev min^{-1}. Aliquots (5 µl) of each cell culture were then transferred to fresh 96-well plates via Freedom EVO platform (TECAN) multidrop robot to 95 µl of VMM containing desired inhibitor supplements and 200 µg ml^{-1} geneticin. Plates were homogenised by shaking for 30 seconds before being read at 595 nm on a Tecan plate reader. Plates were sealed again, placed in plastic lunch boxes containing soaked blue paper towel and incubated overnight at 30°C, 200 rev min^{-1}. OD_{600} of plates were read at 6 h and 24 h with a Sunrise (TECAN) multiwell plate reader, resuspended and homogenised by shaking before each absorbance reading.

2.2.17. Thiol-reactivity of DPI

0.5 mM of DPI (dissolved in DMSO) or solvent-match control was incubated at room temperature for 30 min in the presence or absence of 0.5 mM glutathione. Ellman's reagent was added to a final concentration of 0.5 mM. Absorbance was measured at 412 nm immediately before and immediately after the addition of Ellman's reagent using a fluorescence plate reader as the yellow-coloured product of the reaction between Ellman's reagent and sulfhydryl groups shows strong absorbance at 412 nm with a extinction coefficient of 3,600M^{-1} cm^{-1}.

2.2.18. *Z. tritici* gene deletions

2.2.18.1. Designing plasmids for *Agrobacterium*-mediated transformation of *Z. tritici*

The following genes of interest were targeted for deletion in *Z. tritici: pos5*, *sod2*, and *yap1*. Sequences of interest were identified from Ensembl, 2 kb of sequence before the start and 2 kb after the end of the sequence. The start site and end site of each gene was identified. 1 kb upstream of the start site and 1 kb downstream from the relevant stop codon were labelled as the "recombination flanks". *Z. tritici* gene deletion, mediated by *Agrobacterium tumefaciens*, will occur via homologous recombination at these 1 kb regions, to replace the region between the recombination flanks with a hygromycin resistance marker, leading to whole deletion of *pos5*, *sod2*, or *yap1* genes. For this, three pNOV2114 plasmids (Bowler *et al*., 2010) were synthesised by TWIST Bioscience (one for each gene to be deleted) with one recombination flank immediately upstream from the start of a *trpC* promoter and the other recombination flank immediately downstream of the end of the hygromycin resistance marker.

2.2.18.2. Transformation of *Agrobacterium tumefaciens*

Chemically competent *A. tumefaciens* EHA105 (prepared as in Xu and Li., 2008) from frozen stocks were thawed on ice until just becoming liquid. 1 µg plasmid DNA was added, with mixing by agitation. Samples were frozen in liquid nitrogen for 5 min and then incubated at 37°C for 5 min. 150 µl YEPD was added, and samples were incubated at 28°C for 2-4 h with gentle shaking. Cells were spread onto LB plates containing 100 µg ml^{-1} rifampicin and 100 µg ml^{-1} spectinomycin and incubated for 2 days at 28°C. Transformants were replated on LB agar containing 100 µg ml^{-1} rifampicin and 100 µg ml^{-1} spectinomycin and incubated for 2-3 days.

2.2.18.3. Colony PCR

Isolated colonies of transformed *Agrobacterium tumefaciens* were picked from LB agar and transferred to a microcentrifuge tube containing 20 µl 5x PCRBIO Rapid Extract Buffer A (1U $µl^{-1}$), 10 µl 10x PCRBIO Rapid Extract Buffer B and 70 µl PCR grade dH_2O. Samples were then incubated at 75°C for 5 min. During this period samples were briefly vortexed twice. Samples were then incubated at 90°C for 10 min to deactivate the protease. 900 µl dH_2O was added and the samples were centrifuged at high speed for 1 min. Supernatant was used directly for PCR to confirm transformation.

2.2.18.4. *Agrobacterium*-mediated transformation of *Z. tritici*

A sterile loop containing successfully transformed *A. tumifaciens* was used to inoculate 10 ml of LB medium containing 100 µg ml^{-1} rifampicin and 100 µg ml^{-1} in a 50 ml falcon tube or 50 ml Erlenmeyer flask. Culture was grown at 28°C for 24 h at 260 rev min^{-1} then diluted to OD_{600} 0.115 in induction medium containing 100 µg ml^{-1} spectinomycin, in a volume of 10 ml in a 50 ml sterile falcon tube or 50 ml Erlenmeyer flask. Cultures were grown at 28°C for 2-3 h at 260 rev min^{-1}. While cultures were growing, a single cellophane disc dipped in water was placed on the centre of each IM plate to be used.

When the *Agrobacterium* cultures reached OD_{600} of ~0.208, *Z. tritici* spores were harvested from 5-day old plates: 2 ml sterile dH_2O was added to *Z. tritici* plates and was spread thoroughly using a plastic spreader. Cell suspensions were then transferred to sterile microcentrifuge tubes. *Z. tritici* spore counts were determined using a haemocytometer and samples were diluted to 10^7 *Z. tritici* spores ml^{-1} in ddH_2O. Equal volumes of the *A. tumifaciens* culture and *Z. tritici* spores were mixed together. 150 µl aliquots of mixtures were plated onto the IM plates with the cellophane discs. These were spread with 4.5 mm sterile glass beads until no free liquid was visible and beads were removed. Plates were then incubated at 19°C for 48 h. After 2 days, the cellophane discs were transferred from IM plates to AMM plates using aseptic technique. Plates were then incubated at 19°C until colonies appeared. Colonies were used to inoculate 24-well PDA plates (2 ml agar per well) amended with 100 µg ml^{-1} streptomycin, 100 µg ml^{-1} ampicillin, 250 µM cefotaxime, and 200 µg ml^{-1} hygromycin, and incubated at 19°C for 7-14 days. Transformants were then verified using colony PCR (Appendix Figure 8.1, Appendix Table 8.3, Appendix Table 8.4, Appendix Table 8.5) to ensure constructs were integrated into the *Z. tritici* genome, replacing the native *pos5*, *sod2*, or *yap*1 genes.

2.2.19. Assay for mitochondrial reactive oxygen species in *Z. tritici*

CYP-DPI checkerboards were prepared in an 8x11 format (usually 8x8) with the final column of a black 96-well plate (see Materials) used as a DMSO standard. The medium used was MMZT containing 23 mM ammonium tartrate (replacing $NaNO_3$). *Z. tritici* strain used was fluorescently tagged for Sso1, a protein localised to the plasma membrane, by translational fusion with mCherry. Checkerboards were incubated for 30-40 min with a brief mix to homogenise. 1.16 µl of 0.5 mM DHR 123 was added. Plates were then imaged using an Opera Phenix Plus High-Content Screening System

(Perkin Elmer). Harmony software (Perkin Elmer) was used to identify *Z. tritici* spores via the mCherry fluorescent tag. Harmony software was used to identify DHR 123 fluorescence (green) within borders of cells and median cell fluorescence for each CYP-DPI treatment was calculated.

2.2.20. Assay of mitochondrial membrane depolarisation (MMD) in *S. cerevisiae*

Exponential phase *S. cerevisiae* W303 cells were treated with cyprodinil and diphenyleneiodonium in a checkerboard format, or with serial dilutions of amphotericin B. Preliminary experiments indicated concentrations of cyprodinil, DPI, or amphotericin B that gave low, mild, or high growth inhibition after 48 h. These concentrations were used for the assay with parallel replica incubations used to indicate the corresponding level of growth inhibition. For the MMD assays, cells were removed from wells after 2 h incubation at 30^{o}C (no shaking) and prepared for flow cytometry. Samples were centrifuged at 1,900 g for 3.5 min, then washed and resuspended in 250 µl PBS. Rhodamine 123 was added to each sample to a final concentration of 20 µg ml^{-1} and mixed by pipetting. Samples were incubated with rhodamine 123 in the dark at 30^{o}C for 30 min. Samples were washed once in PBS and resuspended in 500 µl PBS. Samples were then transferred to FACS tubes. Rhodamine 123 fluorescence was then measured using an ID7000 Spectral Flow Cytometer (blue filter; excitation at 488 nm, emission at 530 nm). Data was analysed in Kaluza.

2.2.21. Infection of wheat using *Z. tritici*

Seeds of *Triticum aestivum* (cultivar Skyfall) were planted in 15 cm pots with two seeds per pot. Plants were grown with a photoperiod of 16 h. Day temperature was 20^{o}C and night temperature was 15^{o}C. 14 days after initial watering of seeds, wheat plants were sprayed with solutions of cyprodinil, diphenyleneiodonium (DPI), neocuproine,

cyprodinil-DPI, or cyprodinil-neocuproine at concentrations as specified below. Compounds were dissolved in 0.04% TWEEN 20. 4 ml of desired solution was sprayed per pot (~2 ml per plant). Sprayed leaves were marked with black permanent marker and plants were left to dry overnight. The next day, half of the wheat plants were inoculated with $3x10^5$ spores ml^{-1} of ROY-UN *Z. tritici* suspended in 0.04% TWEEN 20: 4 ml of spore suspension was sprayed per pot (~2 ml per plant). The other half of wheat plants were sprayed with 0.04% TWEEN 20 that did not contain any *Z. tritici* spores. Plants were covered with plastic bags for 3 days to ensure a high humidity environment to aid infection. After 3 days, bags were removed, and plants were grown for 14 days until infection became apparent on leaves marked with the black pen. Leaves were then cut, and approximate percentages of leaf surface areas apparently infected with *Z. tritici*, causing significant discolouration, were estimated by eye.

Chapter 3 - Searching for novel fungicidal synergies using tavaborole, a leucyl-tRNA synthetase inhibitor

3.1. Introduction

Novel fungicide targets are urgently required to combat reliance on the limited treatments presently available. In the case of the phytopathogen *Zymoseptoria tritici*, current treatments mainly rely on demethylation inhibitors (DMIs) and succinate dehydrogenase inhibitors (SDHIs), as well as a few multisite inhibitors (Hellin *et al*., 2021). As stated in the general introduction (1.4.3), fungal protein synthesis could be a promising alternative target due to the large number of steps of this process and, hence, potential target sites. Some of these protein synthesis targets could include translation fidelity, amino acid transport, sulphate-transport, and amino acid biosynthesis (Vallières *et al*., 2018). Any protein involved in transcription, translation or post-translational modification has the potential to be a fungicidal target of protein synthesis (Kuplińska and Rząd, 2021). This includes proteins from the initiation of transcription, such as RNA polymerase, all the way to proteins involved in post-translational events such as protein folding, potentially comprising hundreds of protein targets (Alamgir *et al*., 2008).

3.1.1. Amino acid availability for protein synthesis

3.1.1.1. Amino acid biosynthesis

Targeting the supply of amino acids themselves can prove effective for growth inhibition (Dor *et al*., 2017). Decreased availability of amino acids for protein synthesis will disrupt metabolism and growth of cells. A range of activities can achieve such effects, including the biosynthesis of distinct families of amino acids. Respective examples of this include the immunosuppressant methotrexate, targeting methionine biosynthesis (Wang and Chiang, 2012), or the herbicide chlorimuron ethyl, targeting the biosynthesis of the branched chain amino acids isoleucine, leucine, and valine (Nemat Alla *et al*., 2008). Unfortunately, many amino acid biosynthesis inhibitors are

used as herbicides, and so are less likely to be applicable for use in crop protection. These include the herbicide families of imidazolinones, sulfonyureas (e.g., chlorimuron ethyl), sulfonylamino carbonytriazolinones, triazolopyrimidines, and amino acid-derivatives. However, it is possible to develop crops resistant to certain amino acid biosynthesis inhibitors, such as glyphosate (Dill, 2005), an inhibitor of the synthesis of three essential aromatic amino acids (phenylalanine, tyrosine, and tryptophan) through targeting the 5-enolpyruvylshikimate-3-phosphate (EPSP) synthase enzyme of the shikimate pathway (Green and Siehl, 2021). Indeed, some of these herbicides are naturally selective, with a preference for undesirable plants such as weeds, suggesting the possibility of amino acid biosynthesis as a selective target also for crop pathogens.

Many fungi, including the wheat pathogen *Zymoseptoria tritici*, are capable of synthesising all proteinogenic amino acids, including the nine essential to human diets as humans do not synthesise them, at least in sufficient quantity, (Jastrzębowska and Gabriel, 2015). In a medical setting, the inhibition of the biosynthesis of these nine amino acids would theoretically be the most appropriate targets for inhibition of human pathogens. However, as plants are capable of synthesising all 20 proteinogenic amino acids, amino acid biosynthesis inhibitors run more risk of causing toxicity to the host plant. While the biosynthetic pathways for amino acids are largely conserved between fungi and plants, there are some exceptions. This includes the α-aminoadipate pathway of L-lysine biosynthesis. This pathway is mostly fungus-specific (Jastrzębowska and Gabriel, 2015) but has been reported in bacteria from the genus *Thermus* (Kosuge and Hoshino, 1999), although bacteria usually utilise the diaminopimelate pathway (Vogel, 1965). In addition, the aspartate family, L-threonine, L-isoleucine, and L-methionine all derive from aspartate via pathways not present in mammals. Jastrzębowska and Gabriel (2015) review fungal amino acid biosynthesis pathways and provide evidence that there are many potential targets here to be

exploited. For example, the α-aminoadipate pathway alone consists of seven enzymes, each a potential target (Schöbel *et al*.,2010). The first three reactions are very specific to higher fungi, while the final four may be evolutionarily diverged enough from mammalian equivalents for specific inhibition (Bhattacharjee, 1985). Homoisocitrate dehydrogenase, catalysing the conversion of homoisocitric acid to α-ketoadipate, has had several compounds designed and synthesised specifically for its inhibition with some success (Yamamoto *et al*., 2007; Yamamoto and Eguchi, 2008).

3.1.1.2. Amino acid transport

In addition to amino acid biosynthesis, amino acid transport is a potential target. Pathogenic fungi are known to obtain large amounts of nutrients, including amino acids, from their hosts. By inhibiting the processes through which these organisms can take up amino acids, it is possible to decrease their growth (Struck, 2015; McCarthy and Walsh, 2018; Silao and Ljungdahl, 2022) – although this is unlikely to completely inhibit growth due to the amino acid prototrophy of many fungi. Nevertheless, in *Cryptococcus neoformans* it was shown that two amino acid permeases (membrane proteins involved in the transport of amino acids into the cell) were essential for the organism's virulence (Calvete *et al*., 2019). Furthermore, despite common amino acid transport pathways between pathogenic fungi and host (Wipf *et al*., 2002), as with the case for some inhibitors of aminoacyl-tRNA synthetases, it is possible that evolutionary divergence might be sufficient to allow for selective inhibition (McCarthy and Walsh, 2018).

3.1.2. Aminoacyl-transfer RNA synthetases as targets for inhibition

In organisms, protein synthesis is a highly conserved core biological process that is necessary for biological function and survival. Aminoacyl-transfer RNA synthetases (aaRSs) are enzymes that catalyse loading of the correct amino acids onto the

appropriate tRNAs, making them available for protein synthesis during translation. The reaction is described below:

$$aa + ATP + aaRs \rightleftharpoons aaRS - (aa - AMP) + PPi$$

$$(aaRS - aa - AMP) + tRNA \rightleftharpoons (aa - tRNA) + aaRS + AMP$$

Figure 3.1. **Aminoacylation reaction**. aa = amino acid; ATP = adenosine triphosphate; aaRS = aminoacyl-tRNA synthetase; AMP = adenosine monophosphate; PPi = inorganic pyrophosphate. '–' indicates molecules are chemically bound. The first step yields an aminoacyl-adenylate intermediate from the reaction between the amino acid and ATP. The amino acid moiety is then transferred to its cognate tRNA.

In eukaryotes, there are 20 different types of aaRS molecule, each corresponding to one amino acid of the standard genetic code. These are essential to protein synthesis and hence to the survival of any cell (Ochsner *et al*., 2007). The indispensable nature of these proteins makes each aaRS a potential drug target for inhibiting growth of non-desirable organisms. While the structures of these molecules are conserved in prokaryotes and eukaryotes (Vondenhoff *et al*., 2011), there has been enough divergence to allow for selective inhibitors (Ibba and Söll, 2000). Interestingly, it appears that almost all aaRS families have evolved independently with only LeuRS and TyrRS seeming to follow the division of kingdoms (Wolf *et al*., 1999; Woese *et al*., 2000).

Natural mechanisms for inhibition of aminoacyl-tRNA synthetases as defence/attack strategies already exist in some organisms. Mupirocin, an antibiotic originally isolated from *Pseudomonas fluorescens,* selectively inhibits isoleucyl-tRNA synthetase (Parenti *et al*., 1987). At one stage, mupirocin was the most widely used topical antibiotic for relieving patients of MRSA infections (Boyce, 2001). In addition to its success at inhibiting (Gram-positive) bacteria, mupirocin is structurally unrelated to other topical or systemic antibiotics, limiting the potential for the development of cross-resistance

(Drugbank, 2019). This compound is a good example of how effective targeting of protein synthesis (specifically tRNA synthetases) can be at inhibiting undesirable organisms. For these reasons, a list of known tRNA synthetase inhibitors was consulted in the present project and (initially) one was selected for use here due to strong inhibitory effects on fungi at low concentrations, in the nanograms per millilitre range (see 3.1.3).

3.1.3. Tavaborole

3.1.3.1. Background

Tavaborole, marketed as "Kerydin" (Sharma *et al*., 2015), is an antifungal drug used to treat onychomycosis (fungal infection of the nail bed). It is a relatively low molecular weight drug (151.93 g mol^{-1}, roughly half that of other onychomycosis drugs) which allows it to penetrate deep into the nail. Tavaborole targets the essential cytosolic leucyl tRNA synthetase that is a required enzyme for protein synthesis. The lack of leucine-charged leucyl-tRNAs (leu-$tRNA^{Leu}$) in the cell inhibits protein synthesis and thus impairs cell growth. Additionally, tavaborole is over 1000x more specific to fungal leucyl-tRNA synthetase than to human leucyl-tRNA synthetase, giving a large "margin of safety" (Jinna and Finch, 2015). Another reason why tavaborole is such an effective drug is thought to be because leucine makes up 11.79% of the amino acid composition in fungal membrane proteins, and 9.49% in fungal non-membrane proteins, the most abundant in both cases (Gaur, 2014). At the starting point of this PhD research, tavaborole was believed to be a strong candidate for a potential crop fungicide, and, due to its role in inhibition of protein synthesis, a component in a fungicidal synergy (Vallières *et al*., 2018).

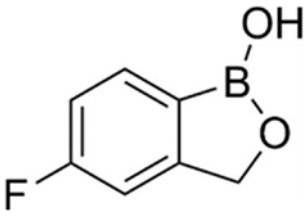

Figure 3.2. **Chemical structure of tavaborole**.

3.1.3.2. Mode of action

The mode of action of tavaborole (an oxaborole) hinges on its boron atom, which binds the leucyl-tRNA synthetase in its editing site, trapping the $tRNA^{Leu}$ molecule, so leaving it unable to be charged with leucine (Rock *et al*., 2007; Jinna and Finch, 2015).

Tavaborole inhibits the translation of mRNA, but it is not known whether the molecule causes mistranslation, i.e., inaccurate translation during protein synthesis resulting in amino acid sequences within proteins not reflecting those specified within the genetic code. It is also not known whether tavaborole also targets the mitochondrial leucyl-tRNA synthetase. However, Rock *et al.* (2007) found that *S. cerevisiae* mutants resistant to tavaborole had all acquired a mutation in the editing site domain of the *CDC60* gene. *CDC60* encodes cytoplasmic leucyl-tRNA synthetase, suggesting that this is the primary target. While the mt-LeuRS gene, *NAM2*, is encoded by the nuclear genome, the aminoacylation of mitochondrial tRNA molecules occurs in the mitochondria (Tyynismaa, 2012; Watanabe, 2010). Therefore, tavaborole would need to access the mitochondria to trap the mitochondrial $tRNA^{Leu}$ molecules. If tavaborole were capable of inhibiting mitochondrial LeuRS, it may work well in combination with a drug that increases the permeability of the mitochondrial membrane, for example, depending on how easily tavaborole may already access the organelle.

At the outset of the work described in this chapter, it was hypothesised that tavaborole could result in mistranslation of proteins. While a lack of one amino acid can lead to the (mis)incorporation of another (Wong *et al*., 2018), it is not known if a

lack of functioning leucyl-tRNA synthetase will lead to the increased use of another aaRS, causing mistranslation, or if translation is simply halted due to a lack of the required correctly-charged tRNA caused by this inhibition. Knowing tavaborole's full mode of action and the consequences it has on the organism gives a greater chance of trying to predict synergies with this already effective drug.

3.1.3.3. Synergistic potential of tavaborole

As a relatively potent inhibitor of translation, tavaborole has potential for drug synergies with other inhibitors of protein synthesis (Vallières *et al*., 2018), although there are resistance concerns due to the (presumed) single target mechanism.

Common mechanisms of drug synergies include one drug enhancing the uptake of another (Jawetz and Gunnison, 1953; Plotz and Davis, 1962), one drug protecting the other from cell defence mechanisms (Ball., 2007), drugs having a physical interaction (with each other or their target, for example) that leads to gain of activity (Bollenbach, 2015) or agents acting at two molecular targets of a common process or function (Vallières *et al*., 2018). If resistance were to develop against tavaborole in which it was degraded or inhibited, a synergy similar to that of amoxicillin and clavulanic acid could be a potential outcome (Brown, 1986; Drawz *et al.*, 2010). As an inhibitor of an essential protein, tavaborole has potential for syncretic and congruous synergies (1.4.1). If tavaborole does induce mistranslation, then there could be a higher chance of a synergistic effect with other compounds that impair translation fidelity by other mechanisms (Vallières *et al*., 2018).

3.1.4. Dual reporters for mistranslation

Dual reporters have become a valuable tool for assaying mistranslation events in cells. The system involves two different reporter genes, such as the firefly and *Renilla reniformis* (sea pansy) luciferases. Luciferase enzymes are a class of oxidative enzymes

that produce bioluminescence. Bioluminescence is thought to have evolved independently at least 40 times in the tree of life (Davis *et al*., 2016) and is an extremely efficient process with 85-90% of input energy turned into light. The firefly and *Renilla* luciferase reactions are depicted below (Matthews *et al*., 1977; Baldwin, 1996; Fraga *et al*., 2006).

$$LH_2 + ATP - Mg^{2+} \rightleftharpoons LH_2 - AMP + PPi - Mg^{2+}$$

$$LH_2AMP + O_2 \rightarrow \ oxyluciferin + AMP + CO_2$$

$$oxyluciferin^* \rightarrow oxyluciferin + light$$

Figure 3.3. **Reactions catalysed by firefly luciferase**. LH_2 = luciferin; ATP = adenosine triphosphate; AMP = adenosine monophosphate; PPi = inorganic pyrophosphate; LH_2-AMP = luciferyl adenylate. '– ' indicates molecules are chemically bound.

$$coelenterazine + \ O_2 \rightarrow coelenteramide + \ CO_2 + light$$

Figure 3.4. **Reaction catalysed by *Renilla reniformis* luciferase**. Coelenterazine is the *Renilla* luciferin.

As with dual-luciferase reporters, reporters utilising dual-fluorescence have also been developed, and both types of system have been optimised for yeast (McNabb *et al*., 2005; Altamura *et al*., 2016). Unlike bioluminescence, biofluorescent proteins do not produce their own light, but absorb light of one wavelength and emit another (Lamb and Davis, 2020). Both systems can be effective tools for measuring mistranslation such as stop codon readthrough, where a stop codon separates the two reporter genes (Loughran *et al*., 2014; Altamura *et al*., 2016), or misincorporation, in which an amino acid essential for fluorescence or bioluminescence has been changed so that the protein is non-functional in terms of light emission, unless the wild-type sequence is restored by misincorporation (McNabb *et al*., 2005; Gomes *et al*., 2016).

3.1.5. Chapter aims

The research set out to test whether tavaborole promotes mistranslation. If so, this would raise the likelihood of tavaborole having synergistic effects on cell growth if combined with other mistranslation-inducing compounds (Moreno-Martinez *et al.*, 2015; Vallières *et al.*, 2018). The third aim was to investigate the potential for fungicidal or fungistatic synergies involving tavaborole (and/or other aaRS inhibitors) and the mechanistic bases for any identified synergies.

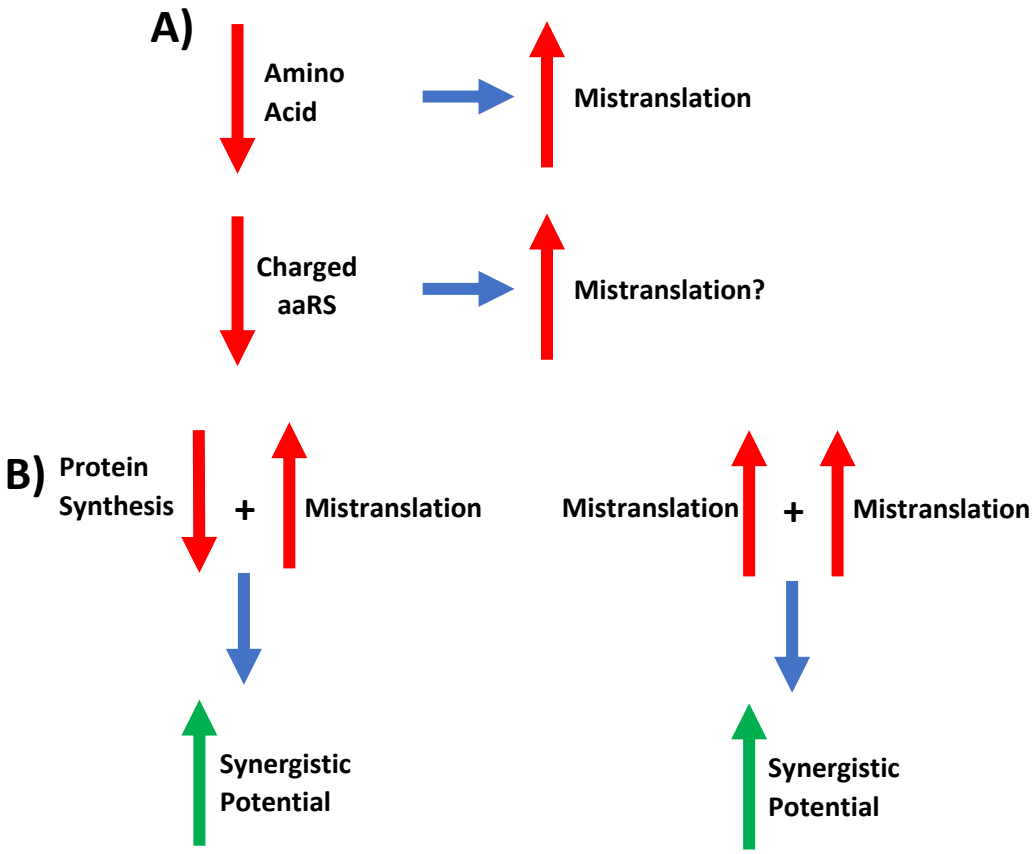

Figure 3.5. **Schematic of potential of tavaborole for synergistic interactions**. A) decreases in amino acid levels are known to lead to increases in mistranslation rates (Wong *et al.*, 2018) but decreases in charged aaRS molecules are not known to have the same effect. B) Tavaborole is a known inhibitor of protein synthesis, but it is not known if tavaborole is an inducer of mistranslation. The same question applies to other aaRS inhibitors. Tavaborole is predicted to have synergistic potential with inducers of mistranslation based on its known and hypothesised modes of action.

3.2. Results

3.2.1. Tavaborole-induced mistranslation

3.2.1.1. Determining MIC and SIC for tavaborole

First, to determine appropriate working concentrations for yeast, various concentrations of tavaborole were tested for their inhibitory effects on the organism. In YEPD medium, the sub-inhibitory concentration (SIC) of tavaborole was ≥219 nM (33 ng ml^{-1}), while the MIC was >1.75 µM (532 ng ml^{-1}) (Figure 3.6).

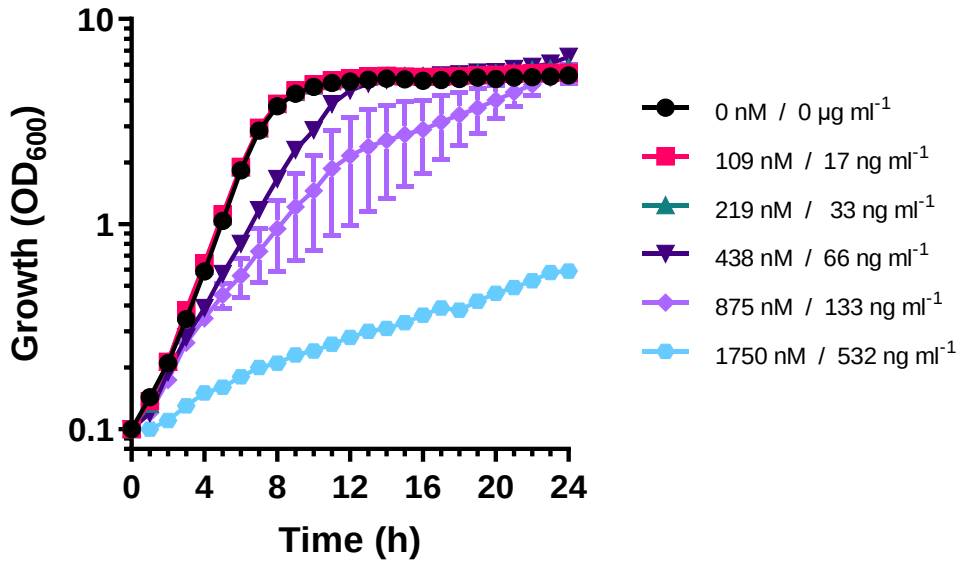

Figure 3.6. **Determining tavaborole SIC and MIC in *S. cerevisiae***. Data shows growth curves of *S. cerevisiae* BY4743 during incubation with varying concentrations of tavaborole. 1 µl of tavaborole stock concentrations were added to 299 µl of OD_{600} 0.1 exponential phase culture in YEPD medium. Plates were incubated shaking in an Epoch 2 plate reader at 30°C for 24 hours. Key represents tavaborole concentration. Bars represent standard deviation. n = 3.

3.2.1.2. Utilising dual-reporter systems to test for tavaborole-induced mistranslation

To test the hypothesis that tavaborole may promote mistranslation, two separate dual-luciferase (DL) constructs, DL^{TAAT} and DL^{868}, were utilised. DL^{TAAT} tested for stop codon readthrough, while DL^{868} tested for the mistranslation of an arginine to a histidine at residue 868 (Figure 3.7). Although tavaborole is known to specifically

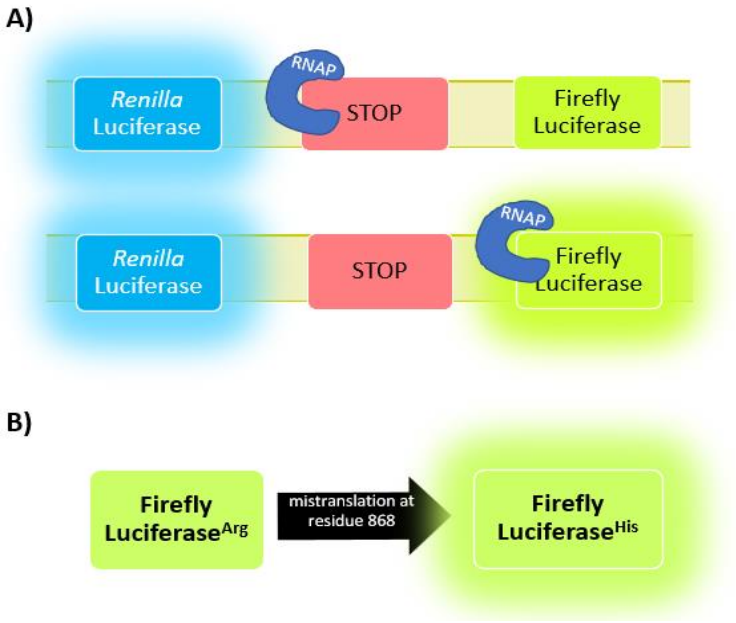

Figure 3.7. **Schematic illustrating the dual-luciferase reporters**. A) DL^{TAAT}. Stop codon readthrough causes RNA polymerase to transcribe the firefly luciferase gene. B) DL^{868}. Misincorporation of the arginine residue at position 868 with a histidine, essential for firefly luciferase bioluminescence. *Renilla* luciferase is still present in this dual-luciferase construct.

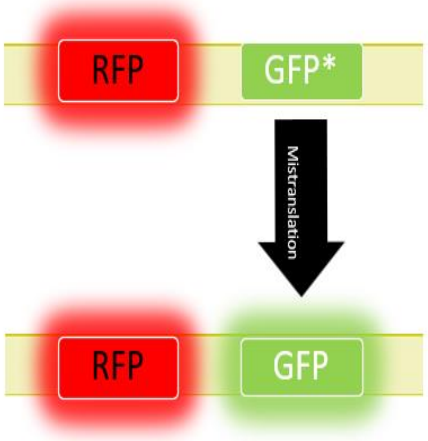

Figure 3.8. **Schematic illustrating the dual-fluorescence reporters.** GFP has been edited at residue 65, part of the fluorophore, to leucine codon TTG so that the protein does not fluoresce. Mistranslation can cause misincorporation of an amino acid residue essential to fluorescence, (threonine or serine) restoring fluorescence.

inhibit the leucyl-tNRA synthetase (LeuRS), i.e., not one of the residues relevant to the mistranslation constructs, there is the possibility of tavaborole causing more general mistranslation. It was hypothesised that as inhibition of LeuRS creates an effect similar to inhibition of leucine biosynthesis (i.e., lack of charged $tRNA^{Leu}$), and as amino acid

starvation is known to induce mistranslation (Wong *et al*., 2018), that tavaborole may therefore lead to increased mistranslation.

Appendix Figure 8.2 shows that tavaborole does not cause significant mistranslation of the dual-luciferase constructs, especially when compared to the positive control paromomycin (PM), a known inducer of broad mistranslation (Davis, 1987).

Next, dual-fluorescence constructs, potentially more tailored to the mode of tavaborole action, were employed. These reporter plasmids contained an unaltered gene for red fluorescent protein (RFP) followed by a modified gene for green fluorescent protein (GFP), as illustrated in Figure 3.8. In the modified version, an ACG codon for a threonine residue (Thr65, construct referred to as 'GFP^{Thr}'), optimal for fluorescence in bacteria, (Cormack *et al*., 1996) has been altered to either the TCG codon for serine (also fluorescent, construct referred to as 'GFP^{Ser}') or to the TTG codon for leucine (non-fluorescent, construct referred to as 'GFP^{Leu}'). The rationale was that a tavaborole-induced lack of available $tRNA^{Leu}$ molecules charged with leucine (leu-$tRNA^{Leu}$), may result in enhanced misincorporation of near-cognate amino acids in GFP^{Leu}, including serine (ser-$tRNA^{Leu}$), which would be detectable as restored fluorescence.

Initial experiments showed that the GFP^{Leu} reporter was not functioning as it should: the unaltered RFP was not consistently fluorescing under control conditions. GFP and RFP fluorescence of GFP^{Ser} and GFP^{Thr} yeast cells under a fluorescence microscope showed relatively strong fluorescence (Figure 3.9A). Cells transformed to express GFP^{Leu} had variable and comparatively weak RFP fluorescence. GFP^{Leu} cells showing GFP fluorescence were not seen (Figure 3.9B). This problem with a lack of the expected cellular fluorescence persisted in every GFP^{Leu} transformant tested (data not shown).

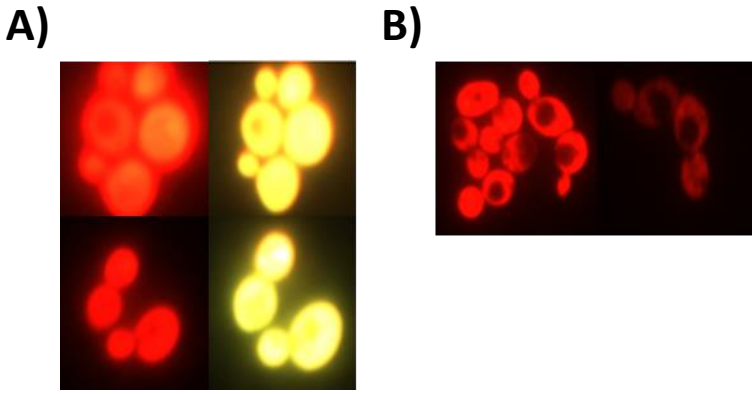

Figure 3.9. **Dual-fluorescent reporters under fluorescence microscope**. Untreated yeast transformed with different dual-fluorescence reporter constructs. A) Clockwise from top-left: RFP fluorescence from GFP^{Thr}; GFP fluorescence from GFP^{Thr}; RFP fluorescence from GFP^{Ser}; GFP fluorescence from GFP^{Ser}. B) Variable RFP fluorescence in cells expressing GFP^{Leu} cells. Cells shown are representative of whole populations. GFP fluorescence from GFP^{Leu} cells not shown.

3.2.1.3. Utilising flow cytometry to test for tavaborole-induced mistranslation

Flow cytometry was carried out to add quantitative support to the microscopical observations. Furthermore, tavaborole-induced mistranslation, if it occurs, is perhaps a relatively rare event. Therefore, an increase in GFP fluorescence due to mistranslation may be eclipsed when looking at an entire population and taking average readings of tens of thousands of cells. By utilising flow cytometry, it was possible to check for mistranslation at a single cell resolution.

Without treatments, flow cytometry data-distributions for cells expressing GFP^{Ser}, GFP^{Thr} or GFP^{Leu} were reproducible (while distinct between the strains). When compared to cell autofluorecence (Figure 3.10), the GFP^{Thr} and GFP^{Ser} reporters were functioning as intended, with most cells showing both GFP and RFP fluorescence (Figure 3.11). There were higher numbers of GFP-positive cells in the GFP^{Thr} strain with 99.5% of total cells showing GFP fluorescence, compared to 87.9% of total cells GFP^{Ser} cells. This is consistent with the knowledge that threonine is the optimal amino acid at

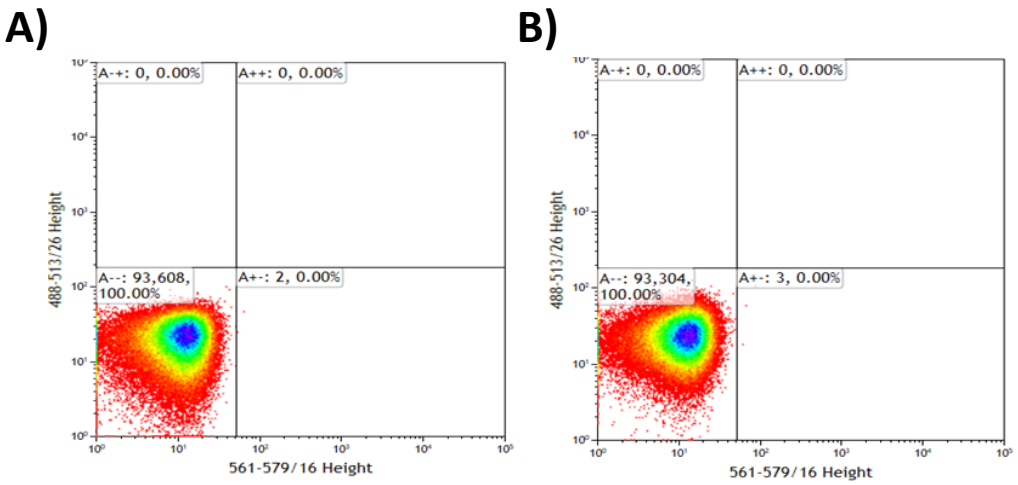

Figure 3.10. **S. cerevisiae autofluorescence.** Exponential phase S. cerevisiae cells without fluorescent reporters were treated overnight in YNB medium with A) DMSO (control); B) 25ng/ml tavaborole. Both conditions had 75% (572 µM) of the leucine that is normally added to YNB medium (762.5 µM) and were supplemented with 475 µM serine. Gates for fluorescence were previously determined with cells without fluorescence reporters grown in YNB with 762 µM leucine and no additional serine. GFP fluorescence is shown on the y-axis and RFP fluorescence is shown on the x-axis. Numbers show total cells in each gate and their percentage as part of the whole population. Each dot represents one cell. All flow cytometry data were analysed with Kaluza software.

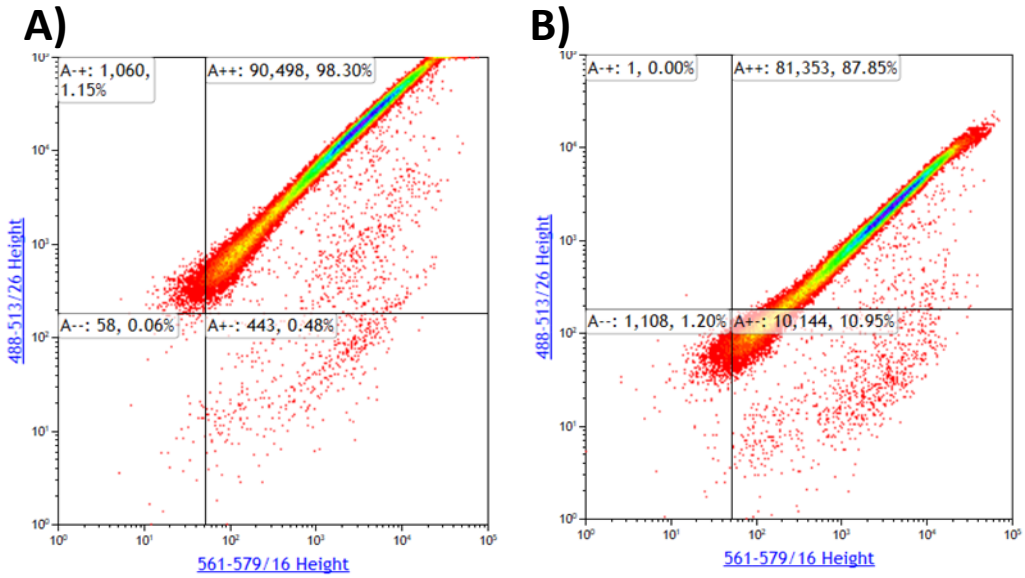

Figure 3.11. **Fluorescence distributions of cells expressing GFP^{Thr} or GFP^{Ser}.** Exponential phase cells transformed to express A) GFP^{Thr} or B) GFP^{Ser} were incubated overnight in YNB medium including DMSO. There was no leucine starvation, serine supplementation, or treatment with tavaborole. GFP fluorescence is shown on the y-axis and RFP fluorescence is shown on the x-axis. Numbers show total cells in each gate and their percentage as part of the whole population. Each dot represents one cell. Bottom-left quadrant shows non-fluorescent cells; top-left quadrant shows GFP-expressing cells; bottom-right quadrant shows RFP-expressing cells; top-right quadrant shows cells expressing both GFP and RFP.

position 65 for GFP fluorescence (Cormack *et al.*, 1996). Figure 3.12 and Figure 3.13 show the GFP^{Leu} expressing cells to comprise two distinct subpopulations, varying in

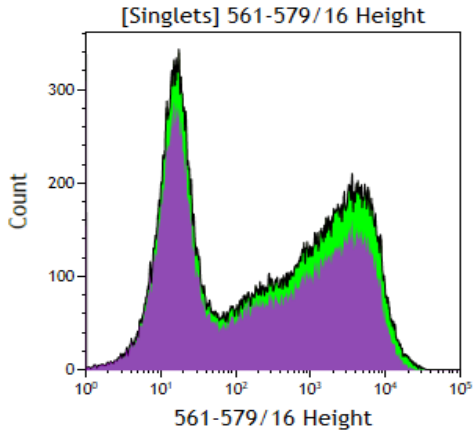

Figure 3.12. **RFP variation in GFP^{Leu}.** RFP fluorescence intensity of untreated exponential-phase GFP^{Leu} cells after 16 h of growth. RFP fluorescence is on the x-axis, number of cells is on the y-axis.

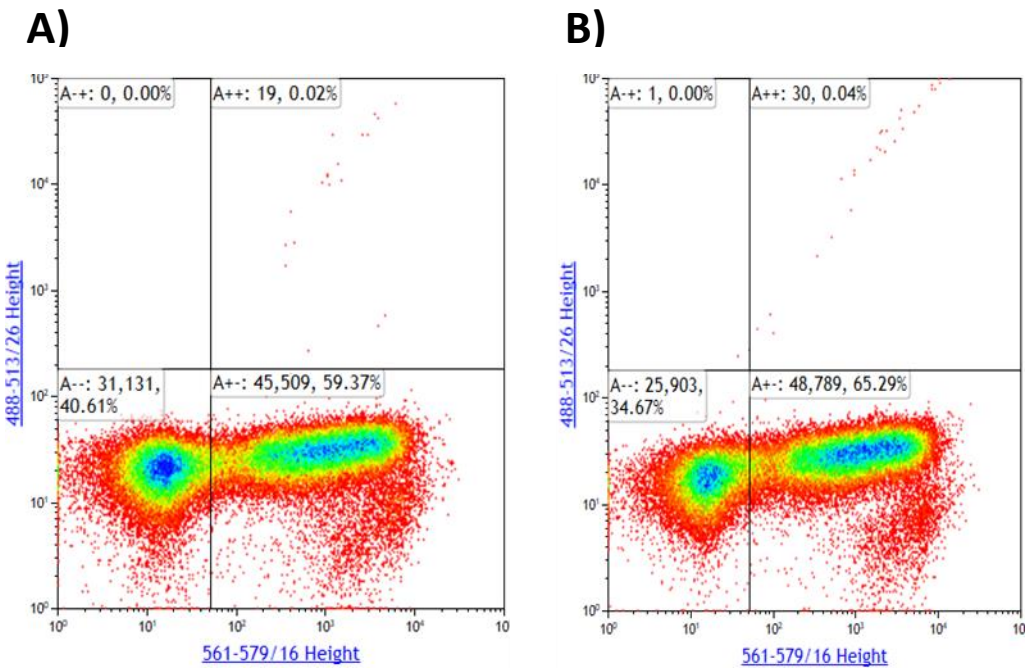

Figure 3.13. **GFP^{Leu} fluorescence heat maps with and without leucine limitation**. Exponential phase GFP^{Leu} cells were incubated overnight in YNB media at 30°C with different levels of leucine: A) 762.5 µM (100%); B) 572 µM (75%). There was no treatment with tavaborole or serine supplementation. GFP fluorescence is shown on the y-axis and RFP fluorescence is shown on the x-axis. Numbers show total cells in each gate and their percentage as part of the whole population. Each dot represents one cell. Bottom-left quadrant shows non-fluorescent cells (GFP$^-$RFP$^-$); *t*op-left quadrant shows GFP$^+$RFP$^-$ cells; bottom-right quadrant shows GFP$^-$RFP$^+$ cells; *t*op-right quadrant shows GFP$^+$RFP$^+$ cells.

their levels of RFP fluorescence. This corroborated that the GFP^{Leu} construct was not working as anticipated. RFP fluorescence in GFP^{Leu}-expressing cells should have been unaffected by the GFP point mutation unless incorrect folding was a consequence. Within the populations expressing GFP^{Thr} and GFP^{Ser}, approximately 99% had RFP

fluorescence (Figure 3.11). In the GFP^{Leu}-expressing cells, this percentage was only 59.4% (Figure 3.13A). Decreasing the leucine availability of GFP^{Leu} cells by supplementing with leucine at only 75% of its normal concentration (no tavaborole treatment) increases the number of cells that were positive for both RFP and GFP fluorescence, albeit only from 19 to 30 cells out of total populations of between 74,000-76,000 cells (Figure 3.13). While this increase was minimal as a proportion of the total, the proportion of GFP^{Leu}-expressing cells positive for RFP fluorescence increased from 59.4% to 65.3% when comparing cultures with leucine at 100% or 75% the normal availability (Figure 3.13). These initial flow cytometry experiments, not involving tavaborole, show that the GFP^{Leu} reporter is not working as intended. This is because the unaltered RFP protein should be as fluorescent as it is in the GFP^{Thr} and GFP^{Ser} strains. Limiting leucine, potentially mimicking low-level tavaborole inhibition, did not cause mistranslation.

When treated with tavaborole, there was only a very small increase in the number of GFP-positive GFP^{Leu}-transformed cells (Figure 3.15): from 14 RFP/GFP-positive cells in the control (0 ng ml^{-1} tavaborole) to 28 and 20 such cells with 12.5 ng ml^{-1} and 25 ng ml^{-1} tavaborole, respectively, out of a total gated population >77,000 cells. It was noted that the few cells that were both RFP- and GFP-positive in Figure 3.13 and Figure 3.15 showed similar distribution as the GFP^{Thr} and GFP^{Ser} strains, i.e., with RFP fluorescence and GFP fluorescence showing a linear, positive correlation in these cells.

Finally, combinations of tavaborole treatment and/or leucine and serine supplementation (to increase chances of serine misincorporation at Leu codons) were tested to see if conditions expected to be more conducive to GFP^{Leu} mistranslation may provoke measurably increased numbers of RFP-/GFP-positive cells in the GFP^{Leu}-transformed cell population (Figure 3.14). However, there was no evidence of

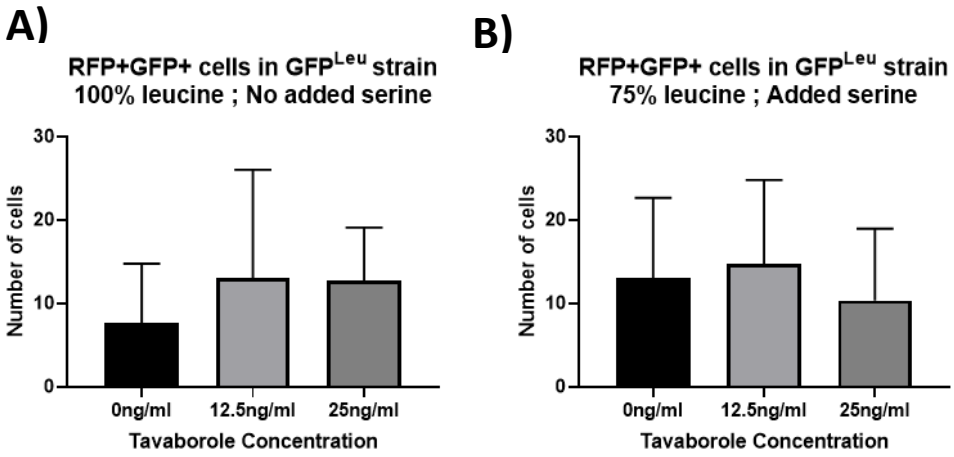

Figure 3.14. **Number of RFP-/GFP-positive GFP^{Leu}-expressing cells with or without leucine starvation, serine and/or tavaborole**. Exponential phase GFP^{Leu}-expressing cells were incubated overnight at 30°C with different concentrations of tavaborole as indicated: A) 762.5 µM leucine (100%), no additional serine; B) 572 µM (75%), 475 µM serine. Data shows the number of cells positive for both RFP and GFP fluorescence in each treatment. Bars represent standard deviation. n = 3. Ordinary one-way ANOVA multiple comparisons show no statistical significance between any conditions.

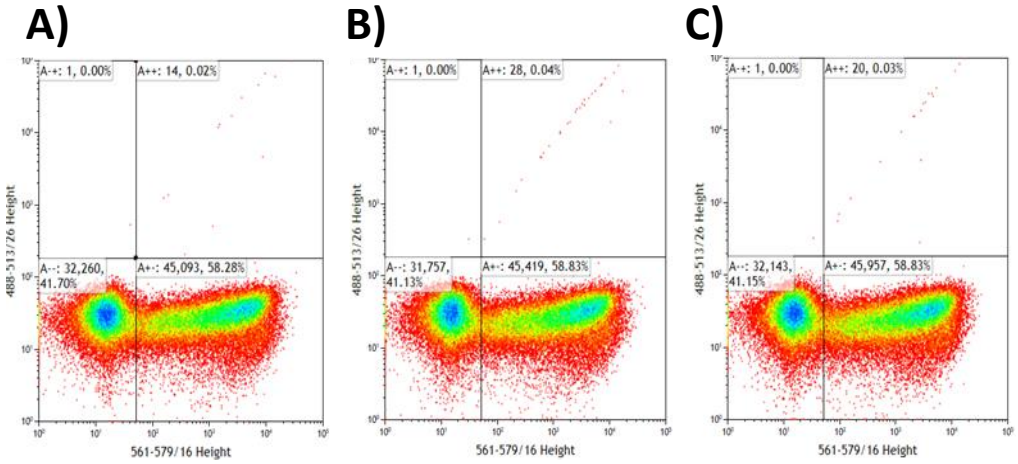

Figure 3.15. **Effect of tavaborole on the fluorescence of GFP^{Leu}-expressing cell populations**. Exponential phase GFP^{Leu}-expressing S. cerevisiae was incubated overnight at 30°C with different concentrations of tavaborole: A) 0 ng ml -1; B) 12.5 ng ml-1; C) 25 ng ml-1. There is no leucine starvation or serine supplementation. GFP fluorescence is shown on the y-axis and RFP fluorescence is shown on the x-axis. Numbers show total cells in each gate and their percentage as part of the whole population. Each dot represents one cell. Bottom-left quadrant shows non-fluorescent cells; top-left quadrant shows GFP(only)-expressing cells; bottom-right quadrant shows RFP(only)-expressing cells; top-right quadrant shows cells expressing both GFP and RFP.

mistranslation that significantly differed between the various treatments either with or without tavaborole.

It remained unclear why the RFP fluorescence appeared hindered in the GFP^{Leu} construct under control conditions when compared to the GFP^{Thr} and GFP^{Ser}

constructs, with a substantial cell-subpopulation showing no RFP fluorescence in the former case (Figure 3.12). The RFP and GFP proteins are synthesised as a single polypeptide without a stop codon in between. If, somehow, the leucine residue at position 65 on GFP caused an issue for RFP fluorescence (e.g., from errors in GFP folding), it would be expected that mistranslation causing serine misincorporation would not only restore GFP fluorescence, but also RFP fluorescence. However, this was not the case. Only RFP fluorescence was increased by leucine starvation (marginally and for unknown reasons), but GFP fluorescence was not (Figure 3.13). Again, this could be due to the leucine residue potentially both removing fluorescence and interfering with the overall structure of the GFP. This could negatively influence the attached RFP protein leading to the lack of RFP fluorescence seen. However, this effect seemingly differs between individual cells, as a large proportion of GFP^{Leu} cells had relatively normal RFP fluorescence when compared to the GFP^{Thr} and GFP^{Ser} strains.

3.2.1.4. Mistranslation-prone mutants may help detection of tavaborole-induced mistranslation

With the GFP^{Leu} dual-fluorescence reporter not functioning as intended, it was decided to use a different approach for assessing potential mistranslation defects. One reason that mistranslation was undetected in previous experiments could have been that the mistranslation rate was too low. Therefore, an alternative approach using mistranslation-prone mutants was planned. This involved the use of *S. cerevisiae* strains L1494, L1583, and L1597. Strain L1583 has decreased translational accuracy, L1597 has increased translational accuracy, and L1494 has 'normal' translational accuracy (in relation to these strains) (Holland *et al*., 2007).

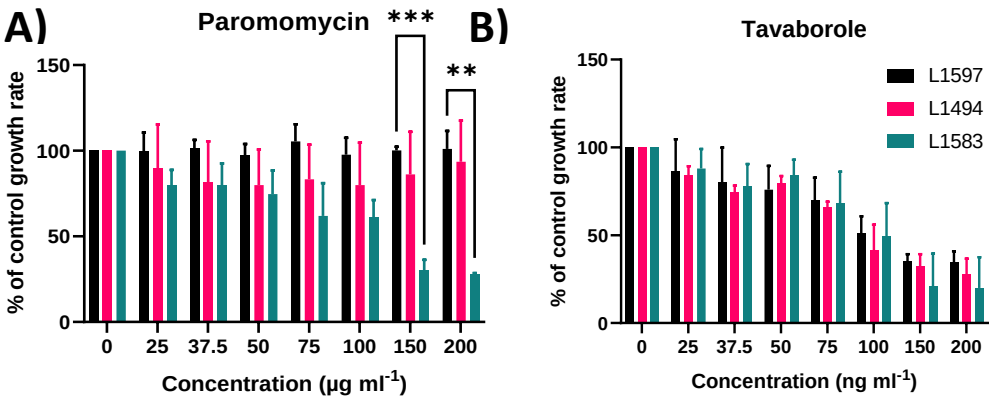

Figure 3.16. **Growth rate of translational fidelity mutants when treated with paromomycin or tavaborole.** S. cerevisiae strains L1494 (wild-type), L1597 (high fidelity), and L1583 (low fidelity) were grown in the presence of different concentrations of either paromomycin or tavaborole (with H_2O and DMSO solvent controls respectively), for 24 hours with readings every 30 min. Growth rate was calculated using doubling time during exponential phase (see Materials and Methods). This was compared to growth rate of the control treatment for each strain. n = 3 biological replicates; ** = p<0.01; *** = p<0.001. P-values calculated from multiple unpaired t-tests.

First, the growth rates of these strains were compared in the absence or presence of the known inducer of mistranslation, paromomycin, as a control to establish the anticipated phenotypes (Figure 3.16). Treatment with paromomycin significantly decreased the growth of strain L1583 compared to the L1597 strain at concentrations of 150 µg ml^{-1} and 200 µg ml^{-1} (Figure 3.16A). This shows the suspected phenotype: the strain with decreased translational fidelity having decreased growth when treated by a compound known to cause mistranslation. The high translation fidelity strain (L1597) showed improved growth versus wild-type at some paromomycin doses, but a statistically significant effect was not discernible over the range of concentrations tested, which only mildly affected the control strain. In contrast to paromomycin, tavaborole inhibited growth of all strains at similar rates, with no significant differences between the strains at any concentration (Figure 3.16B). This result corroborated that tavaborole did not cause notable mistranslation, at least not at any level with significant effect in the assays used to this point.

3.2.1.5. Qualitatively measuring mistranslation with stop codon readthrough mutants

Although used as a control strain in the preceding experiments, the L1494 strain itself carries a particular mutation of usefulness here: an *ade1-14* UGA codon which renders the strain auxotrophic for adenine (Holland *et al*., 2007). If nonsense-mistranslation occurs at this premature stop codon, readthrough allows the strain to recover production of adenine and survive on adenine-limited medium. The *S. cerevisiae* laboratory strain, W303, carries a similar mutation: *ade2-1* UAA (Kokina *et al*., 2014). Additionally, the build-up of an adenine precursor causes the colonies of L1494 and W303 strains to have a pink/red colouration (Ugolini and Bruschi, 1996). Therefore, mistranslation events causing readthrough of the stop codons reverts colonies to a white colour. These methods provide qualitative indications of mistranslation, an alternative to the quantitative measurements assayed above.

It was originally hypothesised that tavaborole would cause mistranslation, specifically the misincorporation of non-leucyl amino acids at leucine-designated residues. It was not originally hypothesised that tavaborole would specifically cause stop codon readthrough, but there is precedent for similar carry-over to other mistranslation events, which could arise from downstream imbalances in the translation machinery: for example, chromate is considered to promote mistranslation by limiting availability specifically of sulphur containing amino acids, but also produces substantial stop codon readthrough (Holland *et al*., 2007; Holland *et al*., 2010). As the strains were readily available, it was decided to test this possibility for tavaborole. Interestingly, when grown on agar plates with varying concentrations of tavaborole, a colour change from red to white was visible, indicative of stop codon readthrough (Figure 3.17B).

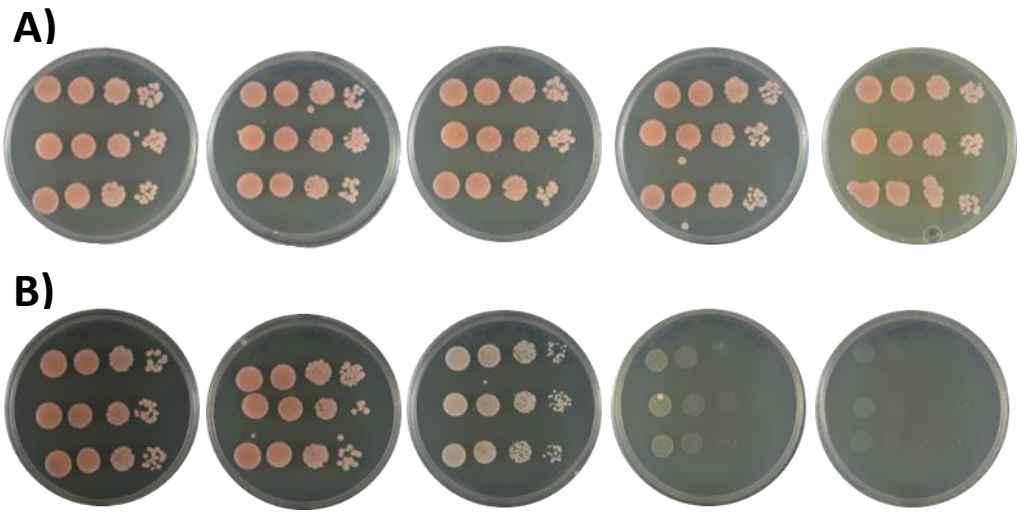

Figure 3.17. **Growth of *S. cerevisiae* W303 on drug-containing agar**. W303 yeast were plated onto YEPD agar containing varying concentrations of A) Paromomycin or B) Tavaborole. Growth is after three days. Each row on a single plate is one technical triplicate, with each colony decreasing in inoculum concentration from left to right (OD600 1, 0.1, 0.01. 0.001; 5 µl added for each spot). A) concentrations from left to right: 0 µg ml^{-1}, 25 µg ml^{-1}, 100 µg ml^{-1}, 200 µg ml^{-1}, 800 ml^{-1}. B) concentrations from left to right: 0 ng ml^{-1}, 12.5 ng ml^{-1}, 75 ng ml^{-1}, 200 ng ml^{-1}, 400 ng ml^{-1}.

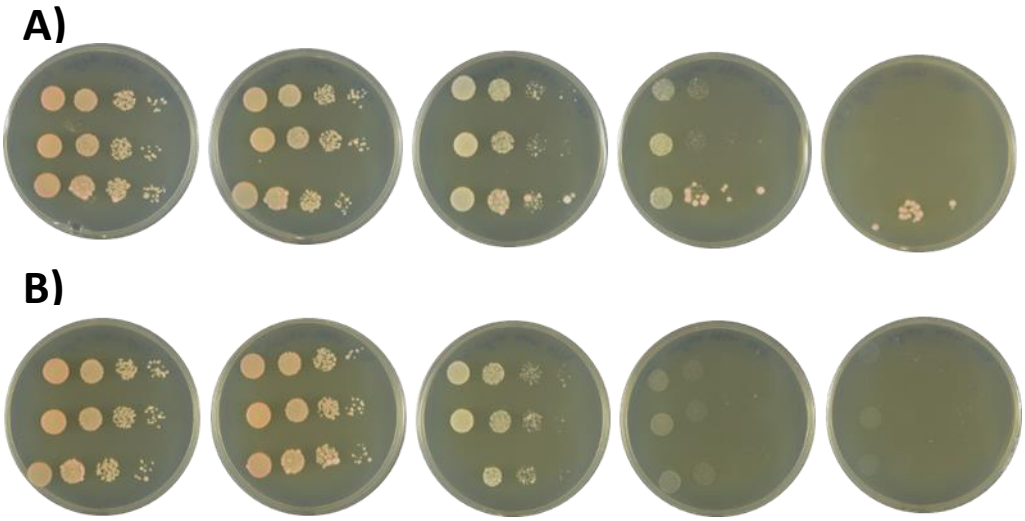

Figure 3.18. **Growth of *S. cerevisiae* L1494 on drug-containing agar.** L1494 yeast were plated onto YEPD agar containing varying concentrations of A) Paromomycin or B) Tavaborole. Growth is after three days. Each row on a plate is one technical triplicate, with each colony decreasing in inoculum concentration from left to right (OD_{600} 1, OD_{600} 0.1, OD_{600} 0.01. OD_{600} 0.001; 5 µl added for each spot). A) concentrations from left to right: 0 µg ml^{-1}, 25 µg ml^{-1}, 100 µg ml^{-1}, 200 µg ml^{-1}, 800 ml^{-1}. B) concentrations from left to right: 0 ng ml^{-1}, 12.5 ng ml^{-1}, 75 ng ml^{-1}, 200 ng ml^{-1}, 400 ng ml^{-1}.

As can be seen in the W303 strain (Figure 3.17A), even at very high concentrations of paromomycin, cells remain uninhibited compared to other concentrations (later experiments show survival at 15 mg ml^{-1}). For this reason, paromomycin was not an

effective positive control for stop codon readthrough experiments in the W303 strain. Nevertheless, at increasing concentrations of tavaborole, colonies increasingly appeared white, suggesting that stop codon readthrough was occurring. For the L1494 strain, both tavaborole and paromomycin showed white colonies at higher concentrations (Figure 3.18). Again, this was originally unexpected for tavaborole as the compound gave no indication of stop codon readthrough with the dual-luciferase experiments.

It was considered that effects other than mistranslation could potentially be causing the white colony phenotype. One known reason is damage to the mitochondria (Pittman *et al*., 1959; Rich *et al*., 2001). To test for this possibly, a triphenyl tetrazolium chloride (TTC) overlay assay was adopted in order to detect respiratory defects that would be indicative of mitochondrial damage. Applying an overlay of agar containing the colourless electron acceptor TTC to colonies comprising cells capable of respiration will enzymatically reduce the compound, restoring a red colour as a stable red formazan precipitate is formed. (Ogur *et al*., 1957; Rich *et al*., 2001; Kim *et al*., 2002). With this assay, the colonies turned a red colour after application of TTC (Figure 3.19), indicating that the original colour change to white was not due to mitochondrial damage.

Another potential reason for colonies turning white in more inhibitory conditions is due to less competition for adenine in the medium, meaning less pressure on cells to (attempt to) synthesise adenine themselves and, consequently, decreased build-up of the pigmented precursor. To attempt to rule this out, strains were cultivated with tavaborole on YNB agar containing no adenine (Figure 3.20). For *S. cerevisiae* W303, no colonies were obtained on YNB agar without adenine for any of the tavaborole or paromomycin conditions (data not shown). Although paromomycin is known to induce

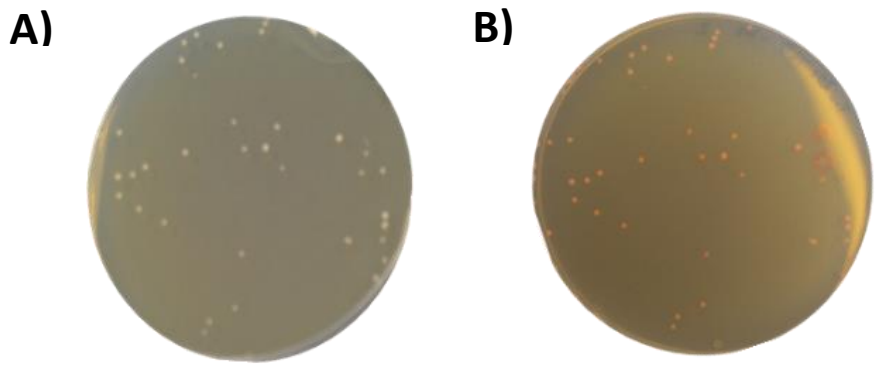

Figure 3.19. **TTC overlay assay for respiratory competence of colonies cultivated with tavaborole**. Pictures shows the same plate of *S. cerevisiae* W303 yeast colonies grown on YEPD agar containing 200 ng ml^{-1} tavaborole for three days, A) before and B) after a TTC overlay. Colonies were cultivated by spread plating 100 µl of OD_{600} 0.001 culture and incubation for 3 d before overlaying with 20 ml of TTC agar (see Materials) and incubation at 30°C for a further 24 h.

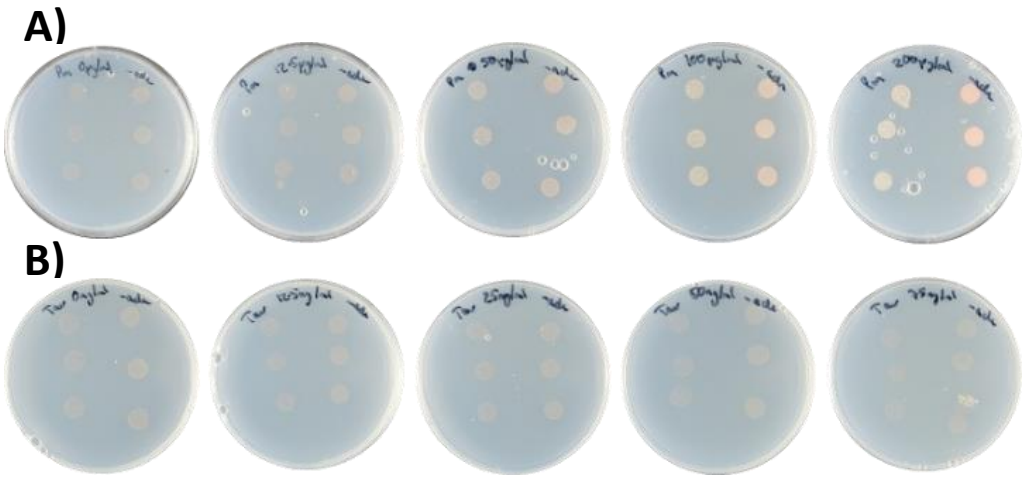

Figure 3.20. **Growth of *S. cerevisiae* L1494 on drug-containing agar without adenine.** L1494 yeast were plated onto YNB agar containing varying concentrations of A) paromomycin or B) tavaborole. Growth is after three days. Each row on a plate is one technical triplicate, with each colony decreasing in inoculum concentration from left to right (OD_{600} 0.1, OD_{600} 1; 5 µl added for each spot). A) Paromomycin concentrations from left to right: 0 µg ml^{-1}, 12.5 µg ml^{-1}, 50 µg ml^{-1}, 100 µg ml^{-1}, 200 µg ml^{-1}. B) Tavaborole concentrations from left to right: 0 ng ml^{-1}, 12.5 ng ml^{-1}, 25 ng ml^{-1}, 50 ng ml^{-1}, 75 ng ml^{-1}.

stop codon readthrough in other tested organisms, W303 cells were not inhibited even at high paromomycin concentrations (in adenine-containing YEPD agar; Figure 3.17A). This suggested no readthrough effects in the present conditions, which may explain the lack of growth when adenine was omitted, i.e., there may not have been enough paromomycin-induced mistranslation to cause sufficient stop codon readthrough to allow growth on adenine-deficient medium. In the L1494 strain, paromomycin at ≥100

mg ml^{-1} successfully restored growth on YNB plates lacking adenine (Figure 3.20A) whereas tavaborole did not restore growth at all (Figure 3.20B). This indicates that tavaborole does not cause sufficient stop codon readthrough to restore growth on adenine-limited media and suggests that stop codon readthrough here is not the cause for the red-white colour change seen (Figure 3.19).

As mitochondrial damage was ruled out, a test for heritability of the white colour was performed. This was because spontaneously arising mutations could potentially give rise to a (heritable) white colour, independent of any (non-heritable) mistranslation effect. White colonies from plates with higher concentrations of tavaborole were picked and plated onto agar not containing the drug. Subsequent colonies were also white (whereas similar sub-culture of red colonies yielded red colonies, not shown). This suggested that the colour change had a genetic basis and was not due to mistranslation. While this raised a possibility that tavaborole provokes DNA mutation, it was unclear what caused the colour changes described above. If white, the colonies theoretically did not have a build-up of the adenine precursor, but they were still unable to grow on medium without adenine (data not shown). One possibility is that mutations occurred upstream of the adenine precursor responsible for the red coloration, preventing its build-up. Another is that the heritability was due to the possession of one or more recessive alleles of adenine genes (Pittman *et al*., 1959). However, that was not explored further as the primary aim of the work was to explore mistranslation-based tavaborole actions and potential synergies.

3.2.2. Searching for tavaborole-based synergies

3.2.2.1. Rational approach

As stated in the chapter introduction, it has been shown that compounds affecting translational fidelity can be synergistic with each other. Alongside trying to determine if tavaborole induces mistranslation, tavaborole was tested in combination with

various other compounds in search for such synergies. These included compounds known to affect translational fidelity, as well as compounds known to be synergistic with these. Unfortunately, tavaborole did not prove synergistic with any of the compounds tested in this way, with FICI values derived from checkerboard assays all >0.5. Table 3.1 shows a list of all the compounds tested in combination with tavaborole in *S. cerevisiae* as well as *Z. tritici* and *B. cinerea*. These negative results for synergy with this selection of compounds added further weight to the preceding evidence that tavaborole does not cause mistranslation. However, one case of synergy with tavaborole was found later in this thesis, when testing aaRS-inhibitors with inhibitors of the biosynthesis of corresponding amino acids (4.2.3).

Table 3.1. **List of mistranslation-associated compounds tested in combination with tavaborole in *B. cinerea*, *S. cerevisiae*, and *Z. tritici*.** Combinations were tested in checkerboard format as appropriate for each organism. None of these combinations resulted in synergy (FICI for all >0.5). AA = amino acid.

Compound	Mechanism	Reference
Bicarbonate	Sulphate-transport inhibitor	Markovich, 2001.
Chromate	Sulphate-transport inhibitor	Markovich, 2001.
Eugenol	AA-transport inhibitor	Darvishi *et al*., 2013.
Hygromycin	Translation inhibitor	Borovinskaya *et al*., 2008.
Malonate	Sulphate-transport inhibitor	Markovich, 2001.
Mancozeb	Targets amino acid function	Dias *et al*., 2010.
Molybdate	Sulphate-transport inhibitor	Markovich, 2001.
Norvaline	Structural analogue of proteinogenic amino acid	Hartman *et al*., 2007.
Orthovanadate	Sulphate-transport inhibitor	Yildiz *et al*., 1994.
Oxalate	Sulphate-transport inhibitor	Markovich, 2001.
Paromomycin	Translation inhibitor	Chawla *et al*., 2011

Probenecid	Sulphate-transport inhibitor	Markovich, 2001.
Quinine	AA-transport inhibitor	Khozoie *et al*., 2009.
Selenate	Sulphate-transport inhibitor	Markovich, 2001.
Streptomycin	Translation inhibitor	Davies *et al*., 1966.
Thiram	Targets amino acid function	Salam *et al*., 2021
Ziram	Targets amino acid function	Cedergreen, 2014; Walker, 2009.

3.2.2.2. Screening the Prestwick Chemical Library against tavaborole

As the compounds related to translation fidelity (Table 3.1) did not synergise with tavaborole, the search for synergy was widened through a combinatorial screen with tavaborole against the Prestwick Chemical Library (PCL); it was considered worthwhile to persist with tavaborole in this way given that the compound inhibits fungi in the nanomolar range, and the compound is already approved for topical use on humans, highlighting its potential. At the time of this study, the PCL contained 1280 compounds that were not only chemically and pharmacologically diverse, but were also known for their bioavailability and safety in humans (further information can be found here: http://www.prestwickchemical.com/libraries-screening-lib-pcl.html). As well as compound libraries, databases also exist that detail known synergies, including one specifically for antifungals (Chen *et al*., 2014). Such databases can theoretically be used to look for synergies involving drugs that may be related to tavaborole, either in mode of action or structure. However, this strategy was not employed due to time constraints.

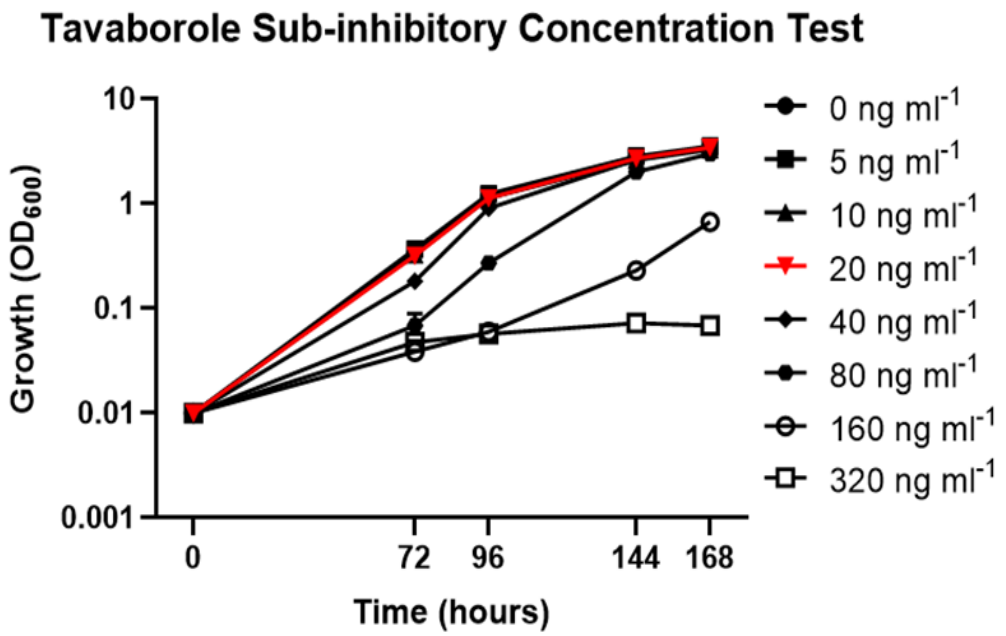

Figure 3.21. **Inhibition of *Z. tritici* growth by tavaborole**. Growth of *Z. tritici* in MCS medium after treatment with different concentrations of tavaborole. 50 µl of tavaborole solutions were added to wells on a 96-well plate containing 50 µl of *Z. tritici* spores to give a final spore concentration of 10,000 spores ml^{-1}. Plates were incubated in the dark at room temperature. OD_{600} was recorded at 0, 72, 96, 144, and 168 h. Bars represent standard deviation. n = 3.

A concentration of 20 ng ml^{-1} tavaborole was deemed to be suitable for screening the PCL for synergies against *Z. tritici*, as that tavaborole concentration was just sub-inhibitory to growth (Figure 3.21). Similarly, it was decided to test the library drugs at a concentration of 10 µM after testing a selection of these for inhibition (Figure 3.22). However, 1 µM may have been more appropriate as other chemicals, such as amphotericin B (Figure 3.22A), showed strong inhibition at 10 µM (Appendix Figure 8.3).

The first and last columns were not in used for each plate, and there were three replicates each for tavaborole and DMSO control plates. With a control well, each 96-well plate contained 79 assays. Therefore, each replicate of each condition required

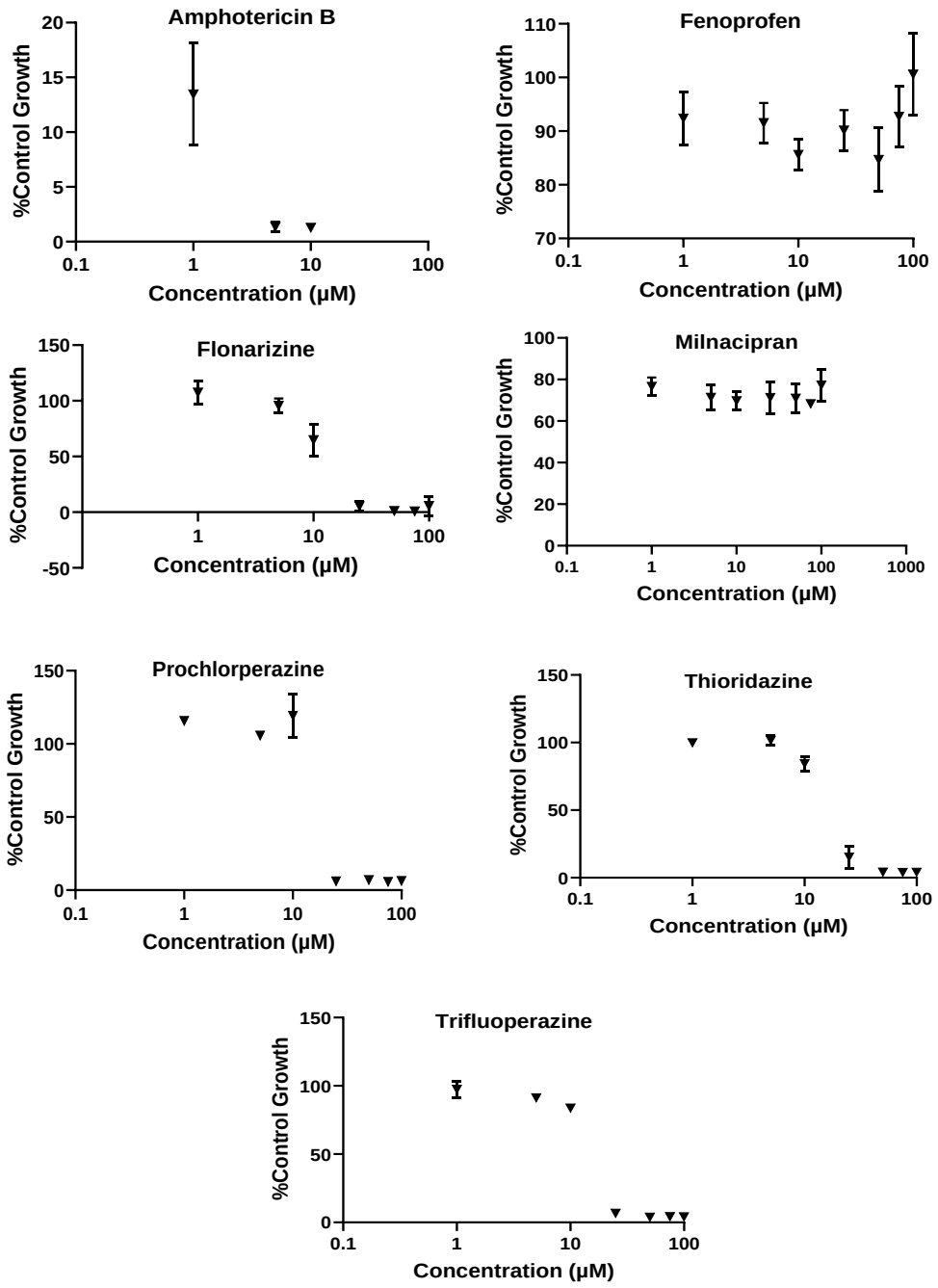

Figure 3.22. **Preliminary dosage testing of the Prestwick Chemical Library.** Growth of *Z. tritici* in the presence of different test drugs from the PCL at different concentrations. Plot points convey growth of treated samples as a percentage of the non-treated samples in DMSO-matched controls. The experiment was carried out in 100 µl MCS medium in 96-well plates with 10,000 spores ml^{-1}. Readings show growth after seven days. n = 3.

17 96-well plates and the whole screen involved the assay of *Z. tritici* in a total 102 different 96-well plates. Examination of the inoculated plates for subsequent growth revealed a clear "edge effect" (Mansoury *et al*., 2021) on each individual plate, with more growth at plate edges and in particular in the four corner wells (Figure 3.23A).

A)

3.385527344	2.99772	2.76118	2.73062	2.62073	2.60256	2.6776	2.74548	2.87489	3.17878
2.839531928	2.65199	2.49865	2.43927	2.43186	2.39651	2.41578	2.45064	2.56032	2.78767
2.869059964	2.58111	2.30922	2.32073	2.29189	2.28281	2.34113	2.34756	2.44417	2.74984
2.84821677	2.51306	2.40396	2.27406	2.29344	2.25656	2.31788	2.35758	2.4627	2.71667
2.892668389	2.56516	2.31406	2.30014	2.21056	2.26781	2.25147	2.33298	2.45201	2.77666
2.938913968	2.56174	2.41156	2.31833	2.35958	2.26422	2.36907	2.35754	2.44573	2.78497
2.943002211	2.69001	2.57069	2.50167	2.54758	2.46398	2.49844	2.49314	2.59934	3.02607
3.156666667	2.88778	2.82032	2.75626	2.74648	2.69147	2.67643	2.73365	2.93903	3.24145

B)

2.272643293	2.29357	2.20173	2.28439	2.13056	2.10573	2.22863	2.28676	2.18438	2.27349
2.303663973	2.29344	2.35047	2.29714	2.27693	2.25925	2.27125	2.30544	2.29344	2.29536
2.256590416	2.27452	2.30922	2.32073	2.29189	2.28281	2.34113	2.21542	2.26593	2.25605
2.246115904	2.2134	2.40396	2.27406	2.29344	2.25656	2.31788	2.35758	2.27867	2.13453
2.279798902	2.25758	2.31406	2.30014	2.21056	2.26781	2.25147	2.33298	2.26902	2.27572
2.317594223	2.25535	2.41156	2.31833	2.35958	2.14729	2.36907	2.35754	2.26646	2.30255
2.323486389	2.4453	2.35425	2.26219	2.31849	2.25843	2.29164	2.24151	2.29344	2.47975
2.27091725	2.1662	2.32843	2.2837	2.27373	2.23085	2.22454	2.26008	2.2973	2.64079

Figure 3.23. **Representation of edge effect**. A) Raw average OD_{600} of all *Z. tritici*-containing wells on all 102 plates before edge effect correction. B) Raw average OD_{600} of all *Z. tritici*-containing wells on all 102 plates after edge effect correction/normalisation according to equations shown in *Figure 3.24*. Colour scale uses shades of green to represent the lowest value(s), shades of red to represent the highest value(s), and shades of yellow to represent middle values. The same colour scale spans both A) and B) (e.g., no red in B as values not as high as in A). Each black box in A) contains a group of wells whose data were normalised separately from others. The red box in the middle was used to calculate the "Average Control Well OD" as the values within are all very similar and contain the control well. First and last columns were not used on each plate, and so 10*8 wells are shown here.

This edge effect is likely the result of two main factors causing differential evaporation: stacking of plates within the confined environment in which they were incubated; and not adding liquid to empty wells to help homogenise temperature distribution across each plate. This led to both intra- and inter-plate variation. It was decided to normalise for the edge effects using these equations:

$$\frac{Average\ Edge\ Well\ OD_{600}}{Average\ Control\ Well\ OD_{600}} = x$$

$$\frac{Individual\ Edge\ Well\ OD_{600}}{x} = Normalised\ Value$$

Figure 3.24. **Equations used to normalise for the observed "edge effect" in the PCL screen**.

The averages calculated for these equations were not pooled across all affected wells in the experiment, as the strength of effect differed for different parts of the plate.

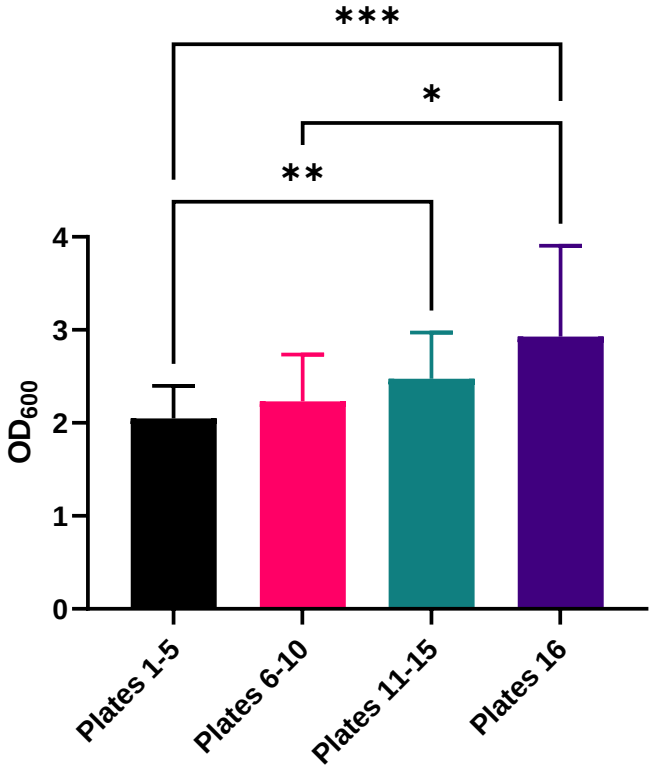

Figure 3.25. **Plate stack-position effect**. *Z. tritici* OD_{600} values of control (minus drug) wells of different groups of PCL-screen plates after 168 h incubation at room temperature. Data for plates were grouped based on their layer when stacked for incubation. Higher numbered plates were at a higher level. *p < 0.05; **p < 0.01; ***p < 0.001. Plates 1-5, n = 30; plates 6-10, n =30; plates 11-15, n = 30; plate 16, n = 6. Error bars show standard deviation. p values calculated from ordinary one-way ANOVA multiple comparisons.

Instead, several independent averages were calculated and applied to different parts of the plate illustrated in Figure 3.23A.

In addition to normalising different sectors within plates, whole groups of plates were also normalised separately. These groups were based on the layer in which they were stacked during incubation, e.g., bottom layer versus middle layer. It was found that plates at different layers in a stack had different growth values for their control-growth wells (i.e., growth without drug) (Figure 3.25). The combination of these correction methods addressed both intra- and inter-plate variation. As well as layer-to-layer variation between replicates, there was often additional plate-to-plate variation. Plates of the same replicates were stacked on the same layers, and so were normalised together. The variation between replicates led to the large error bars seen in Figure

3.26, which shows the finalised PCL screen data after normalisation methods were applied. The compounds of interest are closer to the x-axis, and further from the y-axis, as these are the compounds where the combination with tavaborole elicit inhibition of growth of *Z. tritici*. This includes cefepime hydrochloride (red point, Figure 3.26B) which was taken forward, along with other chemicals, for a further screen that was carried out in a similar fashion, as seen in Figure 3.27. A total of 28 compounds were retested.

Only a limited number of compounds were used per plate, with unused wells filled with medium in an effort to prevent any edge effect. Only wells in the central red box shown in Figure 3.23A were used. Despite the promise shown by cefepime hydrochloride in the initial PCL screen, there was no suggestion of synergy with tavaborole in the more focused further assays. One compound, mefloquine hydrochloride (highlighted in red) appeared a relatively good candidate at 72 h, but not at 96 or 168 h (Figure 3.27). As the follow-up screen did not suffer from an edge effect, and given that it had three biological replicates, each with three technical triplicates, this experiment should have been more robust that the initial screen. Therefore, it appears that cefepime hydrochloride, a compound with good initial promise from the first screen, does not have a synergistic interaction with tavaborole, along with the other compounds carried forward.

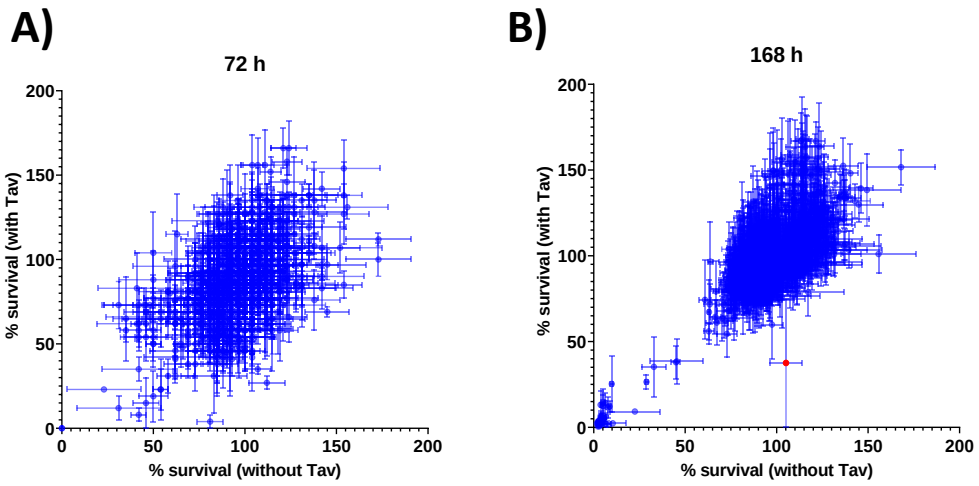

Figure 3.26. **PCL screen results**. Percentage growth of *Z. tritici* after culture with 10 µM PCL compounds without (x axis) or in combination with (y axis) 20 ng ml^{-1} tavaborole (Tav), compared to untreated control growth. Each dot represents a different compound. Red dot in B represents cefepime hydrochloride A) 72 hours growth. B) 168 hours growth. n = 3 technical replicates which were prepared at the same time with the same media and drug stocks. Technical replicates were on separate 96-well plates.

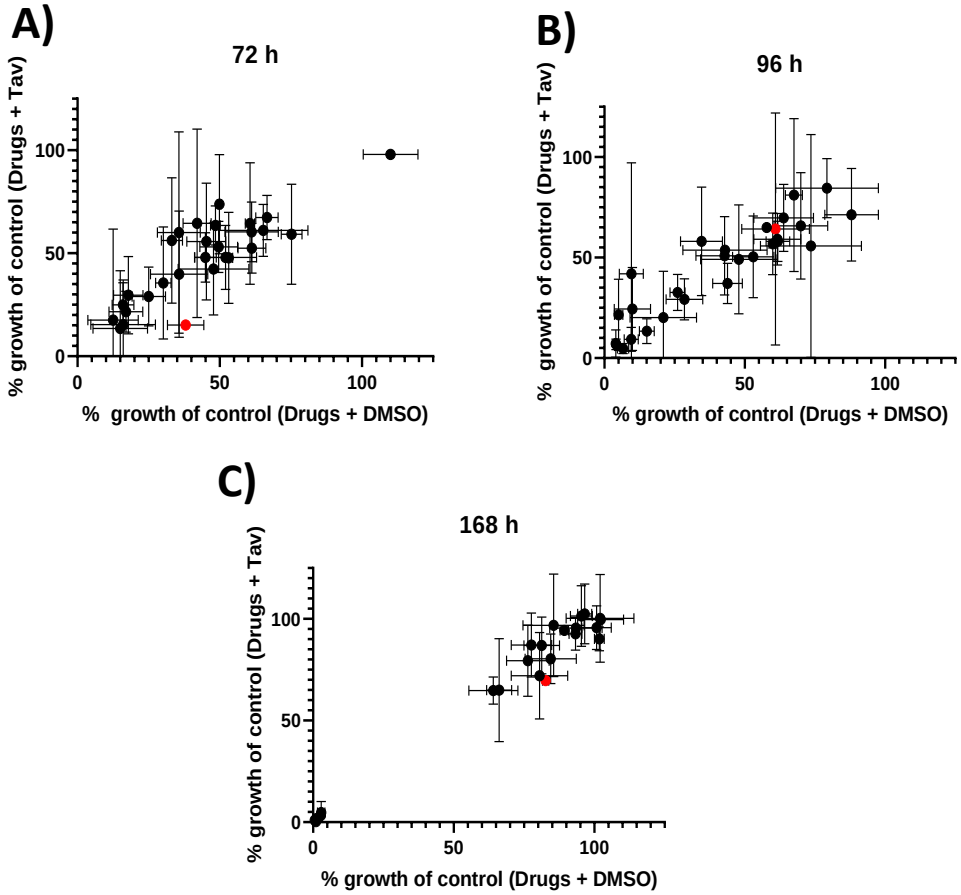

Figure 3.27. **PCL screen follow up**. Percentage growth of *Z. tritici* after culture with 10 µM selected compounds of interest from the Prestwick Chemical Library alone or in combination with 40 ng ml^{-1} tavaborole (Tav) compared to untreated control growth. Each dot represents a different compound. Red dot indicates mefloquine hydrochloride. A) 72 hours growth; B) 96 hours growth; C) 168 hours growth. n = 3 biological replicates, each with 3 technical replicates.

3.3. Discussion

3.3.2. Tavaborole and mistranslation

Using a range of experimental techniques, it was established that tavaborole does not cause detectable mistranslation in yeast; namely, the misincorporation of amino acids near-cognate to leucine or stop codon readthrough. By looking at whole populations, or even at single cells, significant mistranslation could not be detected when cells were treated with tavaborole. The original hypothesis behind this line of enquiry was that amino acid starvation is a known potential cause of increased mistranslation in cells (Wong *et al*., 2018), and tavaborole causes a similar downstream effect through inhibiting the charging of $tRNA^{Leu}$ molecules with leucine. In addition, the high abundance and importance of leucine in cells (as the amino acid with the highest % composition in fungal proteins, Gaur, 2014) suggests that there might have been as strong a chance of a LeuRS inhibitor causing misincorporation than an inhibitor of any other aaRS, or of the biosynthesis of any other amino acid.

As mentioned previously, RFP fluorescence in GFP^{Leu}-expressing cells were hypothesised to have been unaffected by the GFP point mutation. One possible explanation for this is the induction of protein misfolding caused by the SNP in the essential fluorophore, or of the truncation of protein synthesis due to a lack of charged LeuRS molecules at other positions in the protein where leucine was coded for. One method to determine if cessation of protein translation was a consequence of tavaborole would be to connect unaltered GFP and RFP proteins with a chain of linking leucine molecules. Additionally, 2A self-cleaving peptides could have been utilised to induce ribosomal skipping, causing the potential misfolding of GFP to lead to an unaffected RFP protein (Sharma *et al*., 2012).

Mistranslation associated with aaRS enzymes is normally due to the aminoacyl tRNA synthetase mischarging a tRNA with the incorrect amino acid (Schimmel, 2011). It may be that tavaborole's mode of action is simply incompatible with causing mistranslation. For example, as tavaborole acts by trapping the $tRNA^{Leu}$ molecule within the leucyl-tRNA synthetase, the $tRNA^{Leu}$ is not available to be mischarged by another aaRS. Therefore, there is theoretically less chance of a different aminoacyl-tRNA synthetase mischarging $tRNA^{Leu}$ with a non-cognate amino acid than if tavaborole did not trap the $tRNA^{Leu}$ molecule. Consequently, there would be less chance of misincorporation at a leucine-dedicated residue. Indeed, it has been shown that inhibition of either enzymatic step of aminoacylation leads to the accumulation of uncharged tRNA molecules and to the interruption of protein synthesis; this includes inhibition by granaticin, another inhibitor of leucyl-tRNA synthetase (Ogilvie et al., 1975).

3.3.3. Tavaborole and synergies

In concordance with a lack of detectable mistranslation, tavaborole was not synergistic with any of the mistranslation-related synergising compounds described in Vallières *et al*. (2018). As the hypothesis was that mistranslation-inducing compounds would be synergistic with each other, the lack of synergies found by tavaborole was not unexpected given the absence of detectable tavaborole-induced mistranslation. Moreover, synergies with tavaborole were also undetectable after screening the inhibitor in combinations with the 1280 compounds of the Prestwick Chemical Library. Since this research was carried out, the size of the PCL has increased to 1580 chemicals. It would be interesting to see if tavaborole found synergy with any of these extra 300 molecules, although there are of course many other chemical compound collections available. A recent study, similarly, has failed to identify antifungal synergies involving the food preservative sorbic acid (Harvey *et al*., 2023). This was

despite high synergy hit rates in other combinatorial synergy screens with fungi (Vallières *et al*., 2018; Augostine and Avery, 2022). It was postulated that the multifactorial modes of sorbic acid action may dampen synergies that arise at individual targets of the weak acid (Harvey *et al*., 2023). Although speculative, this could suggest the possibility that tavaborole has more diverse actions in cells than currently known, or simply that its specific target is not one that is conducive to synergies with other agents, e.g., there is negligible scope for targeting interacting steps in the common process that's relevant here, unlike other examples where synergy does occur.

3.3.4. Final remarks

With tavaborole a potent inhibitor of fungal LeuRS, there is still the potential for its use as a fungicide, expanding on its current application to treat onychomycosis. The compound requires only nanomolar concentrations to inhibit the fungal phytopathogen *Z. tritici* and has already been approved for treatment of onychomycosis. However, as no synergies were yielded with tavaborole in this part of the PhD research, it was not tested whether tavaborole would remain effective against fungal phytopathogens when applied directly to plants. It may be the case that tavaborole does not effectively control *Z. tritici* infections on plants, despite existing as a potent inhibitor in a laboratory setting. Since the time this research with tavaborole was carried out (2018/2019), at least one paper has been published detailing the potential of tavaborole against a fungal phytopathogen, *Botrytis cinerea* (Zhao *et al*., 2022).

However, one synergy involving tavaborole, an inhibitor of LeuRS, and chlorimuron ethyl, an inhibitor of branched-chain amino acid (isoleucine, leucine, and valine)

biosynthesis was found during the course of this PhD research. This type of combination is described in the next chapter.

Finally, although it was not known if a lack in charging of a particular aaRS molecule led to increased mistranslation, since this work with tavaborole was carried out McFarland *et al*. (2020) showed that despite the depletion of the yeast glutamine aaRS (GlnRS) gene inducing an amino acid starvation response, mistranslation rates were not increased and the GlnRS-depleted strains were not more sensitive to the translation error-inducing drug hygromycin B. However, Parker *et al*. (2017) and Sorensen (2001) did show that starvation of a single amino acid caused a decrease in levels of the corresponding aaRS molecule, leading to mistranslation. This work was carried out in *E. coli*, however, and so the effect of amino acid and/or aaRS starvation may be dependent on the organism in which the research is conducted.

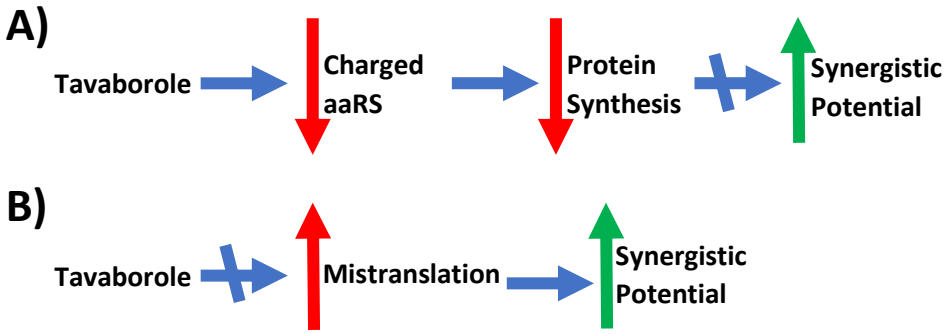

Figure 3.28. **Summary of tavaborole synergistic potential**. A) Although tavaborole is known to lead to inhibition of protein synthesis via a decrease in charged LeuRS, this did not lead to increased synergistic potential with other compounds. B) Tavaborole was not found to cause significant mistranslation which likely contributed to a lack of synergies found when tested in combination with mistranslation-inducing compounds.

Chapter 4 - Discovering novel fungicidal synergies involving aminoacyl-tRNA synthetase inhibitors

4.1. Introduction

Drug synergies can be searched for either with high-throughput methods, such as screening chemical libraries, or through rational approaches, such as testing compounds hypothesised to be synergistic based on known properties and effects. Both techniques are valid and have the potential to uncover effective synergies (Vallières *et al*., 2018; Augostine and Avery, 2022). This chapter, however, mostly explores the rational approach. Specifically, REP3123 dihydrochloride (REP3123), an inhibitor of methyl-tRNA synthetase (MetRS), and compounds hypothesised potentially to synergise with this molecule are investigated.

4.1.1. Aminoacyl-transfer RNA synthetases

As outlined in 3.1.2, aminoacyl-transfer RNA synthetases (aaRS) are essential proteins in all organisms with the dedicated function of "charging" (sometimes referred to as "loading") tRNA molecules with the correct corresponding amino acid. These reactions are carried out in two steps. First, the appropriate aaRS utilises ATP to catalyse the production of an intermediate aminoacyl-adenylate, releasing inorganic pyrophosphate. The aaRS then transfers the amino acid moiety to its cognate tRNA. Figure 3.1 summarises these reactions. Once charged, the tRNA is delivered to the ribosome for protein synthesis.

There are 20 types of aaRS molecules, one for each proteinogenic amino acid. These can be divided into two classes, each consisting of ten enzymes (Eriani *et al*., 1990). Class I aaRS molecules are usually monomeric or dimeric and have two highly conserved sequence motifs. These aminoacylate at the 2'-OH of a terminal adenosine nucleotide on tRNA. Class II aaRS molecules are usually dimeric or tetrameric and have three highly conserved sequence motifs. Except for phenylalanine-tRNA synthetase, class II aaRS molecules aminoacylate at the 3'-OH of a terminal adenosine nucleotide

on tRNA (Eriani *et al*., 1995). Through aminoacylation, amino acids are attached to the hydroxyl group of the adenosine via the carboxyl group (Delarue, 1995). aaRS classes are categorised based on the homology of the catalytic domain, with members of one class having homology with each other but not with members of the other class. The catalytic domain of aaRS molecules is where the reactions seen in Figure 3.1 take place. Another domain, the anticodon-binding domain, interacts mostly with the anticodon region of tRNA (Pang *et al*., 2014).

aaRSs are often referred to as having "superspecificity" (or "hyperspecificity") due to the lack of errors that they introduce into protein synthesis (Bosshard, 1976; Fersht and Kaethner, 1976; Favorova, 1984; Martin *et al*., 2004). In addition to having specific binding and activation for their affiliated amino acids, several aaRS molecules also contain an editing site. The structural or chemical similarities of various amino acids to one another causes difficulties for aaRS molecules. To help distinguish cognate versus noncognate amino acids, some aaRSs employ a "double sieve" editing mechanism (Moras, 2010). This includes AlaRS, IleRS, LeuRS, PheRS, ThrRS, and ValRS (Dock-Bregeon *et al*., 2000; Fukai *et al*., 2000). The first "coarse" sieve acts to reject amino acid molecules that are larger than the cognate amino acid. This occurs at the active site. The second "fine" sieve, located at the aaRS editing site, eliminates noncognate mischarged non-cognate amino acids via hydrolysis (Moras, 2010). This editing can be pretransfer of misactivated aminoacyl adenylates or post-transfer of misacylated tRNA (Lue and Kelley, 2005). In the former, hydrolysis separates the misactivated amino acid back to the amino acid and AMP, whereas in the latter, a misaminoacylated tRNA is hydrolysed to yield the amino acid and tRNA (Lincecum *et al*., 2003).

4.1.1.1. Methyl-tRNA synthetase

While some aaRSs are involved in preventing mistranslation through their editing activities, MetRS is sometimes involved in the potentially beneficial misincorporation of methionine into proteins (mismethionylation). Methionine is an atypical amino acid in that it can become stably oxidised by reactive oxygen species (ROS) to produce methionine sulfoxide (MetO) which can later be reduced by methionine sulphide reductases (MSRs). Both free methionine and methionine within proteins can act as ROS scavengers, alleviating potential oxidative stress (Koc *et al*., 2004). In response to elevated levels of ROS, extracellular signal-related kinase (ERK1/2) activity phosphorylates MetRS at Ser209 and Ser825, causing MetRS to gain increased affinity for non-cognate tRNAs, increasingly charging these with methionine (Lee *et al*., 2014). Under conditions of stress, this misacylation of non-methyl-tRNA with methionine can occur at frequencies of up to 10% in mammalian and yeast cells (Netzer *et al*., 2009; Wiltrout *et al*., 2012).

4.1.2. REP3123

As seen in the previous chapter, the leucyl-tRNA synthetase inhibitor tavaborole yielded no synergies in the chemical combinations tested. As aaRS molecules are still a fungicide target of interest (Hurdle *et al*., 2005; Kwon *et al*., 2019), aaRS inhibitors other than tavaborole should be tested in the search for synergies. REP3123 is a methionyl-tRNA synthetase inhibitor with a different mechanism to that of tavaborole. Instead of trapping the appropriate amino acid in the editing site, REP3123 is believed to dock across both binding sites of the essential methionyl-tRNA synthetase (Al-Moubarak and Simons, 2011). Due to the function of MetRS in increasing misincorporation of methionine into

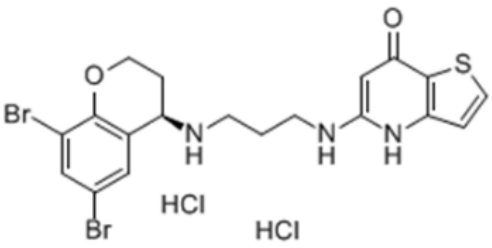

Figure 4.1. **Chemical structure of REP3123**.

proteins in response to oxidative stress, REP3123 could have the additional consequence of subduing an organism's ability to cope with oxidative stress, potentially providing additional opportunities for synergy.

Research determining the mode of action of REP3123 (and the similar compound REP8839) was carried out using *Clostridium difficile* (Al-Moubarak and Simons, 2011). Literature searches suggest there has been no previous work involving REP3123 and fungi, leaving open the possibility that the compound could be a potent inhibitor of fungal phytopathogens.

Regarding synergies, it was hypothesised that REP3123 might be synergistic with compounds that negatively impact methionine biosynthesis. In this way, the incorporation of methionine into proteins would be undermined in two ways: inhibition of biosynthesis resulting in less of the amino acid available; and inhibition of MetRS resulting in a decreased rate of aminoacylation. In addition, based on the role of MetRS in mismethionylation, it was hypothesised that REP3123 might work well with compounds that induce oxidative stress.

4.1.3. Sulphur-transport inhibitors

Inorganic sulphate (SO_4) is required for normal cell function. SO^{2-}_4 is a hydrophilic anion, and so cannot passively cross the lipid bilayer of cell membranes; therefore, transport processes are required for the influx and efflux of this essential molecule. Once inside the cell, SO_4 feeds into various biosynthetic pathways. This includes production of homocysteine which is used in the synthesis of cysteine and methionine, the only two sulphur-containing amino acids. Inhibiting sulphate transport processes provokes starvation of these amino acids (Markovich, 2001). Chromate, sodium bicarbonate, sodium orthovanadate, and sodium selenate are all sulphate transport inhibitors (Ohtake *et al* 1987; Markovich, 2001; Holland *et al*., 2010; Moreno-Martinez

et al., 2015). Sulphate uptake has been shown to be inhibited by bicarbonate as it competes for the sulphate-anion exchanger, sat-1 (Krick *et al*., 2009). As inhibitors of methionine biosynthesis, it was hypothesised that these compounds could work in synergy with the MetRS inhibitor, REP3123.

4.1.4. Cyprodinil and NADH kinases

At the start of this PhD research, cyprodinil, an anilinopyrimidine fungicide used against the phytopathogen *Botrytis cinerea*, was believed to be an inhibitor of methionine biosynthesis (FRAC, 2018). This was based on evidence that supplementation with methionine prevented the inhibition by cyprodinil (Masner *et al*., 1994). However, a paper on anilinopyrimidine resistance in *B. cinerea* (Mosbach *et al*., 2017) as well as personal communications (Andy Corran, Syngenta) suggested that cyprodinil is in fact an inhibitor of the mitochondrial NADH kinase, Pos5p.

NADH kinases are responsible for the production of cellular NADPH in the reaction:

$$ATP + NADH \rightleftharpoons ADP + NADPH$$

Figure 4.2. **Reaction catalysed by NADH kinases**.

NADPH is a molecule vital for all cellular life and is required as a cofactor for a range of activities. It is the redox-equivalent in biosynthesis reactions. Examples include the recycling of antioxidants and methionine sulfoxide reductases via their reduction. These processes are essential as part of cellular response to oxidative stress.

A lack of mitochondrial NADH has many known effects (Table 4.1). This includes increased sensitivity to oxidative stress, defective biosynthesis of enzymes containing iron-sulphur clusters, and arginine auxotrophy (Miyagi *et al*., 2009).

Regardless, as it was methionine biosynthesis that was thought to be the mechanism at the start of this research, this seemed an appropriate target at which to anticipate

a synergy in combination with the MetRS-inhibitory action of REP3123. The potential role of cyprodinil as an inhibitor of NADH phosphorylation in the mitochondria and implications for synergies are explored further in the next chapter.

Table 4.1. **Proven and hypothetical consequences of MetRS inhibition (e.g. by REP3123) and NADH kinase inhibition (e.g. cyprodinil)**.

Consequences of MetRS inhibition	**Consequences of mitochondrial NADH kinase inhibition (Miyagi *et al*., 2009)**
Inhibition of protein synthesis (Green *et al*., 2008)	Increased sensitivity to oxidative stress
Decrease in levels of charged $tRNA^{Met}$ (Green *et al*., 2009)	Slow growth on non-fermentable carbon sources
Inhibition of incorrectly loading methionine to other tRNA synthetases (mismethionylation) in response to oxidative stress (Wiltrout *et al*., 2012)	Defective biosynthesis for enzymes containing iron sulphur cluster(s)
Increased sensitivity to oxidative stress (Wiltrout *et al*., 2012)	Up-regulated transcription of genes for iron uptake
Accumulation of free methionine in cell?	Abnormal accumulation of iron in the mitochondria
	Accumulations of mutations in mtDNA
	Arginine auxotrophy

4.1.5. Chapter aims

The research in this chapter aimed to find synergies involving inhibitors of amino acid biosynthesis and/or inhibitors of aminoacyl-tRNA synthetases. If such synergies were found, this would be precedent to presume that similar synergies are possible, vastly increasing the number of combinations potentially available to synergistically inhibit undesirable organisms.

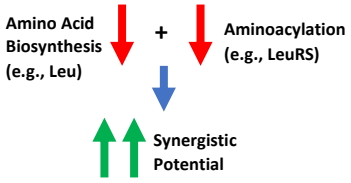

Figure 4.3. **Schematic showing prediction of synergistic potential between amino acid biosynthesis inhibitors and inhibitors of aminoacylation**. It is hypothesised that inhibitors of aminoacylation, such as tavaborole and REP3123 are likely to be synergistic with inhibitors of (corresponding) amino acid biosynthesis.

4.2. Results

4.2.1. Testing for synergies between REP3123 and sulphur-transport inhibitors

Despite the search for synergies with tavaborole proving unsuccessful (see previous chapter), aaRSs were still an attractive target for potential synergy discovery. For this reason, the MetRS inhibitor REP3123 was procured. It was hypothesised first that REP3123 may be synergistic with sulphate-transport inhibitors due to their hindering of methionine biosynthesis in combination with prevention of methionine charging of $tRNA^{Met}$ by REP3123. REP3123 was tested in combination with sodium bicarbonate (NaBIC), sodium orthovanadate (NaVAN), and sodium selenate (NaSEL). These S-transport inhibitors were each found to have synergies against *Z. tritici* when in combination with REP3123 (Figure 4.4). The combinations of REP3123 with NaBIC, NaVAN, and NaSEL gave mean FICI values of 0.375, 0.5, and 0.5 respectively, although NaVAN and NaSEL were non-synergistic according to certain individual replicates.

While a combined impact on $tRNA^{Met}$ aminoacylation with methionine was hypothesised to be the synergistic mechanism-of-action, it was considered that the high concentrations of S-transport inhibitors required to inhibit *Z. tritici* may have had affected the pH of the medium (Vallières *et al*., 2018), which could have non-specific effects. To attempt to rule this out, the pH of MCS medium (used as *Z. tritici* growth medium) was measured at different concentrations of the S-transport inhibitors (Figure 4.5A). MCS medium is prepared at pH 6.4. However, higher concentrations of S-transport inhibitors affected the pH, especially with NaVAN. This included concentrations where synergies with REP3123 were found (Figure 4.5A).

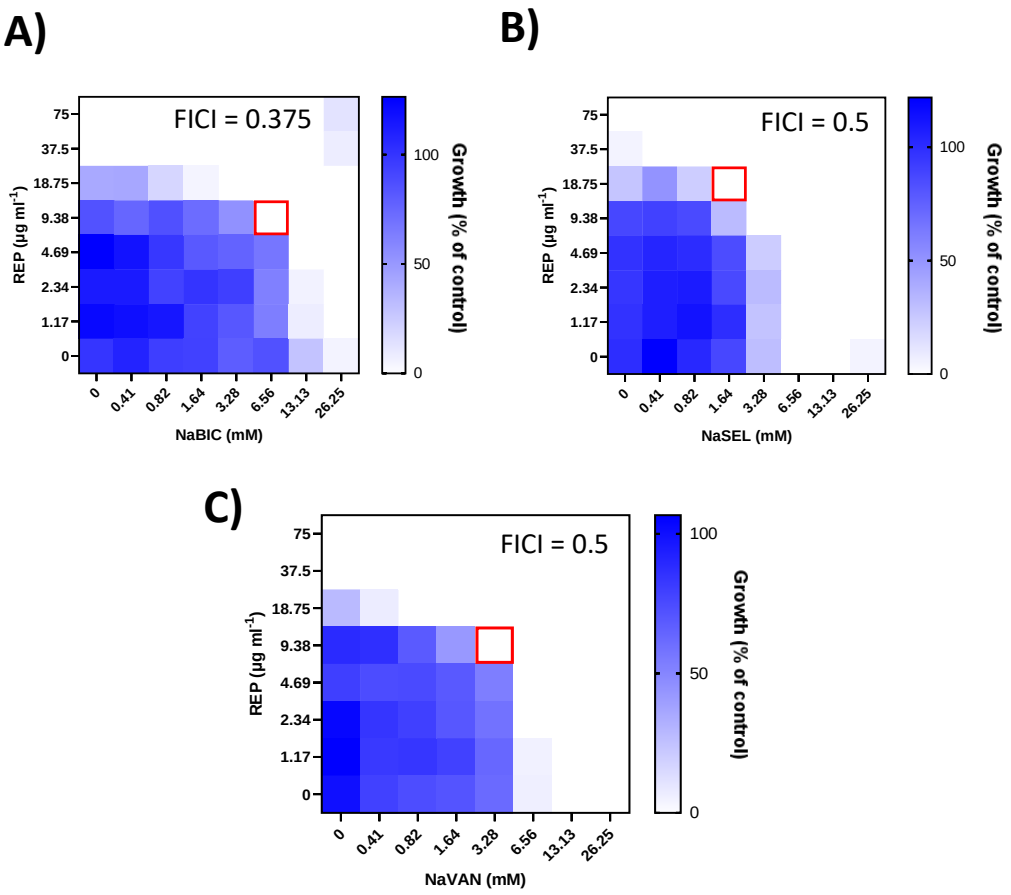

Figure 4.4. **REP3123 and S-transport inhibitor synergies.** Assays were performed according to the EUCAST procedure at the indicated concentrations of REP3123 and different sulphate transport inhibitors: A) sodium bicarbonate; B) sodium orthovanadate; C) sodium selenate. Growth values (scale to the right) represent means from three independent experiments, calculated as percentages of growth (OD_{600}) with compounds relative to the minus-compound control. *Z. tritici* was grown in MCS medium at room temperature and data were collected at 0 h and 168 h. Growth values <5% were assigned as no-growth. Red squares indicate concentrations used to calculate FICI value.

The inhibitory effects of REP3123 over a range of pH values were then also tested. Figure 4.5B shows that REP3123 activity was affected by pH. At pH 6.4, REP3123 completely inhibits *Z. tritici* at a concentration of 37.5 µg ml^{-1}. At pH ≥ 6.7, such as attained at concentrations of certain S-transport inhibitors that gave synergy with REP3123 (indicated by '*' in Figure 4.5A), the REP3123 MIC against *Z. tritici* was reduced. For example, NaVAN is synergistic with REP3123 at combination concentrations of 3.28 mM and 9.38 µg ml^{-1}, respectively (Figure 4.4C). Both concentrations represent the minimum four-fold decrease of respective MICs required in combination to achieve synergy. At this 3.28 mM concentration of NaVAN, the pH

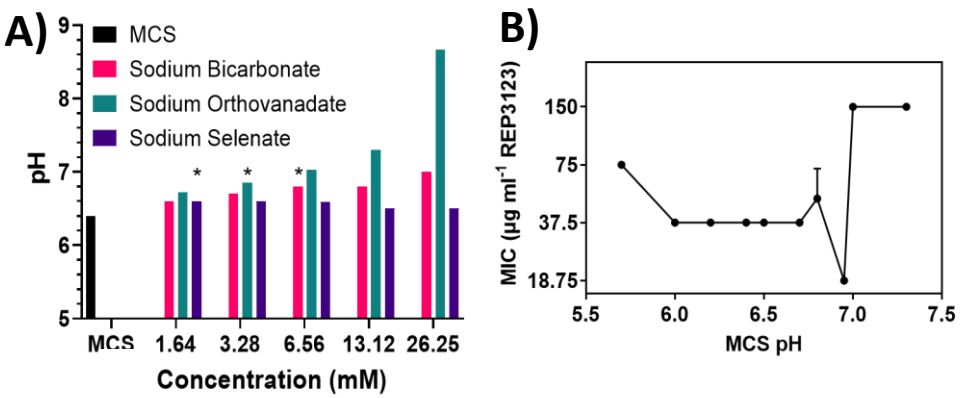

Figure 4.5. **Testing relevance of pH in S-transport inhibitor synergies with REP3123.** A) pH of MCS medium supplemented with different concentrations of S-transport inhibitors. '*' denotes concentrations that were synergistic with REP (FICI ≤ 0.5) as seen in *Figure 4.4*. B) Inhibitory effects of REP3123 against *Z. tritici* after 168 h growth in MCS medium made to different pH values. Scale bar in B shows percentage growth of control. n = 3.

of MCS medium was increased from 6.4 to 6.9 (Figure 4.5A) and this pH effect alone accounts for a halving of the MIC of REP3123 (Figure 4.5B). This still does not match the level of reduction in NaVAN concentration that allows complete inhibition of *Z. tritici* growth when in combination with REP3123. This is the case for all three of the synergies: the effects (on REP3123 MIC) of pH changes associated with adding the S-transport inhibitors are not sufficient to account for the effects on MIC of the S-transport inhibitors themselves, only accounting for a two-fold reduction. However, as four-fold reductions in REP3123 MIC are shown (Figure 4.4), the second two-fold reduction still needs to be accounted for. The results are consistent with the hypothesis that inhibition of sulphate uptake (expected to cause methionine limitation) in combination with MetRS inhibition produces synergistic growth-inhibition of *Z. tritici.* However, this effect alone may not be strong enough to provide a synergistic effect.

4.2.2. Testing REP3123 with the proposed methionine-biosynthesis inhibitor, cyprodinil

4.2.2.1. Initial discovery and tests

As mentioned earlier, cyprodinil was originally thought to be a methionine biosynthesis inhibitor (see 4.1.4.). Following the indication that methionine limitation (via sulphate transport inhibition) may synergise with REP3123 (Figure 4.4), a synergy was also found between REP3123 and cyprodinil against *Z. tritici*: an FICI of 0.375 was recorded consistently across all replicates (Figure 4.6).

In case of a similar effect as with the S-transport inhibitors, cyprodinil was tested for effects on pH of the medium (Figure 4.7). Increasing concentrations of cyprodinil increased the pH of MCS medium from pH 6.4-6.65 at 200 µM cyprodinil. At concentrations where the FICI for REP3123 with cyprodinil was calculated as synergistic (indicated by *, Figure 4.7), pH may be affected enough to increase strength of REP3123 inhibition (Figure 4.6). The effect on pH due to cyprodinil could account for a halving of the REP3123 MIC. However, this would not be sufficient to explain one of the synergistic combinations (red squares, Figure 4.6; 4.69 µg ml^{-1} REP, 50 µM CYP). This suggested that a pH effect was not the (sole) cause behind this synergy.

In addition to the combination concentrations giving synergy, there was another area within the Figure 4.6 checkerboard in which there was decreased growth (shown by black outline). Here growth was between 8.1-10% of the control when replicates for each well were averaged. This was still above the 5% growth cut-off considered as strong inhibition for the purposes of calculating FICI (see Materials and Methods). However, this seems to be an effect of cyprodinil addition rather than the combination, as it also occurred in wells that did not contain any REP3123.

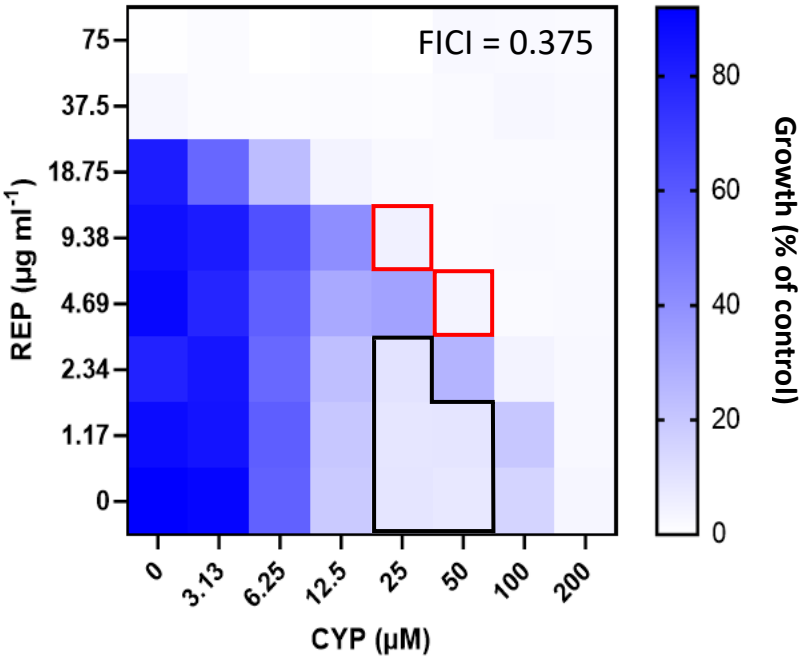

Figure 4.6. **REP3123-cyprodinil synergy in *Z. tritici*.** Checkerboard of REP3123 vs Cyprodinil in *Z. tritici* in MCS medium, based on OD_{600} after 168 hours. Scale bar shows percentage growth versus control (minus drugs). Values are means of three biological replicates. FICI at red squares = 0.375.

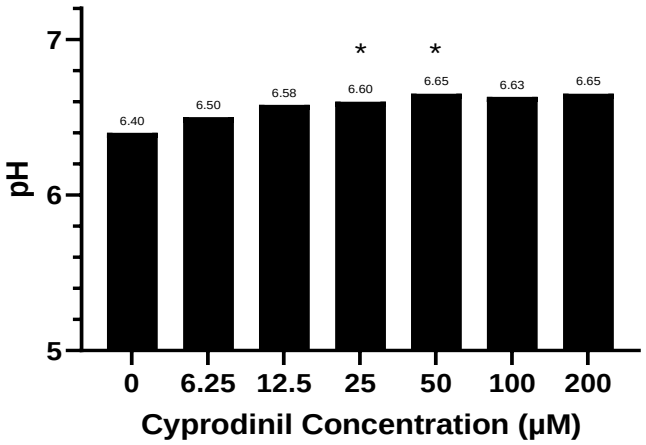

Figure 4.7. **pH of MCS medium at varying cyprodinil concentrations.** MCS medium was aliquoted into 50 ml centrifuge tubes. Each tube was made to a different concentration of cyprodinil used in checkerboards. pH was measured for each concentration. * = Concentrations which were measured to be synergistic with REP3123.

Interestingly, at higher REP3123 concentrations, there was increased growth at these cyprodinil concentrations (25 µM and 50 µM), before the yet-higher REP3123 concentrations produced synergy (Figure 4.6). This effect was unexplained but did not undermine the synergy evident at other concentrations. It may be a similar case as is seen with echinocandins, in which growth can paradoxically come back at higher

concentrations despite inhibition at lower concentrations (Wagener and Loiko, 2017). Due to visual inspection of all checkerboards for noticeable volume differences in wells, the higher evaporation of some wells over others is unlikely to cause this.

Despite the preliminary suggestion above for a synergistic interaction between inhibition of methionine biosynthesis and MetRS inhibition by REP3123, it was at this stage of the project that it was realised that the mode of cyprodinil action may in fact be by inhibition of Pos5p, a mitochondrial NADH kinase. However, this research was carried out in *B. cinerea* and so targeting of Pos5p can only be presumed in *Z. tritici* at this stage (Mosbach *et al*., 2017; Personal Communications, Andy Corran), and could indeed be a different target.

4.2.2.2. Testing oxidative stress as a mechanism for cyprodinil

A BLAST protein search revealed that there was a potential *pos5* gene in *Z. tritici* with 54% identity to its *B. cinerea* counterpart, and an E value of $3e^{-151}$. This was a good indication that the protein products of these genes serve similar functions, and so *pos5* resistance mutations here might also work for *Z. tritici*.

As such, the known and potential consequences of REP3123 and/or cyprodinil inhibition were outlined (Table 4.1). It can be seen here that oxidative stress could play a role in the synergistic mode of action between these compounds. That is, inhibition by cyprodinil of the mitochondrial NADH kinase, Pos5p, may decrease the ability of *Z. tritici* to recycle its antioxidants in response to oxidative stress. One cellular response to oxidative stress might normally be increased misincorporation of ROS-consuming methionine into proteins, protecting them from oxidative stress (Wiltrout *et al*., 2012). However, through inhibition of MetRS, REP3123 may suppress this defence process, both halting this survival mechanism and hindering general protein synthesis. To reiterate, under oxidative stress it is MetRS that mischarges other tRNAs with

methionine, rather than a different aaRS mischarging its cognate tRNA with methionine (Netzer *et al*., 2010). In short, the hypothesis was that cyprodinil increases (sensitivity to) oxidative stress, while REP3123 weakens the cellular response.

To support this hypothesis, REP3123 was tested in combination with known oxidative stress-inducing compounds (list shown in Table 4.2), to see if these mimicked the combinatorial effect seen with cyprodinil. However, REP3123 was not synergistic with any of the prooxidants tested (Figure 4.8). Checkerboard assays of REP3123 in combination with diamide, mefloquine, and paraquat all appeared very similar to the REP3123-menedione checkerboard (Figure 4.8D) and so are not shown. Among these pro-oxidants, REP3123 was tested in combination with electrolysed water (EW, Figure 4.9), an oxidising sanitiser generated from clean water and salt (Huang *et al*., 2008).

Table 4.2. **Oxidative stress-inducing compounds tested in combinations with REP3123**.

Compound Name	**Reference**
Amodiaquine	Tafazoli and O'Brien, 2008
Cumene hydroperoxide	Jovanovic and Jovanovic, 2013
Diamide	Mawatari *et al*., 2008
Electrolysed water (Sourced from Ozo Innovations)	Wohlgemuth *et al.,* 2020
H_2O_2	Poehlmann *et al*., 2013
Mefloquine	Gunjan *et al*., 2016
Menadione	Loor *et al*., 2010
Paraquat	Wang *et al*., 2014
Primaquine	Lalève *et al*., 2016
Tert-butyl hydroperoxide	Li *et al*., 2011

The REP3123-EW interaction (Figure 4.9) showed similarities with that of REP3123-cyprodinil (Figure 4.6). In particular, there appeared to be an intermediate set of

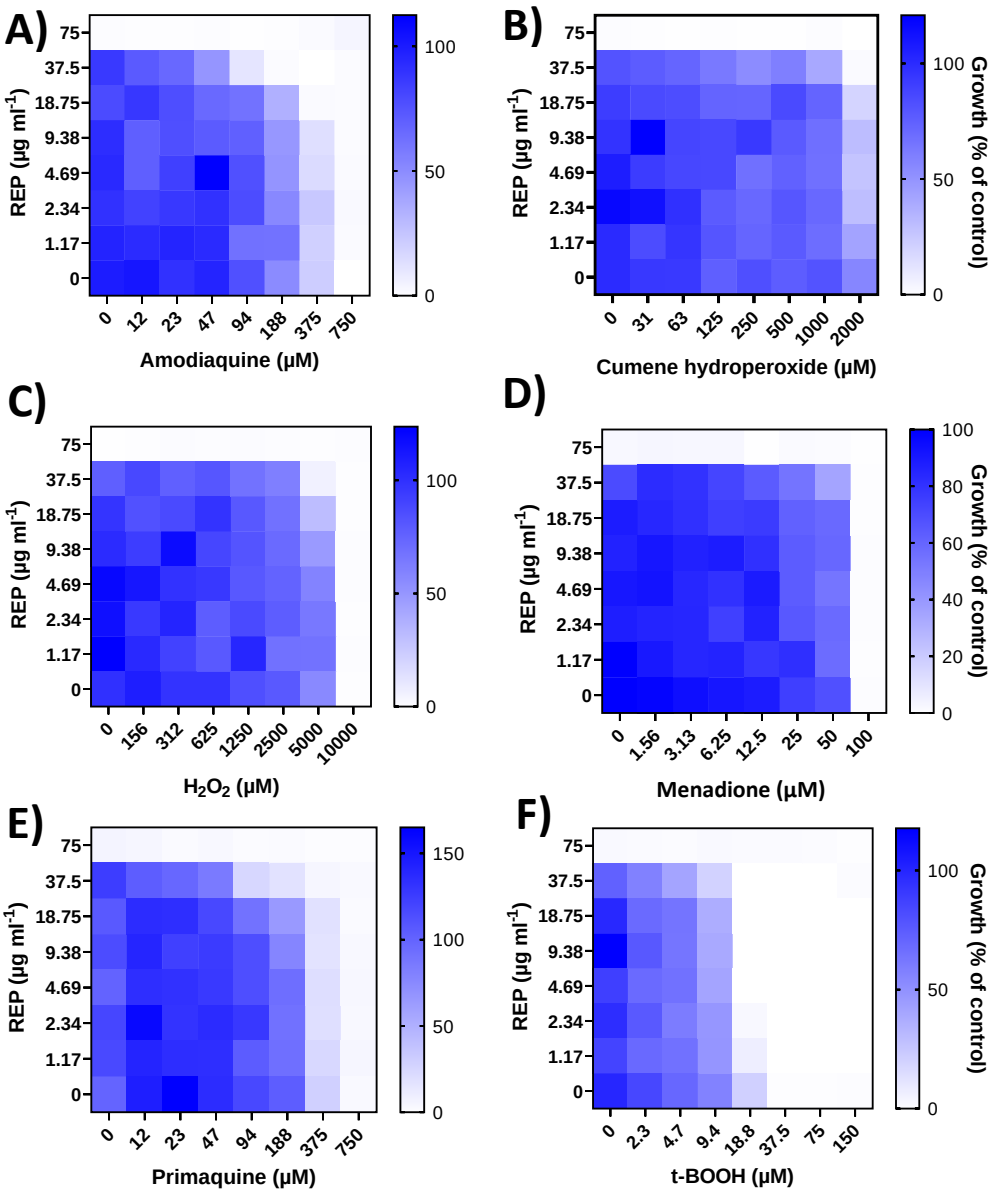

Figure 4.8. **REP3123 in combination with different prooxidants**. Assays were performed according to the EUCAST procedure at the indicated concentrations of REP3123 and prooxidants: A) amodiaquine; B) cumene hydroperoxide; C) hydrogen peroxide; D) menadione; E) primaquine; F) tert-butyl hydroperoxide. Growth values (scale to the right) represent means from three independent experiments, calculated as percentages of growth (OD_{600}) with compounds relative to the minus-compound control. Data were collected at 0 h and 168 h, with incubation at room temperature. Growth values <5% were assigned as no-growth.

concentrations of EW in which there was a greater level of inhibition than at certain higher concentrations and before a clearer MIC was reached. However, the growth inhibition at these intermediate concentrations precluded potential detection of synergy (i.e., FICI ≤ 0.5), unlike in Figure 4.6. Nevertheless, REP3123 did appear to increase sensitivity to EW: at an EW concentration of 1.13%, the REP3123

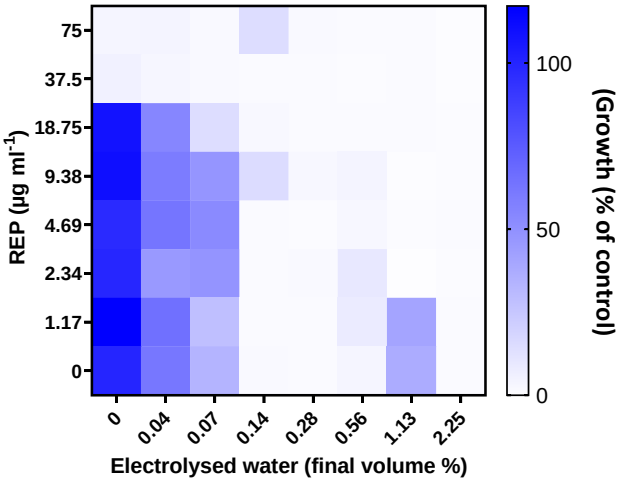

Figure 4.9. **REP3123 in combination with electrolysed water**. 1 ml electrolysed water (EW) solutions were prepared in brown 50 ml conical centrifuge tubes in HPLC-grade H_2O. Aliquots (100 µl) were combined with 100 µl of *Z. tritici* spores were added at a concentration of $1x10^6$ spores ml^{-1}. Spores were treated in the dark at room temperature for five exactly five minutes before adding 1 ml of YEPD to deactivate the EW (Wohlgemuth *et al*., 2020). Subsequently spore suspension (50 µl) was combined with 50 µl REP3123 solutions to create the checkerboard format. Data were collected at 0 h and 168 h, with incubation at room temperature. Growth values <5% were assigned as no-growth.

concentration required to reach inhibition decreased 16-fold from 37.5 µg ml^{-1} to 2.34 µg ml^{-1} (Figure 4.9). This is stronger than any interaction seen in Figure 4.8. In contrast to Figure 4.8, *Z. tritici* spores were pre-treated with EW prior to the addition of REP3123 as EW can be inactivated by culture medium and by extracellular amino acids. Therefore, to ensure that the inhibitory effect of EW was more consistent, spores were pre-treated with EW before the deliberate inactivation with YEPD.

Different ROS are present in EW, and it may be that one or more of these species are specifically responsible for this interaction with REP3123. H_2O_2 is known to be present in EW (Jeong, 2006), but it is unlikely to be the active participant as H_2O_2 is not synergistic with REP3123 (Figure 4.8C). Other ROS, as well as free activated chlorine (FAC) are also present. FAC has been shown to have a primary role in reactivity of EW with cysteine and methionine (Wohlgemuth *et al*., 2020), and amino acids with antioxidant properties (Taylor and Richardson, 1980; Levine *et al*., 1996). In addition,

FAC is known to be highly reactive with iron sulphur cluster (FeS) proteins (Albrich *et al*., 1981). It may be that this is a common target between EW and cyprodinil.

It should be noted that for these experiments and for all future experiments involving cyprodinil, DMSO was used instead of water as a solvent for cyprodinil and the stock was subsequently stored at 4^{o}C instead of room temperature. This was on recommendation from Dr Andy Corran (Syngenta) to improve stability and reproducibility of the cyprodinil data. This coincided with a large four-fold increase in cyprodinil MIC, from 200 µM to 800 µM for *Z. tritici* in MCS medium (see in Figure 4.10). Despite this large increase in MIC, the synergy remained.

One difference between cyprodinil and the oxidants tested is the specific effect of cyprodinil on NADPH, needed for the recycling of antioxidants. The REP3123-cyprodinil combination was therefore supplemented with three different antioxidants: ascorbic acid, glutathione, and *N*-acetylcysteine (Figure 4.10). Ascorbic acid appeared to increase resistance to cyprodinil and REP3123, while completely removing the REP3123-cyprodinil synergy (Figure 4.10B). In one replicate (data not shown), glutathione protected against cyprodinil alone but had little effect on the synergy as a whole – although at higher cyprodinil concentrations, it offered some protection against the addition of REP3123 (Figure 4.10C). Due to this increase in cyprodinil resistance, the FICI was decreased, technically leading to a stronger recorded synergy when glutathione was supplemented. However, three of four replicates showed no protection against cyprodinil, REP3123, or the synergy (Figure 4.10C). In the control, the average FICI was 0.5 (Figure 4.10A), and supplementation of glutathione yielded recorded FICIs of 0.5 (Figure 4.10C) or 0.28 (replicate not shown).

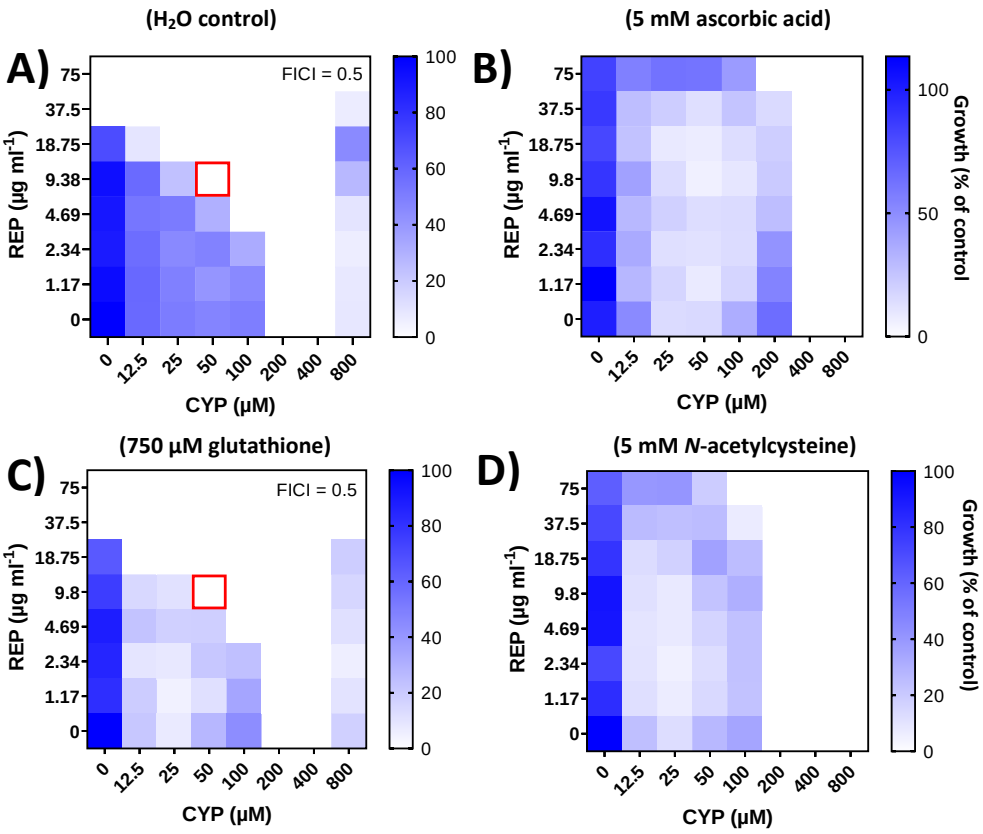

Figure 4.10. **REP3123-cyprodinil combination supplemented with antioxidants**. The data represent *Z. tritici* growth. A) H_2O control; B) 5 mM ascorbic acid; C) 750 µM glutathione; D) 5 mM *N*-acetylcysteine. Growth values (scale to the right) represent data from four independent experiments, calculated as percentages of growth (OD_{600}) with compounds relative to the minus-compound control. Data were collected at 0 h and 168 h, with incubation at room temperature. Growth values <5% were assigned as no-growth. FIC values rounded to two decimal places. Coloured boxes correspond to coloured FIC value calculated from that well.

Results from replicate experiments with *N*-acetylcysteine were also slightly variable (Figure 4.10D), but this antioxidant appeared to protect against REP3123 when compared to the control in three of four replicates (Figure 4.10D), in which the FICI was >0.5.

To summarise, experiments involving the supplementation of different antioxidants in their reduced forms (ascorbic acid, glutathione, and *N*-acetylcysteine) were variable between the different antioxidants. In addition, glutathione and *N*-acetylcysteine were also somewhat variable between replicates). Overall, it appears that ascorbic acid and *N*-acetylcysteine can prevent the REP3123-cyprodinil synergy, whereas

glutathione did not seem capable of doing so at the concentration tested, perhaps due to its autooxidation in aerobic medium (Nuhu *et al*., 2020).

The oxidised form of methionine, methionine sulfoxide (MetO) was expected to exacerbate the inhibitory effects of REP3123 and cyprodinil. Similar to the pro-oxidants tested, it was thought that MetO would increase the demand on cells for antioxidants, and of cellular NADPH that would be needed for the recycling of such antioxidants. While the pro-oxidants were believed to increase the demand on various different antioxidants, it was thought that MetO would specifically increase the demand on methionine sulfoxide reductases (MSR), proteins specifically evolved for the reduction of MetO. It is possible that the oxidative damage involved in the REP3123-cyprodinil synergy is less general, and may focus on certain targets, such as the ROS-sensitive FeS clusters. MSRs are known to preserve the function of FeS clusters (Sideri *et al*., 2009) and so exacerbation of the synergy by MetO supplementation might suggest a role for oxidative damage of FeS clusters in the REP3123-cyprodinil synergistic mechanism.

Supplementation of the REP3123-cyprodinil checkerboard with 5 mM methionine sulfoxide decreased the MIC of cyprodinil in *Z. tritici* two-fold (Figure 4.11B) when compared to the control (Figure 4.11A). *Z. tritici* also appeared more sensitive to REP3123 although there was no MIC change. However, rather than enhancing the synergistic effect, methionine sulfoxide supplementation suppressed the synergy (Figure 4.11).

Checkerboards of REP3123 against methionine sulfoxide showed no clear interaction (Figure 4.11C). However, no MIC for methionine sulfoxide could be reached and it cannot be ruled out that there is any interaction, synergistic or otherwise, between REP3123 and MetO. REP3123 theoretically prevents increases in the levels of

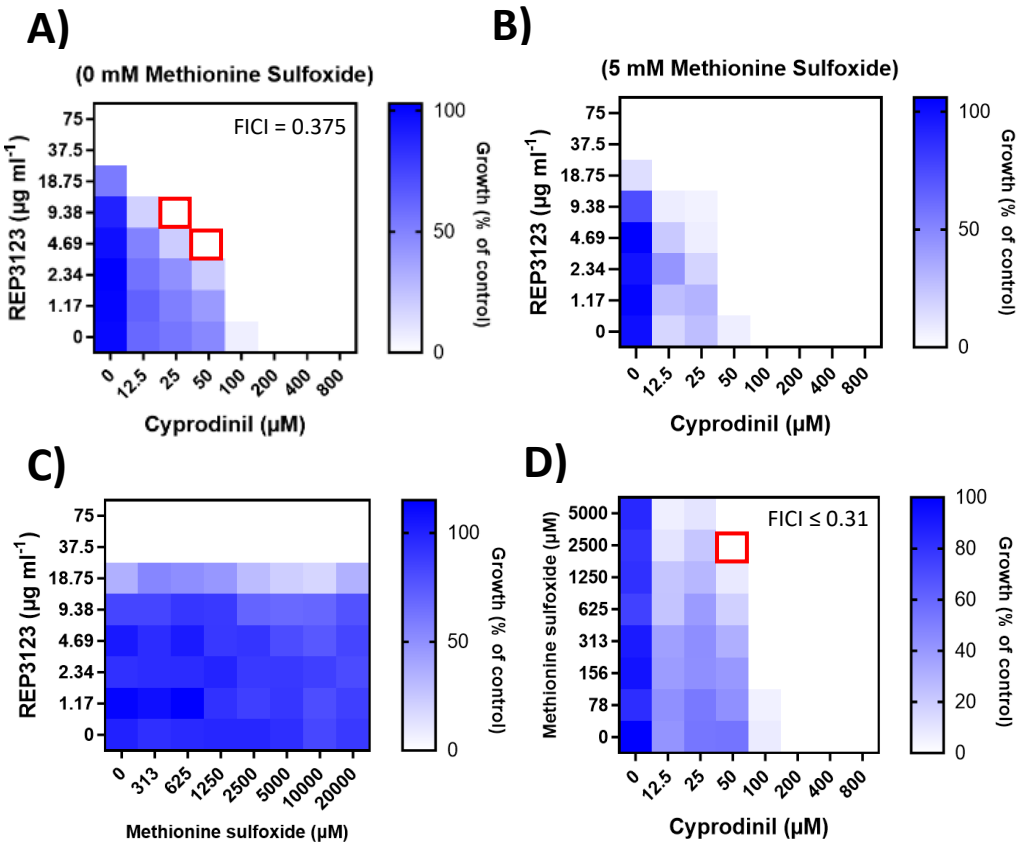

Figure 4.11. **Combinations of REP3123 and cyprodinil with methionine sulfoxide**. Data show Z. tritici growth after different combinatorial treatments: A) H2O control; B) REP3123 vs cyprodinil with 5 mM MetO supplemented to the medium; C) REP3123 vs MetO; D) MetO vs cyprodinil. Growth values (scale to the right) represent means from two independent experiments, calculated as percentages of growth (OD_{600}) with compounds relative to the minus-compound control. Data were collected at 0 h and 168 h, with incubation at room temperature. Growth values <5% were assigned as no-growth. FIC values rounded to two decimal places. The 0.31 value for FICI shown in (D) assumes MIC of MetO is 40 mM using values from ©. Red squares represent wells used for FICI calculations.

methionine misincorporated into proteins in response to elevated oxidative stress while additional methionine sulfoxide will increase the demand on methionine sulfoxide reductases (if it enters the cell).

The highest concentration tested, 5 mM, did not appear to have a strong effect on *Z. tritici* sensitivity to REP3123 (Figure 4.11C). A clearer interaction could be seen with methionine sulfoxide and cyprodinil (Figure 4.11D). At 5 mM methionine sulfoxide, growth achieved, on average, 84.2% that of the untreated control. When in combination with 12.5 µM cyprodinil (which alone gave an average growth of 41.7%) growth was at 6.1% of the untreated control. In these experiments, an FICI value ≤

0.31 was apparent (Figure 4.11D). This suggests that REP3123 and MetO may have similar effects in their (synergistic) interactions with cyprodinil. Increasing the levels of methionine sulfoxide creates a larger demand on methionine sulfoxide reductases and the NADPH they require for recycling. Specifically, MSRs are known to be involved in the preservation of function of ROS-sensitive FeS clusters (Sideri *et al*., 2009). If the mode of action of cyprodinil in *Z. tritici* is the inhibition of the mitochondrial NADH kinase Pos5p, then this synergistic effect makes sense. However, evidence gathered later during this project, while investigating another synergy, suggests that this may not be the (sole) target for cyprodinil, with the specific mode of action ultimately remaining unknown (see next chapter).

Up to this point, experiments had mostly focused on the potential actions of cyprodinil and their downstream consequences. This included supplementing the combination with antioxidants (Figure 4.10), and testing REP3123 in combination with prooxidants (Figure 4.8 and Figure 4.9). To focus more on the specific role of REP3123 in the synergy with cyprodinil, diphenyleneiodonium (DPI) was tested in combination with cyprodinil (Figure 4.12). DPI is known to decrease intracellular levels of ROS and has previously been used to inhibit the ERK-mediated mismethionylation pathway which relies on ROS signalling (Lee *et al*., 2014), so it was hypothesised that DPI would inhibit mismethionylation as REP3123 is expected to do. When tested together, DPI and cyprodinil were strongly synergistic with an FICI value much lower than that of the REP3123-cyprodinil combination. Across three replicates (all showing synergy), the cyprodinil-DPI combination had a mean FICI of 0.229. The strongest replicate showed 16-fold MIC decreases for both cyprodinil and DPI (Figure 4.12A, red square). REP3123 and DPI were not synergistic (Figure 4.12B).

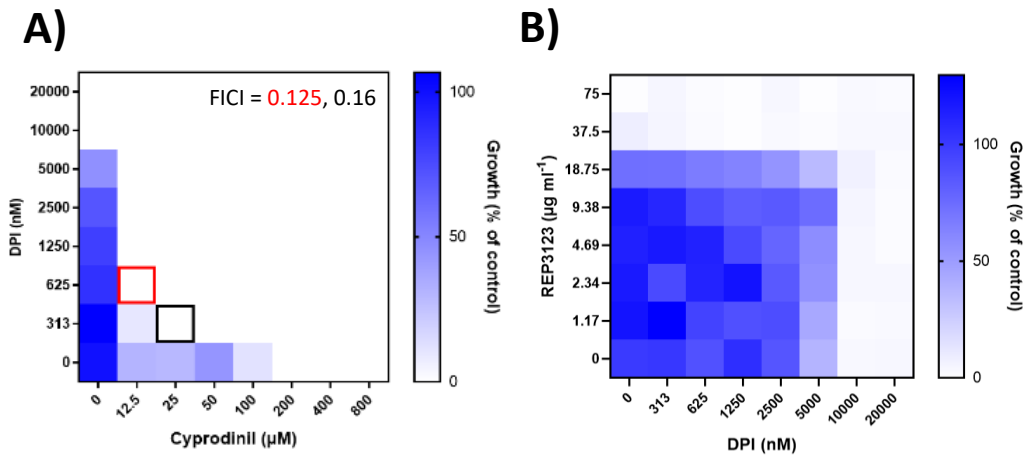

Figure 4.12. **Testing diphenyleneiodonium in combinations**. *Z. tritici* spores were treated with diphenyleneiodonium in combination with A) cyprodinil and B) REP3123. Growth values (scale to the right) represent percentage of growth (OD_{600}) with compounds relative to the minus-compound control. Data were collected at 0 h and 168 h, with incubation at room temperature. Growth values <5% were assigned as no-growth. Red and black squares correspond to FICI values calculated from those wells.

As the cyprodinil-DPI synergy was particularly potent, the focus on cyprodinil was shifted to this combination and away from REP3123-cyprodinil interaction. DPI alone was far more inhibitory than REP3123 alone, requiring low namomolar concentrations to completely inhibit the growth of *Z. tritici*, compared to the low micromolar range of the more expensive REP3123.

4.2.3. Aminoacyl tRNA inhibitors in combination with amino acid biosynthesis inhibitors

As mentioned, cyprodinil was initially understood to be a methionine biosynthesis inhibitor. It had therefore been tested in combination with REP3123 based on the hypothesis that inhibition of the biosynthesis of an amino acid and inhibition of aminoacylation would be synergistic. While cyprodinil is suspected to have an alternative mode of action (inhibition of Pos5p), the underlying rationale for testing it in combination with REP3123 was extended to targeting other amino acids in this 'double attack' on their incorporation into proteins. *B. cinerea* and *Z. tritici* are prototrophic for all amino acids and so can grow in defined media lacking all amino

acids. Therefore, there was no limitation here for which amino acid targets could be tested. Synergies based on this 'double attack' mechanism were tested with four amino acids: methionine, leucine, isoleucine, and tyrosine, for each of which both potential tRNA synthetase inhibitors and biosynthesis inhibitors were available (Table 4.3).

Table 4.3. **Compounds targeting amino acid biosynthesis or aminoacyl-tRNA synthetases**.

Amino acid	tRNA synthetase inhibitor (Reference)	Amino acid biosynthesis inhibitor (Reference)
Isoleucine	Mupirocin C (Paulander *et al*., 2010)	Chlorimuron Ethyl ((Alla and Hassan, 2019)
Leucine	Tavaborole (Jinna and Finch, 2015)	Chlorimuron Ethyl (Alla and Hassan, 2019)
Methionine	REP3123 (Al-Moubarak and Simons, 2011)	Methotrexate (Wang and Chiang, 2012)
Tyrosine	Epigallocatechin gallate (Skupinska *et al*., 2017)	Glyphosate (Geiger and Fuchs, 2002)

Checkerboard experiments were carried out to find any synergies among these inibitor combinations. The leucyl-tRNA synthetase inhibitor tavaborole in combination with chlorimuron ethyl (Figure 4.13), an inhibitor of branched chain amino acid biosynthesis (including leucine), gave an FICI value indicating synergy only in *Z. tritici* in the rich PDB medium (and not MCS), and showed no synergy in *B. cinerea* or in an *S. cerevisiae* strain prototrophic for leucine. The synergy for *Z. tritici* in PDB (Figure 4.13F) had an FICI of 0.375, with two- and four-fold MIC decreases for tavaborole and chlorimuron ethyl, respectively. This particular synergy was then tested in the presence of different branched chain amino acid supplements in the medium, to ascertain whether the synergistic effect was removed when the targeted amino acids were provided (Figure 4.14). Unexpededly, addition of leucine and isoleucine seemed to increase the sensitivity of *Z. tritici* to chlorimuron ethyl, whereas the addition of valine to the

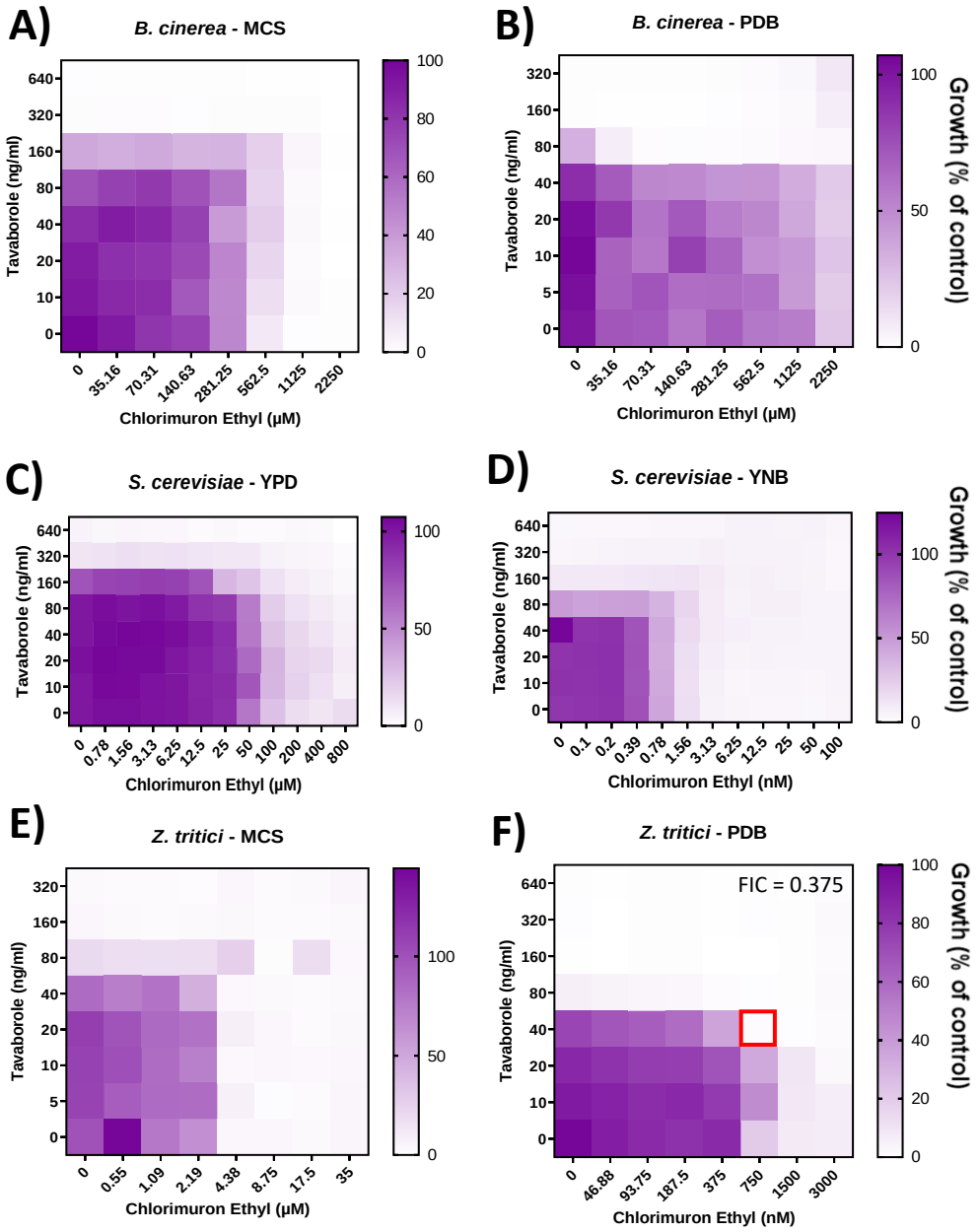

Figure 4.13. **Tavaborole vs chlorimuron ethyl growth-effects in different fungi and media.** Tavaborole and Chlorimuron ethyl were tested against each other in different conditions A) *B. cinerea*, MCS medium ; B) *B. cinerea*, PDB medium ; C) *S. cerevisiae* (leucine prototroph), YEPD ; D) *S. cerevisiae* (leucine prototroph), YNB ; E) *Z. tritici*, MCS ; F) *Z. tritici*, PDB. Growth values (scale to the right) represent means from three independent experiments, calculated as percentages of growth (OD_{600}) with compounds relative to the minus-compound control. Data were collected at 0 h and 168 h (*B. cinerea*, *Z. tritici*), 0 h and 24 h (*S. cerevisiae*. YEPD), and 0h and 48 h (*S. cerevisiae*, YNB). For *B. cinerea* and *Z. tritici*, incubation was at room temperature. For *S. cerevisiae*, incubation was at 30°C. Growth values <5% were assigned as no-growth.

combination did not. According to FICI determinations, leucine and isoleucine suppressed the synergy (Figure 4.14C), although not to the extent evident from the appearance of checkerboards for other fungi for this combination (Figure 4.13). The

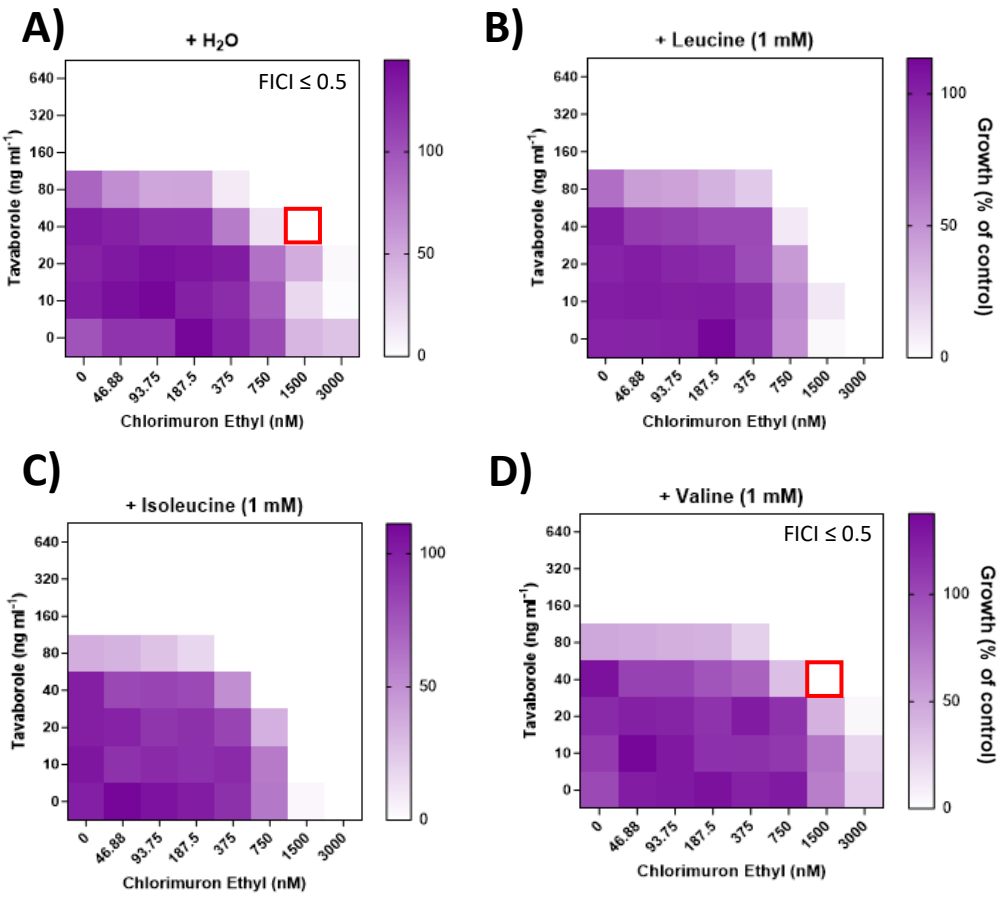

Figure 4.14. **Tavaborole-chlorimuron ethyl combination against Z. tritici in PDB with branched-chain amino acid supplements.** Checkerboards of tavaborole and chlorimuron ethyl against Z. tritici in PDB with branched-chain amino acid supplements in the medium as follows: A) No supplement ; B) 1 mM Leucine ; C) 1 mM Isoleucine ; D) 1 mM Valine. Growth values (scale to the right) represent means from three independent experiments, calculated as percentages of growth (OD_{600}) with compounds relative to the minus-compound control. Data were collected at 0 h and 168 h, with incubation at room temperature. Growth values <5% were assigned as no-growth.

synergy still remains with the valine supplement (Figure 4.14D) and is largely unchanged from the control (both FICI ≤ 0.5).

Following this, combinations of tRNA synthetase inhibitors and amino acid biosynthesis inhibitors that targeted isoleucine, methionine, and tyrosine were tested (Figure 4.15A-F). REP3123 in combination with methotrexate, a reported methionine biosynthesis inhibitor, proved synergistic in both *B. cinerea* (FICI ≤ 0.25, Figure 4.15A) and *Z. tritici* (FIC ≤ 0.375, Figure 4.15B) in PDB medium. In MCS, a possibility of synergy could not be ruled out as the concentrations of methotrexate used did not reach the MIC but were the maximum possible based on solubility and without exceeding 3%

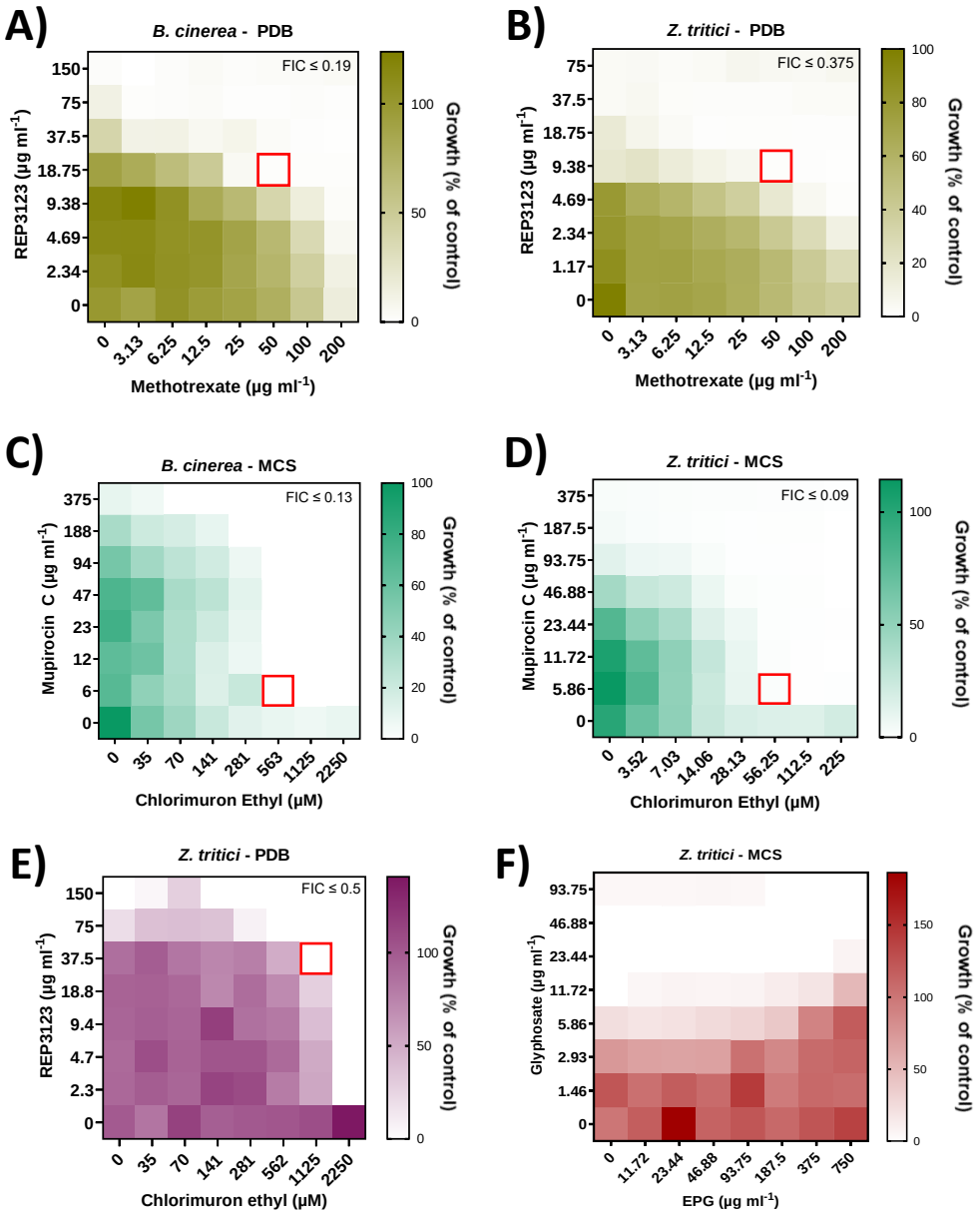

Figure 4.15. **Selected checkerboards of aminoacyl-tRNA synthetase inhibitors in combination with amino acid biosynthesis inhibitors**. *B. cinerea* or *Z. tritici* were treated with different combinations of compounds inhibiting amino acid biosynthesis and tRNA aminoacylation. A) *B. cinerea*, REP3123 vs methotrexate, PDB medium; B) Same combination in *Z. tritici*, PDB; C) *B. cinerea*, mupirocin C vs chlorimuron ethyl, MCS medium; D) Same combination in *Z. tritici*, MCS; E) *Z. tritici*, glyphosate vs epigallocatechin gallate, MCS; F) *Z. tritici*, REP3123 vs chlorimuron ethyl, PDB. Growth values (scale to the right) represent means from four independent experiments, calculated as percentages of growth (OD_{600}) with compounds relative to the minus-compound control. Data were collected at 0 h and 168 h, with incubation at room temperature. Growth values <5% were assigned as no-growth.

DMSO solvent concentration (Appendix Figure 8.6). In PDB, the calculated FICI values propose an MIC for methotrexate of 400 µg ml^{-1} (the next concentration in the series, which could not be tested) so returned values are a potential underestimate. Further

supporting the 'double attack' hypothesis, synergies between mupirocin C, an isoleucyl-tRNA synthetase inhibitor, and chlorimuron ethyl were found in *B. cinerea* (FIC ≤ 0.5, Figure 4.15C) and *Z. tritici* (FIC ≤ 0.16, Figure 4.15D, black square). In contrast to the tavaborole and chlorimuron ethyl synergy, these occurred in MCS medium but not in PDB (Appendix Figure 8.6). The tyrosyl-tRNA synthetase inhibitor, epigallocatechin gallate, was not synergistic with the tyrosine biosynthesis inhibitor, glyphosate. In fact, this combination appeared to be antagonistic, although an accurate MIC could not be determined for reasons similar to those explained above (Figure 4.15F).

Each amino acid biosynthesis inhibitor and aaRS inhibitor was then cross-tested with each other. This was to determine whether synergies only arose with inhibitor combinations that targeted the same amino acid (as tested above). Only one of the eight alternative pairwise permutations showed synergy (Figure 4.15E), with the rest showing no synergy (data not shown). The metRS inhibitor REP3123 was synergistic with the branched chain amino acid inhibitor chlorimuron ethyl against *Z. tritici* in PDB medium (but not MCS). Chlorimuron ethyl has been shown to cause production of reactive oxygen species (Cobb and Reade, 2010; Caverzan *et al*., 2019), which could be a potential explanation for this synergy. As mentioned previously, REP3123 was hypothesised to be synergisitic with ROS-inducers due to its role in preventing increased mismethionylation, although earlier tests with various pro-oxidants (described above) did not support that. To summarise, there was a higher frequency of synergies in combinations of tRNA synthetase inhbitors and amino acid biosynthesis inhibitors that targeted the same amino acid (3 in 4) than those that did not (1 in 8). This was supportive of the 'double attack' hypothesis as a rational approach to finding these antifungal synergies, even though synergy was not seen for every combination, and the media condiditons were variable.

4.2.4. Screening the Prestwick Chemical Library against REP3123

Whereas this chapter largely focuses on rational approaches taken for discovering synergies, high throughput methods can also be used to 'fish' for chemical-chemical interactions (He *et al*., 2018; Flobak *et al*., 2019; Augostine and Avery, 2022). In the previous chapter, the Prestwick Chemical Library (PCL) was screened against the leucyl-tRNA synthetase inhibitor, tavaborole. It was reasoned that this higher throughput approach may increase the chances of finding synergies with this compound. Unfortunately, none were found. During this experiment, the 28 best-performing compounds in combination with tavaborole were retested in a smaller screen and the results from this experiment were shown in the previous chapter. REP3123 was also tested against these 28 compounds (Figure 4.16). At the 72 h timepoint one compound showed some potential for synergy, with around ~25% growth when supplied alone, but complete inhibition in combination with REP3123 (Figure 4.16A). However, at the 96 and 168 h timepoints, this compound showed complete inhibition both alone and in combination. Therefore, as with tavaborole these 28 chemical compounds from the PCL did not show synergy when in combination with REP3123. That is not to say that other compounds from the PCL might prove synergistic with REP3123 in a wider screen.

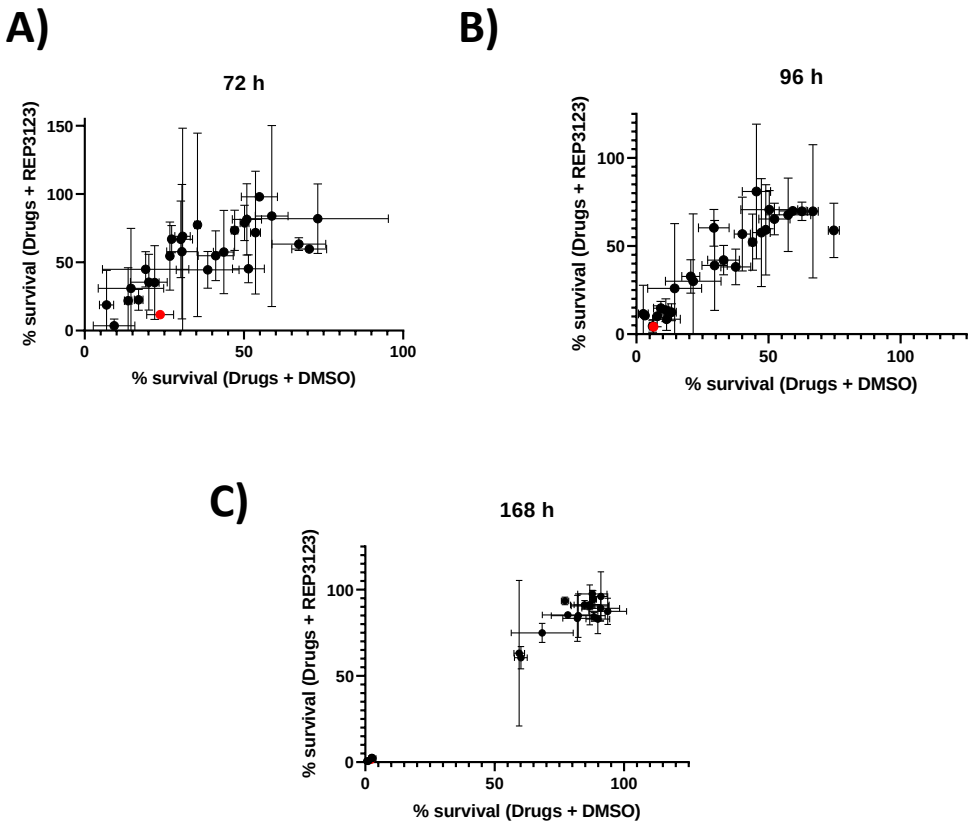

Figure 4.16. **PCL screen follow up**. Percentage growth (compared to untreated control) of *Z. tritici* after culture with 10 µM selected compounds of interest from the Prestwick Chemical Library alone or in combination with REP3123 after A) 72 h; B) 96 h; C) 168 h. Each dot represents a different compound. n = 3.

4.3. Discussion

4.3.1. REP3123 and S-transport inhibitors

The apparent resistance of tavaborole to synergy that was evident from the previous chapter contrasted to the success of the rational-driven approach for discovering novel synergies in this chapter. With REP3123 and S-transport inhibitors, the proposed mechanism of synergy was based on inhibition of methionine biosynthesis, caused by impaired sulphur transport (Pereira *et al*., 2008; Holland and Avery, 2011), working in concert with REP3123-mediated inhibition of $tRNA^{Met}$ charging (Al-Moubarak and Simons, 2011). This synergy was the first trial of the amino acid/aminoacylation 'double attack' in which the availability of a particular amino acid for protein synthesis is targeted two ways: i) decreased amino acid availability through inhibition of biosynthesis, and ii) inhibition of the aaRS required for aminoacylation of the cognate tRNA. However, it is possible that this was not the sole mechanism involved in the REP3123/S-transport inhibitor synergies. It was shown that sodium bicarbonate, sodium orthovanadate, and sodium selenate all caused the pH of the MCS medium to increase, conditions which could account for REP3123 being twice as effective at inhibiting *Z. tritici*. *Z. tritici* itself, however, has been shown to have similar growth from pH 4.5-8 (Lynch *et al*., 2016). Combinations are described as synergistic if the FICI value is ≤ 0.5. This translates to a minimum of a four-fold decrease in MIC for each compound when in combination as opposed to when applied individually. Therefore, the changes in pH alone could not account for the full effect on MIC values that were needed to achieve synergy. In addition, unlike REP3123, the four-fold decreases in MIC of the S-transport inhibitors (when combined with REP3123) could not be explained by a pH effect, strengthening the case that the proposed strategy could be a viable one for antifungal synergies. It was noted that there was considerable variability

between replicate experiments, with only the REP3123-sodium bicarbonate synergy consistently evident between replicates. This might suggest that the REP3123-NaBIC combination holds the greatest promise for a fungicidal treatment. Despite attempts, the experiment-experiment variation could not be controlled and may have arisen from variables outside reasonable control, e.g., day to day fluctuations in laboratory temperature, or water quality.

4.3.2. REP3123 and cyprodinil

Unfortunately, the mode of action of cyprodinil has been contested for the duration of this PhD. It was originally thought to be a methionine biosynthesis inhibitor (Masner *et al*., 1994), hence the reason for testing this compound in combination with REP3123. However, subsequent information indicated that the mode of action for cyprodinil was instead through inhibition of the mitochondrial NADH kinase, Pos5 (Mosbach *et al*., 2017, Andy Corran, Syngenta).

Due to the role of NADPH in the recycling of oxidised antioxidants, the role of cyprodinil in this synergy could be to raise the level of oxidative stress. However, with REP3123 not proving to be synergistic with methionine sulfoxide or any of the ten pro-oxidant compounds tested, this hypothesis was considered unlikely. Of these ten, electrolysed water (EW) showed the most promising checkerboard results. However, a synergistic FICI was not recorded. Cyprodinil may act by several mechanisms with more than one required to achieve synergy with REP3123, although such scenarios have been proposed to be less likely to yield synergies (Harvey *et al*., 2023).

Although the range of experiments performed here did not pinpoint cyprodinil's role in the synergy, some progress was made in elucidating that of REP3123. Methionine sulfoxide (MetO) mimicked the action of REP3123 in synergising with cyprodinil. In this case, MetO potentially may increase sensitivity to oxidative stress by increasing the

demand on antioxidants (and the NADH required to recycle them), specifically increasing potential harm to FeS clusters (Sideri *et al*., 2009). Via inhibition of MetRS, REP3123 also theoretically increases sensitivity to oxidative stress by preventing increased levels of mismethionylation which would normally protect proteins from damaging reactive oxygen species (Wiltrout *et al*., 2012).

As *Z. tritici* is currently not as amenable to genetic manipulation as certain other fungi (Talbot, 2015), this tool was not utilised to improve understanding of the REP3123-cyprodinil synergistic mechanism. It was unfortunate that this synergy was not present in *S. cerevisiae*, as that could have opened a wide range of genetic tools. Dual fluorescence reporters of amino acid misincorporation were considered for helping to find the mode of synergistic action. Application of a construct involving TagRFP, a red fluorescent protein with a methionine essential for fluorescence (Lee *et al*., 2014), could have helped explore whether; i) the mismethionylation-inhibiting mechanism of REP3123 was involved in the synergy, and/or ii) that cyprodinil specifically enhanced this effect. However, as the cyprodinil-diphenyleneiodonium synergy proved significantly stronger, at this stage the focus of research moved to that combination.

4.3.3. Amino acid 'double attack'

The hypothesis that synergies would be found between compounds that inhibit amino acid biosynthesis and compounds that inhibit tRNA aminoacylation was generally supported. In total, four combinations were found (excluding REP3123-cyprodinil, given uncertainty over the cyprodinil mode of action), including one for tavaborole for which no synergy was found in the previous chapter. While limited assays were carried out to test the proposed synergy mechanisms for these combinations, the reported mechanisms for each of these compounds leaves this 'double attack' mechanism as a possibility. For the tavaborole-chlorimuron ethyl synergy, it was shown that

supplementation with leucine and isoleucine suppressed the synergistic effect, supporting the proposed mechanism. However, it is important to be mindful that such a test was exactly how cyprodinil was (mis)identified as a methionine biosynthesis inhibitor (Masner *et al*., 1994), although methionine has the notable other property of being an antioxidant. Nevertheless, further support could have been added here by carrying out similar amino acid supplementation tests with all the combinations of interest, to see if the relevant targeted amino acid could suppress synergy. It is also important to understand why the synergy was only present in certain media. A further angle could be genetic manipulation (where feasible); for example, by altering expression level of the relevant tRNA synthetase and testing for altered strength of synergy.

While it was expected that aaRS inhibitors would be synergistic with inhibitors of cognate amino acid biosynthesis, cross-testing was carried out to see if attacking the incorporation of two separate amino acids via these mechanisms could be synergistic. As shown in Figure 4.15, cross-testing an amino acid biosynthesis inhibitor with an inhibitor of a non-cognate aminoacyl-tRNA synthetase can give synergy. While this was achieved with chlorimuron ethyl, an inhibitor of biosynthesis of three amino acids, this suggested that there are, at minimum, 400 combinations to be tested when considering the possibility of compounds that only target one amino acid/aaRS each. In addition, another 380 combinations could be carried out with two different (single) amino acid biosynthesis inhibitors, and again another 380 combinations with two inhibitors of different aminoacyl-tRNA synthetases. Although cross-testing only yielded one synergy of eight combinations tested, extrapolating this 12.5% success rate would give 195 synergies if consistent. In addition, this does not cover potential inhibitors of tRNA molecules themselves (Chopra and Reader, 2015), which would exponentially increase the number of possible combinations.

Being eukaryotes, fungi offer a limited number of realistic targets for the types of drug interactions to explore here. Target proteins should ideally have diverged enough from their human and plant counterparts in order to decrease toxicity concerns. As outlined in the previous chapter (see 3.1), the protein synthesis machinery is relatively conserved between eukaryotes. However, in the case of a synergy, it might not be the case that both compounds need have a fungus-specific target. If one of the compounds of a synergistic pair had specificity for a fungal target and the combinatorial synergy was potent enough, then the second inhibitor might only be needed at concentrations low enough to preclude potential cytotoxicity concerns. With amino acid biosynthesis (Jastrzębowska and Gabriel, 2015), aminoacyl-tRNA synthetases (Hurdle *et al*., 2005; Kwon *et al*., 2019; Chakraboti *et al*., 2021; Kushwaha and Capalash, 2022), and even tRNAs themselves (Chopra and Reader, 2015) seen as therapeutic targets with potential, it is possible that synergies may alleviate some concerns, while increasing the promise of these targets.

4.3.4. REP3123 and the Prestwick Chemical Library (PCL)

As with tavaborole (3.3.3), the high-throughput method of screening REP3123 for synergy did not yield any synergies. However, in this case REP3123 was only tested in combination with the 28 most promising compounds taken forward from the initial screen with tavaborole, and not with the entirety of the 1280 chemicals of the PCL library. It is quite possible that REP3123, with its extra action of preventing mismethionylation, could have had more potential for synergy than tavaborole and broader screens than done here could prove worthwhile.

4.3.5. Final Remarks

This research was initiated because of the perceived potential for aminoacyl-tRNA synthetase inhibitors as components of synergistic fungicidal combinations. While the

previous chapter did not reveal clear synergies involving the LeuRS inhibitor, tavaborole, the research carried out in this chapter was successful in identifying several combinatorial synergies involving aaRS inhibitors. Although the mechanisms of synergy were not fully corroborated here, most of these synergies are hypothesised to exist due to the combined effect (on an amino acid's availability for protein synthesis) of inhibiting amino acid biosynthesis and inhibiting aminoacyl-tRNA synthetases. While some of the compounds used are considered toxic to humans, this research shows that these combinations are effective at killing fungal pathogens of crops, namely *B. cinerea* and *Z. tritici*. If more selective inhibitors can be discovered or developed, the strategy pursued here, and potentially strategies involving tRNA inhibitors also (i.e., in addition to aaRS inhibitors and amino acid biosynthesis inhibitors), could allow for at least 1200 possible combinations. This has implications not just for fungal phytopathogens, but potentially also other undesirable fungi, and could offer fresh direction for protein synthesis as a legitimate target for fungal inhibition.

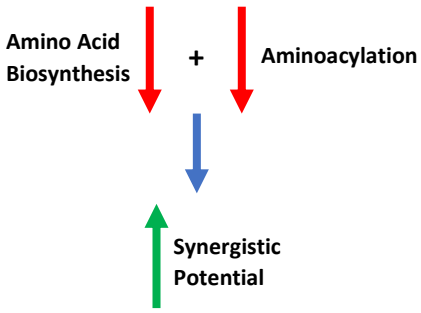

Figure 4.17. **Schematic of synergistic potential between agents inhibiting amino acid biosynthesis and agents inhibiting aminoacylation.** Several synergies were discovered between inhibitors of amino acid biosynthesis and inhibitors of aminoacylation. However, this combination type did not always lead to synergy. An increase in molecules exhibiting theses modes of action could increase the arsenal against fungal pathogens.

Chapter 5 - Unravelling bases for synergistic inhibition of fungal growth by cyprodinil combined with diphenyleneiodonium

5.1. Introduction

5.1.1. Background

This PhD was initially concentrated on discovering novel fungicidal synergies utilising compounds targeting protein synthesis with a focus on (possible) mistranslation. The compound that was the focus of initial interest, tavaborole, is a leucyl-tRNA synthetase (LeuRS) inhibitor that was hypothesised to cause mistranslation – and therefore to have an increased chance of synergy with other mistranslation-inducing compounds (Moreno-Martinez *et al*., 2015). However, no synergies were found between tavaborole and other mistranslation-inducing compounds. In addition, evidence did not support that tavaborole induces mistranslation (3.3.2). Therefore, tavaborole was not pursued further and another aminoacyl-tRNA inhibitor, REP3123, was explored.

REP3123, an inhibitor of MetRS (Al-Moubarak and Simons, 2011), was hypothesised to have a greater chance of synergy with compounds acting in other ways (compared to tavaborole) due to the additional function of MetRS in the mismethionylation of non-cognate tRNA molecules (Netzer *et al*., 2010), which can increase methionine misincorporation and aid in the protection of proteins from reactive oxygen species (ROS). REP3123 in combination with cyprodinil, which was originally believed to be an inhibitor of methionine biosynthesis but is now considered a likely inhibitor of mitochondrial NADH kinase Pos5p (Mosbach *et al*., 2017; personal communication, Andy Corran, Syngenta), proved to be synergistic against the wheat pathogen *Zymoseptoria tritici* (Fones and Gurr, 2015). To understand if inhibition of mismethionylation was involved in the REP3123-cyprodinil synergy, cyprodinil was tested in combination with diphenyleneiodonium (DPI), a known inhibitor of this pathway (Lee *et al*., 2014). This cyprodinil-DPI (CYP-DPI) combination proved to be far more potent than that of CYP-REP3123 (Figure 4.6). The focus of the PhD then shifted

towards trying to understand the mechanism behind this novel synergy and exploring its potential to provide protection from *Z. tritici* growth and infection.

5.1.2. Cyprodinil

Cyprodinil is a systemic, broad-spectrum anilinopyrimidine fungicide commonly used in the control of different ascomycete fungal phytopathogens, including *B. cinerea* (Rupp *et al*., 2017).

NADH kinases are responsible for the production of cellular NADPH, which is essential for the recycling of antioxidants such as N-acetyl cysteine, glutathione, and ascorbic acid, as well as for the recycling of the methionine sulfoxide reductases (MSRs) that reduce oxidised methionine (methionine sulfoxide) (Jamieson, 1998; Carmel-Harel and Storz, 2000; Weissbach *et al*., 2002). This recycling is especially vital in the mitochondria (where Pos5p is localised), as mitochondrial processes generate harmful reactive oxygen species (Boveris and Cadenas, 1982). The phosphorylation catalysed by Pos5p is thought to be the main source of NADPH in the mitochondria (Outten and Culotta, 2003), as NADPH molecules are unable to cross into (and out of) this organelle (Lewis *et al*., 2014; Nikiforov *et al*., 2011). In addition to the recycling of antioxidants, NADPH functions to provide the reducing equivalents for biosynthetic reactions and, in some organisms, enabling generation of free radicals by NAD(P)H oxidases for defence or signalling purposes (Takemoto *et al*., 2007).

SWITCH, a fungicide mixture of cyprodinil and fludioxonil, is a 'hyperactivator' of the high osmolarity glycerol signalling pathway (Yoshimi *et al*., 2005) and is currently used for treating *B. cinerea* infections (Saito *et al*., 2016). The development of alternative combinations involving cyprodinil would be valuable for broadening the treatment options (particularly in the face of growing fungicide resistance), including against other fungal phytopathogens such as *Z. tritici*.

5.1.3. Diphenyleneiodonium

Diphenyleneiodonium (DPI) is a compound that is known to broadly inhibit NAD(P)H oxidases (Riganti *et al*., 2004). NAD(P)H oxidases (Nox) are membrane-bound complexes found in a range of different organisms (Segal, 2008). Fungi possess three Nox subfamilies: NoxA, NoxB, and NoxC and, although there are large similarities across the fungal kingdom, these three families are not always all present in certain fungi and can even serve different purposes in different fungal species (Aguirre *et al*., 2005; Takemoto *et al*., 2007).

Reactive oxygen species (ROS) generated by Nox enzymes serve a multitude of signalling roles in fungal cellular differentiation. This includes hyphal tip growth, spore germination, and sexual development (Takemoto *et al*., 2007). Deletion of Nox genes in some phytopathogenic species is reported to reduce pathogenicity – including in *Z. tritici* (Choi *et al*., 2016) – and deletion of Nox genes in some mutualistic fungi is associated with fungal overgrowth and plant death (Takemoto *et al*., 2007).

Inhibition of these molecules has several downstream effects, including disruption of the processes regulated by Nox proteins (Tanaka *et al*., 2006). DPI is a general NAD(P)H oxidase inhibitor and is known to inhibit the fungal-specific NADH dehydrogenases. These enzymes are bound to the inner mitochondrial membrane (von Jagow and Klingenberg, 1970) and offer an alternative route for electrons to be donated to the electron transport chain (ETC), bypassing complex I (Joseph-Horne *et al*., 2001). DPI has also been shown to inhibit complex I in non-fungal mitochondria (Fato *et al*., 2009). Therefore, DPI can disrupt cellular respiration, decreasing mitochondrial ROS (mROS) and, inevitably, ATP production (Li and Trush, 1998). As mentioned, inhibition of Nox by DPI has also been used as a research tool to prevent the increase in mismethionylation in response to elevated ROS levels (Lee *et al*., 2014), or simply to

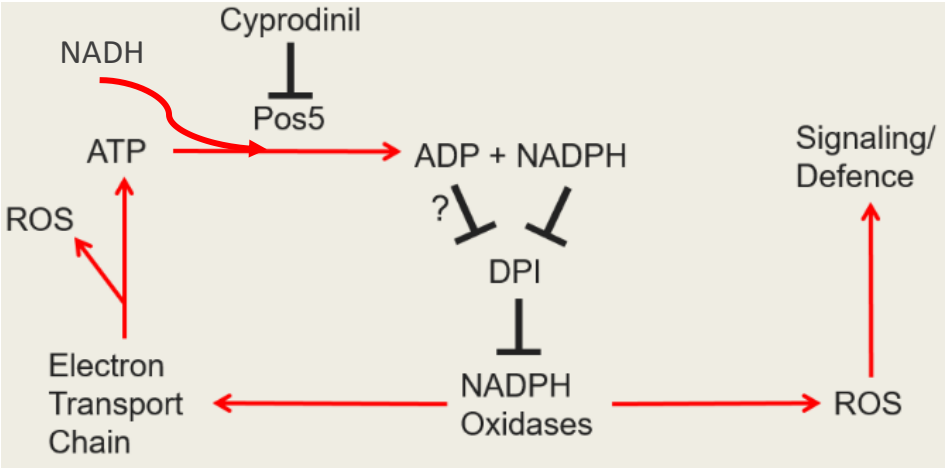

Figure 5.1. **Schematic of potential interactions between cyprodinil and diphenyleneiodonium**. DPI can inhibit the electron transport chain, decreasing ATP production. Cyprodinil leads to a decrease in mitochondrial NADPH. NADPH has been shown to block DPI inhibition. This schematic does not highlight downstream inhibitory effects of each compound. Arrows indicate links between cellular processes/proteins/products. Black shapes indicate inhibition.

decrease ROS levels within cells of interest (Li and Trush, 1998). In addition, NADPH has previously been shown to prevent *in vitro* inhibition of mouse macrophage flavoproteins by DPI (Stuehr *et al*., 1991), suggesting that cyprodinil may also decrease the natural defence against DPI within the mitochondria. This is summarised in Figure 5.1.

However, Riganti *et al*. (2004) have suggested that due to DPI's non-specific, broad range inhibition, that results from *in vitro* and *in vivo* experiments with DPI should be "interpreted with caution". It was shown that DPI significantly inhibited both the pentose phosphate pathway (PPP) and the tricarboxylic acid (TCA) cycle, increased ROS generation (in contrast to decreased ROS levels mentioned above), lipoperoxidation, and leakage of lactate dehydrogenase activity in the extracellular medium. In addition, DPI decreased the glutathione/glutathione disulfide ratio in N11 glial cells (among other cell types), while increasing the efflux of glutathione out of the cells (Riganti *et al*., 2004). It was also shown that cells were protected from these effects of DPI inhibition when supplemented with glutathione. Ultimately, Riganti *et al* suggested that DPI inhibited the PPP and TCA cycle through broad inhibition of

different NAD(P)-dependent enzymes, such as glucose 6-phosphate dehydrogenase, glyceraldehyde 3-phosphate dehydrogenase, and lactate dehydrogenase. While an initial hypothesis behind the synergism between was based on the mechanisms outlined in Figure 5.1, it is important to keep in mind all of the potential targets of DPI and the subsequent consequences on the cell.

5.1.4. Chapter aims

This chapter aims to understand the mechanism behind the powerful synergy between cyprodinil and diphenyleneiodonium. Through understanding this mechanism, it is possible that more, similar synergies may be identified that could aid in combatting fungal phytopathogens.

5.2. Results

5.2.1. Testing the cyprodinil-diphenyleneiodonium synergy in different organisms

The synergy between REP3123 and cyprodinil found in the previous chapter was only present against *Z. tritici*, limiting the tools that were available/feasible to characterise the synergistic mechanism. The cyprodinil-diphenyleneiodonium (CYP-DPI) synergy was first tested *B. cinerea* and corroborated in *Z. tritici* (Figure 5.2). In this set of experiments, the synergy was present in *Z. tritici* with an average FICI of 0.19. In the strongest replicate (all of which were synergistic), the MIC of both cyprodinil and DPI decreased 16- and 32-fold, respectively, when in combination. When tested against *Botrytis cinerea*, a phytopathogen against which cyprodinil is currently an approved treatment, the FICI in two of three replicates was 0.5, with one replicate non-synergistic. These four-fold reductions in MIC are considerably smaller than when the combination is applied to *Z. tritici*, although are still synergistic. However, these experiments show that *Z. tritici* is far more sensitive to the combination than *B. cinerea*.

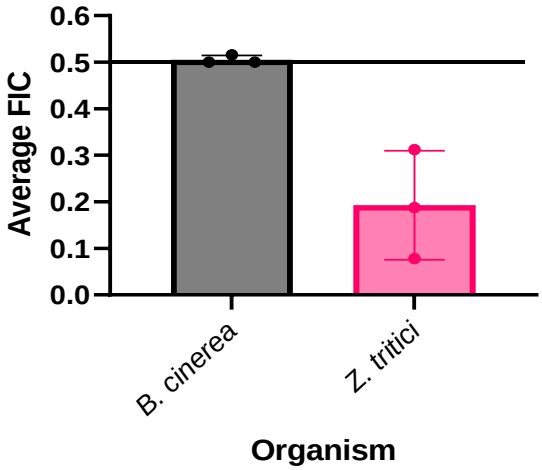

Figure 5.2. **CYP-DPI synergy is present in *B. cinerea* and *Z. tritici***. *B. cinerea* and *Z. tritici* spores were treated with cyprodinil and DPI in checkerboard format. Data were collected at 0 h and 168 h, with incubation at room temperature. Growth values <5% were assigned as no-growth. Bars show FICI from three independent experiments calculated as described (see 2.2.7.4). Error bars show standard deviation. Horizontal black bar shows FICI cut-off for synergy.

5.2.2. Testing the initial hypothesis of combined activity against NADPH production in the mitochondria

As a proposed inhibitor of Pos5p, cyprodinil is believed to inhibit the production of NADPH in the mitochondria. The phosphorylation of NADH to NADPH requires ATP, most likely generated via the electron transport chain.

5.2.2.1. CYP-DPI synergy is still present in rho^0 yeast

Figure 5.3A shows that the CYP-DPI synergy is also present against *S. cerevisiae*. Therefore, a wider set of genetic tools can be utilised, especially when compared to the REP3123-CYP synergy that was found only in *Z. tritici*.

Diphenyleneiodonium (DPI), an inhibitor of NAD(P)H oxidases, is known to inhibit the yeast alternative NADH dehydrogenases present in the electron transport chain (Fang and Beattie, 2003). As such, DPI may inhibit the production of ATP. As ATP is required by the phosphorylation reaction catalysed by Pos5, this could be (part of) the mechanism of the CYP-DPI synergy. Both compounds may introduce limiting factors for the reaction catalysed by Pos5p, i.e., limiting the phosphorylation of NADH to produce NADPH; i) DPI may decrease the availability of the ATP substrate. ii) Cyprodinil may decrease the availability/activity of Pos5p. To see if the ATP generated by the ETC was crucial for the synergy, the combination was applied to rho^0 *S. cerevisiae* that had previously been generated under artificial growth conditions utilising ethidium bromide (Grant *et al*., 1996; Kukat *et al*., 2008). Rho^0 strains possess dysfunctional mitochondria and so do not have a fully functioning electron transport chain. More evidence was gained for this by an inability to grow using the respiratory substrates ethanol and glycerol (data not shown). However, although the ethidium bromide

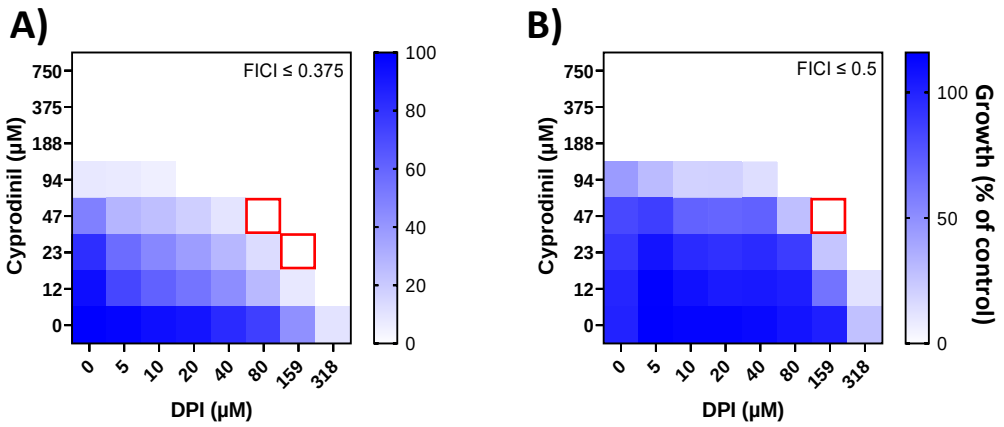

Figure 5.3. **CYP-DPI synergy is present in yeast with or without functioning mitochondria**. Exponential phase W303 *S. cerevisiae* were treated with cyprodinil and diphenyleneiodonium in a checkerboard format. Different strains used were A) Wild-type W303; B) rho^0 W303 (see Materials and Methods). Growth values (scale to the right) represent means from three independent experiments calculated as percentages of growth (OD_{600}) with compounds relative to the minus-compound control. *S. cerevisiae* was grown in YNB medium at 30°C, and data were collected at 0 h and 24 h. Growth values <5% were assigned as no-growth. DPI MIC assumed to be 636 μM for FICI calculation. Red squares indicate concentrations used to calculate FICI values.

method has often been used for the generation of rho^0 mutants, the results could indicate a defect in gluconeogenesis and so measurements directly measuring the respiratory activity of mitochondria may have been more appropriate.

Synergistic action of the CYP-DPI combination was retained in rho^0 *S. cerevisiae*, although the recorded FICI was weaker than that of the WT strain that possessed fully functional mitochondria (Figure 5.3). The control strain showed four- and eight-fold decreases of cyprodinil and DPI MICs when in combination (Figure 5.3A), while the rho^0 strain showed only four-fold decreases for the MIC of both compounds. Note, as no MIC was reached for DPI, it was assumed that 636 μM was the MIC. As an assumption must be made regarding MIC, it is possible that the true FICI values are lower, meaning stronger synergies. (This method of assuming an MIC is utilised throughout as needed.) Additionally, while a lack of MIC difference between the WT and rho^0 strains suggests that the ETC is not important for the mechanism of action for either compound, this is not certain for DPI as the MIC was not reached. It is

unfortunate that tests looking into defects in gluconeogenesis were not carried out as it cannot be stated for certain whether these strains truly had defects in the ETC.

5.2.2.2. Anaerobic conditions do not consistently remove the CYP-DPI synergy

In addition to rho^0 yeast, the CYP-DPI synergy was applied to *S. cerevisiae* grown in anaerobic conditions. Under anaerobic conditions the oxygen-dependent electron transport chain cannot function. If the ETC was the synergistic target, then it would be expected that the synergistic effect is lost in anaerobic conditions. When grown in aerobic conditions, the FICI of W303 *S. cerevisiae* was ≤0.16 (Figure 5.4A) compared to an FICI of ≤0.31 under anaerobic conditions (Figure 5.4B). As the synergy is present in both conditions, it is unlikely that inhibition of the ETC is the (sole) target for synergy, and that one of the other effects of DPI inhibition is at play. Nevertheless, the synergy is weaker in anaerobic conditions, as it was in the rho^0 mutant (Figure 5.3), although this is not significant (p value = 0.4549, paired t-test.

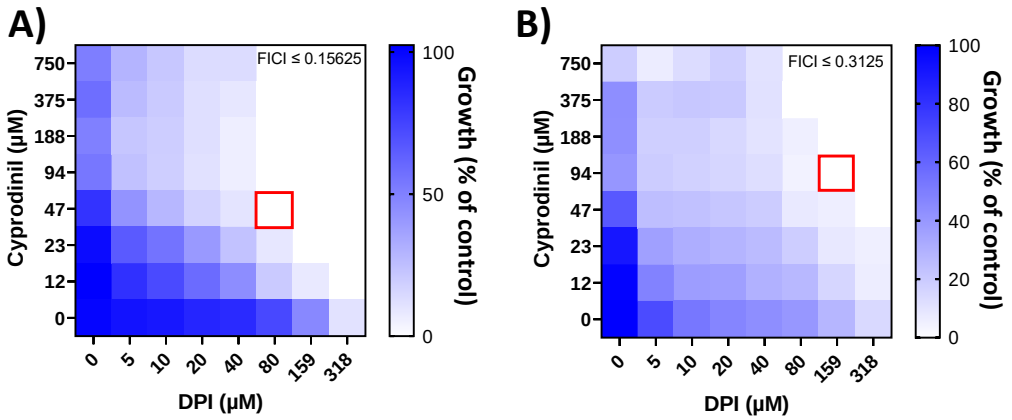

Figure 5.4. **CYP-DPI synergy in aerobic and anaerobic conditions.** Exponential phase *S. cerevisiae* were treated with cyprodinil and diphenyleneiodonium in a checkerboard format. A) W303, aerobic, YEPD; B) W303, anaerobic, YEPD. Growth values (scale to the right) represent means from three independent experiments calculated as percentages of growth (OD_{600}) with compounds relative to the minus-compound control. Plates were incubated at 24°C, and data were collected at 0 h and 24 h. Growth values <5% were assigned as no-growth. Cyprodinil and DPI MICs assumed to be 1500 μM and 636 μM, respectively, for FICI calculations. Red squares indicate concentrations used to calculate FICI values.

5.2.3. Screening heterozygous yeast deletant library to identify individual cyprodinil and DPI targets involved in synergy

5.2.3.1. Relevance of the screen

As the synergy was not (or only partially) reliant on the ETC, a broader approach was adopted. Screening a heterozygous yeast deletion library may help characterise proteins targeted by one or both compounds involved in the synergy, especially as the heterozygous library encompasses essential gene functions unlike the homozygous deletants. Haploinsufficiency as a result of heterozygosity for essential gene functions can be amplified by drugs that target those functions (Lum *et al*., 2004). Here, if inhibition of an essential protein by cyprodinil was important for the synergy, then a yeast strain containing only one copy of the corresponding gene would be expected to be more sensitive to DPI than a control strain with both copies. In this study, the heterozygous yeast deletant library of essential genes was screened with the aim of identifying potential targets involved in the CYP-DPI synergy. Strains with deletions of non-essential genes under standard growth conditions are not included in the library used.

5.2.3.2. Library screen revealed both resistant and sensitive mutants to the CYP-DPI synergy

Cyprodinil and DPI were tested at concentrations that were on average only slightly inhibitory compared to a DMSO control. This equated to ~88% growth compared to the control for cyprodinil and ~82% growth compared to the control for DPI (Figure 5.5). For the combination, there was a large difference between the two technical replicates with ~68% and 38% growth compared to the control (Figure 5.5). Such variation may impact the discovery of genes relevant to the synergy. Genes that showed either a >10% increase (considered resistant) or decrease (considered

sensitive) in percentage growth compared to the upper and lower quartiles of control growth, respectively, were considered hits. 33 strains were taken forward for further testing out of a total of 1180 (2.8% of strains tested).

These selected heterozygous strains were then used in dedicated growth-curve assays in plate readers, enabling calculation of maximum growth rate and the time of culture after which that maximum growth rate was attained, for each strain against every condition (Figure 5.6). In these assays, the control strain *S. cerevisiae* BY4743 appeared to grow more slowly than most of the deletion strains tested, even under control conditions, achieving lower maximum growth rates and longer time to reach the maximum growth rates (Figure 5.6A). All strains used were diploid with the same auxotrophies.

The results for the wild-type were considered unreliable for this particular experiment as their growth rate was much lower than each deletion mutant tested. Occasional similar experiences in the past have usually been corrected after replacing with a fresh stock from the freezer. Instead, mutants were compared with each other to indicate those with the greatest resistance or sensitivity, according to maximum growth rate and/or culture time needed to reach that maximum compared to the median value in each condition calculated from all 33 strains. There were 33 deletion strains tested. As such, the median maximum growth rate and the median time to reach maximum growth rate of these 33 strains were used as benchmarks for determining increased sensitivity/resistance. In each experimental condition, there were strains that met one or more of these criteria. First, it was noted that seven strains reached exponential

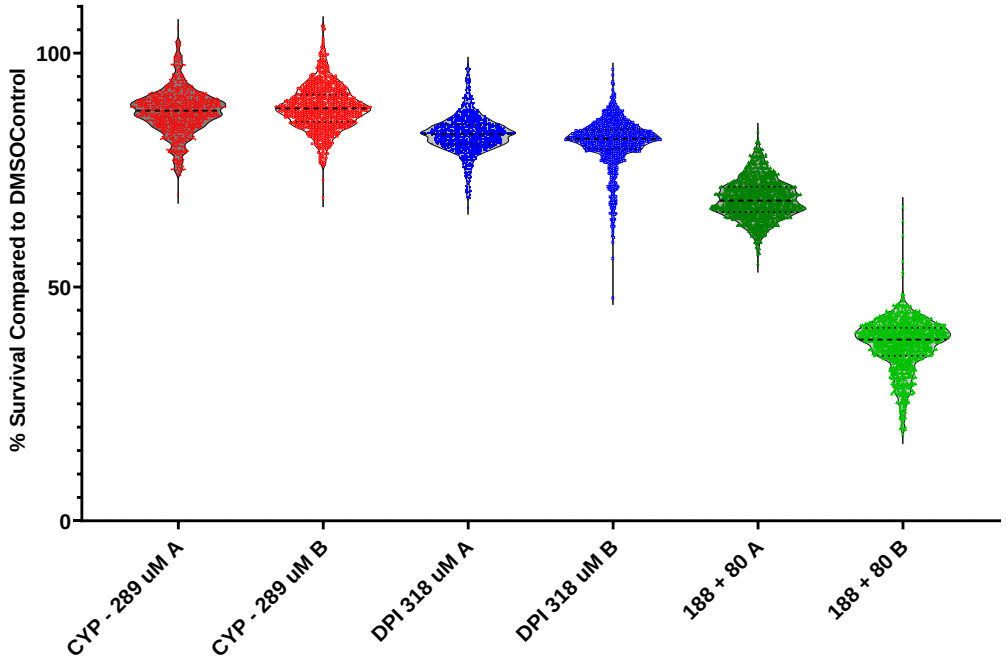

Figure 5.5. **Sensitivity of heterozygous yeast deletion strains sensitivity to cyprodinil, DPI, and the combination**. Heterozygous deletion strains of *S. cerevisiae* (BY4743 background) stored in 96-well plates were thawed from -80°C and 80 µl of YEPD containing 200 µg ml^{-1} geneticin was added to each well. Plates were covered with a gas-permeable plastic seal and incubated overnight at 30°C at 200 rev min^{-1}. 5 µl of each cell culture was then added to 95 µl of YEPD medium containing desired treatment. Plates were homogenised by shaking for 30 seconds before being read at 595 nm on a Tecan plate reader. Plates were sealed again, placed in plastic lunch boxes containing soaked blue paper towel and incubated overnight at 30°C at 200 rev min^{-1}. '188 + 80' indicates 188 uM CYP + 80 uM DPI Plates were read at 6 h and 24 h. n = 2 biological replicates (both shown).

phase slower (~3.5-8 h) than all other strains (~3 h) in the control DMSO treatment, with 26 strains reaching exponential phase ~3 h (Figure 5.6A). Strains were considered sensitive or resistant to a treatment if they were ≥10% higher or lower than the median for either of these measures, with a higher maximum growth rate considered resistant, and an earlier (lower) time point to achieve this growth rate considered resistant. Strains that showed opposite phenotypes between Figure 5.5 and Figure 5.6 were discounted as they were not consistent in different assays.

When treated with 50 µM cyprodinil, four individual strains showed particular resistance for both measures. Some strains showed resistance in only one of the two measures (Figure 5.6B). When 250 µM of cyprodinil was used, five individual strains showed resistance by both measures (Figure 5.6C). However, there was no overlap in

strains between these two concentrations of cyprodinil. Some strains did show resistance at both concentrations, but not across both measures.

The *nop8/NOP8* strain, heterozygous for the Nop8 nuclear protein, required for 60S ribosomal subunit biosynthesis (Zanchin and Goldfarb, 1999), showed increased sensitivity in both measures to both cyprodinil concentrations. However, this strain also showed resistance to the CYP-DPI combination (Figure 5.5). Another strain, *rtp1/RTP1*, encoding a protein for the nuclear import and biogenesis of RNA polymerase II (Gómez-Navarro *et al*., 2013), showed resistance to both cyprodinil concentrations in all measures except growth rate to 250 µM cyprodinil.

Interestingly, the *yah1/YAH1* heterozygote showed as a hit and conferred increased resistance to both cyprodinil concentrations in all four measures except growth rate to 50 µM cyprodinil. Overexpression of *yah1* is known to increase sensitivity to ROS (Vallières *et al*., 2017), suggesting that reactive oxygen species play a role in the mode of action of cyprodinil. Experiments involving *yah1* overexpression are shown in section 5.2.8.

For DPI, no heterozygotes gave an increased resistance in terms of an earlier exponential phase. However, six different strains showed increased maximum growth (i.e., >10% above median) rate across both 50 µM (Figure 5.6D) and 250 µM (Figure 5.6E) treatments. This included strains heterozygous for genes that encode: an RNA polymerase III subunit (*RPC11*); an inner plaque spindle pole body component (*SPC29*); an actin-related protein involved in transcriptional regulation (*ARP9*); a protein implicated in the assembly of the DNA replication machinery (*SLD5*); a protein required for the nuclear import and biogenesis of RNA polymerase II (*RTP1*); and a nuclear protein required for S- and M-phase cyclin degradation and mitotic control (*UBC9*).

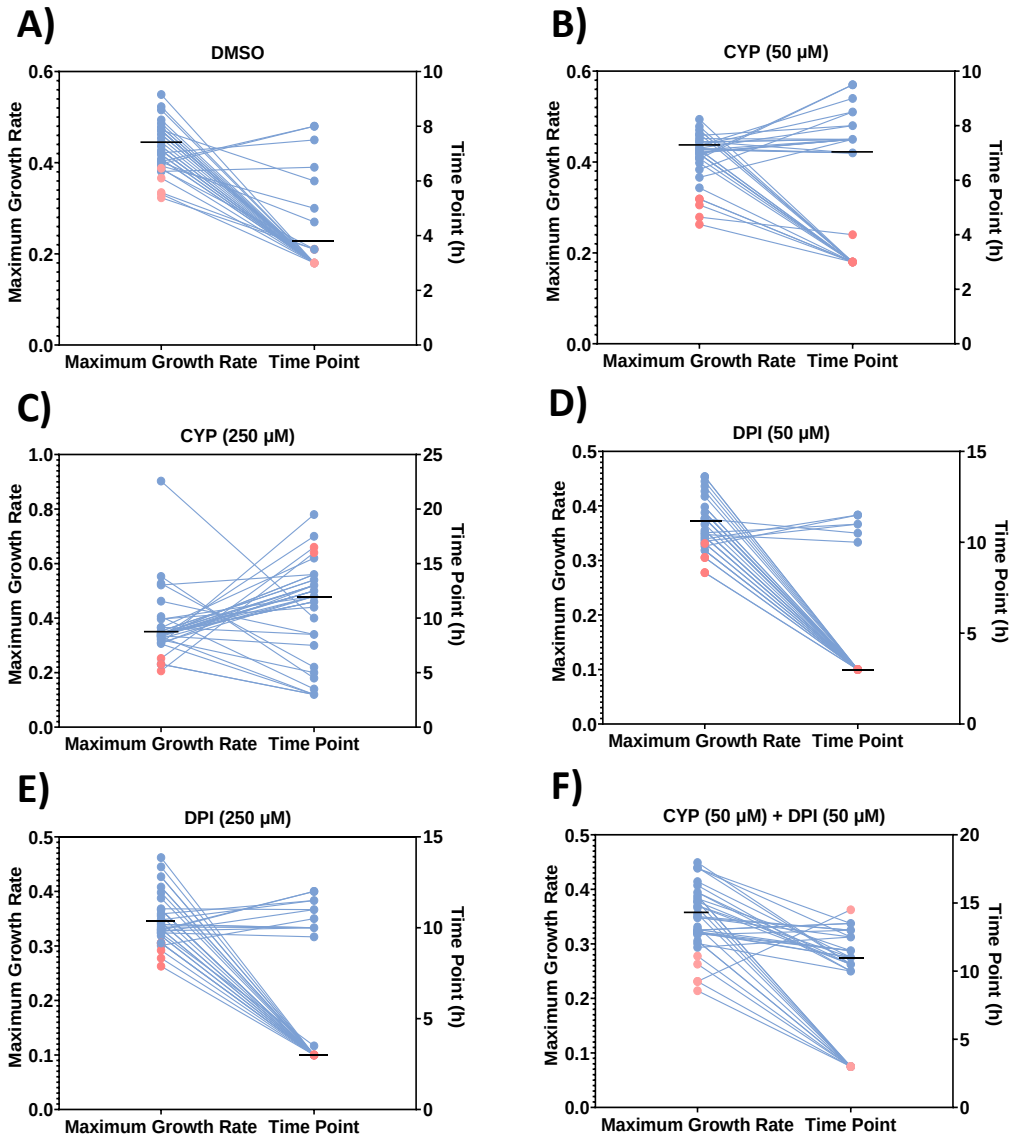

Figure 5.6. **Yeast heterozygous deletion screen follow-up**. Exponential phase *S. cerevisiae* cells were incubated at 30°C for 48 h in YNB minimal media containing A) DMSO; B) 50 µM cyprodinil; C) 250 µM cyprodinil; D) 50 µM DPI; E) 250 µM DPI; F) 50 µM cyprodinil and 50 µM DPI. OD_{600} was read every 30 minutes. Maximum growth rate was calculated as: µmax = ln2/g, where g is cell doubling time. 'Time Point' indicates time taken for culture to reach maximum growth rate. Blue points indicate deletion strains, while pink points represent different WT cultures. Blue lines connect 'Maximum Growth Rate' and 'Time Point' for individual strains. n = 2 biological replicates. Black lines indicate median values. Knockdowns tested: YPL126W, YOL144W, YGR115C, YBR237W, YBR190W, YLR305C, YOR194C, YLR277C, YLR276C, YKL195W, YOR103C, YPL252C, YGR029W, YIL033C, YOR149C, YNL026W, YOR250C, YDR164C, YOR116C, YLR397C, YBR234C, YGR083C, YOR098C, YFL038C, YHR005C-A, YDL043C, YPL124W, YDR045C, YOR148C, YMR033W, YDR489W, YDL064W, YMR185W.

In the case of the CYP-DPI combination, heterozygosities in *DBP9* (required for 27S rRNA processing), *SPC29*, *YPT1* (involved in ER-to-Golgi step of secretory pathway), *BCY1* (regulatory subunit of cyclic AMP-dependant protein kinase), *STT4* (involved in

PKC1 protein kinase pathway) and YGR115C (a dubious open reading frame) all gave increases in sensitivity to the CYP-DPI combination for maximum growth rate (Figure 5.6). These genes show no obvious links to the proposed mechanism of increased oxidative stress (presumably in the mitochondria).

This experiment did not yield obvious targets for cyprodinil or DPI, and may provide evidence for a synergy with multiple mechanisms of action. None of the heterozygosities conferring sensitivity to cyprodinil were of those found to give resistance to cyprodinil in *B. cinerea* due to SNPs (Mosbach *et al*., 2017). Additionally, none of the gene deletions conferring sensitivity to DPI were known NAD(P)H oxidases.

5.2.4. Screening of yeast overexpression library to find CYP-DPI resistant mutants

5.2.4.1. Initial screens yield resistant colonies

Continuing the broad approach to determining the synergistic mechanism an *S. cerevisiae* overexpression library was utilised. The ATCC® 37323™ overexpression library contains thousands of different high-copy plasmids that overexpress individual genes from the yeast genome, with genome-wide coverage (Kruppa et al., 2001). Similar to the heterozygous deletion library, the objective was to isolate and identify genetic suppressors of the cyprodinil/DPI synergy. Four iterations of this experiment were carried out, two with concentrations of cyprodinil and DPI at 94 µM and 625 nM, respectively (Figure 5.7A), and two with the concentrations doubled to 188 µM and 1250 nM DPI, respectively (Figure 5.7B): the MIC of DPI in yeast were found to be lower when grown on agar than in liquid media. For cyprodinil alone, the MIC ranged between 188 µM and 375 µM, whereas for DPI, the MIC was between 1.25 µM and 2.5 µM (data not shown).

The first attempt at this overexpression screen, with cyprodinil at 94 µM and DPI at 625 nM (Figure 5.7A), yielded hundreds of colonies, compared to thousands for the untreated control. The four largest colonies (R1-R4) were picked for later use, and the experiment was repeated. The second attempt (at the same concentrations) produced a similar number of colonies growing on cyprodinil + DPI, but in this case >100 of the colonies (R5-R112) appeared noticeably larger than the rest. Figure 5.7C shows an example control well containing no cyprodinil or DPI. Control wells contained 400-500 colonies. With 36 wells per condition, this equated to more than the 10,000 colonies required for total coverage of the library.

The screen was then repeated twice with double the concentration of cyprodinil and DPI. The higher concentrations had the effect of removing the large number of smaller colonies. The first attempt yielded five resistant colonies (R113-R117), while on the

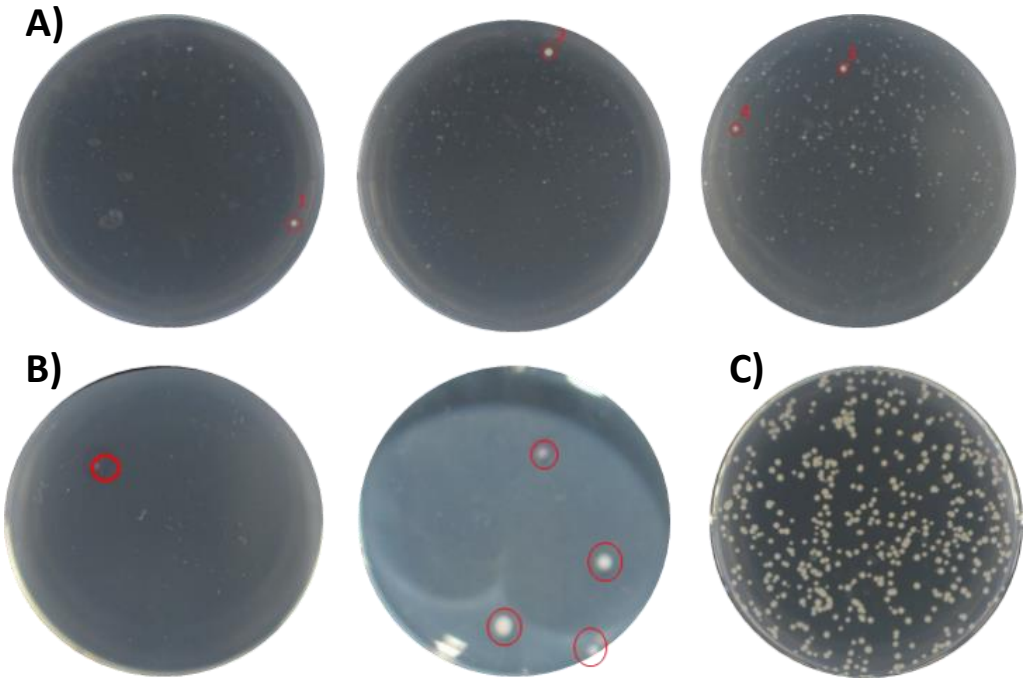

Figure 5.7. **ATCC®37323™ overexpression library yielded mutants resistant to CYP-DPI synergy**. W303 *S. cerevisiae* transformed with the ATCC®37323™ overexpression library were spread onto agar containing A) 94 uM CYP and 625 nM DPI; B) 188 uM CYP and 1250 nM DPI. Agar was set in wells of 6-well plates. C) shows example control well containing no CYP or DPI. Control wells contained between 400-500 colonies. There were 36 wells per condition leading to ~16,000 transformants. Plates were viewed every day for 144 h. Examples of 'resistant' colonies are shown circled in red. Colonies were picked and propagated onto selective media.

second attempt, no further resistant colonies were found among ~16,500 transformants screened (Figure 5.7B).

5.2.4.2. Growth curves confirm phenotypes of resistant mutants

To corroborate the resistance of transformant isolates described above, the strains (R1-R117) were grown in broth in different conditions. Of all the strains, only R113-R117 showed clear resistance to the synergy (Figure 5.8A), indicating that the screen carried out with lower concentrations of cyprodinil and DPI did not yield any true resistant mutants. Isolate R113 was more resistant than the WT control to both cyprodinil and DPI, as well as the combination (Figure 5.8B). Strains R114-117 showed similar results (Appendix Figure 8.7). All overexpression strains showed resistance to both cyprodinil and DPI individually, as well as the synergy.

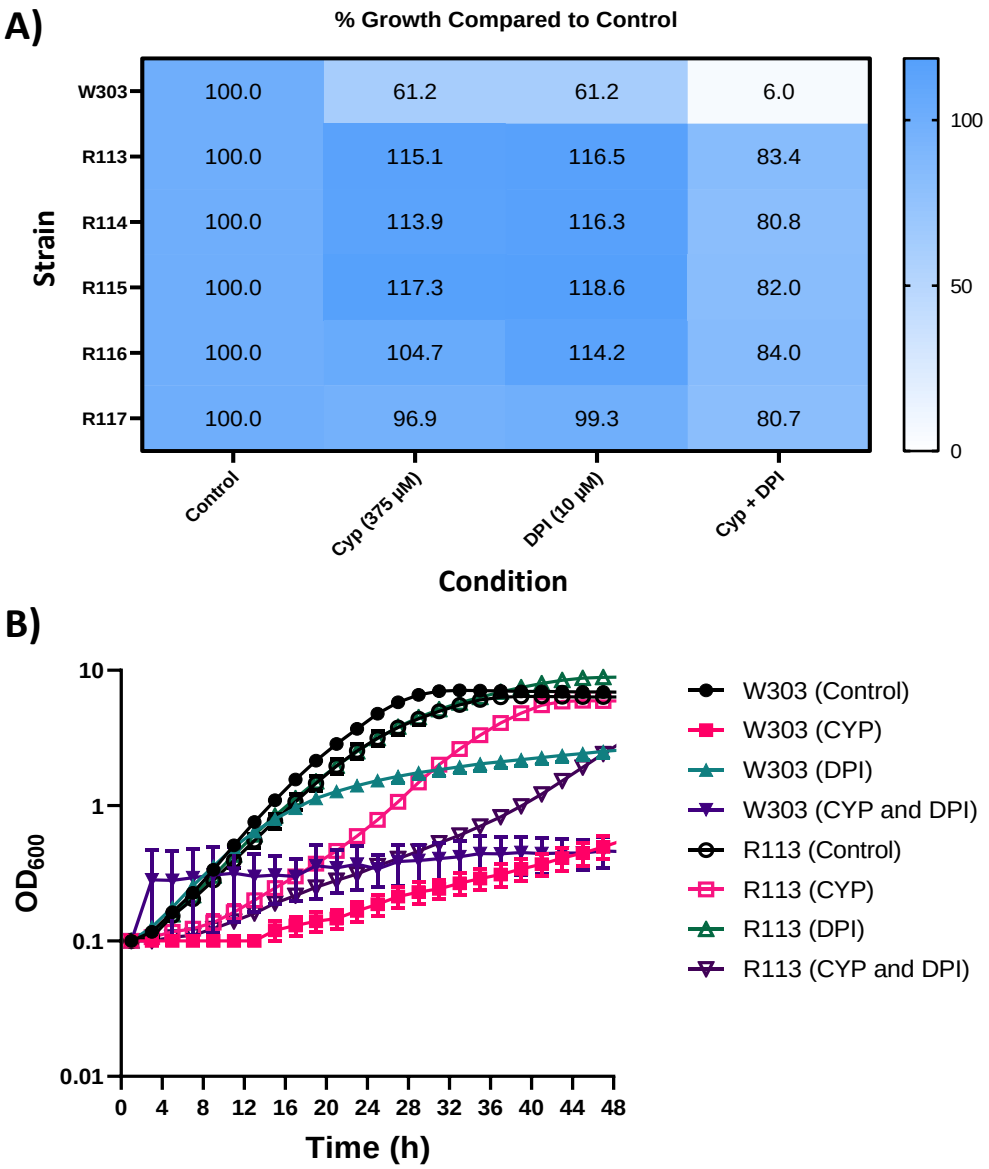

Figure 5.8. **Corroborating transformant phenotypes from ATCC®37323™ overexpression-library screen**. A) Exponential phase WT and transformants of interest (R113-117) were incubated statically at 30°C for 48 hr in YNB medium containing DMSO, cyprodinil, DPI, or a combination. Numbers represent growth as a percentage when compared to final OD_{600} of each strain in control conditions. B) Growth curves of WT and a representative resistant strain (R113) incubated statically at 30°C for 48 hr in YNB medium containing either DMSO, 375 µM cyprodinil, 10 µM DPI, or a combination of 375 µM cyprodinil and 10 µM DPI. Readings taken every 30 min (each reading preceded by brief agitation). Bars show standard deviation of three biological replicates. n = 3. Corresponding data for strains R114-R119 are shown in Appendices Figure Appendix Figure 8.7.

5.2.4.3. Sequencing of resistance-conferring constructs reveals *SGE1* (encoding a plasma membrane multidrug transporter) as a resistance gene

In total, plasmid sequences were acquired for seven different resistant transformants (R113-R119). Primers were designed to amplify the regions of DNA within the cloning sites of high-copy plasmids conferring resistance. The S*GE1* gene encoding a plasma membrane multidrug transporter was present in all the high-copy plasmids successfully sequenced (Figure 5.9). R116 could not be successfully sequenced. In addition, plasmid sequences from strains R115, R117 and R119 included gene for a putative maltose-responsive transporter factor. YPR196W, as well as *ARR1* and *ARR2* (Figure 5.9), are genes involved in resistance to arsenicals (Stefanini *et al*., 2022). However, the sequence generated from strain R118 began more than halfway into the putative maltose-responsive transcription factor ORF and finished before the *ARR1* and *ARR2* ORFs (Figure 5.9). Three other sequences were encompassed by these DNA regions: ARS1631, an autonomously replicating sequence, Ty4 LTR, a retrotransposon, and a dubious open reading frame that is unlikely to encode a functional protein. Despite the presence of these sequences on the high-copy plasmids conferring resistance, it was presumed that overexpression of *SGE1* was the cause of resistance in all resistant mutants. As Sge1p has plasma-membrane multidrug transporter function, this was considered likely to be cause of cyprodinil/DPI resistance rather than a function directly suppressing the molecular target of synergy. This may indicate that the synergy works to target multiple essential genes at once, and so the overexpression of a single target protein gene is unable to confer resistance. This data might suggest that more than one inhibitory target of DPI is involved (Riganti *et al*., 2004). In addition, as *Z. tritici* is known to have a plethora of efflux pumps (discussed

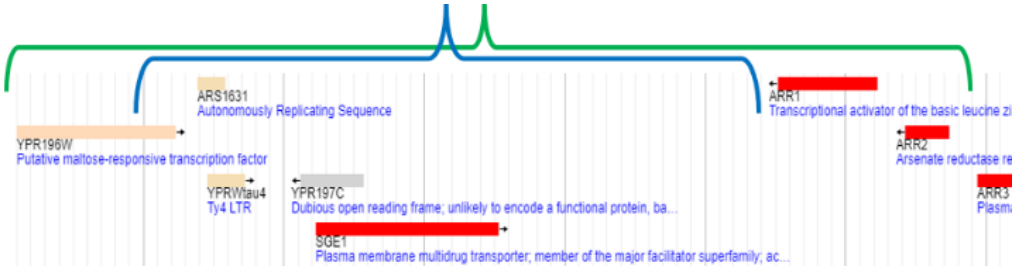

Figure 5.9. **Gene sequences included in different gene-overexpression transformants.** Polymerase chain reaction was carried out with plasmid templates isolated from transformant yeast strains resistant to the CYP-DPI synergy. The figure shows the sections of DNA included in the different resistance strains. Green: R115, R117, R119. Blue: R118. Sequence taken from Saccharomyces Genomic Database viewed and viewed on JBrowse. The region shown encompasses nucleotides 931376 (start of YPR19W) to 939922 (start of the *ARR3* ORF) of *S. cerevisiae* chromosome XIV.

in 1.3.2), this may give the fungal phytopathogen a simple method to overcome the CYP-DPI synergy (although the combination is far stronger in this organism than in yeast).

5.2.5. Cyprodinil-diphenyleneiodonium synergy is not due to auxotrophy of amino acid requiring mitochondrial NADPH

Arginine biosynthesis has an NADPH-requiring step which takes place within the mitochondria that is catalysed by *N*-acetylglutamyl phosphate reductase (Jauniaux *et al*., 1978). Deletion of *pos5* (considered a target of cyprodinil) has been shown to lead to arginine auxotrophy in *S. cerevisiae* as well as defective biosynthesis of enzymes containing iron-sulphur (FeS) clusters (Outten and Culotta, 2003). In addition, various other amino acids require FeS-containing enzymes in their biosynthesis.

To help understand if either of these consequences of Pos5p inhibition might be relevant to the mechanism of CYP-DPI synergy, different amino acids were supplemented to *S. cerevisiae* W303. Average FICI values for these checkerboard assays are shown in Figure 5.10. Arginine supplementation ('+R') did not suppress the synergistic effects of CYP-DPI against *S. cerevisiae* growth. Cysteine, glutamic acid, isoleucine, lysine, leucine, methionine, glutamine, and valine are all amino acids that

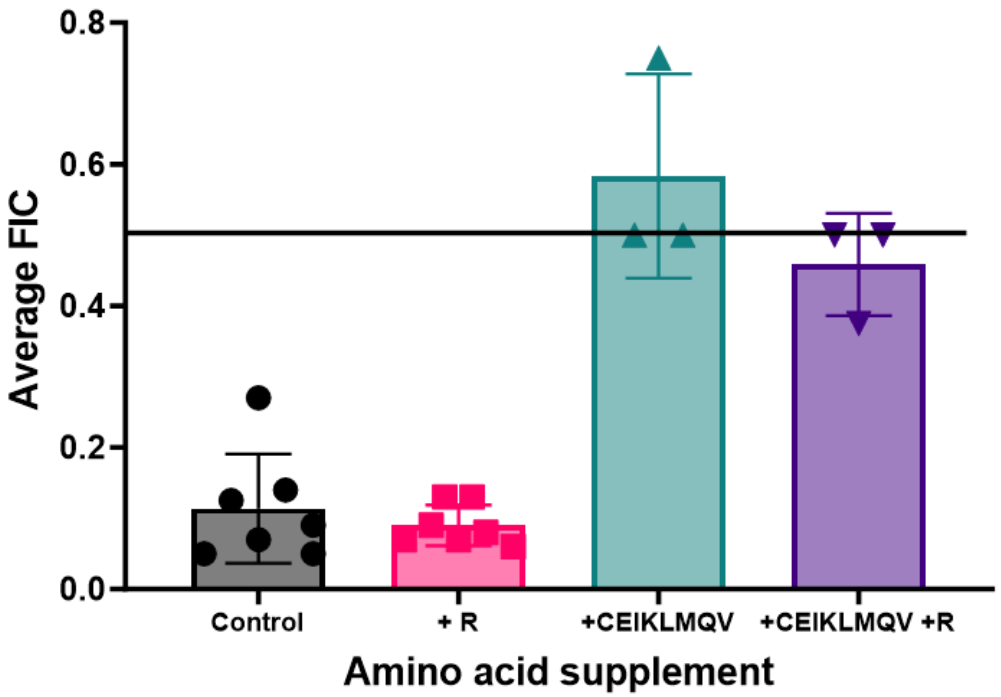

Figure 5.10. **Effects of amino acid supplements on CYP-DPI synergy against yeast.** Exponential phase *S. cerevisiae* W303 cells were treated with cyprodinil and diphenyleneiodonium in a checkerboard format. Cells were grown in minimal medium at 30°C. In all conditions, cells were supplemented with the amino acids essential for growth of strain W303: histidine, leucine, and tryptophan. YNB medium was used. Bars show mean of FICI values calculated from checkerboards. Individual data points show synergistic FICI values from wells for each of three replicate checkerboards. Error bars show standard deviation. Horizontal bar represents FICI cut-off for synergy.

require FeS cluster proteins during at least one step of their biosynthesis. When these amino acids were supplemented as a group to CYP-DPI checkerboards, FICI was markedly increased. This suggested that biosynthesis of amino acids requiring FeS cluster-containing enzymes could be involved in the mechanism of CYP-DPI synergy. Aspartic acid and tyrosine were not tested due to issues dissolving these amino acids.

Subsequently, each FeS-requiring amino acid was supplemented separately (Figure 5.10). Supplementation of either cysteine or methionine to the medium conferred resistance to DPI (Figure 5.11C) and to the combination (Figure 5.11D). In retrospect, a higher concentration of cyprodinil should have been used as the levels of inhibition by this agent alone were too small to accurately determine potential resistance due to amino acid supplementation. Nonetheless, cysteine and methionine were two amino

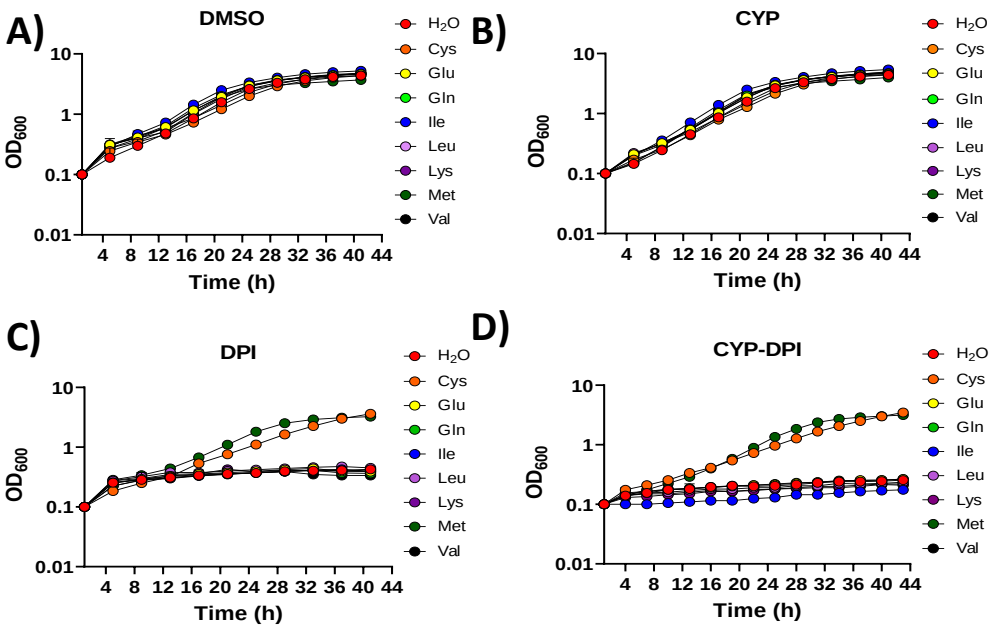

Figure 5.11. **CYP-DPI combination in *S. cerevisiaie* W303 supplemented with different amino acids requiring FeS-containing enzymes for their biosynthesis**. Exponential phase *S. cerevisiae* W303 was treated with A) DMSO; B) 50 µM cyprodinil; C) 60 µM DPI ; 50 µM cyprodinil and 60 µM DPI. Media were supplemented to final concentrations of 66.67 mg ml^{-1} of specified amino acids. Cells were incubated at 30°C for 48 h. Readings taken every 30 min. Bars show standard deviation. n = 2.

acids that rescued growth with both DPI and CYP-DPI. Given that other amino acids requiring FeS for biosynthesis did not have this effect, combined with the fact that cysteine and methionine are known to have protective roles against reactive oxygen species (Bin *et al*., 2017), the results pointed more to a role for oxidative stress than Fe-S cluster integrity impairing amino acid biosynthesis in the CYP-DPI synergy.

5.2.6. Diphenyleneiodonium potentially interacts with sulfhydryl groups of antioxidants

5.2.6.1. Utilising Ellman's reagent to test for -SH reactivity of DPI

Following a mode of action (MoA) screen (involving a series of plate-based assays) that was carried out by Syngenta (methodology not available), DPI was noted to be active against *Z. tritici* and yeast in minimal but not rich medium. In the same MoA screen, DPI was shown to be 'weakly active' in an assay looking at reactivity with glutathione

(internal experiments carried out by Syngenta). One potential cause for this could be reaction of DPI with free -SH groups, which occur in antioxidants such as glutathione and *N*-acetylcysteine, which are also likely to be more abundant in rich media. Such an action of DPI could inhibit glutathione (GSH) function in counteracting oxidative stress, while inhibition of NADPH formation (in the mitochondria) by cyprodinil would exacerbate this by slowing the recycling of glutathione (Lushchak, 2012).

In an attempt to corroborate DPI reactivity with -SH groups Ellman's reagent (5,5'-dithiobis-(2-nitrobenzoic acid), or DTNB) was used. DTNB rapidly reacts with thiols (compounds containing an -SH group) to cleave the molecule's disulphide bond, releasing 2-nitro-5-thiobenzoate (TNB^-). TNB^- ionises to the dianion TNB^{2-} which can be quantified by spectrophotometry, with one mole of thiol releasing one mole of TNB (Reiner *et al.*, 2002). The yellow colour of TNB^{2-}, which requires pH >7, also allows for visual confirmation. Mistakenly, the media was not buffered, and pH was not checked – although visual conformation was seen. Glutathione with DPI gave decreased absorbance from Ellman's reagent compared with glutathione with DMSO (Figure

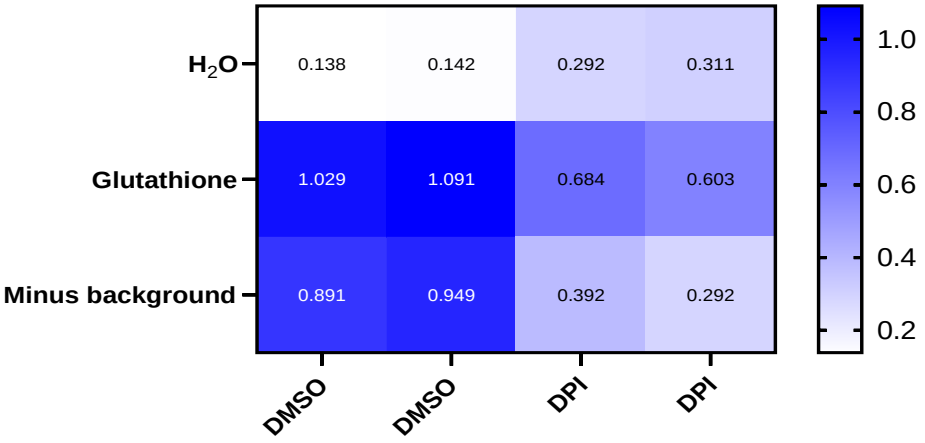

Figure 5.12. **DPI decreases available -SH groups for Ellman's reagent reaction**. 0.5 mM of DPI or DMSO equivalent was incubated with either 0.5 mM glutathione or H_2O not containing glutathione. 0.5 mM Ellman's reagent was added after 30-minute incubation. Absorbance was measured at 412 nm immediately before and immediately after the addition of Ellman's reagent using a microplate reader. Bottom row is not a reading but shows final absorbance after background (top row) was subtracted from middle row. Data shows two replicates.

5.12). This might be evidence that DPI has some glutathione reactivity, preventing the thiols from cleaving Ellman's reagent and the ultimate production of TNB^{2-}. This is consistent with a hypothesis that DPI's role in the CYP-DPI synergy could be the inhibition of -SH-containing antioxidants, so increasing sensitivity to ROS. However, DPI may have been interfering with the dianion, preventing colour formation in the appropriate conditions. To test for this DPI could have been added after the reaction of glutathione with DTNB to see if it was able to "destain" the solution. DPI's ability to interact with thiol groups is therefore not conclusive.

5.2.6.2. Thiol-containing antioxidants alleviate the CYP-DPI synergy in *S. cerevisiae*

Figure 5.12, as well as assays carried out by Syngenta, suggested that DPI might have reactivity with glutathione, although this is not conclusive. If DPI is reacting with thiol groups in glutathione, then it may also do so with the thiol groups in other antioxidants. The CYP-DPI synergy was therefore tested in *S. cerevisiae* W303 and supplemented with different antioxidants. These included the thiol-containing glutathione and *N*-acetylcysteine as well as ascorbic acid, an antioxidant without a thiol group, and mitoquinol (Figure 5.13), a non-thiol-containing antioxidant that is selective for the mitochondria (Kelso *et al*., 2000).

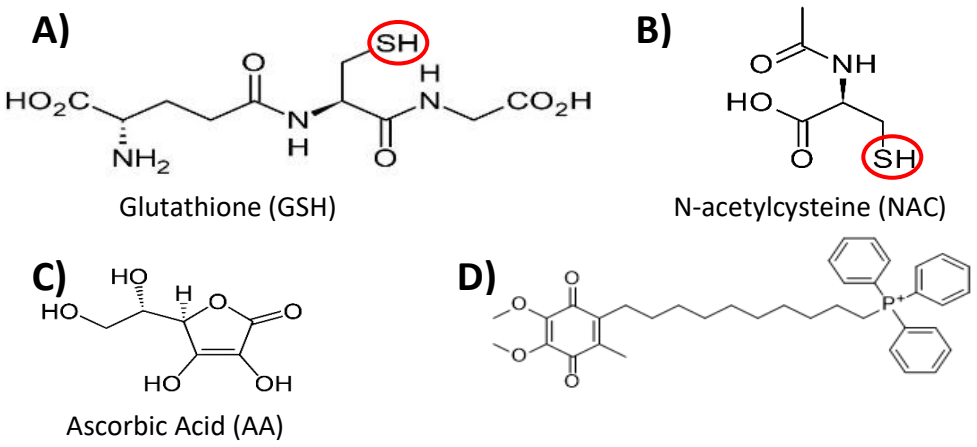

Figure 5.13. **Chemical structures of different antioxidants**. Figure shows the chemical structures of A) glutathione; B) *N*-acetylcysteine; C) ascorbic acid; D) mitoquinol. -SH groups are circled in red.

Compared to the untreated DMSO control (Figure 5.14A), both glutathione and *N*-acetylcysteine at 2 mM helped suppress growth inhibition by cyprodinil (Figure 5.14B). Ascorbic acid (250 µM) also helped alleviate the inhibitory effects of cyprodinil, although this was less effective than the thiol-containing antioxidants (Figure 5.14B). This may be due to ascorbic acid acting as a comparatively weaker antioxidant. It is also possible that ascorbic acid may not enter the cells with a similar efficiency. Glutathione and *N*-acetylcysteine also helped protect against inhibition by DPI (Figure 5.14C) and the CYP-DPI combination (Figure 5.14D). Ascorbic acid and mitoquinol did not allow restored growth under these conditions (see 6.2.5 for cyprodinil-mitoquinol synergy). These results further support an important role for -SH containing antioxidants in the synergy of CYP-DPI, potentially via reactivity of DPI with -SH groups, or, perhaps more likely, through the alleviation of induced oxidative stress. The absence of thiol groups from mitoquinol or ascorbic acid may explain the lack of protection they conferred against the synergistic combination.

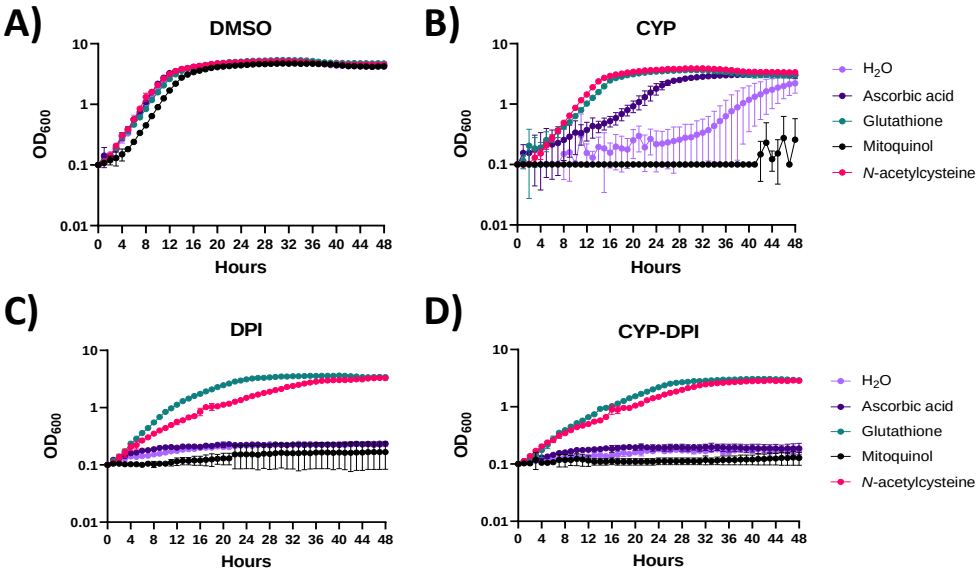

Figure 5.14. **Thiol-containing antioxidants alleviate CYP-DPI synergy**. Exponential phase *S. cerevisiae* W303 were treated with A) DMSO; B) 188 µM CYP; C) 318 µM DPI; D) 94 µM CYP + 94 µM DPI. Cells were grown in YNB and supplemented with either H_2O, 2 mM glutathione, 2 mM ascorbic acid, 2 mM *N*-acetylcysteine or 250 µM mitoquinol. Plates were incubated shaking at 30°C for 48 h. Error bars show standard deviation. n = 4 biological replicates.

5.2.7. Inhibition of yeast is stronger when cyprodinil or diphenyleneiodonium are combined with hydrogen peroxide

As there was reason to believe that both cyprodinil and diphenyleneiodonium may increase sensitivity to oxidative stress (CYP via Pos5p inhibition, DPI via potential thiol-reactivity/glutathione efflux (Riganti *et al.*, 2004)), hydrogen peroxide was tested in combination with each compound (Figure 5.15). When in DMSO, 0.625 mM H_2O_2 delayed the onset of exponential phase growth by ~6 hours compared to the H_2O-DMSO control, though with little effect on subsequent growth rate, potentially due to the action of cellular catalase (Martins and English, 2014). Cyprodinil (200 µM) and DPI (500 µM) also impacted growth, delaying the onset of exponential phase by ~8 hours and ~3 hours, respectively, when compared to the control. These effects were markedly accentuated with the inclusion of 625 µM H_2O_2, where entry to the exponential growth phase was delayed by >24 hours and ~40 hours with DPI and cyprodinil, respectively. This evidence – that H_2O_2 exacerbates the inhibitory actions of both cyprodinil and DPI – is consistent with an impaired defence against reactive oxygen species underlying the CYP-DPI synergy.

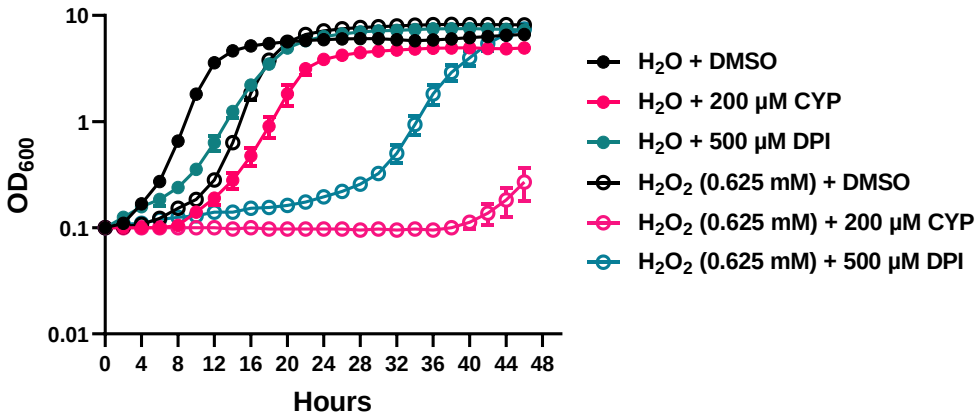

Figure 5.15. **BY4743 yeast treated with H_2O_2 in combination with cyprodinil or DPI.** Exponential phase BY4743 yeast were treated with different combinations of H_2O, H_2O_2, DMSO, cyprodinil, and DPI. Plates were incubated at 30°C for 48 h with shaking. n = 3 biological replicates.

5.2.8. *YAH1* overexpression increases sensitivity to DPI and to the CYP-DPI synergy

As cyprodinil is believed to act on Pos5p, a mitochondrial protein, an oxidative stress-based synergistic action could involve unchecked ROS damaging crucial ROS-sensitive mitochondrial proteins, such as those involved in iron-sulphur cluster biosynthesis. While the rho^0 yeast utilised in 5.2.2.1 were assumed to not possess a functional electron transport chain, the process of mitochondrial FeS biogenesis is essential for cell viability and thus must still be functional in the strain, leaving open the possibility that such a process could be targeted by the CYP-DPI combination.

Iron-sulphur (FeS) clusters are essential cofactors used in various reactions such as amino acid biosynthesis, DNA synthesis and repair, mRNA translation, the TCA cycle, and FeS-protein biogenesis itself (Brancaccio *et al*., 2017, Macomber and Imlay, 2009, Tan *et al*., 2017). FeS proteins are notoriously ROS labile, most commonly those with surface exposed FeS clusters. FeS clusters are also susceptible to Fe displacement by metals such as Cu, Ag, and Hg (Xu and Imlay, 2012). If the synergistic mechanism of cyprodinil and DPI is related to ROS and/or weakened ROS defence, FeS proteins may be at greater risk of damage by oxidative stress. ROS stress can potentially be exacerbated by increased expression of nonessential FeS proteins. This causes a larger pool of labile FeS, which, following turnover (e.g., ROS-mediated), leads to the accumulation of free Fe. This can further the potential for ROS stress via Fe-catalysed Fenton chemistry (Keyer and Imlay, 1996; Liochev and Fridovich, 1999). However, increased expression of an essential FeS protein targeted by ROS may help counter ROS-mediated inhibition.

Different genes involved in FeS cluster biogenesis or genes encoding FeS-containing proteins were overexpressed in *S. cerevisiae* (Table 5.1) and treated with cyprodinil, DPI, and the combination (Figure 5.16).

Table 5.1. **List of FeS-related genes overexpressed in Figure 5.16**.

Gene	Function / Relevance	SGD references
CFD1	Essential FeS cluster binding protein localised in the cytoplasm. Involved in FeS protein assembly in the cytosol.	https://www.yeastgenome.org/locus/S000001265
ISU1	Performs a scaffolding function during FeS cluster assembly in the mitochondria.	https://www.yeastgenome.org/locus/S000006056
NAR1	Subunit of the cytosolic FeS protein assembly machinery. Essential protein required for normal resistance to oxidative stress.	https://www.yeastgenome.org/locus/S000005184
RLI1	Essential cytosolic FeS protein required for ribosome biogenesis.	https://www.yeastgenome.org/locus/S000002498
YAH1	Essential, mitochondrial FeS ferredoxin required for the formation of FeS cluster proteins.	https://www.yeastgenome.org/locus/S000006173
YFH1	Mitochondrial matrix iron chaperone involved in oxidisation and storage of iron.	https://www.yeastgenome.org/locus/S000002278

In the control (+DMSO) or with 187.5 µM cyprodinil, all yeast strains grew at similar rates with minor differences in their growth curves (Figure 5.16A,B). When treated with 318 µM DPI, cells overexpressing the mitochondrial ferredoxin *YAH1* showed increased sensitivity, with a ~6-hour delay in reaching exponential phase when compared with the control strain (Figure 5.16C). Overexpression of *YAH1* in *S. cerevisiae* has previously been noted to cause increased sensitivity to ROS (Vallières *et al*., 2017). Therefore, although resistance to ROS was being tested for in other overexpression strains, the *YAH1* overexpression mutant was a good candidate to search for ROS-sensitivity. When treated with a sub-lethal combination of cyprodinil

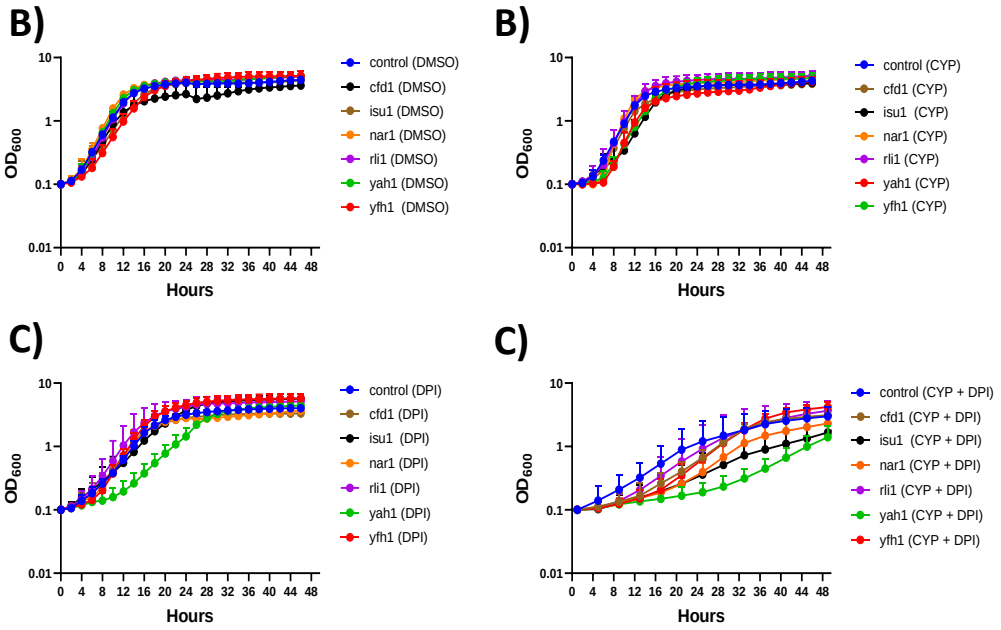

Figure 5.16. **Overexpression of iron-sulphur cluster-related genes in *S. cerevisiae* and effects on CYP/DPI resistance**. Exponential phase *S. cerevisiae* BY4743 cells were treated with A) DMSO; B) 187.5 µM cyprodinil; C) 318 µM DPI; D) 94 cyprodinil + 80 µM DPI. Cells were cultured in YNB medium at 30°C with shaking. OD_{600} was measured every 30 minutes. Keys represent different genes overexpressed using the high-copy pCM190 plasmid. Error bars show standard deviation. n = 3 biological replicates

and DPI together, every overexpression strain showed at least slight sensitivity compared to the control, with the strain overexpressing *YAH1* showing the strongest sensitivity: here there was a ≥24-hour delay before exponential phase (Figure 5.16D). As *YAH1* overexpression is known to cause pro-oxidant hyper-sensitivity (Vallières *et al*., 2017), the data support the theory that the CYP-DPI combination increases ROS levels and/or the sensitivity of a cell to ROS.

5.2.9. Testing *pos5*, *sod2*, and *yap1* deletion strains of *S. cerevisiae* and *Z. tritici*

5.2.9.1. *sod2Δ* and *yap1Δ S. cerevisiae* are more susceptible to the CYP-DPI synergy

The manganese superoxide dismutase, Sod2p, is a mitochondrial protein that helps to protect cells against oxidative stress by converting (dismutating) superoxide radicals into O_2 and the less harmful hydrogen peroxide (Wang *et al*., 2018). The Yap1p

transcription factor is activated by H_2O_2 (including that produced by Sod2p) to trigger relevant oxidative stress responses (Zyrina *et al*., 2017). In *S. cerevisiae* strains carrying deletions of either of these genes, an increase in sensitivity to the CYP-DPI combination was seen (Figure 5.17). In this particular experiment, the CYP-DPI combination did not produce an FICI ≤0.5 (indicative of synergy) in the *S. cerevisae* BY4741 control (Figure 5.17A); however, this is a possible under-estimate as an MIC for DPI was not attained (but a 636 µM value was assumed for FICI calculation). Nevertheless, *sod2Δ* (Figure 5.17B) and *yap1Δ* (Figure 5.17C) deletants conferred increased sensitivity such that a synergistic FICI was attained. The *sod2Δ* strain also showed sensitization to each compound alone, albeit effects too mild to change the

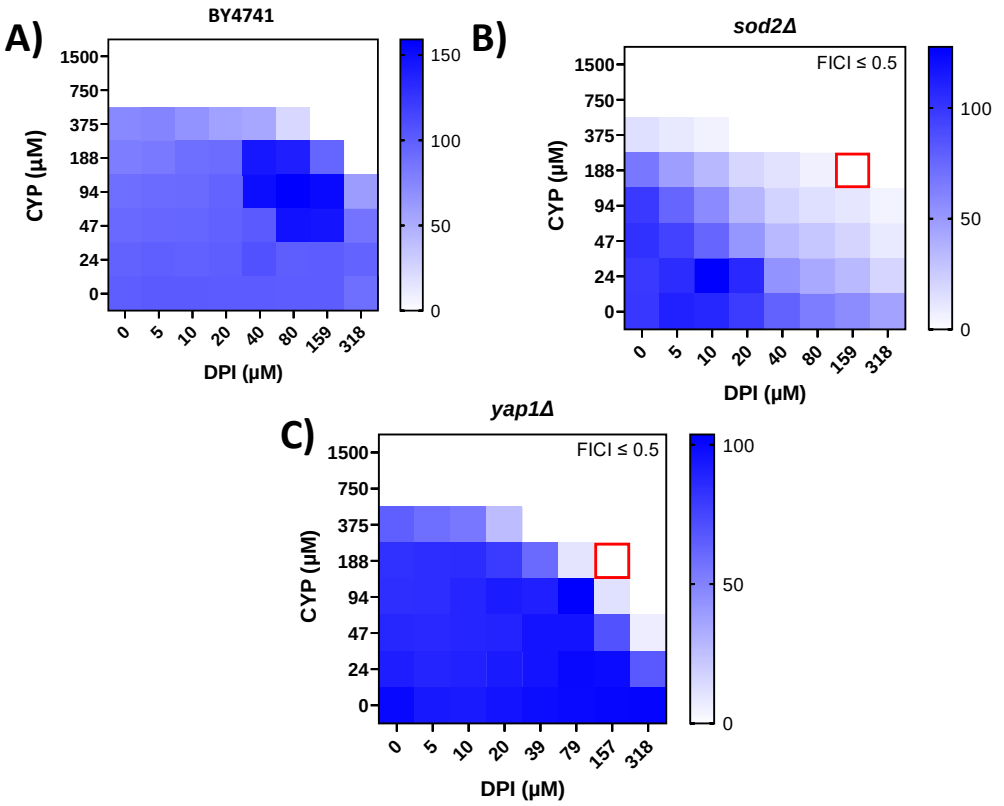

Figure 5.17. **Deletion of genes involved in oxidative stress response increases the sensitivity of yeast to the CYP-DPI synergy.** Exponential phase *S. cerevisiae* cells A) BY4741 control; B) *sod2Δ*, and C) *yap1Δ* were treated with cyprodinil and diphenyleneiodonium in a checkerboard format. Cells were in YEPD. Growth values (scale to the right) is calculated as percentages of growth (OD_{600}) with compounds relative to the minus-compound control. Plates were incubated at 30°C, and data were collected at 0 h and 24 h. Growth values <5% were assigned as no-growth. DPI MIC was assumed to be 636 µM for FICI calculations. Red squares indicate concentrations used to calculate FICI values.

MIC. The hypersensitivity of these ROS-response mutants to CYP-DPI synergy further supported a synergistic mechanism involving oxidative stress.

5.2.9.2. CYP-DPI synergy is significantly stronger in *pos5Δ S. cerevisiae* compared to wild-type

Pos5p, an NADH kinase located in the mitochondria is a proposed target of cyprodinil. Mutations in additional genes also gave resistance to cyprodinil in *B. cinerea* (Mosbach *et al*., 2017), suggesting additional possible targets, although there may be different reasons for such phenotypes. It was therefore of interest to test if *POS5* deletion had an impact on the resistance to cyprodinil and to the combination.

If Pos5p is a principal target of cyprodinil involved in the synergy, then it would have been expected for the deletion strain alone to show increased sensitivity to DPI alone compared to the WT (because deletion of *pos5* should have similar effects as Pos5p inhibition by CYP). However, across all replicates, the MIC of DPI was the same in the WT and *pos5Δ* strains. This suggested that Pos5p was not the target of cyprodinil at least in the case of *S. cerevisiae* (the Pos5p target of cyprodinil was proposed from results obtained with *B. cinerea*, Mosbach *et al*., 2017). Nonetheless, deletion of *pos5* did sensitize yeast to the synergistic effect of CYP-DPI. Pos5p is known to contribute to the detoxification of ROS (Strand *et al*., 2003) and so, if the CYP-DPI mechanism was ROS-related, it could be expected that a *pos5Δ* strain would be more sensitive to this. Therefore, while the results for DPI effectively rule out a role for Pos5 inhibition as a major target in the mechanism of (relatively weak) CYP-DPI synergy in yeast, the results remain consistent with an oxidative stress-based mechanism.

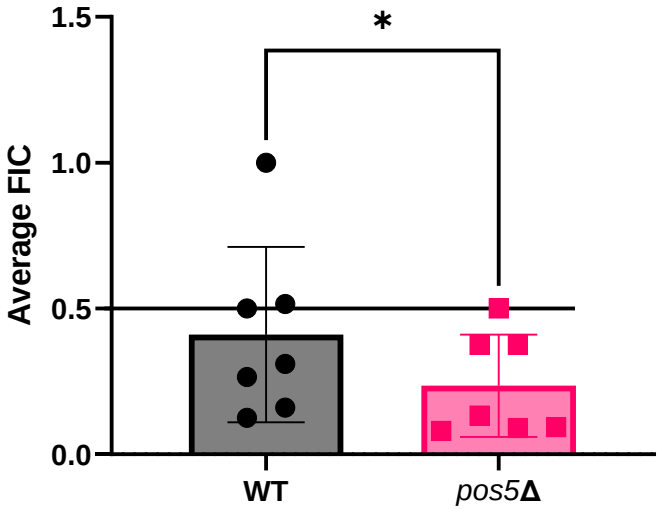

Figure 5.18. **Average FICs of WT and *pos5Δ* CYP-DPI checkerboards**. Exponential phase *S. cerevisiae* cells were treated with cyprodinil and diphenyleneiodonium in a checkerboard format. Cells were grown in minimal media at 30°C. Bars show mean of FICI values calculated from final checkerboards. Individual data points show synergistic FICI values of wells from each of three replicate checkerboards. Some checkerboards had multiple wells from which to calculate FICI values. Error bars show standard deviation. Horizontal bar represents FICI cut-off for synergy. Paired t-test: **P* value of 0.0246.

The yeast *pos5Δ* deletant gave increased sensitivity to the CYP-DPI combination when compared to the WT: although there was variability between replicates, the mutant was always more sensitive than the wild-type within the same experiment and this effect was significant (Figure 5.18).

5.2.9.3. *Z. tritici* deletion strains are not significantly altered in FICI values for CYP-DPI

While the yeast *pos5Δ* deletant did not exhibit altered DPI sensitivity, it was desirable to test effect of the deletion in *Z. tritici*. During a placement at the industrial sponsor for this PhD, Syngenta, it was possible to carry out gene deletions in *Z. tritici*. *Z. tritici* strains with deletions of either *POS5*, *SOD2*, or *YAP1* genes were generated. These genes were identified based on homology to *S. cerevisiae* counterparts (Table 5.2). The *sod2* homologue has been identified as a superoxide dismutase, and the *yap1* homologue as a transcription factor. However, the *pos5* homologue is an

uncharacterised protein, although it does possess a BLAST Expect Value of $6e^{-64}$ with a 92% query cover and a 35.95% identity.

Table 5.2. **BLAST search results comparing *S. cerevisiae* and *Z. tritici* genes of interest**.

***S. cerevisiae* gene name**	**Query Cover**	**BLAST Expect Value**	**Percentage Identity**	**Link**
POS5	92%	$6e^{-64}$	35.71%	Potential *Z. tritici POS5*
SOD2	93%	$4e^{-88}$	56.44%	Potential *Z. tritici SOD2*
YAP1	25%	$1e^{-13}$	43.12%	Potential *Z. tritici YAP1*

The *Ku70* gene (Protein Accession EGP88672.1) was knocked out in all strains (except the original IPO3123 laboratory strain of *Z. tritici*) to aid with the generation of these strains. The *Ku70* gene is involved in the repair of DNA double strand breaks (Sidhu *et al*., 2015). A *Ku70* knockout interrupts the non-homologous end-joining repair mechanism thereby increasing the frequency of homologous recombination (used in *Agrobacterium*-mediated gene deletion in *Z. tritici*). No consistent differences in MIC to cyprodinil or DPI were seen among the strains (Figure 5.19). This might suggest that neither Pos5, Sod2 nor Yap1 are important for the actions of these agents in *Z. tritici*.

For the mechanism of CYP-DPI synergy hypothesised earlier, it had been suggested that Pos5p was the relevant molecular target of cyprodinil in *S. cerevisiae* and *Z. tritici*, as it is (thought to be) in *B. cinerea*. However, the subsequent experiments with *S. cerevisiae* implicated oxidative stress but not Pos5p as important for the synergy mechanism between cyprodinil and DPI, with the specific action of cyprodinil in that

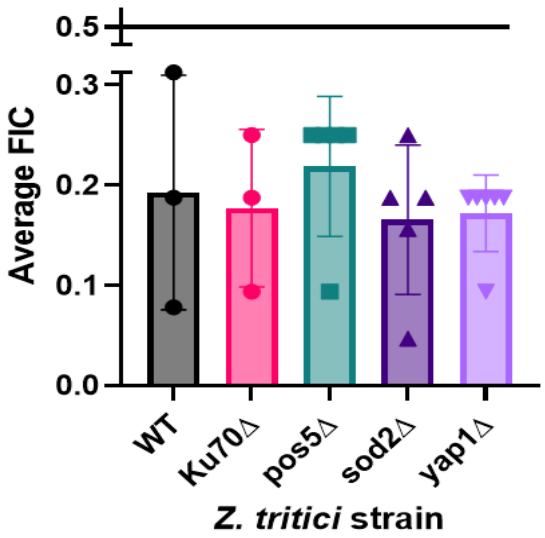

Figure 5.19. **Average FICI for *Z. tritici* deletion strains treated with CYP-DPI combination**. *Z. tritici* spores were treated with cyprodinil and diphenyleneiodonium in a checkerboard format in MCS medium. Plates were incubated at room temperature. Bars show mean of FICI values calculated from final checkerboards. Individual data points show synergistic FICI values of wells from each of three replicate checkerboards. Some checkerboards had multiple points of synergy. Error bars show standard deviation. Horizontal bar represents FICI cut-off for synergy.

synergy unclear. This may undermine the hypothesised oxidative stress mechanism of the CYP-DPI synergy in *Z. tritici*.

5.2.10. ROS assay suggests there is no synergistic increase in reactive oxygen species due to the CYP-DPI combination

DHR-123 is a non-fluorescent molecule that fluoresces upon oxidation. This lipophilic molecule localises to the mitochondria and is often used as an indicator of ROS within this organelle (Balaiya and Chalam, 2014). DHR-123 was used to see if ROS was synergistically increased in the mitochondria when a combination of cyprodinil and DPI were applied in *Z. tritici*. DPI alone tended to lower slightly the levels of ROS detected in the mitochondria (bottom row, Figure 5.20). Cyprodinil alone increased DHR-123 fluorescence (first column, Figure 5.20). There was no clear evidence for a synergistic increase in ROS detection when the two agents were combined. The data was normalised to the average cell fluorescence per well of all groups of cells identified by the Opera Phenix confocal imager (Figure 5.20B).

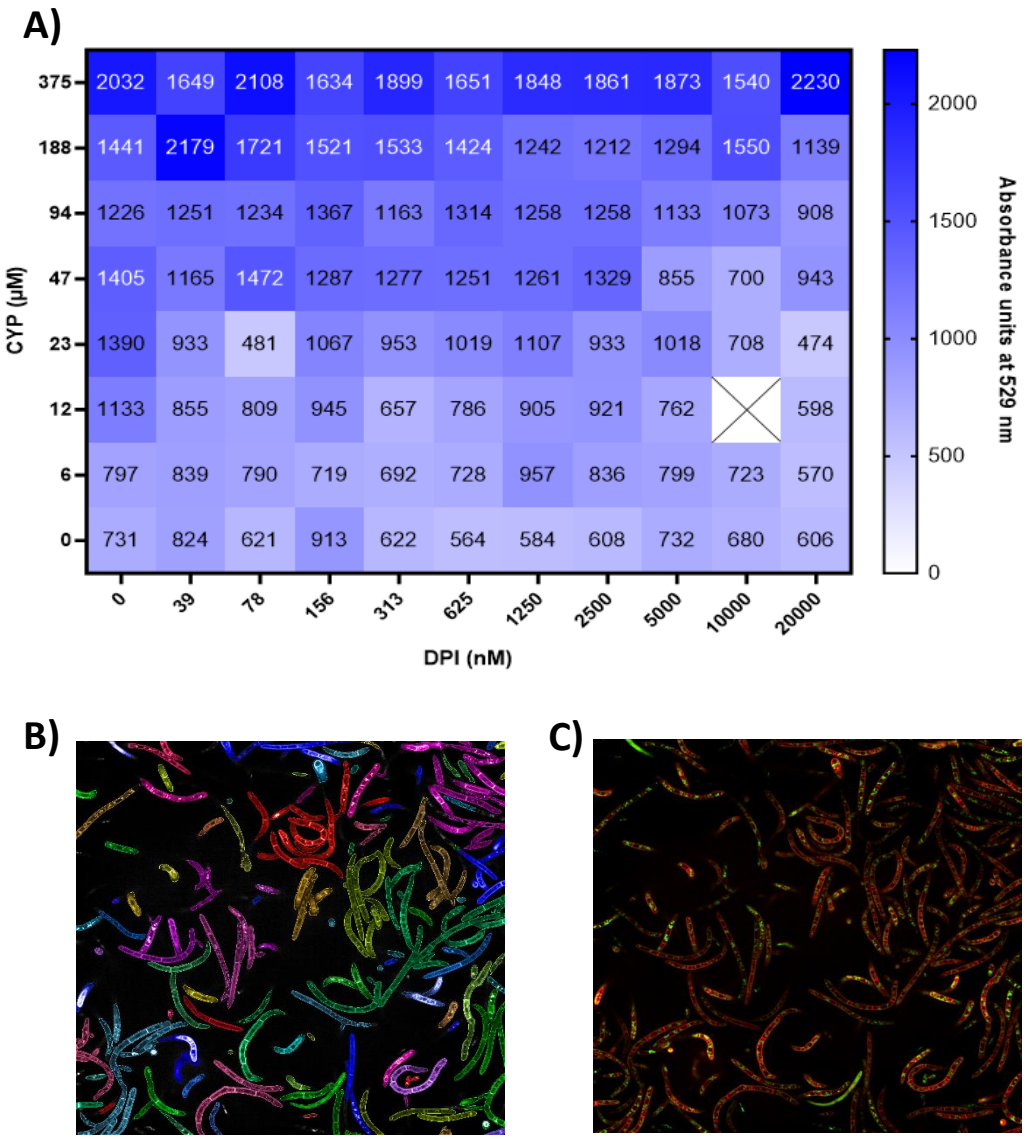

Figure 5.20. **DHR-123 fluorescence in *Z. tritici* cells after treatment with CYP-DPI**. *Z. tritici* with mCherry-tagged Sso1 was incubated in MMZT medium for 48 h. Cyprodinil and DPI were then added in a checkerboard format before addition of DHR-123 to each well. Plates were then imaged using an Opera Phenix confocal imager. Harmony software was then used to identify cell outlines using the Sso1-fluorescent tag. Total DHR-123 fluorescence was measured (absorbance at 529 nm) within each group of cells and divided by total cell area. An average was then calculated for the entire well based on the number of expected cells. A) Average DHR-123 fluorescence per spore group in each well; B) example of imaging software identifying groups of spores (false colouration); C) Same image as B instead showing Sso1 (red) and DHR-123 (green) fluorescence. Images taken from well treated with 375 µM cyprodinil and 20 µM DPI. n = 1.

This seemed to conflict with previous experiments supporting an action for ROS. While it is known that DPI may help protect against ROS-production by inhibiting NAD(P)H oxidases (Li and Trush, 1998), DPI has also been reported to cause increased levels of ROS (Riganti *et al.*, 2004). It is also speculated here that DPI has thiol-reactivity,

potentially affecting antioxidants (5.2.6). If true, this presumably decreases the ability of organisms to defend against oxidative stress. It is possible that a mixed effect of DPI-based inhibition of NAD(P)H oxidases and of the potential DPI-based interference with antioxidant thiols, as well as the unknown relative impact of depleted antioxidant defence versus elevated ROS production, could give rise to sensitivity that is not reflected in synergistically elevated ROS levels. This may be particularly so considering the high reactivity of many ROS – meaning they do not persist long (Collin, 2019) – and potential non-specificity of ROS probes (Winterbourn, 2014). Nonetheless, the result could suggest that ROS many be less important for CPI-DPI synergy in *Z. tritici* than in *S. cerevisiae*, for which a range of evidence was attained, albeit not all in agreement (see below).

5.2.11. Recap of results to this point

5.2.11.1. ETC is not essential to CYP-DPI synergy

The synergy was present in rho^0 mutants and in WT *S. cerevisiae* grown anaerobically. As a functional ETC would have been a major source of ROS, it is unclear as to where ROS responsible for the hypothesised mechanism of CYP-DPI action may originate. However, synergy was less potent in the rho^0 mutant (Figure 5.3) and in anaerobic conditions (Figure 5.4). Despite anaerobic indicator test strips indicating that the anaerobic chamber was truly anaerobic, it is possible that all oxygen was not successfully removed from the media/materials prior to the set-up of the experiment.

5.2.11.2. Discrepancies in the role of DPI in the synergy

Despite reported ROS-inducing activities (Riganti *et al*., 2004), DPI is a recognised inhibitor of NAD(P)H oxidases (Reis *et al*., 2020), enzymes known to be responsible for producing ROS for signalling purposes (Takemoto *et al*., 2007). DPI is often used as an inhibitor of ROS production, which would conflict with a ROS-based synergistic

mechanism. However, as overexpressed *YAH1* conferred increased sensitivity to DPI (Figure 5.16C), DPI alone may induce ROS or increase ROS sensitivity arising from elevated FeS cluster turnover (Vallières *et al*., 2017). In addition, Reis *et al* (2020) state that DPI inhibition can come from non-specific reactions with both flavin and heme cofactors. This gives DPI a very large range of potential targets and the inhibition of any (combination) of these may be contributing to the synergy with cyprodinil. To reiterate what is stated in the text, the ability for DPI to react with antioxidants is speculation and was not confirmed (or denied) by the experiments carried out in this thesis. Different controls could have been used to confirm the hypothesis, such as the addition of DPI to a completed reaction of glutathione and DTNB, as well as the addition of excess DTNB to the reaction of glutathione and DPI.

5.2.11.3. The role of cyprodinil in synergy with DPI

Pos5p, the proposed target for cyprodinil, is indirectly required for efficient FeS cluster biogenesis in *S. cerevisiae* (Pain *et al*., 2010). Deletion of the *pos5* gene in *S. cerevisiae* is characterised (among other things) by FeS cluster deficiency (Outten and Culotta, 2003), as well as increased minus-one frameshift mutations in mitochondrial DNA, increased petite colony formation, sensitivity to hydrogen peroxide and exogenous copper, and an increase in mitochondrial biogenesis (Strand *et al*., 2003). Despite the essentiality of FeS cluster biogenesis in cells, Δ*pos5 S. cerevisiae* strains are viable (although with defects), and so another source of mitochondrial NADPH must be available to support some FeS cluster biogenesis (Jo *et al*., 2001; Outten and Culotta, 2003).

None of the overexpressed FeS-related genes conferred increased sensitivity to cyprodinil alone (Figure 5.16B). Higher cyprodinil concentrations could also have been used when supplementing with different amino acids Figure 5.11B). Regardless,

overexpression of different FeS-related genes did confer sensitivity to the CYP-DPI combination (Figure 5.16D).

5.2.11.4. Proposed synergistic mechanism

Evidence gained thus far points towards reactive oxygen species playing a role in the synergistic mechanism of the cyprodinil-diphenyleneiodonium combination. This includes: DPI potentially interacting with thiol antioxidants (5.2.6); increased sensitisation to both cyprodinil and DPI with hydrogen peroxide (5.2.7); increased potency of the combination against strains overexpressing *YAH1* (5.2.8); increased sensitivity to the synergy in *pos5Δ*, *sod2Δ* and *yap1Δ* strains of *S. cerevisiae* (5.2.9). While the individual target of cyprodinil is in question, the ultimate synergistic mechanism appears to be increased sensitivity to reactive oxygen species. Of course, the experiments with the rho^0 yeast and under anaerobic conditions conflict with this hypothesis.

As discussed in Table 4.1, inhibition of mitochondrial NADH kinase has the consequence of defective biosynthesis for enzymes containing iron sulphur cluster(s). This includes enzymes involved in the TCA cycle such as aconitase and succinate dehydrogenase. It may therefore be possible that the synergistic mechanism derives from the potential ability of both cyprodinil and DPI to inhibit enzymes involved in the TCA cycle. In addition, while DPI may or may not interact directly with the thiol groups in glutathione, DPI is known to increase the efflux of the antioxidant (Riganti *et al*., 2004). If cyprodinil is inhibiting Pos5p, then recycling of oxidised glutathione is likely decreased through a decrease in mitochondrial NADPH. Therefore, each compound may directly or indirectly negatively impact the capability of glutathione to respond to oxidative stress in the cell.

5.2.12. Testing for potential synergy of cyprodinil-diphenyleneiodonium against insect cells

To see if the cyprodinil-DPI combination was potentially toxic against non-target organisms, the insect (*Spodoptera frugiperda*) cell line SF21 was used. Instead of using OD_{600} and measuring growth, an MTT (3-(4,5-dimethylthiazol-2-yl)-2,5-diphenyl tetrazolium bromide) assay was carried out. This is a colorimetric assay that assesses cell metabolic activity. A synergistic effect was visibly apparent against SF21 cells suggesting that the CYP-DPI synergy may not be specific to fungi (Figure 5.21). However, no MIC was reached at the concentrations used. As 5% growth compared to the control was used as a cut-off for checkerboard assays measuring OD_{600}, this was also used for the MTT assay. As such, no wells reach total inhibition of growth and so FICI could not be calculated (Figure 5.21).

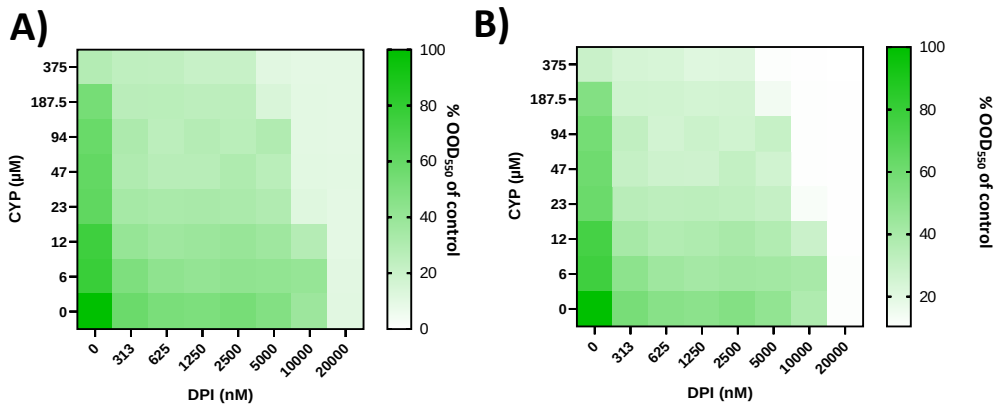

Figure 5.21. **CYP-DPI combination against SF21 insect cells**. Cyprodinil and DPI were prepared in a checkerboard format in 96-well plates. *Spodoptera frugiperda* SF21 cells at 10^4 per well were then added, and the plates incubated for four days at 27°C in a humidified box. Plates were then read at 570 nm as an indicator of metabolic activity.

5.3. Discussion

5.3.1. Library screens did not help to corroborate underlying mechanisms of the antifungal synergies

Screening of chemical or strain libraries is a useful tool for assaying a wide range of phenotypes or genotypes relatively quickly. *Zymoseptoria tritici* was the main organism of interest for this PhD but large deletant or gene-overexpression libraries were not available. Therefore, readily available libraries for the model organism *S. cerevisiae* in which the CYP-DPI synergy was also effective, were used.

5.3.1.1. Screen of yeast gene-overexpression clones

The results from the gene-overexpression screen did not give clear new insight to cellular mechanism(s) of synergy. Although resistance to the cyprodinil-DPI synergy (in yeast) could be overcome by the overexpression of a multidrug transporter, this activity would be expected to alter cellular accumulation of the agents rather than mechanism of intracellular action. This could suggest that the synergistic mechanism has multiple relevant targets that cannot be solved through a single mutation in the gene for one target protein. Furthermore, apart from *SGE1* (and a few other DNA regions unlikely to independently cause resistance), no other protein-coding genes were found among overexpressed genes conferring resistance. The absence of candidates apart from the multidrug transporter could suggest that a single protein function is not the main target of the cyprodinil-DPI synergy. It may also suggest that the synergistic mechanism may have non-protein targets. Possible non-protein-targeting mechanisms include inhibition/efflux of antioxidants such as glutathione (Riganti *et al*., 2004), degradation of lipid droplets (Fu *et al*., 2021; Kovacs *et al*., 2021), and direct DNA-binding to block transcription (Leung *et al*., 2013). However, these final

mechanisms were only thought of during the write up of this thesis and so were not able to be investigated experimentally.

Interestingly, *Z. tritici* is known to gain multidrug resistance through the overexpression of the major facilitator gene *MFS1* (Omrane *et al*., 2017). This might suggest that strains of *Z. tritici* employing this method of resistance, may naturally be resistant to the CYP-DPI synergy. However, the multidrug resistance conferred by *Z. tritici* is more effective at combatting azole fungicides, with only low resistance levels towards SDHIs recorded.

5.3.1.2. Yeast heterozygous deletion strain library

More than 1,100 diploid yeast strains that possessed only one copy of known essential genes were screened against cyprodinil-DPI. As the combination lethally inhibits cell growth (Appendix Figure 8.14), it seemed likely that one or more essential genes could be the target. However, this may not be so likely if the synergistic mechanism was based around ROS and oxidative stress, for example (unless a specific ROS-sensitive protein was the target).

The initial screen yielded 33 strains that were considered hits based on the growth yield (according to OD_{600}) being in the top/bottom 10% of all strains grown in media containing different combinations of cyprodinil and DPI. These hits were retested by dedicated assay of exponential-growth kinetics, rather than reading a single growth time-point. When looking at the growth curves for all strains under each different condition, there were no stand-out strains with an obvious drastic increase/decrease in resistance to cyprodinil, DPI, or the combination.

One strain, heterozygous for *YAH1* encoding a mitochondrial ferredoxin, showed resistance to cyprodinil (Figure 5.6). Previously, *yah1* overexpression was shown to

confer increased sensitivity to DPI and to the CYP-DPI combination (Figure 5.16). Overexpression of *yah1* is known to confer hypersensitivity to the prooxidant paraquat (Vallières *et al*., 2017). This was thought to occur due to the increased availability of FeS clusters which are released upon protein damage and participate in Fenton chemistry, aggravating oxidative damage. However, this relies on the speculation that during overexpression, all proteins receive a cluster and are then targeted by this potential synergistic mechanism.

5.3.2. Thoughts on the mechanism of CYP-DPI synergy

In this chapter, several experiments implicated oxidative stress as important for the CYP-DPI synergy (although this was contradicted by rho^0 and anaerobic experiments). DPI is often used in research as an inhibitor of ROS production (Li and Trush, 1998), and this was the initial reason ROS were tested here with DPI exposed cells (4.2.2.2). However, DPI is a non-specific inhibitor capable of targeting a wide range of enzymes (Riganti *et al*., 2004; Massart *et al*., 2014). While it has been suggested here that DPI has reactivity with thiol groups in the antioxidant glutathione (Figure 5.12), and that thiol-containing antioxidants protect against DPI-mediated inhibition (Figure 5.14C), glutathione has previously been shown to reverse the effects of DPI (Souri *et al*., 2021). In the literature cited, this was to prevent a DPI-mediated boost to arsenic toxicity. Interestingly, *arr2*, the gene for an arsenate reductase, was found in several of the DNA sequences returned from the CYP-DPI resistant mutants isolated from the overexpression library (Figure 5.9). ARR2 is required for arsenate (salt or ester of arsenic acid) resistance, acting by converting arsenate to arsenite, which can then be exported from cells by Arrp3 (Mukhopadhyay *et al*., 2000). In addition, GSH was required for ARR2 activity, which may have been pumped out of the cell due to DPI (Riganti *et al*., 2004). However, as one sequence did not include *arr2*, and all sequences

included the multidrug transporter *sge1*, it is less likely that arsenic is involved in the CYP-DPI synergistic mechanism.

DPI is known to increase oxidative stress (Riganti *et al*., 2004). This is thought to occur through DPI-mediated inhibition of the pentose phosphate pathway and tricarboxylic cycle. Although evidence here suggests that inhibition of mitochondrial NADPH production by cyprodinil may not be important in the synergy, it is interesting to note that DPI can inhibit NADPH production in the cytosol (Riganti *et al*., 2004). Additionally, in inhibiting the mitochondria-based citric acid cycle, DPI could decrease production of NADH in the mitochondria and the pool of NADH available for phosphorylation to NAPDH by the mitochondrial protein Pos5 (the potential cyprodinil target). This combination of effects appears to suggest a potential mechanism for CYP-DPI synergy. However, although resistance to the synergy increased somewhat, deletion of *pos5* did not increase sensitivity to DPI (Figure 5.18 and Figure 5.19), suggesting that inhibition of the Pos5 protein (e.g. by cyprodinil) should not cause sensitisation to DPI. However, as deletion of *pos5* is known to cause growth by fermentation, there may have been a decrease in generation of oxidative stress for the mechanism of DPI to potentially synergise with.

Although this study did not pinpoint a precise molecular target of cyprodinil involved in the synergy, there is evidence pointing towards a role for oxidative stress in the synergistic action of the CYP-DPI combination. This includes the alleviation of synergy by thiol-containing compounds such as glutathione and *N*-acetylcysteine (Figure 5.14), as well as thiol-containing amino acids methionine and cysteine (Figure 5.11C) and overexpression of *YAH1* and other FeS proteins conferring sensitivity to the synergy (Figure 5.16). Deletion of *SOD2* and *YAP1*, encoding proteins involved in oxidative stress responses, also gave increased sensitivity to the combination (Figure 5.17). In

addition, both cyprodinil and DPI appeared to have a combinatorial effect with H_2O_2 (Figure 5.15). Later, it is shown that mitochondrial membrane depolarisation, a deleterious effect linked to increased ROS in the mitochondria (Suzuki-Karasaki *et al*., 2014; Zorov *et al*., 2014), also occurred during incubation of yeast cells with cyprodinil, DPI, and the combination (see Figure 6.11), although this effect itself was not synergistic.

Although some evidence gathered here (Figure 5.20) and literature may conflict with this hypothesis, there is a lot of data to suggest that the inhibitory mechanism of CYP-DPI synergy is due to oxidative stress (at least as a final consequence). DPI *may* be contributing to the synergy by directly binding to thiol-containing antioxidants (although more experiments were needed to prove this), or by causing an efflux of glutathione, preventing the molecules from alleviating oxidative stress. Cyprodinil has been shown to cause increased ROS (Figure 5.20), although it is not clear specifically how the molecule executes this effect. Therefore, cyprodinil may be increasing intracellular ROS levels and oxidative stress, while DPI decreases the ability of the cell to respond, as well as causing additional oxidative stress.

5.3.3 Final remarks

In the previous chapter, a powerful synergy was found between cyprodinil and diphenyleneiodonium against the prevalent fungal phytopathogen *Zymoseptoria tritici*. Work carried out in this chapter aimed to understand the mechanism behind this synergy.

For CYP-DPI, the synergistic mechanism appears to be related to increases in reactive oxygen species caused by cyprodinil, and a simultaneous increase in sensitivity to oxidative stress caused by DPI. The rho^0 and anaerobic experiments seem to suggest that ROS, if indeed involved in the synergistic mechanism, is not generated via the ETC.

In addition, a specific molecular target of cyprodinil involved in this synergy is still not understood.

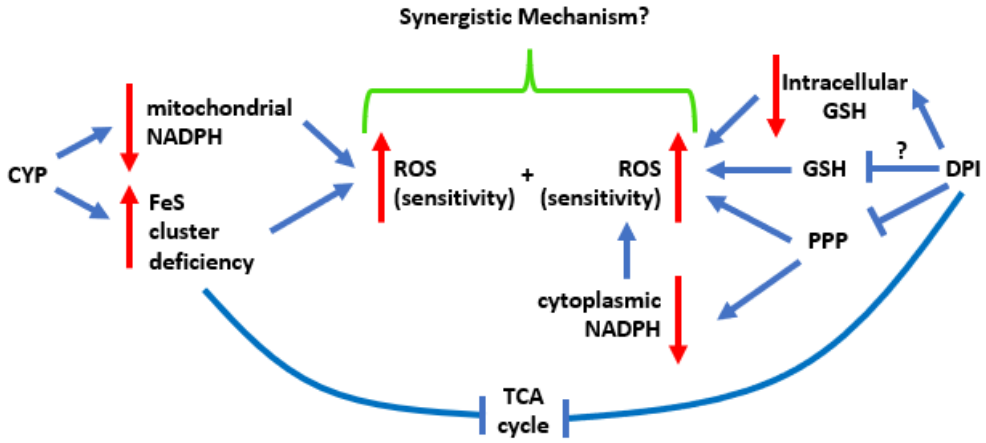

Figure 5.22. **Schematic of possible cyprodinil and diphenyleneiodonium interactions leading to synergy**. Through the potential inhibition of Pos5p, cyprodinil may lead to a decrease in mitochondrial NADPH, as well as an increase in FeS cluster deficiency, both leading to an increase in sensitivity to ROS. Diphenyleneiodonium is known to decrease levels of intracellular glutathione, and may potentially directly decrease glutathione activity, leading to an increase sensitivity to ROS. A similar consequence is seen through the inhibition of the pentose phosphate pathway. Additionally, through known mechanisms, both compounds have the potential to inhibit the tricarboxylic acid cycle. Blue arrows show a flow of consequences, while red arrows show increases or decreases of certain effects.

Chapter 6 - Discovery of synergistic copper and neocuproine combinations

6.1. Introduction

6.1.1. Background

In the late 19th century Alexis Millardet discovered the ability of neutralised copper sulphate to reduce grapevine downy mildew (Millardet, 1881; Ayres, 2004), providing the first effective tool to control various phytopathogens (Tamm *et al*., 2022). This concoction of copper sulphate, lime, and water was known as *Bordeaux mixture*, and introduced widespread use of copper as a fungicide. Even as early as 1807, copper sulphate (known as bluestone) was used to disinfect seeds (Johnson, 1935). Today, copper-based products are still widely used for the protection of plants in both organic and conventional agriculture. Copper has many advantages, including activity against a broad spectrum of organisms (Gessler *et al*., 2011). Such target organisms include ascomycetes, basidiomycetes, and oomycetes, including the causative agent of potato blight, *Phytophthora infestans*.

More recently, blocs such as the European Union have been aiming to reduce the application of copper-based treatments in agriculture. As copper cannot be degraded, it can bioaccumulate in ecological systems causing toxicity to non-target organisms, continuously cycling in the environment after release from its initial application (Eisler, 1998). One possible method of decreasing the amount of copper that accumulates in the environment, while retaining the advantages of its application, is through inclusion in fungicidal synergies.

6.1.2. Inhibitory mechanisms of copper

Copper is an essential micronutrient for all living organisms, primarily playing the role as a cofactor for several enzymes (Adamo *et al*., 2012). While copper deficiency can lead to impaired function of key enzymes, such as copper dependant oxidoreductases

and monooxygenases (Jaiser and Winston, 2010) an excess of copper can generate reactive oxygen species (ROS) or displacement of other metal ions in cells. As such, active homeostatic mechanisms work across concentration gradients to maintain low levels of intracellular copper, preventing accumulation (Kim *et al*., 2008). In fact, research suggests that there is less than one free copper ion per cell (Rae *et al*., 1999; Lippard, 1999). Metallochaperones guide transition metal ions within the cell, delivering them safely to the appropriate protein receptors (Pufahl, 1997). One such example is the yeast protein yCCS, which delivers copper to SOD1, activating the antioxidant enzyme (Rae *et al*., 1999).

Copper-based solutions act through the cupric ion (Cu++) which non-specifically leads to the denaturation of structural and enzymatic proteins, negatively impacting the cell membrane semi-permeability and blocking respiratory activity, preventing germination (La Torre *et al*., 2018). The modes of action of copper and its overall inhibitory effects on the cell appear broad. However, recent research indicates that copper action is dependent on mitochondrial respiration and involves targeting of the mitochondrial ferredoxin (Vallières *et al*., 2017) or direct binding to lipoylated components of the tricarboxylic acid cycle. This leads to a form of cell death known as cuproptosis (Tsvetkov *et al*., 2022).

6.1.3. Copper resistance

It is because of the multimodal activity of copper that resistance is unlikely to develop, with no resistance by oomycetes and fungi reported to various copper compounds (FRAC, 2018). Despite this, some bacterial phytopathogens have developed resistance (Marco and Stall, 1983; Bender and Cooksey, 1986; Sholberg *et al*., 2001) through mechanisms such as efflux pumps, copper oxidases, and copper transporters (La Torre, 2018). It is possible, as was seen from the CYP-DPI overexpression library experiment

(2.2.15.1), that synergies involving copper may also be resisted through efflux mechanisms.

Impairment in intracellular copper levels, copper transport, and copper localisation are implicated in several human diseases (Waggoner *et al*., 1999; De Freitas *et al*., 2003). While various mechanisms of copper-induced cell death have been reported, it seems that the recently discovered cell death mechanism termed cuproptosis is the true underlying mechanism. It was recently discovered that deletion of either *FDX1*, a reductase known to reduce Cu^{2+}, and *LIAS* (lipoyl synthase) in the human ovarian clear cell carcinoma cell line (OVISE) conferred resistance to cuproptosis induced by copper ionophores elesclomol, disulfiram, NSC319726, Thiram, 8-HQ, and Zn-Prithione. However, this resistance was lost at high concentrations of elesclomol suggesting that off-target mechanisms may occur at high ionophore concentrations (Tsvetkov *et al*., 2022).

S. cerevisiae is well known for its naturally high resistance to copper, which has been purportedly having evolved due to the spraying of vines with copper salts and/or due to the use of copper-containing storage vessels and fermenters (Mortimer, 2000). In *S. cerevisiae*, copper resistance is known to be granted by several genes, including *CUP1* and its regulator, *ACE1*. If intracellular copper levels become abundant, Ace1 becomes loaded with cuprous ions and activated (Buchman *et al*., 1989; Pena *et al*., 1998). CUP1, and other proteins responsible for copper detoxification, are then upregulated to confront the threat of excess copper. Sod1 is also upregulated to aid in the removal of harmful radicals (Mehta *et al*., 2018).

CUP1 encodes a metallothionein, low molecular weight, cysteine-rich proteins that are ubiquitous in eukaryotes. Metallothionines decrease the toxic potential of copper by chelating copper ions (Kägi, 1991). Adaptation to high levels of copper toxicity by *S,*

cerevisiae occurs primarily through *CUP1* gene amplification (Whale *et al*., 2022). Resistance to copper is also gained by regulating the uptake of copper into cells (White and Gadd, 1986) and increased antioxidative activities (Perrone *et al*., 2008).

Copper uptake in yeast is highly regulated, consisting of both high and low affinity transporters (Radisky and Kaplan, 1997). The high affinity transporters are more selective for target metals (e.g., copper) and are tightly regulated according to metal need whereas the low affinity transporters are less responsive to needs for metal and are less selective for the metals they transport. These mechanisms allow yeast cells to maintain metal homeostasis, in conditions of either metal excess or limitation. The same mechanisms apply to iron, manganese, and zinc, as they do for copper (Radisky and Kaplan, 1997).

For *Z. tritici*, I was unable to find literature that detailed the mechanisms of copper homeostasis and detoxification in *Z. tritici*. However, it is entirely possible that copper resistance in *Z. tritici* could be overcome by mechanisms similar to those mentioned of *S. cerevisiae*. Interestingly, cells reliant on mitochondrial respiration were nearly 1000-fold more sensitive to copper ionophores than cells undergoing glycolysis (Tsvetkov *et al*., 2022). This might suggest that filamentous fungi, such as *Z. tritici*, undergoing aerobic growth, will be far more sensitive to copper ionophores than, for example, *S. cerevisiae* undergoing fermentative growth. Interestingly, however, it was shown that, that carbon in yeast metabolism directly affects redox status and cellular physiology (Maslanka *et al*., 2020). In the study mentioned, fermentative metabolism, which was triggered by high levels of glucose, led to increased levels of the superoxide anion.

6.1.4. Copper chelators

Chelating agents are molecules that have the ability to bind to metal via multiple points of contact, forming metal complexes. In pharmacology, chelators are generally used in therapeutic treatments for the removal of metals from the body. Ionophores, a subset of chelating agents, typically form lipophilic metal complexes that lead to intracellular access for the complexed metal (Helsel and Franz, 2015).

Copper chelators are often used for studying copper-related biological functions in areas such as cancer, neurodegeneration, and microbial diseases (Hunsaker *et al*., 2019; Oliveri, 2020). Neocuproine is one such copper chelator (Castro *et al*., 2014). This membrane-permeable ionophore primarily chelates Cu^{1+}, but can also bind Cu^{2+} (Nunes *et al*., 2018). Copper sulphate ($CuSO_4$), which was used throughout this project, yields Cu^{2+}, and so a Cu^{2+}-neocuproine complex (Figure 6.1) is the most relevant.

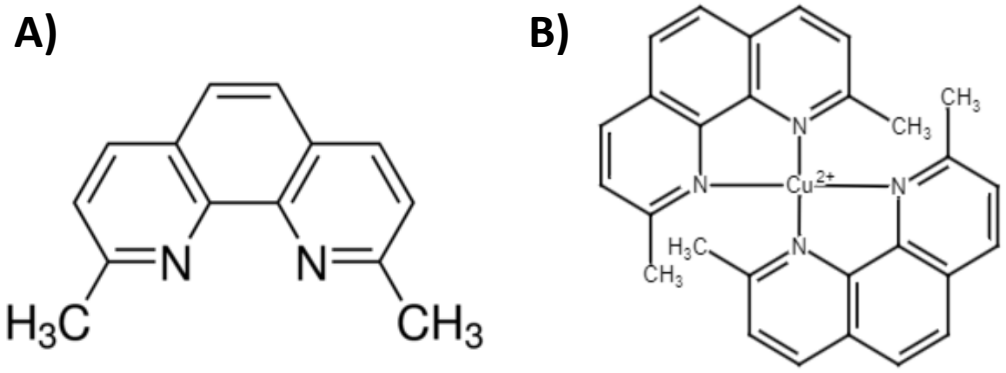

Figure 6.1. **Chemical structure of neocuproine and copper**. A) Chemical structure of neocuproine. B) Neocuproine-copper complex. Two neocuproine molecules bind to one copper atom. Structures obtained from Pubchem and drawn using Chemspace.

As a copper ionophore, neocuproine has been shown to cause increased uptake of copper into cells (Castro *et al*., 2014). 2-(6-benzyl-2-pyridyl)quinazoline (BPQ), a copper chelator similar to neocuproine, was found to enhance and potentiate damage to mitochondria by copper, suggesting that at least some of the bound copper is released into this organelle. This copper-delivery of BPQ bypassed the resistance mechanisms of *S. cerevisiae* that have evolved to protect mitochondrial iron-sulphur

clusters (Foster *et al*., 2014). Neocuproine may therefore lead to the same consequences as BPQ when each form lipophilic complexes with copper and deliver the metal into cells.

Zinc pyrithione (ZPT) is used in antidandruff products and antifouling paints and works to inhibit cells through an increase in cellular copper levels which in turn leads to a loss of activity of iron-sulphur clusters. The pyrithione acts as a copper ionophore, causing increased copper influx into intracellular organelles such as mitochondria. Reeder *et al*. (2011) suggest that the increased levels of copper decreases the activity of iron sulphur cluster-containing enzymes, similar to the mechanisms of copper inhibition reported against Escherichia coli (Macomber and Imlay, 2009) and Bacillus subtilis (Chillappagari et al., 2010).

Tardito *et al*. (2011) state that ligands disassociate from their bound metal mostly in the extracellular environment where copper is sequestered by binding to competitors such as amino acids and serum proteins. The proportion of copper that remains complexed, following diffusion law, equilibrates between the extracellular and intracellular spaces.

6.1.5. Ziram

A dithiocarbamate is a function group and analogue of a carbamate, in which the two oxygen atoms are replaced by sulphur atoms, with thiocarbamates the result if only one oxygen atom is replaced. Dithiocarbamates can react with metal salts to give a wide variety of transition metal-dithiocarbamate complexes that have different uses, such as in the vulcanisation of rubber (Shi *et al*., 2021), or as fungicides. Ethylene bisdithiocarbamates in the form of complexes with, manganese (maneb), zinc (zineb), or a combination of manganese and zinc (mancozeb) have been used as fungicides since the 1940s (Morton and Staub, 2008).

Shortly before the beginning of this PhD project, copper sulphate ($CuSO_4$) was found to work in synergy against *Zymoseptoria tritici* and *Rhizoctonia solani* with zinc dimethyldithiocarbamate (ziram), a commonly used fungicide (Vallières *et al*., 2018). This synergy was proposed to be related to combined actions on translation fidelity via amino acid availability. Ziram, also known as zinc dimethyldithiocarbamate, is a coordination complex of zinc with dimethyldithiocarbamate, one of the simplest organic dithiocarbamates (Schubart, 2000). The compound modifies thiol-containing amino acids and has also been reported to inhibit enzymes containing copper ions (Walker, 2009; Cedergreen, 2014).

Recent research has shed more light on the primary mode of action (MoA) of ziram and other dithiocarbamate fungicides (Adeyemi and Onwudiwe, 2020). Dithiocarbamates, inhibit via their own synergism with the metal ions they bind, altering the toxicity of the metal whilst simultaneously enhancing their own biological properties (Mamba *et al*., 2010). In these cases, DNA is the most common targeted site of action (reviewed in Adeyemi and Onwudiwe, 2020). The two sulphur atoms present within dithiocarbamates are available for complexation and show strong binding capacity to transition metals such as copper, iron, nickel, and zinc (Manoussakis *et al*., 1987), which can lead to enzyme inhibition (Onwudiwe and Ajibade, 2012). The weak covalent metal-ligand bond is likely to undergo ligand substitution and redox reaction enabling the dithiocarbamates and metal ions to reach their target sites (Adeyemi and Onwudiwe, 2020). Ziram itself has been shown to increase intracellular levels of zinc and copper (Dennis and Valentine, 2015).

Another of the proposed MoAs of dithiocarbamates is the strong inhibition of carbonic anhydrases (CAs). Although that work was carried out in *Leishmania major* promastigotes, their flagellated form (Pal *et al*., 2015), CAs play crucial roles in various

physiological processes (Sly, 1995) and occur in other organisms including fungi (Amoroso *et al*., 2005; Innocenti *et al*., 2009).

6.1.6. Chapter Aims

As part of the present work, it was aimed to test whether neocuproine could synergise with copper and/or ziram in fungi. Such insights can further the understanding of underlying mechanisms of drug action and synergy and potentially help to predict other related synergies.

Secondly, this chapter looks at the discovery of new synergies involving neocuproine and copper, attempting to elucidate the synergistic mechanisms behind them.

Thirdly, this chapter aims to see if two of the most powerful synergies discovered in throughout this research can protect live plants from infection by *Zymoseptoria tritici*. It is possible that the strength of the synergy in a laboratory environment does not translate well to preventing *Z. tritici* pathogenicity.

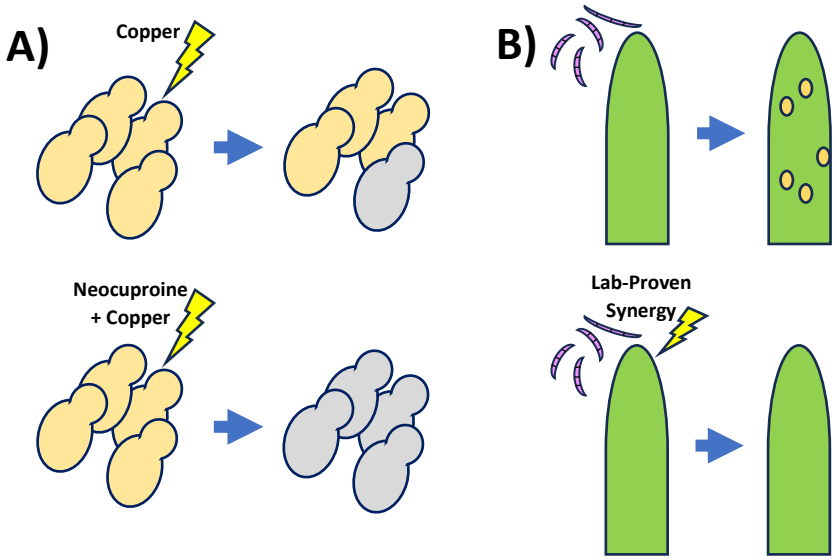

Figure 6.2. **Schematic of chapter hypotheses**. A) Neocuproine will enhance copper uptake to synergistically inhibit fungal cells. B). Lab-proven synergies will protect live wheat plants from *Z. tritici* infection.

6.2. Results

6.2.1. Copper, neocuproine and ziram

Initially, the copper chelator neocuproine was used to help characterise the mechanism behind the anti-fungal copper-ziram synergy found by Vallières *et al*. (2018). Neocuproine was hypothesised to increase the uptake of copper into cells (Castro *et al*., 2014; Foster *et al*., 2014), potentially enhancing the synergistic effect of the copper-ziram combination and so the strength of phenotype with which to elucidate the mechanism.

At high enough $CuSO_4$ and ziram concentrations, the media changed colour to a bright orange (Figure 6.4). This is indicative of copper chelation (Foster *et al*., 2014) and suggests that these molecules are interacting directly with one another and that a copper-ziram complex is formed. Similarly, addition of neocuproine to copper sulphate, at high enough concentrations, also showed this colour change to orange. It should be noted that ziram does this more effectively, with comparatively more intense colour changes at the same concentrations. The colour changes in YEPD with copper for both ziram and neocuproine occurred in the presence or absence of cells. In YEPD without copper, the same concentrations did not lead to colour change.

The previously-reported copper-ziram synergy was corroborated here in *S. cerevisiae* (Figure 6.3A, FICI = 0.375) and *Zymoseptoria tritici* (Figure 6.3B, FICI = 0.28). *Z. tritici* is more sensitive to both ziram and copper. The ziram MIC for *Z. tritici* in PDB (synergy was not detected in MCS medium) is 500 ng ml^{-1}, 100-fold lower than that of *S. cerevisiae*. Similarly, *Z. tritici* is at least 3.5-fold more sensitive to copper sulphate, with an MIC of 31.25 µM.

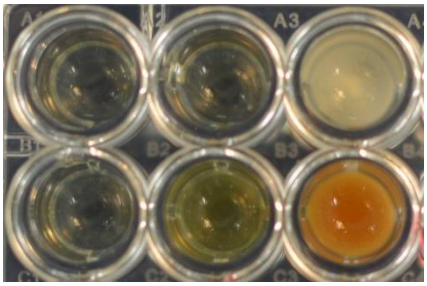

Figure 6.4. **Visualisation of copper chelation in YEPD medium**. Wells contain YEPD with H_2O (top row) or 1 mM $CuSO_4$ (bottom row). Middle column contains 5 mM neocuproine; right column contains 5 mM ziram.

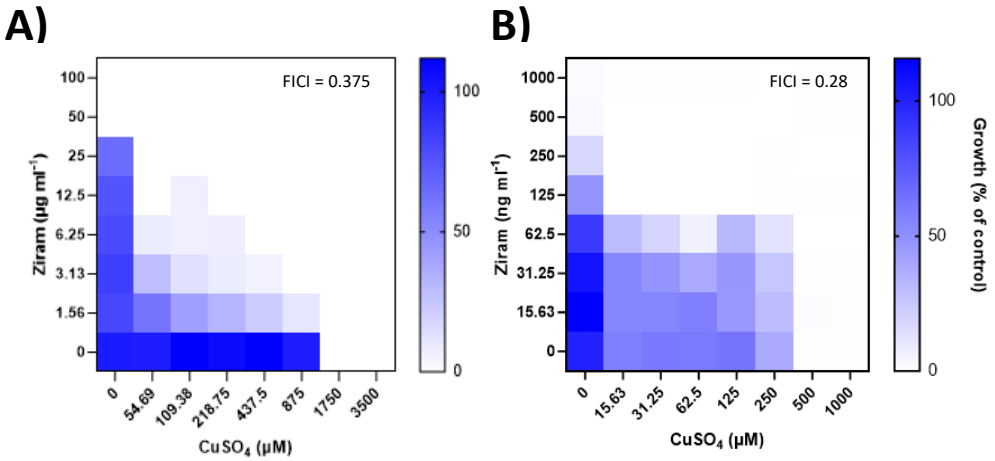

Figure 6.3. **$CuSO_4$-ziram checkerboards in *S. cerevisiae* and *Z. tritici*.** Assays were performed according to the EUCAST procedure at the indicated concentrations of ziram and copper sulphate with A) *S. cerevisiae* (BY4743) in YNB broth containing 2% glucose and B) *Z. tritici* in PDB. Growth values (scale to the right) represent means from three independent experiments, calculated as percentages of growth (OD_{600}) with compounds relative to the minus-compound control. For *S. cerevisiae*, data were collected at 0 h and 48 h during incubation at 30°C. For *Z. tritici*, data were collected at 0 h and 168 h, during incubation at room temperature. Growth values <5% were assigned as no-growth.

After commencing this work and carrying out several experiments, including three-way checkerboards (data not shown), an older paper by Phinney and Bruland (1997) was found. They proposed that a direct physical interaction between copper and ziram yielded a lipophilic complex that increased copper uptake into cells of phytoplankton. If it is the case that copper (in the form of $CuSO_4$) and ziram bind to each other, my prior work using neocuproine to chelate copper in the hopes of increasing its uptake and enhancing the synergy was inappropriate (data not shown).

To test the Phinney and Bruland hypothesis, a competition experiment was carried out. Copper sulphate, ziram and neocuproine, were included with yeast cells in wells of a 96-well plate in different combinations and orders (Figure 6.5).

It was reasoned that the different levels of inhibition of yeast growth achieved through different treatments would indicate i) if the copper-ziram complex was competitive with the copper-neocuproine complex, ii) which of the two complexes was more inhibitory than the other to yeast cells, and iii) give an approximate indication of how fast the inhibitory process begins. Showing competition for copper binding between neocuproine and ziram would be evidence that the Phinney and Bruland hypothesis is correct.

The $CuSO_4$ and ziram combination concentrations used gave visible inhibition when compared to the control of $CuSO_4$ alone – roughly a four-hour delay in reaching OD_{600} 1 (Figure 6.5A). The concentration of neocuproine was the same as that for ziram (20 µM). This was so that the same number of molecules of each compound were present and available to bind to copper.

When cells are added after a 30-minute incubation (to allow time for prior reaction where two compounds were added at the start, Figure 6.5A), $CuSO_4$ alone, gave the strongest growth. $CuSO_4$ in combination with ziram gave a mild inhibition; final OD_{600} was similar, but there was a four-hour delay in reaching OD_{600} 1 when ziram was present. $CuSO_4$ in combination with neocuproine gave total inhibition of cell growth, indicating a much more potent interaction than that of copper-ziram (Figure 6.5A). Inclusion of ziram rescued the potent inhibition by Cu + neocuproine (regardless of order of addition), showing comparable growth to $CuSO_4$ + ziram. This was consistent with the copper-ziram complex being chemically favoured compared with copper-neocuproine (Figure 6.5A), i.e. ziram binds copper more efficiently than neocuproine.

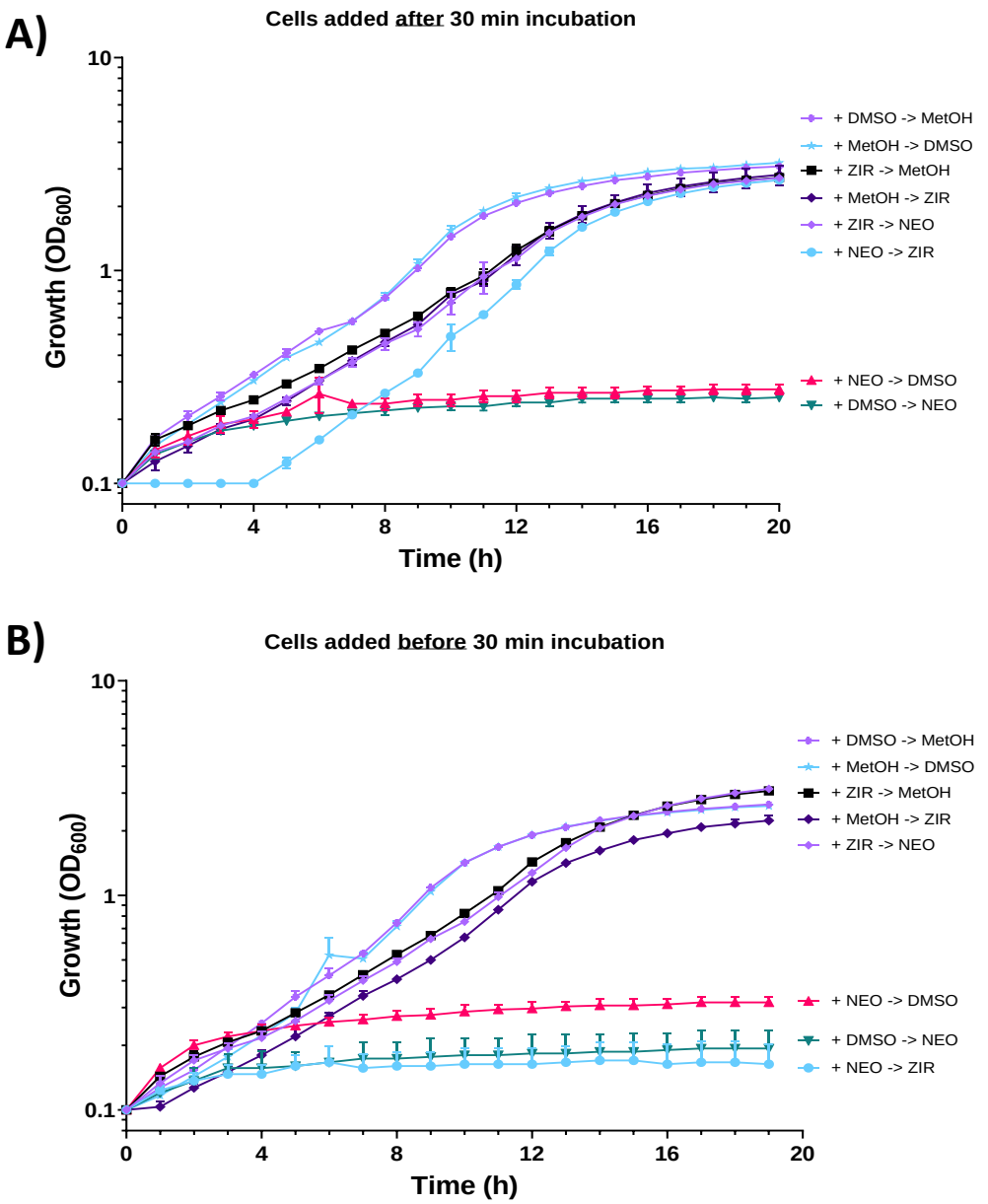

Figure 6.5. **Investigating the combinatorial effects of neocuproine, ziram and copper sulphate.** Growth of *S. cerevisiae* BY4743 with different treatments. Key shows in which order drugs and/or solvents were added to wells. "30" indicates a 30 min incubation at 30°C before addition of the final drug/solvent. H_2O, $CuSO_4$ solvent; DMSO, ziram solvent; methanol (MetOH), neocuproine solvent. $CuSO_4$ concentration, 3.4175 µM; ziram (ZIR) concentration, 20 µM; neocuproine (NEO) concentration, 20µM. A) Cells added after 30 min incubation at 30°C along with final treatment. B) Cells added before 30 min incubation at 30°C along with initial treatment. '+' indicates solution added along with $CuSO_4$. Compounds after '->' were added after 30 min incubation of previous compounds with/without cells. Exponential phase cells were added to a starting OD_{600} of 0.1. Plates were incubated shaking at 30°C in an Epoch 2 plate reader. n = 3.

When cells were added with the initial compound(s) and incubated for 30 minutes before the addition of any third compound (Figure 6.5B), the growth curves were similar to those of Figure 6.5A. A notable exception was loss of the rescue by ziram of

the inhibition by Cu + neocuproine, where the latter two were allowed to react first (Figure 6.5B). This suggests that 30 minutes is enough time for the copper-neocuproine complex to enter cells and initiate strong inhibitory process(es), so long as cells are included before ziram is added.

Nevertheless, when ziram was added along with cells after copper and neocuproine had been incubating alone, there was a 4-hour delay in the initiation of growth (Figure 6.5A). This was consistent with a short-term action of a more potent complex (copper-neocuproine) before the remaining bound extracellular copper may have been displaced by ziram to form a less potent copper-ziram complex.

Together with the visual aid of Figure 6.4, the data support the literature evidence that either ziram (Phiney and Bruland, 1997) or neocuproine (Castro *et al*., 2014) may bind to copper (and do so competitively). This causes increased growth inhibition, presumably via increased uptake into the cells. While $CuSO_4$ and ziram in combination in this experiment were used at low enough concentrations to not completely inhibit growth, the combination of $CuSO_4$ and neocuproine (with neocuproine at the same concentration as ziram), was extremely inhibitory (Figure 6.5). This suggests that while copper chelation and subsequent increased uptake (due to the lipophilic properties of the complexes) may explain the observed effects for both neocuproine and ziram, the copper-neocuproine complex contributes to a far more potent synergy at the concentrations tested. This may be due either to (i) the relative individual effects of neocuproine or ziram once inside the cell, (ii) the relative amounts of copper (or copper-chelator complex) accumulated in the cell, (iii) an effect of chelator on copper localization once inside the cell (e.g., cytosol vs mitochondria). This concept for neocuproine is explored later in this chapter.

The experimental data are consistent with the hypothesis of Phinney and Bruland, as regards to yeast, that copper and ziram are likely synergistic due to a copper-ziram complex which may cause enhanced uptake into cells.

One oversight of this experiment was that the copper-neocuproine complex is thought to require two neocuproine molecules for one copper molecule (Figure 6.1B), whereas Phinney and Bruland hypothesised the copper-ziram complex to require only one ziram molecule (Phinney and Bruland, 1997). This may mean that the concentrations used were inappropriate, as the same concentration of neocuproine would only be able to bind to half as many copper molecules at maximum efficiency. This could be an explanation for growth data that were consistent with ziram outcompeting neocuproine for chelation of copper when mixed. However, as ziram was able to prevent the stronger growth-inhibitory effects of neocuproine with copper when ziram was added along with cells (when compared to being added after copper and neocuproine had incubated with cells), this suggests that the effect of ziram was (at least in part) due to the copper-ziram complex being chemically preferred to copper-neocuproine, rather than simply outcompeting due to potential for binding double the number of copper molecules.

In summary, Figure 6.5 suggests that neocuproine, a copper chelator, is less potent when ziram is present. Along with the colour change indicative of copper chelation seen in Figure 6.4, this suggests that ziram binds to copper and supports the literature suggesting that ziram may increase copper uptake.

Figure 6.6. **Schematic indicating chemical complexes preferences**. When copper, neocuproine, and ziram are mixed, the copper-ziram complex is chemically preferred to the copper-neocuproine complex. However, the copper-neocuproine complex is more inhibitory if allowed to enter cells.

6.2.2. Neocuproine and copper sulphate exhibit a strong synergy when in combination

Neocuproine is a copper chelator known to increase uptake of copper into cells (Castro *et al.*, 2014). As copper is a traditional fungicide, the interaction of copper and neocuproine was considered to be of interest here. As expected, neocuproine was found to be synergistic with copper sulphate when tested in combination against yeast (Figure 6.7). Here, the MIC for neocuproine and copper sulphate decreased 128- and 32-fold, respectively, in combination. In *Z. tritici*, a synergistic interaction also occurred (FICI ≤ 0.02), but unexpectedly appeared to become less effective at higher, intermediate copper concentrations (Figure 6.7B). This effect was seen in three of three biological replicates. A similar effect was seen in earlier experiments relating to the copper-ziram synergy (Appendix Figure 8.10). Despite the checkerboards containing ziram, the effect occurs in wells in which ziram is not present (Appendix Figure 8.10). However, it is unclear what may cause this effect. It is understood that

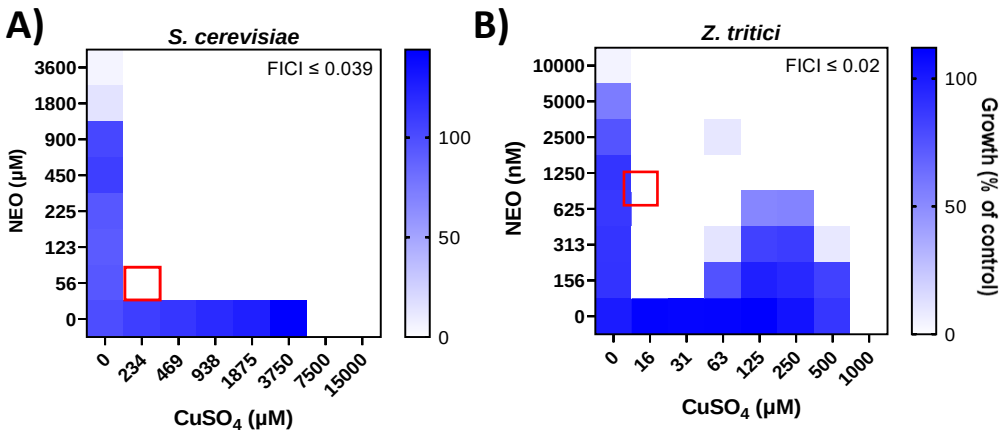

Figure 6.7. **Copper and neocuproine exhibit a strong synergistic effect in *S. cerevisiae* BY4743.** A) Exponential phase *S. cerevisiae* or B) *Z. tritici* spores were treated with neocuproine and copper sulphate in a checkerboard format. Growth values (scale to the right) represent means from three independent experiments calculated as percentages of growth (OD_{600}) with compounds relative to the minus-compound control. Growth pattern shown in B is present in all replicates. *S. cerevisiae* was grown in YNB medium at 30°C, and data were collected at 0 h and 24 h. *Z. tritici* was grown in MCS medium at room temperature and data were collected at 0 h and 168 h. Growth values <5% were assigned as no-growth. Neocuproine MIC assumed to be 7.2 mM for FICI calculations in *S. cerevisiae* and 20 µM for FICI calculations in *Z. tritici*. Red square indicates concentration used to calculate FICI values.

for some compounds, such as echinocandins, growth can paradoxically come back at higher concentrations despite inhibition at lower concentrations (Wagener and Loiko, 2017).

6.2.3. Cyprodinil is synergistic with the copper chelator neocuproine but not with copper

Neocuproine was also found to be synergistic with cyprodinil against *S. cerevisiae* and *Z. tritici* but in not *B. cinerea* (Figure 6.8). The synergy was strongest for *S. cerevisiae* with a FICI of 0.156 (Figure 6.8A). Against *Z. tritici* an FICI of 0.25 was recorded, with the MIC for each compound dropping eight-fold when in combination (Figure 6.8C). The lower growth seen at middle cyprodinil concentrations (in this case 47 µM) compared to higher concentrations was assumed to be an artefact occasionally seen in *Z. tritici* checkerboard replicates throughout the PhD project (e.g. Figures Figure 4.6, Figure 4.10B, Figure 4.10C, and Figure 4.12A) and could not be explained, with following of experimental procedure and standard laboratory practice meticulous. This effect never occurred in *B. cinerea* or *S. cerevisiae* checkerboards.

As neocuproine is thought to act by increasing cellular levels of copper, cyprodinil was also tested in combination with $CuSO_4$. Interestingly no synergy between cyprodinil and copper was found in any organism (Appendix Figure 8.9). Neocuproine and DPI were also synergistic in two of three biological replicates in *S. cerevisiae* (consistent across WT, *pos5Δ* and *pos5* replacement strains) and in three of three biological replicates *Z. tritici* (consistently present but with a varied FICI). In *B. cinerea*, this combination appears antagonistic (Appendix Figure 8.13B).

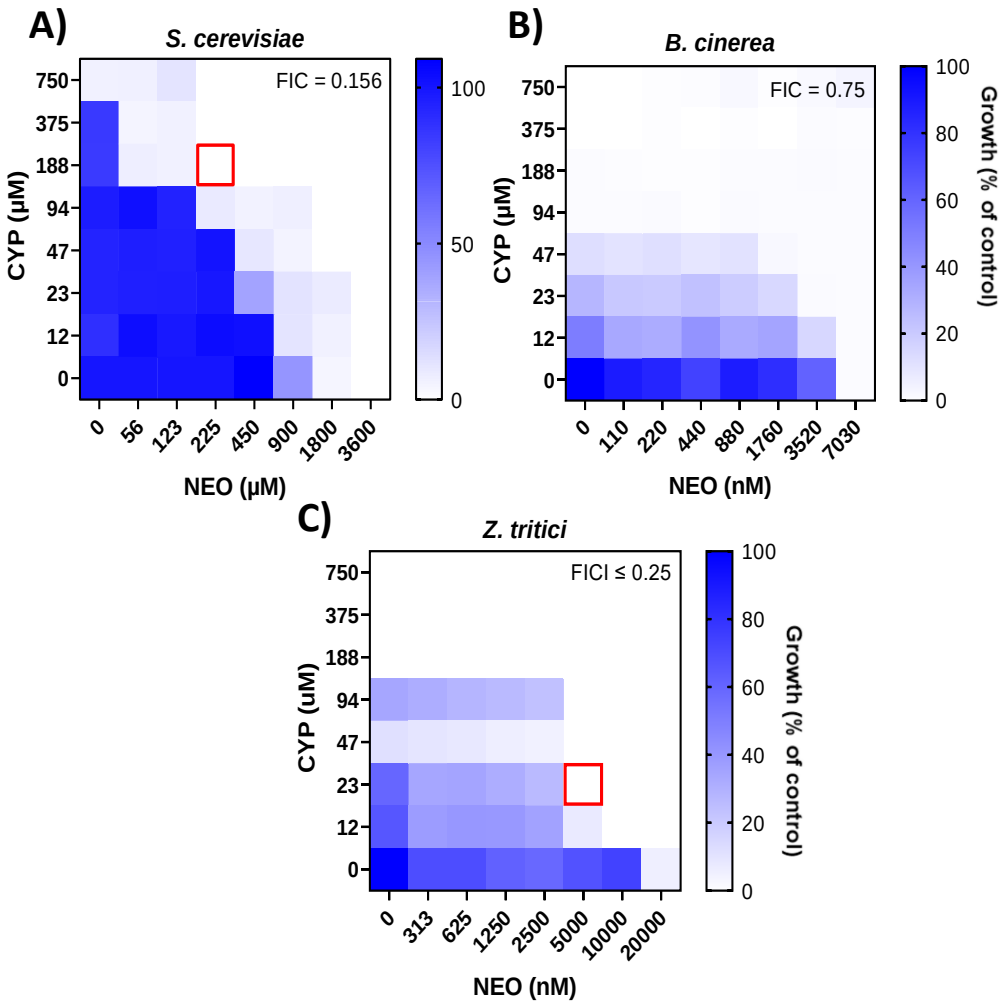

Figure 6.8. **Cyprodinil-Neocuproine checkerboards for different fungal organisms.** A) Exponential phase *S. cerevisiae* BY4743; B) *B. cinerea* spores; or C) Z. *tritici* spores were treated with cyprodinil and neocuproine in a checkerboard format. Growth values (scale to the right) calculated as percentages of growth (OD_{600}) with compounds relative to the minus-compound control. *S. cerevisiae* was grown in YNB medium at 30°C, and data were collected at 0 h and 48 h. *B. cinerea* and *Z. tritici* were grown in MCS medium at room temperature and data were collected at 0 h and 168 h. Growth values <5% were assigned as no-growth. Cyprodinil MIC assumed to be 1.5 mM for FICI calculations in *S. cerevisiae*. Neocuproine MIC assumed to be 40 µM for FICI calculations in *Z. tritici*. Red squares indicate concentrations used to calculate synergistic FICI values.

6.2.4. S. cerevisiae expressing *POS5* from *B. cinerea* or *Z. tritici* shows stronger synergy to cyprodinil-neocuproine combination

As the cyprodinil-DPI and cyprodinil-neocuproine synergies differed in strength between *Z. tritici* and yeast, it was tested to see if this may be due to differences in Pos5p between species. To understand the interspecies differences in sensitivity to the CYP-DPI and CYP-NEO synergies, multicopy plasmids containing *POS5* cloned from

S. cerevisiae, *B. cinerea* or *Z. tritici* were transformed into *pos5Δ S. cerevisiae*. These strains/proteins are referred to as *Sc*Pos5, *Bc*Pos5, and *Zt*Pos5, respectively. The *B. cinerea* and *Z. tritici pos5* genes were codon optimised for *S. cerevisiae*.

As represented for CYP-DPI in Figure 5.19, the CYP-NEO combination in *pos5Δ S. cerevisiae* (Figure 6.9B) show a higher FICI compared to the control (Figure 6.9A), indicative of increased resistance to the synergy. When *Sc*Pos5 is reintroduced into *pos5Δ S. cerevisiae* on a plasmid (Figure 6.9C), sensitivity to the synergy compared to the WT is largely recovered as is the 'shape' of the synergies according to checkerboard appearance. This was not true for complementation with Pos5 from the other species. In these cases, according to the more intense growth seen in WT, *pos5Δ*, and *Sc*Pos5 strains, the synergistic effect appears stronger in *Bc*Pos5 and *Zt*Pos5 strains (Figure 6.9). However, total inhibition is not reached over intermediate combination concentrations against the *Bc*Pos5 or *Zt*Pos5 strains and, as such, among the three strains expressing plasmid-borne *pos5*, the FICI for the *Sc*Pos5 strain gives the strongest synergy (FICI ≤ 0.25, Figure 6.9C), but the 'L' shape of a stronger combinatorial effect is suggested by both the *Bc*Pos5 (Figure 6.9D) and *Zt*Pos5 (Figure 6.9E) strains. These 'L'-shape checkerboards are like those seen for neocuproine-copper combinations (Figure 6.7, Appendix Figure 8.8).

Despite the absence of a CYP-NEO synergy in *B. cinerea*, *S. cerevisiae* expressing *Bc*Pos5p showed hyper-sensitivity to this combination when comparing final OD_{600} (although unable to be shown by FICI values). As the *S. cerevisiae* strains expressing different *pos5* genes grow similarly in control conditions, and as the sequences were codon-optimised for *S. cerevisiae*, the reasoning for this is unclear.

For CYP-DPI, it was expected that the *Zt*Pos5 strain might be more sensitive than the others as this synergy was consistently strongest in *Z. tritici*. In the experiments carried

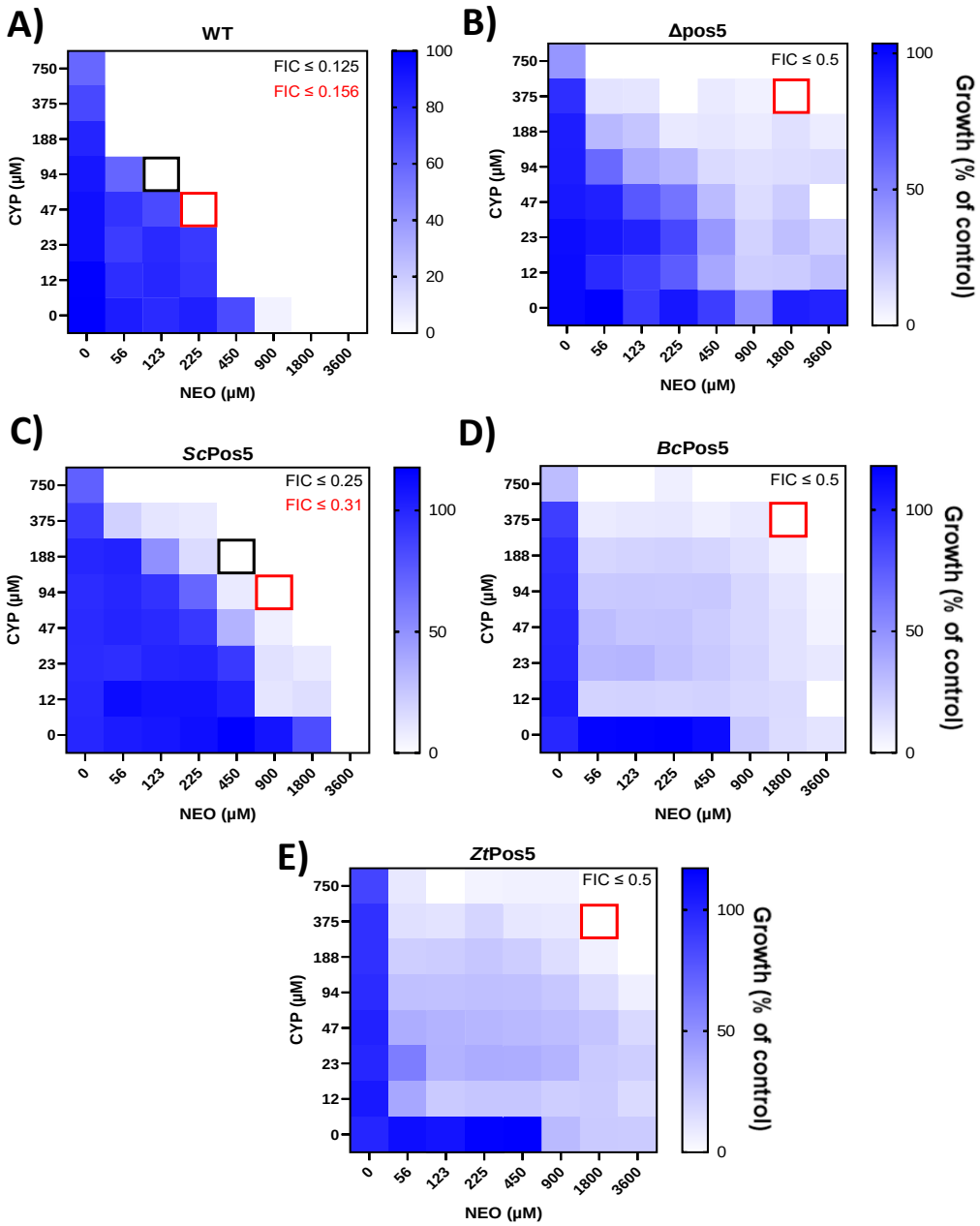

Figure 6.9. **CYP-NEO combination in S. cerevisiae expressing Pos5p of different fungal species**. Exponential phase S. cerevisiae A) Wild-type BY4743; B) pos5Δ; C) pos5Δ+ScPos5; D) pos5Δ+BcPos5; E) pos5Δ+ZtPos5 were treated with cyprodinil and neocuproine in a checkerboard format. Growth values (scale to the right) calculated as percentages of growth (OD_{600}) with compounds relative to the minus-compound control. S. cerevisiae was grown in YNB medium at 30°C, and data were collected at 0 h and 24 h. Growth values <5% were assigned as no-growth. Red and black squares indicate concentrations used to calculate FICI values.

out, it was shown that *Bc*Pos5 (FICI ≤ 0.375) and *Zt*Pos5 (FICI ≤ 0.5) strains showed increased sensitivity to the CYP-DPI combination when compared to the other strains, including the WT (FICI > 0.5) (Appendix Figure 8.12). However, although there was high sequence similarity, it is uncertain if the *B. cinerea* and *Z. tritici* sequences gave a function complementation.

6.2.5. Cyprodinil and neocuproine are synergistic with mitoquinol

When testing the effects of different antioxidants (ascorbic acid, glutathione, *N*-acetylcysteine, and mitoquinol) on the CYP-DPI and CYP-NEO synergies, it was found that both cyprodinil and neocuproine are synergistic with the mitochondrial antioxidant mitoquinol. Growth curves showed that when sub-inhibitory concentrations of mitoquinol were added to sub-lethal concentrations of cyprodinil or neocuproine, there was increased inhibition (Figure 6.10).

At high enough concentrations, mitoquinol is toxic to cells. One mechanism of toxicity is thought to be due to mitoquinol insertion into the mitochondrial membrane,

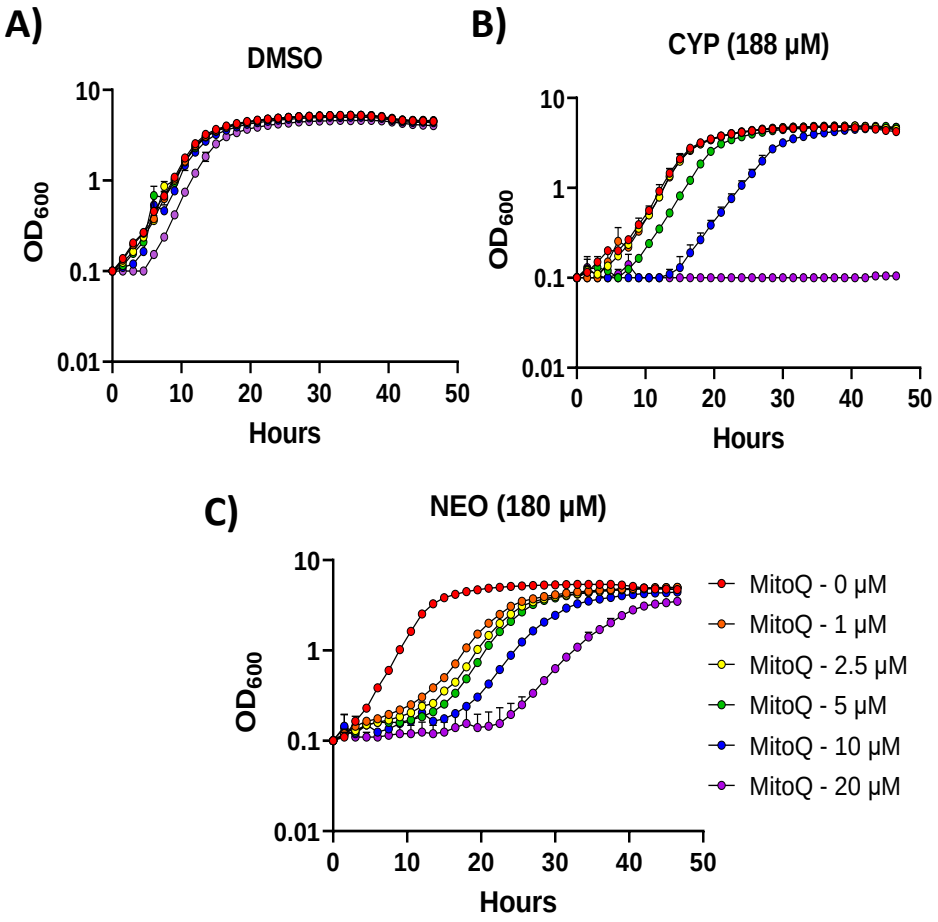

Figure 6.10. **Mitoquinol is synergistic with cyprodinil and neocuproine in *S. cerevisiae***. Exponential phase *S. cerevisiae* W303 grown in YEPD were treated with A) DMSO; B) 188 µM cyprodinil; C) 180 µM neocuproine. Individual wells were supplemented to the specified mitoquinol concentrations (MitoQ). Plates were incubated at 30°C and OD_{600} was read every 30 minutes. Error bars represent standard deviation. n = 4 biological replicates carried out in the same 96-well plate on the same day.

causing mitochondrial swelling and depolarisation (Gottwald *et al*., 2018). Mitoquinol has been reported to increase ROS production in some cancer cells which has been associated with a lowering in mitochondrial membrane potential and mtDNA copy number (Pokrzywinski *et al*., 2016).

6.2.6. Measuring mitochondrial membrane potential in *S. cerevisiae*

As mitoquinol toxicity is reported to depolarise the mitochondrial membrane, this was considered as a basis for the mitoquinol synergies with cyprodinil and neocuproine. Rhodamine 123 is a dye that accumulates in the mitochondrial membrane and fluoresces in a membrane potential-dependent manner. As mitochondrial membrane potential decreases, fluorescence is decreased (Baracca *et al*., 2003). As a positive control, sub-inhibitory and inhibitory concentrations of amphotericin B (Figure 6.11A), known to cause depolarisation of the mitochondrial membrane (Lee *et al*., 2002), led to a 90-100% decrease in rhodamine 123 fluorescence (Figure 6.11C). At cyprodinil and DPI concentrations that give 128% and 87% relative growth when compared to the control (Figure 6.11B), rhodamine 123 fluorescence decreased by 20% and 70%, respectively (Figure 6.11D), suggesting that cyprodinil and DPI both cause depolarisation of the mitochondrial membrane. In combination, growth is significantly lower than that expected for an additive effect (Figure 6.11B). The combination of CYP-DPI at these concentrations leads to (non-significantly) higher rhodamine 123 fluorescence than expected even for an additive effect (Figure 6.11). This indicates that depolarisation of the mitochondrial membrane by these compounds is independent of each other and is not a synergistic effect. Depolarisation of the mitochondrial membrane is therefore unlikely to contribute to the mechanistic basis for the synergy.

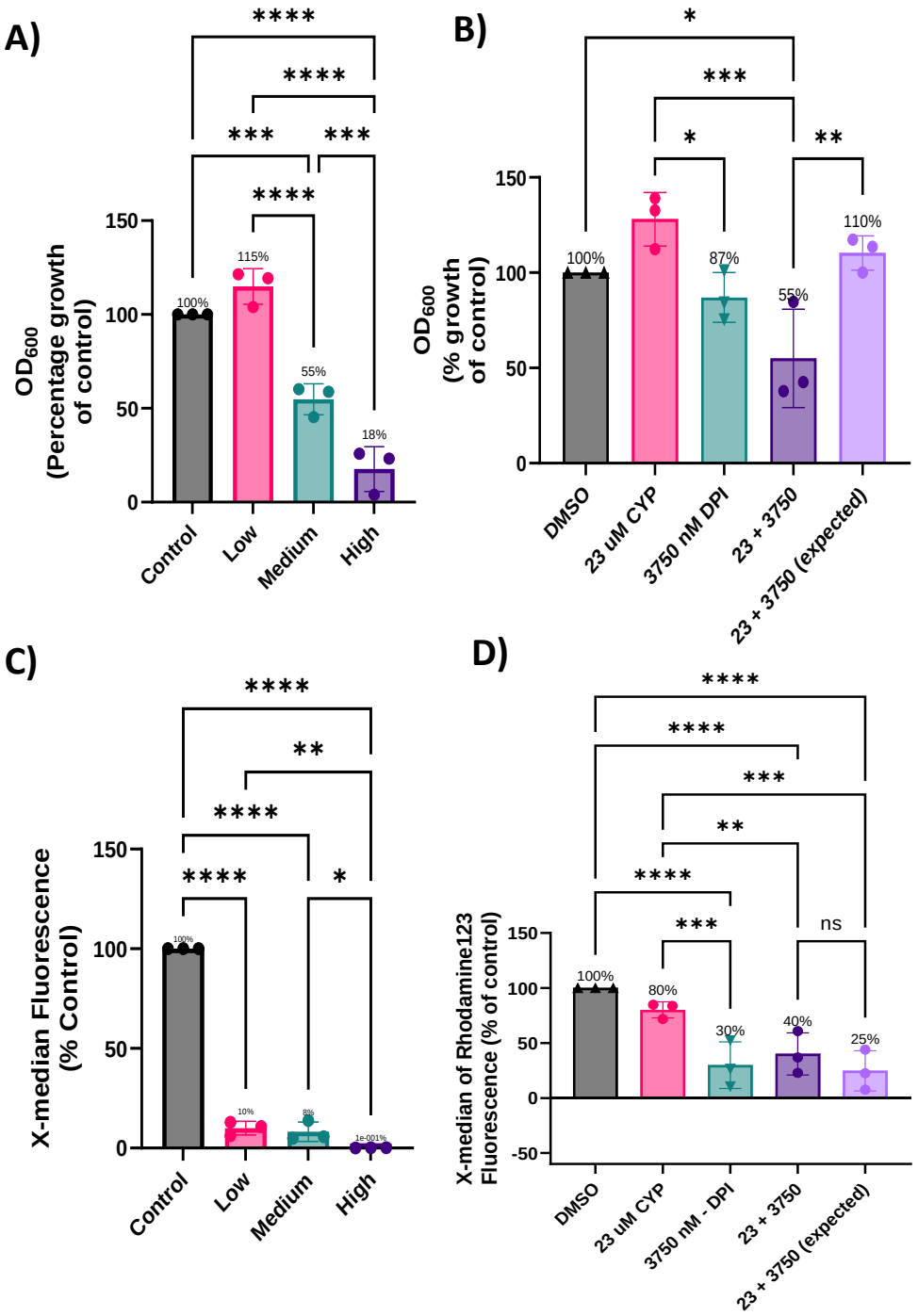

Figure 6.11. **Measuring mitochondrial depolarisation with the CYP-DPI combination.** Exponential phase *S. cerevisiae* W303 were treated with amphotericin B, cyprodinil, DPI, or a CYP-DPI combination. Concentrations used were based on preliminary experiments giving desired levels of inhibition for each compound. After 2 hours cells were removed and prepared for flow cytometry to read rhodamine 123 fluorescence (see Materials and methods). A second set of plates prepared at the same time was left to incubate for 48 h to gauge the level of growth inhibition relevant to the cells removed. A) OD_{600} of amphotericin treated cells; B) OD_{600} of cells treated with DMSO, cyprodinil, DPI, or CYP-DPI combination; C) X-median rhodamine 123 fluorescence of amphotericin treated cells; D) X-median rhodamine fluorescence of cells treated with DMSO, cyprodinil, DPI, or CYP-DPI combination. 'Expected' values for additive effect calculated by multiplying % determinations obtained for the corresponding individual-compound effects. p values generated by One-way ANOVA. *P≤0.05; **P≤0.01; **P≤0.005; ***0.001; ****P≤0.0001.

6.2.7. The cyprodinil-diphenyleneiodonium and cyprodinil-neocuproine combinations did not protect whet from *Z. tritici* infection

6.2.7.1. Corroborating synergies in different *Z. tritici* field isolates

While this PhD has focused on finding and understanding novel fungicidal synergies, all experiments so far had been carried out in a laboratory setting. When applied to *Z. tritici* spores, the CYP-DPI synergy was shown to decrease the MIC of each compound individually by 16- or 32-fold. While this is evidence of a powerful synergy, the goal ultimately for such work is improved protection of wheat plants from *Z. tritici* infection. Therefore, the CYP-DPI as well as the CYP-NEO combinations were applied to wheat plants at various combination concentrations to see if development of *Z. tritici* infection could be prevented.

First, CYP-DPI and CYP-NEO combinations were tested against different field isolates of *Z. tritici*. This was because the laboratory strain IPO323 showed no infection in a previous attempt at this experiment (data not shown). As it was a possibility of poor infectivity potential by this strain, it was decided to carry out the final experiment with an isolate from British wheat fields.

Effectiveness of the CYP-DPI synergy was evident against all the tested *Z. tritici* field isolates except isolate ROY-PZ, with some variation in individual-compound MICs and FICI values (Figure 6.12). For ROY-PZ, the MIC of cyprodinil was the lowest at 3 µM and it is possible that synergy could have been evident over a lower, more appropriate range of cyprodinil concentrations. Nevertheless, ROY-UN 2 was eventually carried forward for the infection experiment (6.2.7.2).

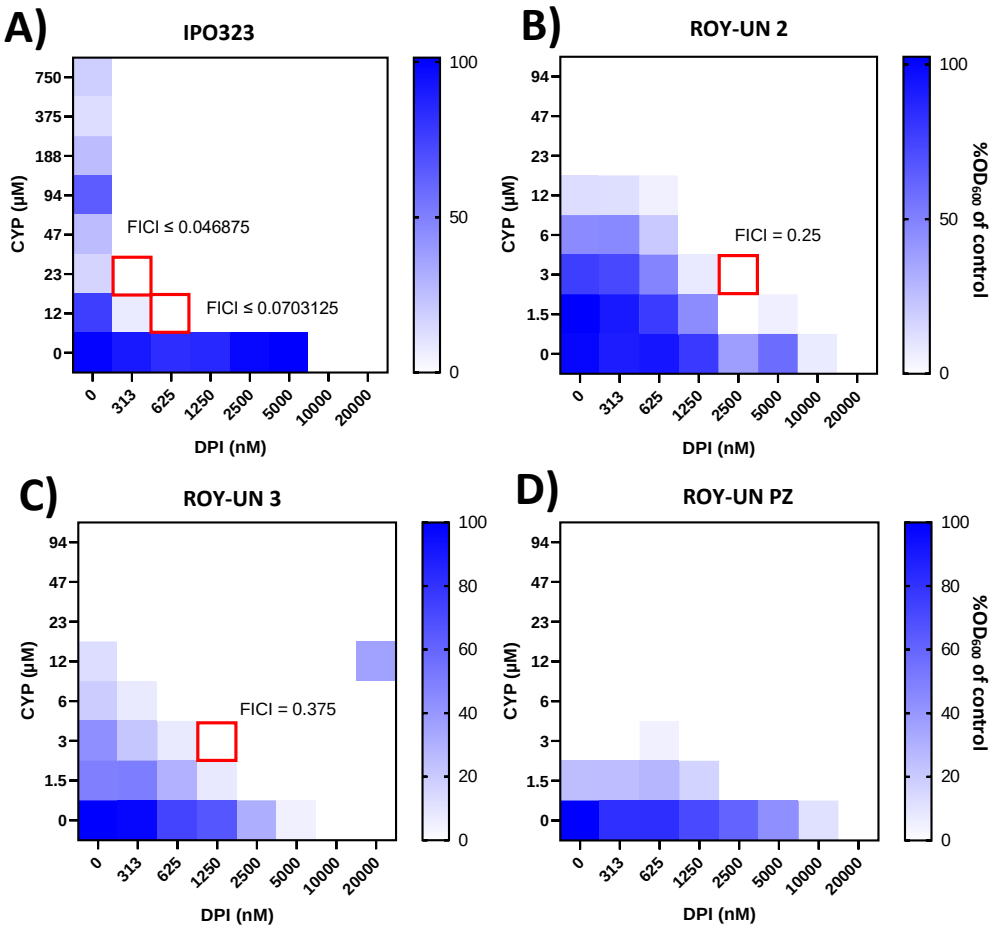

Figure 6.12. ***Z. tritici* field isolates treated with the CYP-DPI combination**. Z. *tritici* spores were treated with cyprodinil and DPI in a checkerboard format. Growth values (scale to the right) calculated as percentages of growth (OD_{600}) with compounds relative to the minus-compound control. *Z. tritici* were grown in MCS medium at room temperature and data were collected at 0 h and 168 h. Growth values <5% were assigned as no-growth. Cyprodinil MIC assumed to be 1.5 mM for FICI calculations in *Z. tritici*. Red squares indicate concentrations used to calculate FICI values.

As with CYP-DPI, CYP-NEO maintained effectiveness against all field isolates except for ROY-PZ (Figure 6.13). Interestingly, despite the CYP-NEO combination showing no synergy against ROY-PZ, the MICs for each compound individually were lower for this isolate than the others (Figure 6.13). The ROY-PZ strain was isolated from Royston, UK, in a field where prochloraz, an azole, was used the previous season. The 'UN' strains indicated there was no treatment in the previous season. However, the 'UN' strains are known to have the triazole insensitivity SNPs L50S, I381V, and Y461H. The ROY-PZ has the same Y461H mutation, with an additional V136C SNP. All SNPs are in the lanosterol 14-alpha-demethylase gene (Steve Rossall, Personal Communications).

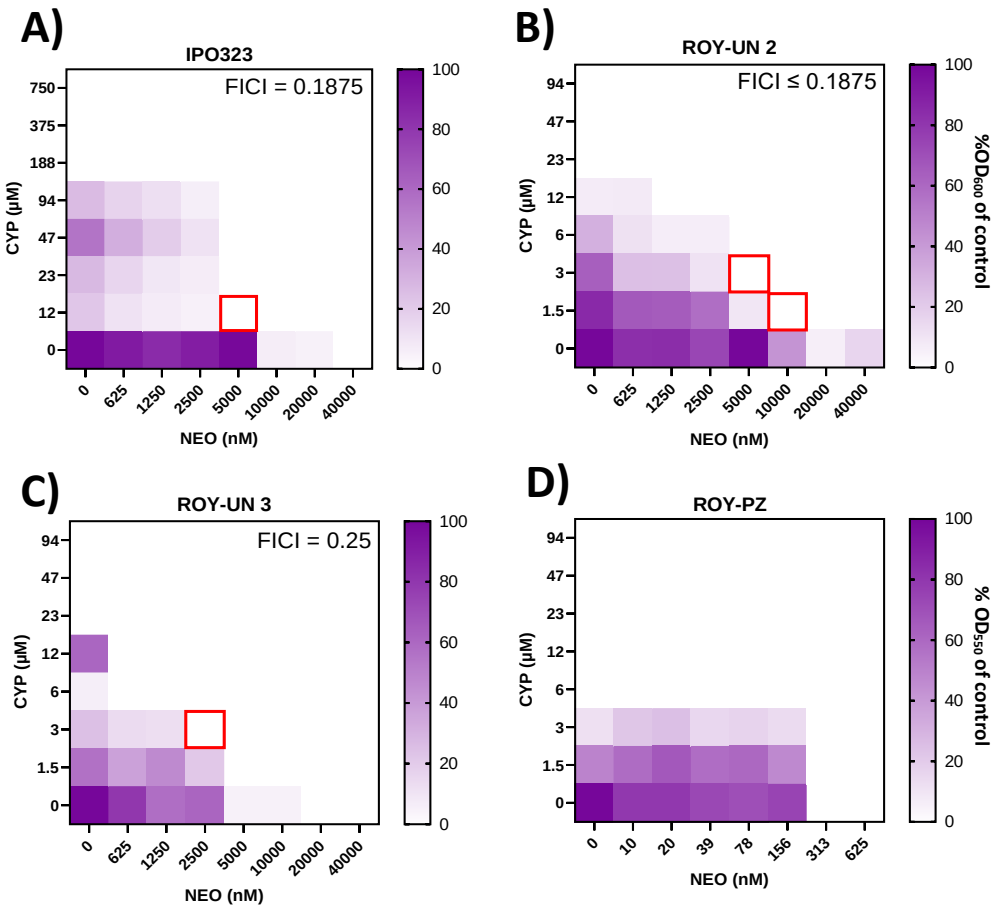

Figure 6.13. ***Z. tritici* field isolates treated with the CYP-NEO combination**. Z. *tritici* spores were treated with cyprodinil and neocuproine in a checkerboard format. Growth values (scale to the right) calculated as percentages of growth (OD_{600}) with compounds relative to the minus-compound control. *Z. tritici* were grown in MCS medium at room temperature and data were collected at 0 h and 168 h. Growth values <5% were assigned as no-growth. Red squares indicate concentrations used to calculate FICI values.

6.2.7.2. Live plant trial

Fourteen-day old wheat plants were sprayed in a greenhouse (located at Sutton Bonington Campus, University of Nottingham) with different CYP-DPI and CYP-NEO treatments. Plants were left to dry for 24 h before inoculation with *Z. tritici* spores. Plants were then left to grow in controlled conditions for a further 21 days and leaves were inspected for signs of infection throughout this period. At the concentrations used, neither cyprodinil, DPI, neocuproine, nor the combinations showed clear

Figure 6.14. **Detached wheat leaves after treatment and inoculation with *Z. tritici*.** 14-day old wheat were sprayed with 1 ml of different treatments. The next day, plants were sprayed with either H_2O (uninfected), or with *Z. tritici* spores (infected). Plants were then grown for 14 days with a photoperiod of 16 h. Day temperature was 20°C and night temperature was 15°C. before Leaves were then detached and checked for infection. A) DMSO, uninfected; B) DMSO, infected; C) cyprodinil (750 µM) + DPI (200 µM), uninfected; D) cyprodinil (750 µM) + DPI (200 µM), infected; E) cyprodinil (750 µM) + NEO (200 µM), uninfected; F) cyprodinil (750 µM) + NEO (200 µM), infected. Black spots are from permanent marker which was used to indicate which wheat leaves were originally treated and/or inoculated. Leaves shown are every leaf that was originally treated under specified condition.

protection against *Z. tritici* infection in live plants (Figure 6.14). Wheat plants that were not inoculated with *Z. tritici* spores remained relatively healthy until the end of the experiment, with most leaves remaining a healthy green colour (Figure 6.14A, C, E), indicating that the treatments themselves do not cause phytotoxicity.

In all cases where wheat plants were inoculated with *Z. tritici* (as opposed to non-inoculated controls), most leaves were brown and shrivelled (Figure 6.14B, D, F). This indicated that, at least at the concentrations used, cyprodinil, DPI, neocuproine, CYP-DPI, and CYP-NEO treatments were ineffective at protecting live plants from infection, in contrast to their effectiveness in laboratory culture. Table 6.1 shows the average percentage of leaf surface infected for the controls and each treatment (only highest concentrations shown). Here, neocuproine alone looks to be the most effective, with only 66.67% of leaf surface area a non-green colour, although the error is high. However, all combination treatments show >85% non-green surface area. When

compared to the untreated and infected controls, there is a suggestion that the combination treatments may offer some slight (up to 15%) protection, but the error is high, and no statistically significant effect was evident (P values > 0.05).

Table 6.1. **Percentage of leaf surface infected determined by eye.** Extent of leaf infection was determined by eye to the nearest 10% of total leaf coverage. Averages per treatment were then calculated and are shown below. Leaves analysed were those shown in Figure 6.14.

Condition	Average % of leaf surface non-green	Standard Deviation (%)
Control - Uninfected	28%	23.93
Control - Infected	100%	0
CYP (750 µM) - Uninfected	30%	20.94
CYP (750 µM) – Infected	88%	20.46
DPI (200 µM) – Uninfected	35%	40
DPI (200 uM) – Infected	87%	23.92
NEO (200 µM) – Uninfected	46%	40.06
NEO (200 µM) – Infected	67%	31.44
CYP+DPI – Uninfected	26%	29.31
CYP+DPI – Infected	86%	24.54
CYP+NEO – Uninfected	25%	30
CYP+NEO – Infected	93%	13.92

6.3. Discussion

6.3.1. Copper-ziram synergy

Based on earlier literature and on results obtained here from the copper/ziram/neocuproine combination experiments, it became apparent that the mechanism behind the copper-ziram synergy is likely to be similar in yeast as previously proposed in phytoplankton. Ziram binds to copper in a proposed 1:1 ratio forming a lipophilic complex which then enters cells (Phinney and Bruland, 1997), presumably helping copper to bypass mechanisms that regulate copper uptake. The present data suggested that although copper-ziram may be a chemically preferred complex, copper-neocuproine (also reported to form a complex, Byrnes *et al*., 1992) is far more potent in its inhibitory action on *S. cerevisiae*. The hypothesis on the chemical preference of the copper-ziram complex over the copper-neocuproine complex could have been tested by spectroscopic analyses and titration experiments. In addition, ziram prefers binding to copper (II), while neocuproine prefers binding to copper (I), which may explain the preference (although does not detract from the results and conclusion around inhibition and the copper-ziram mechanism). Copper (I) and/or reducing agents could have been tested to see if a neocuproine became chemically preferred.

The copper-ziram experiments were not carried out in other fungi, but as the evidence was consistent with a common synergistic mechanism between yeast and phytoplankton, this would suggest that it too is the mechanism for inhibition against of other fungal species such as *Z. tritici*. As well as fungi and phytoplankton, the copper-ziram synergy could be effective against a wide range of organisms and would likely also inhibit via the same mechanisms.

6.3.2. The cyprodinil-neocuproine synergy

Cyprodinil is synergistic with the copper-chelator neocuproine (Figure 6.8) but it is not synergistic with copper alone (Appendix Figure 8.9). This may be due to additional effects of neocuproine, or perhaps due to the specific localisation of copper bound by neocuproine. Indeed, the neocuproine-related copper chelator BPQ has been shown to potentiate damage to the mitochondria (Foster *et al*., 2014), which might suggest this as a target for chelated copper. Neocuproine forms a lipophilic complex with copper (Zhu and Chevion, 2000), potentially bypassing regulatory systems for copper uptake as the complex passes straight through the phospholipid bilayer. Further, it has been shown that neocuproine binds to copper and damages the electron transport chain, suggesting that at least some of the copper that was bound to neocuproine is released in the mitochondria (Gyulkhandanyan *et al*., 2003). It is also possible that unloaded neocuproine is capable of entering cells and directly chelating copper from proteins, although literary evidence for this was unable to be found.

As cyprodinil is thought to be synergistic with DPI through increased oxidative stress, it is possible that this is also the case for the CYP-NEO synergy. As with the CYP-DPI combination, the effects of CYP-NEO were shown to be prevented by supplementation with antioxidants, this time including the non-thiol containing ascorbic acid. In addition, mitoquinol supplementation with the combination showed a further decrease in growth (Figure 6.10). It may be the case that elevated copper in the mitochondria, delivered via chelation with neocuproine, synergises with cyprodinil-induced effects promoting the cycling of copper re-oxidation and Fenton-based ROS production. Neocuproine has previously been shown to synergistically enhance the cytotoxicity of Fenton-type reagents (Burkitt *et al*., 1996; Almeida *et al*., 1999).

One explanation for synergy with neocuproine but not copper might be that, as hypothesised, neocuproine imports extracellular copper to a specific cellular location/organelle such as mitochondria (or at least potentiates damage to within this organelle), as is the case with the similar copper chelator, BPQ (Foster *et al*., 2014). Copper without neocuproine may be distributed more evenly throughout the cell. This could have been tested using methods such as intercoupled plasma mass spectrometry (ICP-MS), measuring the levels of copper in different organelles under different treatments (Garza *et al*., 2021).

Another explanation could relate to the sudden onset of $CuSO_4$ toxicity with increasing concentrations (Appendix Figure 8.10). Unlike most compounds tested, which showed gradually increased inhibition as concentration is increased, $CuSO_4$ showed little inhibition at one concentration followed by complete inhibition at a concentration two-fold higher. This could be due to a sudden overwhelming of copper defence mechanisms that cause total inhibition above a certain threshold, something cells may be particularly sensitive to considering there is usually less than one free copper atom per cell (Rae *et al*., 1999). If that is the case, with the possible exception of agents known to alter copper uptake or localisation (unlike cyprodinil), there could be too small a window reliably to detect synergy considering that two-fold dilution series are used for conventional checkerboards. The effect of neocuproine on copper uptake/localisation could introduce the cyprodinil-copper synergy indirectly. Based on previous experiments with cyprodinil and on knowledge of neocuproine and the related compound BPQ, an effect of neocuproine seems likely to be localisation of copper to the mitochondria (Foster *et al*., 2014). Additionally, it has been found that copper-mediated cell death in human cells is dependent on mitochondrial respiration (Tsvetkov *et al*., 2022), further implicating the role of copper delivered to the mitochondria.

It would also have been interesting to test cyprodinil in combination with copper (I) instead of the copper (II) that was supplied when copper sulphate was used in experiments. As copper (I) sulphate is unstable it requires reduction by thiol compounds. This may exacerbate the demand of cells on glutathione, leading to a decrease in response to oxidative stress which is hypothesised to increase the inhibitory effects of cyprodinil.

6.3.3. Live plant infections

It was important to see whether the combinations detailed in this chapter could protect wheat plants from *Z. tritici* infection. Despite showing potent antifungal synergies in the laboratory, neither CYP-DPI nor CYP-NEO significantly slowed development of infection by *Z. tritici*. It is unclear whether higher concentrations of the compounds might prove more effective. As there were no visible signs of phytotoxicity at the concentrations used, higher concentrations may still be feasible. Unfortunately, due to constraints on chemical concentrations allowed at the site where the wheat plants were incubated, it was not possible to test higher concentrations.

In liquid medium, the CYP-DPI combination decreased the MICs of CYP and DPI by at least 16-fold. If the synergy maintained a similar FICI when applied to plants then, because no synergy was reached with the concentrations used, the MIC for CYP and DPI would be 12 mM and 3.2 mM, respectively. These are far higher than the MICs found when *Z. tritici* is grown in liquid medium. However, as the compounds are applied as sprays to a solid leaf surface, it is inappropriate to assume the concentration sprayed is the same as what might be expected if *Z. tritici* were to encounter the combination in liquid media. In addition, it is unknown if the combinations tested would persist or disappear over time due to rainfall elution, evaporation, growth

dilution, thermal degradation and/or photodegradation (Karthika and Muraleedharan, 2009). It may have been more appropriate to inoculate the plants first, and then treat a day later. This would have decreased the risk of washing off the treatment with the spraying of inoculum (if this is what occurred). Different adjuvants could also have been tested to aid in the attachment and/or dispersal of the fungicides on the leaf surface.

6.3.4. Final remarks

The novel synergy found between cyprodinil and neocuproine may also be based around oxidative stress in the mitochondria as well as copper availability, although less work was carried out on this work due to time constraints.

Despite the strength of the cyprodinil-diphenyleneiodonium and cyprodinil-neocuproine synergies against *Z. tritici* in the laboratory, neither could protect wheat from infection by this phytopathogenic organism. This research highlights the difficulty in finding novel treatments that are viable for real-world applications.

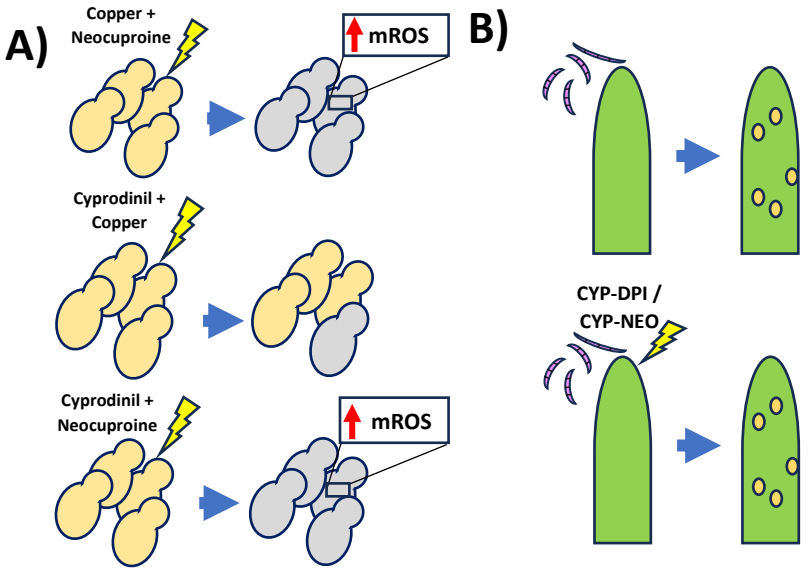

Figure 6.15. **Schematic of chapter results and hypotheses.** A) Similar to the ionophore BPQ, neocuproine facilitates the transport of copper into the mitochondria, synergising with the mode of action of cyprodinil. Copper without neocuproine does not achieve such an affect. B) At the concentrations tested, following the described protocol (2.2.21), lab-proven synergies cyprodinil-diphenyleneiodonium and cyprodinil-neocuproine were not effective at prevent infection by *Z. tritici* of live wheat plants.

7. Summary and Conclusions

7.1. Summary of results

Chapter 3 focused on the leucyl aminoacyl-tRNA synthetase (LeuRS) inhibitor, tavaborole. This oxaborole compound was hypothesised to cause mistranslation, due to the role of LeuRS in protein synthesis (charging leucyl-tRNA molecules with leucine), and therefore to prove synergistic with known inducers of mistranslation. All efforts to measure tavaborole-induced mistranslation indicated that this compound does not cause the hypothesised effect. Despite this, the relatively low price, specificity, and potency of tavaborole, as well as its approval for topical application on humans, denoted that tavaborole was still desirable for use in a fungicidal synergy. As such, tavaborole was tested in combination against more than 1100 compounds. From all the combinations tested, tavaborole showed synergy with only one compound, the branched chain amino acid biosynthesis inhibitor, chlorimuron ethyl. In addition, this synergy was only present against *Z. tritici*, specifically in rich PDB medium. Similar synergies between amino acid biosynthesis inhibitors and aminoacyl-tRNA synthetase inhibitors were found across different organisms in different conditions, suggesting that the method of attacking aminoacylation via two routes (depleting the pool of available amino acid and inhibition of the aminoacylation enzyme) has wider potential. Hundreds of combinations with this mechanism are possible.

In Chapter 4, the anilinopyrimidine fungicide, cyprodinil, was originally used in this project as it was predicted to be an inhibitor of methionine biosynthesis. Despite this no longer being the presumed mode of action, cyprodinil proved synergistic in several synergies. Firstly, cyprodinil was found to be synergistic with REP3123, an inhibitor of MetRS. The role of MetRS in mismethionylation, the increased misincorporation of methionine into proteins in response to oxidative stress, is hypothesised to be part of

this synergy. Inhibition by cyprodinil can be alleviated with the supplementation of antioxidants. While the mechanism of Pos5p inhibition by cyprodinil has been put into question with this research, cyprodinil was shown to cause increased ROS. An increase in ROS in combination with a decrease in the mismethionylation response to ROS is the proposed synergistic mode of action for this combination.

The strongest synergy discovered against a fungal phytopathogen was that between cyprodinil and diphenyleneiodonium (DPI). This combination synergistically inhibited *Z. tritici*. In some replicates the MICs of cyprodinil and DPI decreased 16- and 32-fold when in combination. Again, while the individual molecular target of cyprodinil is not known, evidence gathered suggests a synergistic mechanism based around oxidative stress. Cyprodinil was shown to cause an increase in ROS in the mitochondria, while DPI was theorised to cause the efflux of the antioxidant glutathione, as well as potentially directly decreasing its activity. Despite the strength of this synergy, the combination was ineffective at protecting live wheat plants from *Z. tritici* infection.

7.2. Comments on strategies employed

Various strategies were employed in this thesis to varying degrees of effectiveness. Both rationally thought, low-throughput and high-throughput screening methods were used in attempts to identify synergistic combinations against phytopathogenic fungi. The low-throughput methods had more success, with several synergies discovered (albeit not always deliberately). Despite the unsuccessful nature of the high-throughput screening of the Prestwick Chemical Library, this is likely to be less the fault of the method, and more to do with the synergistic potential of the tavaborole and REP3123 compounds. Although synergies were found with both these compounds through rational means, high-throughput screening for synergies remains a popular and effective scientific tool.

Other high-throughput methods, such as the overexpression and heterozygous gene deletion libraries were employed. The only significant result yielded by the latter was the corroboration of the role of *yah1* in the cyprodinil-diphenyleneiodonium synergy; overexpression leads to increased sensitivity, while a heterozygous deletion strain showed increased resistance. Similarly, the overexpression library did not give the expected results, that one or more genes overexpressed would increase sensitivity/resistance, helping to elucidate the synergistic mechanism. The SGE1 result did reveal that the synergy may in fact be multimodal with the increased expression of efflux pumps the only known overexpression to develop resistance. Despite these limited results, the strategies employed here remain effective search tools for the discovery and understanding of synergies and their underlying mechanisms.

Checkerboard experiments remain a valuable tool for the discovery and understanding of synergies. However, the work carried out in this thesis perhaps relied too heavily on these experiments, and other, more invasive, methods could have been used, particularly for uncovering the mechanisms of the synergies discovered. In addition, due to the use of various different strains throughout this thesis, the measurements of single 24 h or 48 h timepoints in yeast, for example, may not have been the most suitable as different strains have different growth rates. Also, while the same starting optical density was used for the start of each experiment, each yeast strain may not necessarily have been in the same phase of growth, and so differences seen in results could be the result of this, and not the result of the strain genotypes themselves.

Finally, to avoid potential effects such as those seen in experiments with REP3123 and the S-transport inhibitors, all media could have been buffered to a certain pH, to rule out pH change induced by one compound enhancing the effect of the other.

7.3. Future work

Synergies remain a desirable solution to combatting undesirable organisms such as phytopathogenic fungi. With lower concentrations required and potential high specificity to the target organism, synergies have the capability to drastically reduce the cost of pesticide treatment on crops, as well as lowering environmental toxicity.

As the synergy between REP3132 and cyprodinil was only found in *Z. tritici*, the genetic toolbox available was limited. However, one experiment which may prove insightful would be the use of a dual fluorescence reporter in which an essential methionine in the mCherry fluorophore is altered to a cognate amino acid. By inducing ROS production, cyprodinil would theoretically cause increased mismethionylation leading to the restoration of fluorescence. As an inhibitor of MetRS, increasing concentrations of REP3123 should decrease the levels of mismethionylation.

The synergistic mechanism of a 'double attack' on aminoacylation opens hundreds of combinations to be tested. However, there is an obvious bottleneck here of available compounds with the desired mechanisms for these combinations. If these could be developed with high specificity to fungal proteins (or indeed that of other undesirable organisms), then there could be a future wealth of combinatory treatments that could be utilised in fungicide rotational programmes. In addition, a third possible method of attacking aminoacylation is impairing the production or functionality of the tRNA molecules themselves. This would exponentially increase the number of combinations available with the potential of synergistically inhibiting aminoacylation. Copper chelating compounds such as neocuproine may also act as amino acid biosynthesis inhibitors by targeting Fe-S cluster-containing amino acid biosynthesis enzymes such as Leu1 and Met5 in combination with aaRS inhibitors and so could be tested in these combinations.

If hypotheses for the CYP-REP3123, CYP-DPI, CYP-NEO, and synergies are accurate, combinations that synergistically increase oxidative damage appear to be particularly effective at inhibiting *Z. tritici*. Novel combinations that explore these mechanisms could be explored in the future with the hope of discovering multiple powerful synergies. Despite evidence gathered for these hypotheses, more experiments need to be carried out to support the predicted synergistic mechanisms. For the CYP-NEO synergy, it could be investigated whether unloaded neocuproine enters the cells and binds to internal copper (those from proteins), or if it leads to a copper overload through the import of extracellular copper. In addition, inductively coupled plasma mass spectrometry (ICP-MS) could be utilised to determine concentrations of copper in *S. cerevisiae* or *Z. tritici* after different treatments. Whole cell and organelle specific (i.e., the mitochondrion) extracts could be investigated. This has the potential to highlight any differences in localisation of copper when applied individually or in combination with neocuproine. Differences in copper localisation could be the cause for a lack of synergy between cyprodinil and copper, despite the presence of a synergy between cyprodinil and the copper chelator neocuproine. It is also possible that copper was interacting with cyprodinil directly, impairing its function. For CYP-DPI in particular, more experiments could be attempted anaerobically, as there was the possibility that media and materials used carried some oxygen into the anaerobic chamber. However, iron-mediated Fenton reactions can still occur under anaerobic conditions (Luo *et al*., 1996).

Differences in sensitivity of organisms to the synergy between neocuproine and copper could also be explored. In *S. cerevisiae* this combination was extremely synergistic with the MICs of neocuproine and copper, consistently decreasing 128- and 32-fold, respectively, when in combination. Furthermore, lower concentrations were not tested and so the synergy may be even stronger than described here. Against *B.*

cinerea, at the concentrations tested, this combination appeared antagonistic, but it is possible there is synergy at lower concentrations as is the case with *Z. tritici*, although it would be difficult to find these concentrations for field trials. This sudden antagonism at higher concentrations only occurred in the phytopathogens and may indicate different defence mechanisms by the fungi or different molecular targets of copper once imported. A wider range of concentrations across the different organisms should be tested to see if similar patterns of synergy and antagonism occur.

This PhD research has discovered several novel synergistic combinations that effectively inhibit fungal phytopathogens. Although the synergies tested were ineffective at inhibiting infection of live plants at the applied concentrations, it is possible that these combinations may still be effective for application to crops. Finally, the proposed mechanisms outlined provide the foundations for future drug discovery and the finding of novel fungicidal synergies.

8. Appendix

Appendix Table 8.1. **Standard PCR reaction ingredients**.

Reagent	50 µl reaction	Final concentration
5x HF Phusion Buffer	10 µl	1x
dNTPs	1 µl	200 µM
Forward Primer	2.5 µl	0.5 µM
Reverse Primer	2.5 µl	0.5 µM
DMSO	2.5 µl	
Phusion	0.5 µl	
DNA	200 ng	
PCR grade dH_2O	Up to 50 µl	

Appendix Table 8.2. **Standard PCR protocol**.

Cycles	Temperature	Time	Notes
1	98°C	3 min	Initial denaturation and enzyme activation
30	98°C 55°C to 65°C 72°C	30 sec 30 sec 1-90 sec	Denaturation Annealing Extension (30 sec per kb)

Appendix Table 8.3. **Primers used for colony PCR of *A. tumefaciens* and *Z. tritici*.**

Primer ID	Sequence	FWD/ REV	Target	Size	
oe62	ACTGTCGGG CGTACACAA AT	FWD	3' Hyg gene in pNOV2114		
oe71	TCGCGCAGA GGTCGATAA AA	REV	pNOV2114_Mycgr3G74 468_KO ZtPOS5 agro check	593bp	use with oe62
oe72	GAAGTCAGC TGAGTCGAG GG	REV	pNOV2114_Mycgr3G69 430 _KO ZtSOD2 agro check	515bp	use with oe62
oe73	GGATTTGGC TGCGGAAAA GG	REV	pNOV2114__Mycgr3G3 5076_KO ZtYAP1 agro check	561bp	use with oe62

Appendix Table 8.4. **Reagents used for colony PCR.**

Reagent	50 µl reaction	Final concentration
2x PCRBIO HS Taq Mix Red	25 µl	1x
Forward primer (10 µM)	2 µl	400 nM
Reverse primer (10 µM)	2 µl	400 nM
Supernatant	1-2 µl	variable
PCR grade dH_2O	Up to 50 µl	

Appendix Table 8.5. **Programme for colony PCR**.

Cycles	Temperature	Time	Notes
1	95°C	10 min	Initial denaturation and enzyme activation
40	95°C 55°C to 65°C 72°C	15 sec 15 sec 1-90 sec	Denaturation Annealing Extension (15 sec per kb)

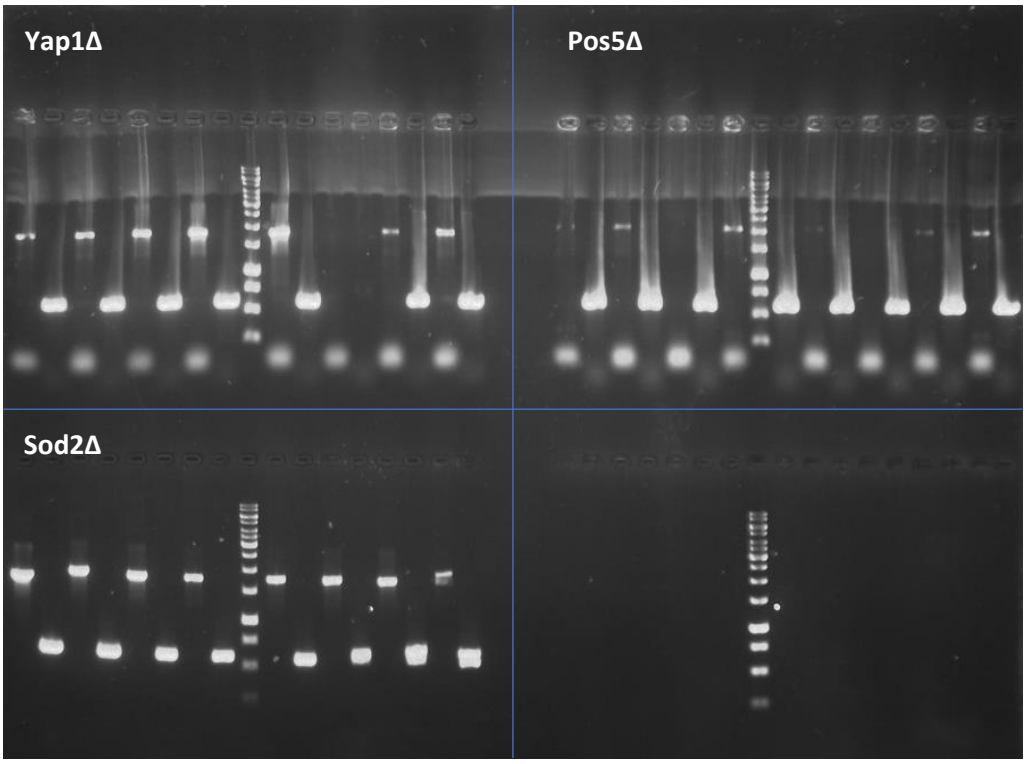

Appendix Figure 8.1. ***Z. tritici* genotype confirmation**. 1% agarose cell showing genotype of different *Z. tritici* transformants following colony PCR. Ladder used was Gene Ruler 1kb. Lanes 1, 3, 5, 7, 10, 12, 14, 16 in each quadrant (except blank bottom-right) are from eight different samples and show correct-sized band for genome replacement of respective genes. Lanes 2, 4, 6, 8 (9 for Pos5Δ), 11, 13, 15, 17 are controls for deleted sequences. Transformants positive for insert and negative for native yap1, pos5, or sod2 genes were taken forward for further experimentation.

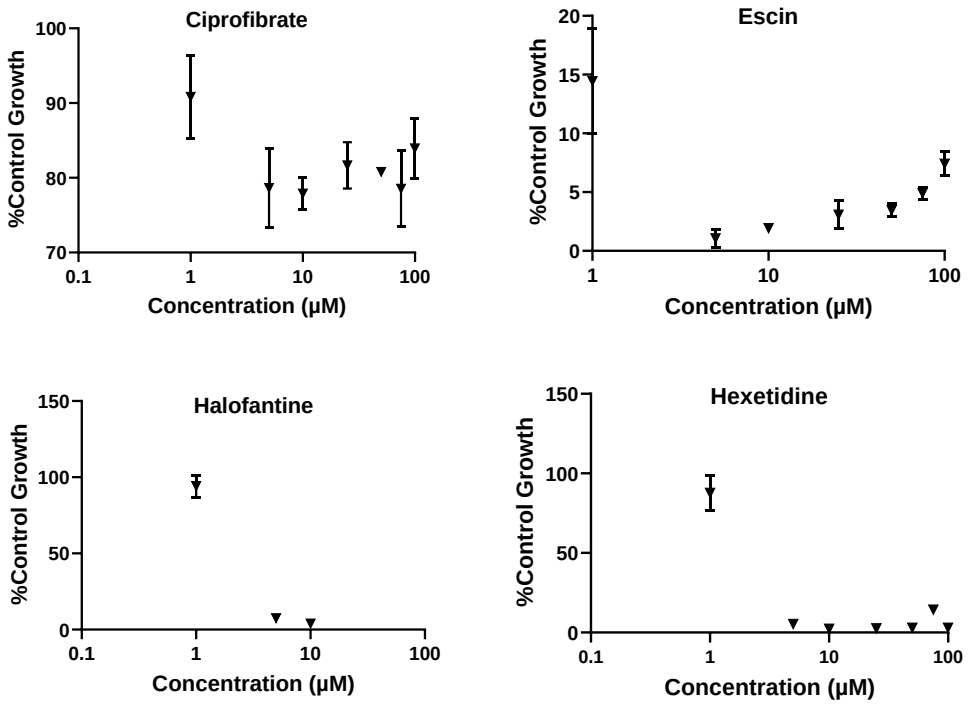

Appendix Figure 8.3. **More compounds used in preliminary dosage for PCL screen**. Growth of *Z. tritici* in the presence of different test drugs from the Prestwick Library at different concentrations. Plot points convey growth of treated samples as a percentage of the non-treated samples in DMSO -matched controls. The experiment was carried out in 100 µl MCS medium in 96-well plates with 10,000 spores ml^{-1}. Readings show growth after seven days. n = 3.

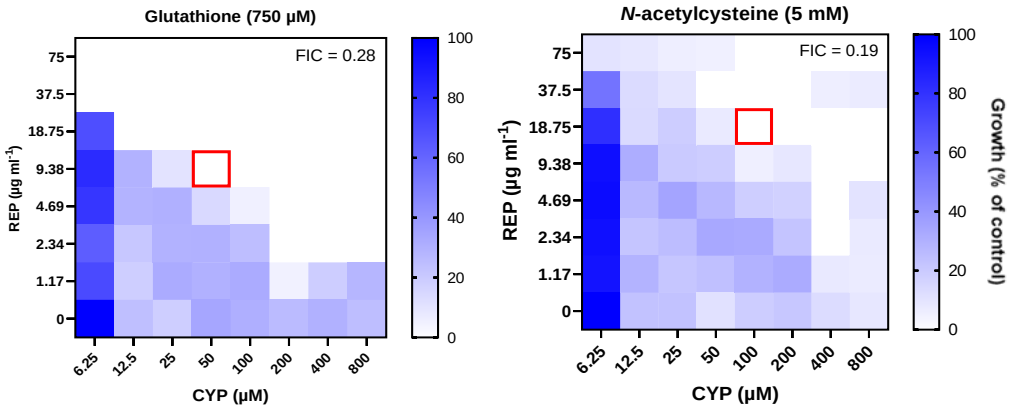

Appendix Figure 8.5. **REP3123-cyprodinil combination supplemented with antioxidants**. The data represent *Z. tritici* growth. A) 750 µM glutathione; B) 5 mM *N*-acetylcysteine. Growth values (scale to the right) represent data from single independent experiments, calculated as percentages of growth (OD_{600}) with compounds relative to the minus-compound control. Data were collected at 0 h and 168 h, with incubation at room temperature. Growth values <5% were assigned as no-growth. FIC values rounded to two decimal places. Coloured boxes correspond to coloured FIC value calculated from that well.

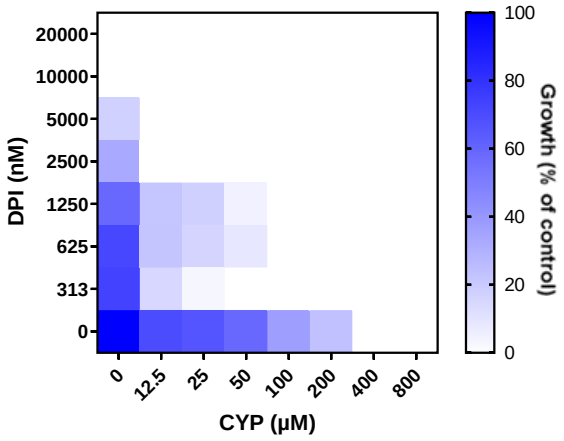

Appendix Figure 8.4. **Testing diphenyleneiodonium in combinations**. *Z. tritici* spores were treated with diphenyleneiodonium in combination with A) cyprodinil and B) REP3123. Growth values (scale to the right) represent mean percentage of growth (OD_{600}) from three biological replicates with compounds relative to the minus-compound control. Data were collected at 0 h and 168 h, with incubation at room temperature. Growth values <5% were assigned as no-growth.

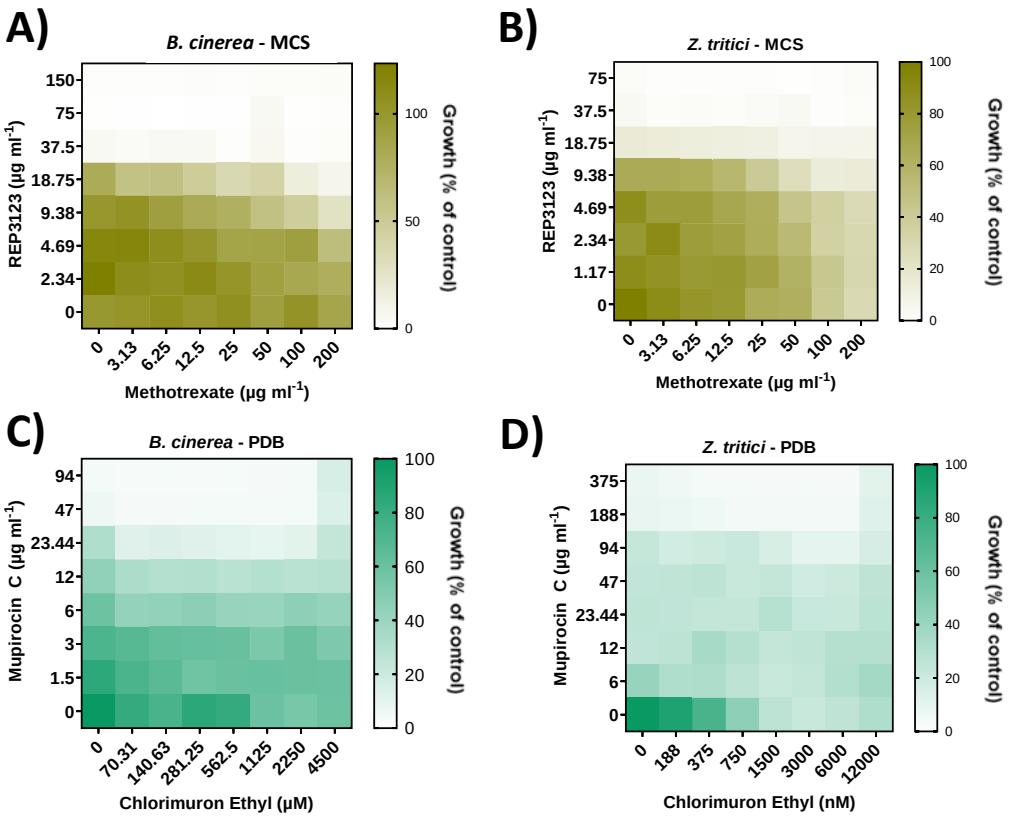

Appendix Figure 8.6. **Selected checkerboards of aminoacyl-tRNA synthetase inhibitors in combination with amino acid biosynthesis inhibitors**. *B. cinerea* or *Z. tritici* were treated with different combinations of compounds inhibiting amino acid biosynthesis and tRNA aminoacylation. A) *B. cinerea*, REP3123 vs methotrexate, PDB medium; B) Same combination in *Z. tritici*, PDB; C) *B. cinerea*, mupirocin C vs chlorimuron ethyl, MCS medium; D) Same combination in *Z. tritici*, MCS; E) *Z. tritici*, glyphosate vs epigallocatechin gallate, MCS; F) *Z. tritici*, REP3123 vs chlorimuron ethyl, PDB. Growth values (scale to the right) represent means from four independent experiments, calculated as percentages of growth (OD_{600}) with compounds relative to the minus-compound control. Data were collected at 0 h and 168 h, with incubation at room temperature. Growth values <5% were assigned as no-growth.

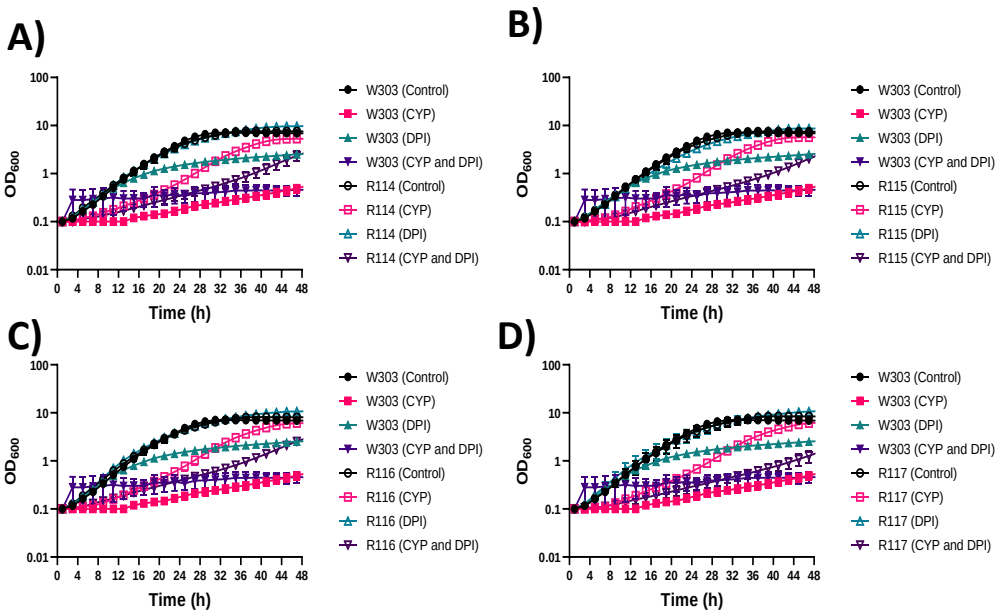

Appendix Figure 8.7. **Growth curves of ATCC®37323™ overexpression library resistant isolates**. Growth curves of WT and resistant strains R114, R115, R116, R117 were incubated statically at 30°C for 48 hr in YNB containing either A) DMSO; B) 375 µM cyprodinil; C) 10 µM DPI; D) 375 µM and 10 µM DPI, . Readings taken every 30 min. Bars show standard deviation. n = 3 biological replicates.

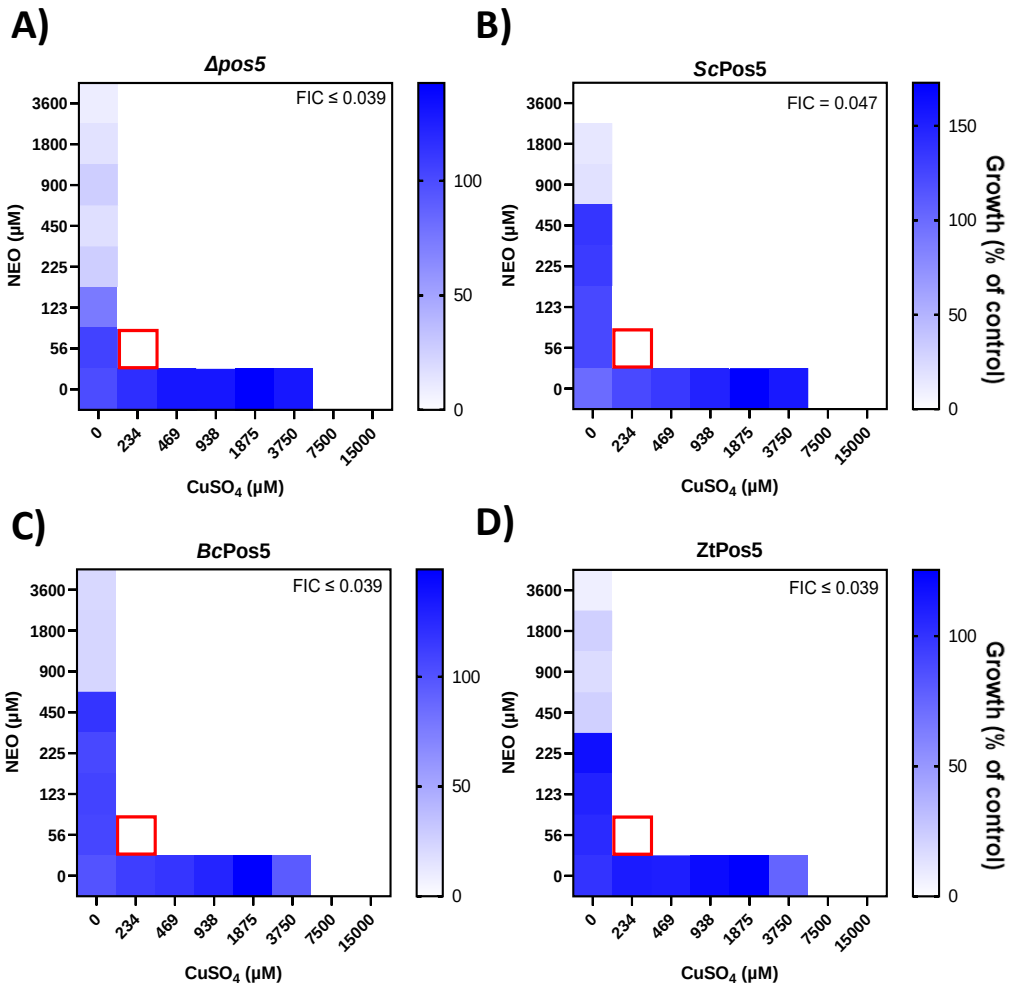

Appendix Figure 8.8. **Neocuproine-copper synergy in *S. cerevisiae* expressing Pos5p of different fungal species**. Exponential phase *S. cerevisiae* (BY4743 background) were treated with neocuproine and $CuSO_4$ in a checkerboard format. A) *pos5Δ*; B) *Sc*Pos5; C) *Bc*Pos5; D) *Zt*Pos5. Growth values (scale to the right) represents mean of three individual experiments calculated as percentages of growth (OD_{600}) with compounds relative to the minus-compound control. *S. cerevisiae* was grown in YNB medium at 30°C, and data were collected at 0 h and 48 h. Growth values <5% were assigned as no-growth. Red squares indicate concentrations used to calculate FICI values.

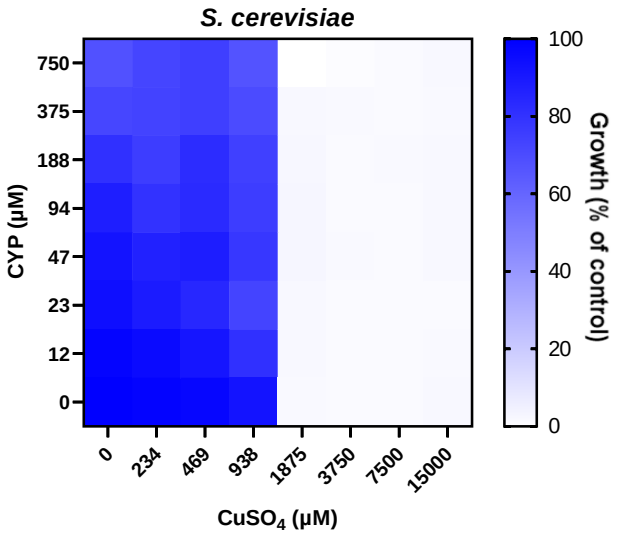

Appendix Figure 8.9. **Cyprodinil and copper sulphate are not synergistic in *S. cerevisiae***. Exponential phase W303 *S. cerevisiae*. were treated with cyprodinil and $CuSO_4$ in a checkerboard format. Growth values (scale to the right) represents mean of three individual experiments calculated as percentages of growth (OD_{600}) with compounds relative to the minus-compound control. *S. cerevisiae* was grown in YNB medium at 30°C, and data were collected at 0 h and 48 h. Growth values <5% were assigned as no-growth.

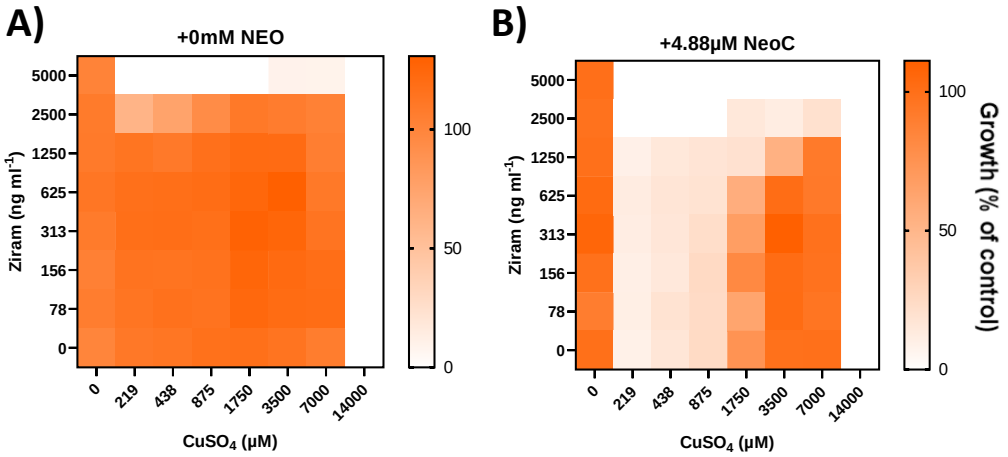

Appendix Figure 8.10. **$CuSO_4$-ziram combination in *S. cerevisiae* with and without neocuproine**. Exponential phase BY4743 *S. cerevisiae*. were treated with ziram and $CuSO_4$ in a checkerboard format. A) without added neocuproine; B) with 4.88 µM neocuproine. Growth values (scale to the right) calculated as percentages of growth (OD_{600}) with compounds relative to the minus-compound control. *S. cerevisiae* was grown in YEPD medium at 30°C, and data were collected at 0 h and 24 h. Growth values <5% were assigned as no-growth. Data from single biological replicates.

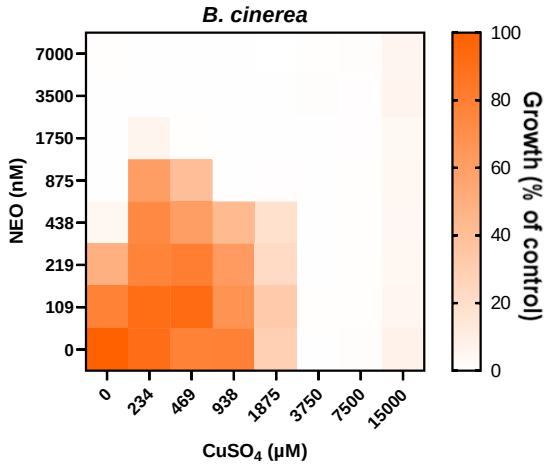

Appendix Figure 8.11. **Antagonistic effect of neocuproine and $CuSO_4$ is also seen in *B. cinerea***. *B. cinerea* spores were treated with ziram and $CuSO_4$ in a checkerboard format. Growth values (scale to the right) calculated as percentages of growth (OD_{600}) with compounds relative to the minus-compound control. *B. cinerea* was grown in MCS medium at room temperature, and data were collected at 0 h and 168 h. Growth values <5% were assigned as no-growth. Data from a single biological replicate.

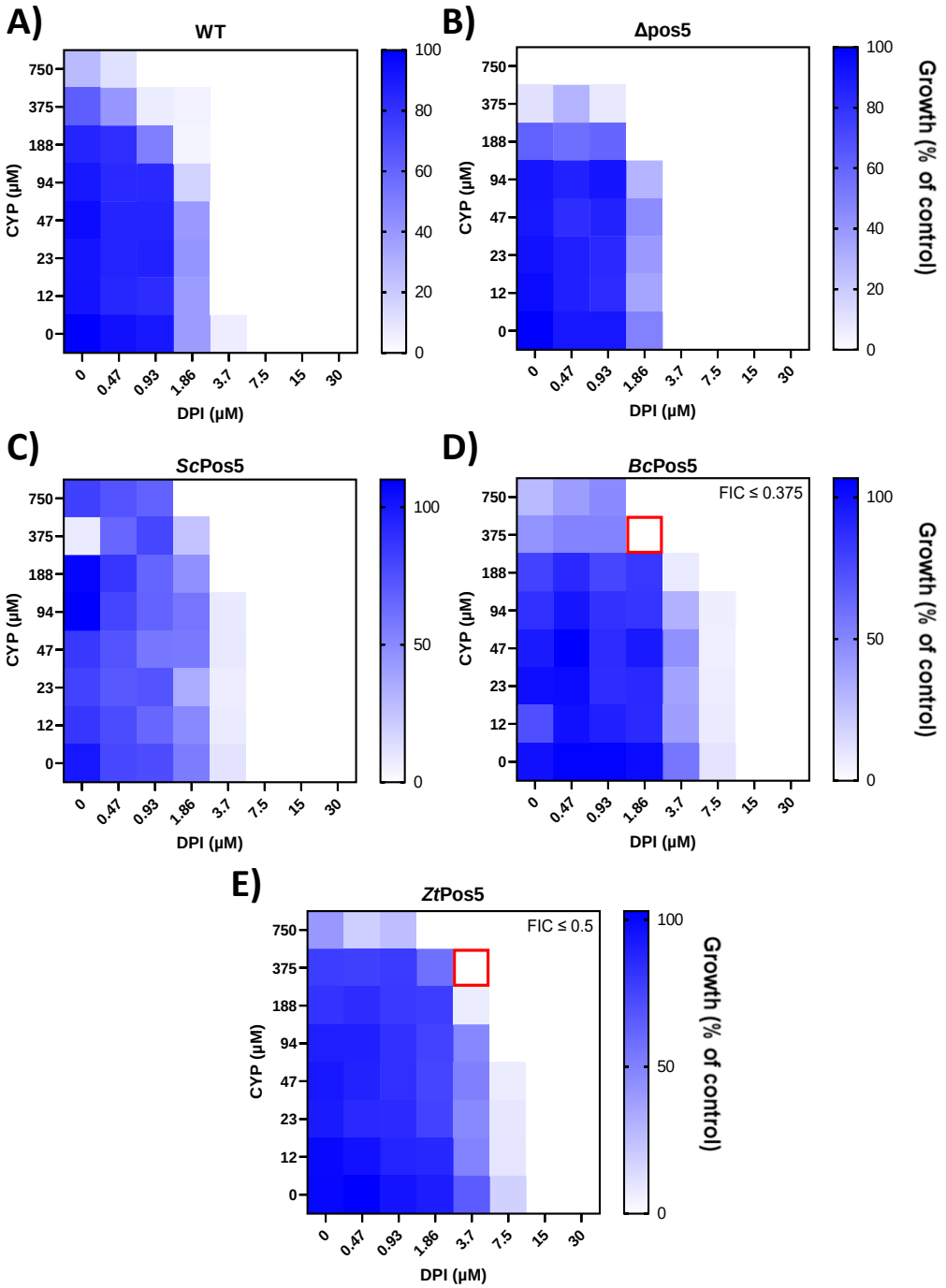

Appendix Figure 8.12. **CYP-DPI combination in *S. cerevisiae* expressing Pos5p of different fungal species.** Exponential phase *S. cerevisiae* (BY4743 background) were treated with neocuproine and $CuSO_4$ in a checkerboard format. A) WT; B) *pos5Δ*; C) *Sc*Pos5; D) *Bc*Pos5; E) *Zt*Pos5. Growth values (scale to the right) calculated as percentages of growth (OD_{600}) with compounds relative to the minus-compound control. *S. cerevisiae* was grown in YNB medium at 30°C, and data were collected at 0 h and 48 h. Growth values <5% were assigned as no-growth. Red squares indicate concentrations used to calculate FIC values.

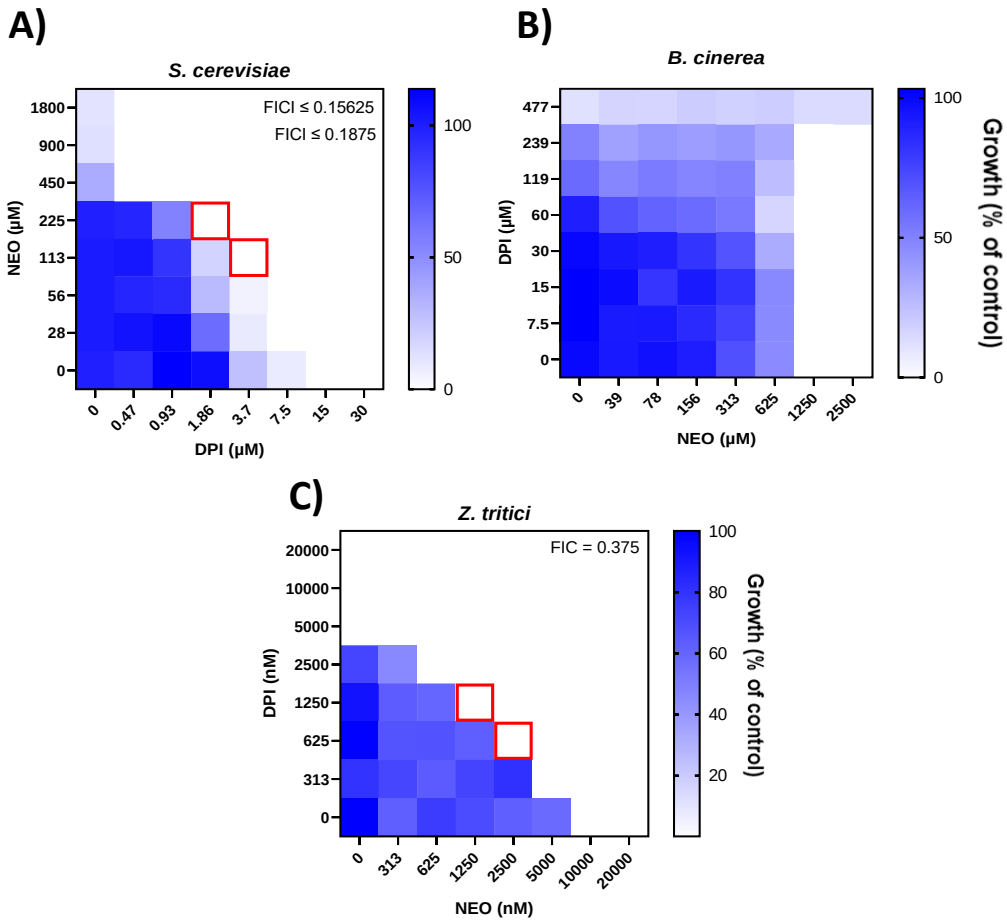

Appendix Figure 8.13. **DPI-NEO combination in different fungal species**. A) Exponential phase *S. cerevisiae*; B) *B. cinerea* spores; or C) Z. *tritici* spores were treated with diphenyleneiodonium and neocuproine in a checkerboard format. Growth values (scale to the right) calculated as percentages of growth (OD_{600}) with compounds relative to the minus-compound control. *S. cerevisiae* was grown in YNB medium at 30°C, and data were collected at 0 h and 48 h. *B. cinerea* and *Z. tritici* were grown in MCS medium at room temperature and data were collected at 0 h and 168 h. Growth values <5% were assigned as no-growth. Cyprodinil MIC assumed to be 7.2 mM for FIC calculations in *S. cerevisiae*. Neocuproine MIC assumed to be 40 µM for FIC calculations in *Z. tritici*. Red squares indicate concentrations used to calculate FIC values.

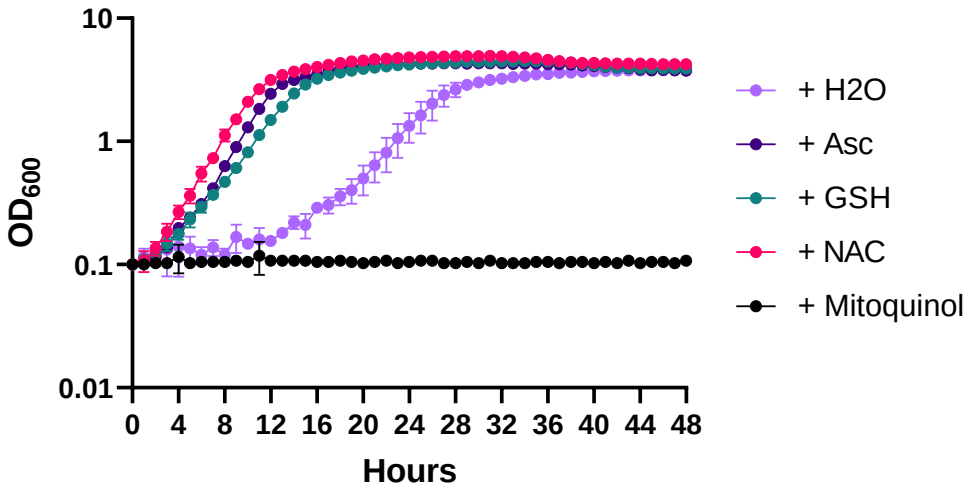

Appendix Figure 8.14. **The effect of different antioxidants on the cyprodinil-neocuproine combination**. Exponential phase W303 cells were treated with a combination of 94 um cyprodinil and 90 uM neocuproine. Different antioxidants (or H_2O for control) were added. Cells were grown in YNB and supplemented with either H_2O, 2 mM glutathione, 2 mM ascorbic acid, 2 mM *N*-acetylcysteine or 250 µM mitoquinol. Plates were incubated at 30°C for 48 h. Error bars show standard deviation. n = 4.

Appendix Figure 8.15. **CYP-DPI synergy is fungicidal against *Z. tritici***. After a standard checkerboard experiment, *Z. tritici* growth was removed from wells and washed in PBS. 5 µl sample were then pipetted onto PDA agar plates containing no cyprodinil or DPI in the same layout as the original checkerboard. Plates were incubated at room temperature for 96 h.

9. References

Adamo, G.M., Brocca, S., Passolunghi, S., Salvato, B. and Lotti, M. (2012). Laboratory evolution of copper tolerant yeast strains. *Microbial Cell Factories*. **11**, 1.

Adeyemi, J.O. and Onwudiwe, D.C. (2018). Organotin(IV) dithiocarbamate complexes: chemistry and biological activity. *Molecules*. **23**, 2571.

Adeyemi, J.O. and Onwudiwe, D.C. (2020). The mechanisms of action involving dithiocarbamate complexes in biological systems. *Inorganica Chim Acta*. **511**.

Agrios, G.N. (2005). Plant Pathology. Fifth edition, Academic Press. New York, 633.

Aguirre, J., Rios-Momberg, M., Hewitt, D. and Hansberg, W. (2005). Reactive oxygen species and development in microbial eukaryotes. *Trends Microbiol*. **13**, 111-118.

Alamgir, Md., Eroukova, V., Jessulat, M., Xu, J. and Golshani, A. (2008). Chemical-genetic profile analysis in yeast suggests that a previously uncharacterized open reading frame, YBR261C, affects protein synthesis. *BMC Genomics*. **9**, 583.

Albrich J.M., McCarthy C.A. and Hurst J.K. (1981). Biological reactivity of hypochlorous acid: implications for microbicidal mechanisms of leukocyte myeloperoxidase. *Proc Natl Acad Sci USA*. **78**, 210-214.

Alhebshi, A., Sideri, T.C., Holland, S.L. and Avery, S.V. (2012). The essential iron-sulfur protein Rli1 is an important target accounting for inhibition of cell growth by reactive oxygen species. *Mol Biol Cell*. **23**, 3582-3590.

Almeida, C.E., Felício, D.L., Galhardo, R.S., Cabral-Neto, J.B. and Leitão, A.C. (1999). Synergistic lethal effect between hydrogen peroxide and neocuproine (2,9-dimethyl 1,10-phenanthroline) in *Escherichia coli*. *Mutat Res*. **433**, 59-66.

Al-Moubarak, E. and Simons, C. (2011). A homology model for *Clostridium difficile* methionyl tRNA synthetase: active site analysis and docking interactions. *J. Mol Model*. **17**, 1679-1693.

Altamura, E., Borgatti, M., Finotti, A., Gasparello, J., Gambari, R., Spinelli, M., Castaldo R. and Altamura N. (2016). Chemical-Induced Read-Through at Premature Termination Codons Determined by a Rapid Dual-Fluorescence System Based on S. cerevisiae. *PLoS ONE*. **11**: e0154260.

Amoroso, G., Morell-Avrahov, L., Müller, D., Klug, K. and Sültemeyer, D. (2005). The gene NCE103 (YNL036w) from *Saccharomyces cerevisiae* encodes a functional carbonic anhydrase and its transcription is regulated by the concentration of inorganic carbon in the medium. *Mol Microbiol*. **56**, 549-558.

Arraiano, L.S. and Brown, J.K. (2017). Sources of resistance and susceptibility to Septoria tritici blotch of wheat. *Mol Plant Pathol*. **18**, 276-292.

Asiimwe, T., Krause, K, Schlunk, I. and Kothe, E (2012). Modulation of ethanol stress tolerance by aldehyde dehydrogenase in the mycorrhizal fungus *Tricholoma vaccinum*. *Mycorrhiza*. **22**, 471-484.

Augostine, C.R. and Avery (2022). Discovery of Natural Products With Antifungal Potential Through Combinatorial Synergy. *Front Microbiol*. **13**, 866840.

Avenot, H.F. and Michailides, T.J. (2019). Occurrence and Extent of Boscalid Resistance in Populations of *Alternaria alternata* from California Pistachio Orchards. *Plant Dis*. **104**, 306-314.

Avery, S.V., Singleton, I., Magan, N. and Goldman, G.H. (2019). The fungal threat to global food security. *Fungal Biol*. **123**, 555-557.

Ayres, P.G. (2004). Alexis Millardet: France's forgotten mycologist. *Mycologist*. **18**, 23-26.

Baibakova, E.V., Nefedjeva, E.E., Suska-Malawska, M., Wilk, M., Serviukova, G.A. and Zheltobriukhov, V.F. (2019). Modern Fungicides: Mechanisms of Action, Fungal Resistance and Phytotoxic Effects. *Annu Res Rev Biol*. **32**, 1-16.

Baker, K.F. (1987). Evolving concepts of biological control of plant pathogens. *Annu Rev Phytopathol* **25**, 67–85.

Balaiya, S. and Chalam, K.V. (2016). An *In vitro* Assay to Quantify Nitrosative Component of Oxidative Stress. *J Mol Genet Med*. **8**, 120.

Baldwin, T.O. (1996). Firefly luciferase: the structure is known, but the mystery remains. *Cell Press*. **4**, 223-228.

Baracca, A., Sgarbi, G., Solaini, G. and Lenaz, G. (2003). Rhodamine 123 as a probe of mitochondrial membrane potential: evaluation of proton flux through F0 during ATP synthesis. *Biochim Biophys Acta*. **1606**, 137-146.

Barthelme, D. Scheele, U., Dinkelaker, S., Janoschka, A., MacMilan, F., Albers, S., Driessen, A.J.M., Stagni, M.S., Bill, E., Meyer-Klaucke, W., Schuönemann, V. and Tampé, R. (2007). Structural organization of essential iron-sulfur clusters in the evolutionarily highly conserved ATP-binding cassette protein ABCE1. *J Biol Chem*. **282**, 14598-14607.

BAYER AG. (2020). Chlorothalonil Loss in May 2020 Poses New Challenges. https://cropscience.bayer.co.uk/blog/articles/2020/02/life-after-chlorothalonil/.

BAYER AG. Listed fungicides: https://cropscience.bayer.co.uk/our-products/fungicides/. Accessed on 18/05/2020.

Bebber, D.P., Ramotowski, M.A.T. and Gurr, S.J. (2013). Crop pests and pathogens move polewards in a warming world. *Nat Clim Change*. **3**, 985-988.

Beebe, K., Ribas de Pouplana, L. and Schimmel, P. (2003). Elucidation of tRNA-dependent editing by a class II tRNA synthetase and significance for cell viability. *EMBO J*. **22**, 668-675.

Bender, C.L. and Cooksey, D.A. (1986). Indigenous plasmids in *Pseudomonas syringae* pv. *tomato*: conjugative transfer and role in copper resistance. *Journal of Bacteriology*. **165**, 534–541.

Berners-Lee, M., Kennelly, C., Watson, R. and Hewitt, C.N. (2018). Current global food production is sufficient to meet human nutritional needs in 2050 provided there is radical societal adaptation. *Elem Sci Anth*. **6**, 52.

Bhattacharjee, J. (1985). α-Aminoadipate pathway for the biosynthesis of lysine in lower eukaryotes. *Crit Rev Microbiol*. **12**, 131-151.

Bin, P., Huang, R. and Zhou, X. (2017). Oxidation Resistance of the Sulfur Amino Acids: Methionine and Cysteine. *Biomed Res Int*. **2017**, 9584932.

Black, B., Lee, C., Horianopoulos, L.C., Jung, W.H. and Kronstad, J.W. (2018). Respiring to infect: Emerging links between mitochondria, the electron transport chain, and fungal pathogenesis. *PLoS Pathog*. **17**, e1009661.

Bollenbach, T. (2015). Antimicrobial interactions: mechanisms and implications for drug discovery and resistance evolution. *Curr Opin Microbiol*. **27**, 1-9.

Bonnemain, H. and Dive, D. (1990). Studies on synergistic toxic effects of copper and dithiocarbamate pesticides with the ciliate protozoan *Colpidium campylum* (Stokes). *Ecotoxicol Environ Saf*. **19**, 320-326.

Borovinskaya, M.A., Shoji, S., Fredrick, K. and Cate, J.H.D. (2008). Structural basis for hygromycin B inhibition of protein biosynthesis. *RNA*. **14**, 1590-1599.

Bosshard, H.R. (1976). Theories of enzyme specificity and their application to proteases and aminoacyl-Transfer RNA synthetases. *Experientia*. **32**, 949-963.

Boveris, A. an dCadenas, E. (1982). Production of superoxide radicals and hydrogen peroxide in mitochondria. In Oberley,L. (ed.), Superoxide Dismutase. CRC Press, Boca Raton, FL, Vol. II, pp. 15–30.

Bowler, J., Scott, E., Tailor, R., Scalliet, G., Ray, J. and Csukai, M. (2010). New capabilities for *Mycosphaerella graminicola* research. *Mol Plant Pathol*. **11**, 691-704.

Boyce, J.M. (2001). MRSA patients: proven methods to treat colonization and infection. *J Hosp Infect*. **48,** 9-14.

Brancaccio, D., Gallo, A., Piccioli, M., Novellino, E., Ciofi-Baffoni, S. and Bacni, L. (2017). [4Fe-4S] cluster assembly in mitochondria and its impairment by copper. *J Am Chem Soc*. **139**, 719-730.

Brent K.J. and Hollomon D.W. (2007). Fungicide Resistance in Crop Pathogens: How Can it be Managed? FRAC Monograph 1. 2nd Ed. Brussels, CropLife International, Brussels: 55.

Brown, A.G. (1986). Clavulanic acid, a novel beta-lactamase inhibitor--a case study in drug discovery and development. *Drug Design and Delivery*. **1**, 1-21.

Buchman, C., Skroch, P., Welch, J., Fogel, S. and Karin, M. (1989). The CUP2 gene product, regulator of yeast metallothionein expression, is a copper-activated DNA-binding protein. *Mol Cell Biol*. **9**, 4091-4095.

Burkitt, M., Milne, L., Nicotera, P. and Orrenius, S. (1996). 1,10-Phenanthroline stimulates internucleosomal DNA fragmentation in isolated rat-liver nuclei by promoting the redox activity of endogenous copper ions. *Biochem J*. **313**, 163-169.

Byrnes, R.W., Antholine, W.E. and Petering, D.H. (1992). Oxidation-reduction reactions in Ehrlich cells treated with copper-neocuproine. *Free Radic Biol Med*. **13**, 469-478.

Calvete, C.L., Martho, K.F., Felizardo, G., Paes, A., Nunes, J.M., Ferreira, C.O., Vallim, M.A. and Pascon, R.C. (2019). Amino acid permeases in *Cryptococcus neoformans* are required for high temperature growth and virulence; and are regulated by Ras signaling. *PLoS ONE*. **14**, e0211393.

Carmel-Harel, O. and Storz, G. (2000). Roles of the glutathione- and thioredoxin-dependent reduction systems in the *Escherichia coli* and *Saccharomyces cerevisiae* responses to oxidative stress. *Annu Rev Microbiol*. **54**, 439-461.

Castro, P.A., Ramirez, A., Sepúlveda, F.J., Peters, C., Fierro, H., Waldron, J., Luza, S., Fuentealba, J., Muñoz, F.J., De Ferrari, G.V., Bush, A.I., Aguayo, L.G. and Opazo, C.M. (2014). Copper-uptake is critical for the down regulation of synapsin and dynamin induced by neocuproine: modulation of synaptic activity in hippocampal neurons. *Front Aging Neurosci*. **6**, 319.

Caverzan, A., Piasecki, C., Chavarria, G., Stewart Jr., C.N. and Vargas, L. (2019). Defenses Against ROS in Crops and Weeds: The Effects of Interference and Herbicides. *Int J Mol Sci*. **20**, 1086.

Cedergreen, N. (2014). Quantifying Synergy: A Systematic Review of Mixture Toxicity Studies within Environmental Toxicology. *PLoS ONE*. **9**, e96580.

Cevestesic, N., Semanjski, M., Soufi, B., Krug, K., Gruic-Sovulj, I. and Macek, B. (2016). Proteome-wide measurement of non-canonical bacterial mistranslation by quantitative mass spectrometry of protein modifications. *Scientific Reports*. **6**, 28631.

Channabasava, A., Lakshman, H.C. and Jorquera, M.A. (2015). Effect of fungicides on association of arbuscular mycorrhiza fungus Rhizophagus fasciculatus and growth of Proso millet (Panicum miliaceum L.). *Journal of Soil Science and Plant Nutrition*. **15**, 35-45.

Chait, R., Craney, A. and Kishony, R. (2007). Antibiotic interactions that select against resistance. *Nature*. **446**, 668–671.

Chakraboti, S., Chhibber-Goel, J. and Sharma, A. (2021). Drug targeting of aminoacyl-tRNA synthetases in Anopheles species and Aedes aegypti that cause malaria and dengue. *Parasit Vectors*. **14**, 605.

Charles, W. and Carter, Jr. (2018). Coding of Class I and II aminoacyl-tRNA synthetases. *Adv Exp Med Biol*. **966**, 103-148.

Chawla, B., Jhingran, A., Paningrahi, A., Stuart, K.D. and Madhubala, R. (2011). Paromomycin Affects Translation and Vesicle-Mediated Trafficking as Revealed by Proteomics of Paromomycin –Susceptible –Resistant *Leishmania donovani*. *PLoS One*. **6**, e26660.

Cheek, M., Lughadha, E.C., Kirk, P., Lindon, H., Carretero, J., Looney, B., Douglas, B., Haelewaters, D., Gaya, E., Llewellyn, T., Ainsworth, A.M., Gafforov, Y., Hyde, K.D., Crous, P.W., Hughes, M., Walker, B.E., Forzza, R.C., Wong, K.M. and Niskanen, T. (2020). New scientific discoveries: Plants and fungi. *Plants, People, Planet*. **2**, 371-388.

Chen, X., Ren, B., Chen, M., Liu, M., Ren, W., Wang, Q., Zhang, L. and Yan, G. (2014). ASDCD: Antifungal Synergistic Drug Combination Database. *PLoS ONE*. **9**, e86499.

Chen, K., Wang, Y., Zhang, R., Zhang, H., Gao, C. (2019). CRISPR/Cas genome editing and precision plant breeding in agriculture. *Annu Rev Plant Biol*. **70**, 667-697.

Cheval, P., Siah, A., Bomble, M., Popper, A.D., Reignault, P. and Halama, P. (2017). Evolution of QoI resistance of the wheat pathogen *Zymoseptoria tritici* in Northern France. *Crop Prot*. **92**, 131-133.

Chillappagari, S., Seubert, A., Trip, H., Kuipers, O.P., Marahiel, M.A. and Miethke, M. (2010). Copper Stress Affects Iron Homeostasis by Destabilizing Iron-Sulfur Cluster Formation in *Bacillus subtilis*. *J Bacteriol*. **192**, 2512-2524.

Choi, Y., Lee, C. and Goodwin, S.B. (2016). Generation of Reactive Oxygen Species via NOXa Is Important for Development and Pathogenicity of *Mycosphaerella graminicola*. *Mycobiology*. **44**, 38-47.

Chopra, S. and Reader, J. (2015). tRNAs as Antiobiotic Targets. *Int J Mol Sci*. **16**, 321-349.

Cobb, A.H. and Reade, P.H.R. (2010). Herbicides and Plant Physiology. 2nd ed. John Wiley & Sons; New York, NY, USA: 2010. 286p.

Cokol, M., Chua, H.N., Tasan, M., Mutlu, B., Weinstein, Z.B., Suzuki, Y., Nergiz, M.E., Constanzo, M., Baryshnikova, A., Giaever, G., Nislow, C., Myers, C., Andrews, B.J., Boone, C. and Roth, F. (2011). Systematic exploration of synergistic drug pairs. *Mol Syst Biol*. **7**, 544.

Cokol, M., Li, C. and Chandrasekaran, S. (2018). Chemogenomic model identifies synergistic drug combinations robust to the pathogen microenvironment. *PLos ONE*. **14**, e1006677.

Collin, F. (2019). Chemical Basis of Reactive Oxygen Species Reactivity and Involvement in Neurodegenerative Diseases. *Int J Mol Sci*. **20**, 2407.

Commission implementing regulation (EU) 2020/2087 of 14 December 2020 concerning the nonrenewal of the approval of the active substance mancozeb, in accordance with Regulation (EC) No 1107/2009 of the European Parliament and of the Council concerning the placing of plant protection products on the market and amending the Annex to Commission Implementing Regulation (EU) No 540/2011. https://eur-lex.europa.eu/legalcontent/EN/TXT/PDF/?uri=CELEX:32020R2087&rid=6.

Cormack, B.P., Valdivia, R.H. and Falkow, S. (1996). FACS-optimized mutants of the green fluorescent protein (GFP). *Gene*. **173**, 33-38.

Costanzo, M., VanderSluis, B., Koch, E.N., Baryshnikova, A., Pons, C., Tan, G., Wang, W., Usaj, M., Hanchard, J., Lee, S.D., Pelechano, V., Styles, E.B., Billmann, M., van Leeuwen, J., van Dyk, N., Lin, Z., Kuzmin, E., Nelson, J., Piotrowski, J.S., Srikumar, T., Bahr, S., Chen, Y., Deshpande, R., Kurat, C.F., Li, S.C., Li, Z., Usaj, M.M., Okada, H., Pascoe, N., San Luis, B., Sharifpoor, S., Shuteriqi, E., Simpkins, S.W., Snider, J., Suresh, H.G., Tan, Y., Zhu, H., Malod-Dognin, N., Janjic, V., Przulj, N., Troyanskaya, O.G., Stagljar, I., Xia, T., Ohya, Y., Gingras, C., Raught, B., Boutros, M., Steinmetz, L.M., Moore, C.L., Rosebrock, A.P., Caudy, A.A., Myers, C.L., Andrews, B. and Boone, C.

(2016). A Global Genetic Interaction Network Maps a Wiring Diagram of Cellular Function. *Science*. **353**, 6306.

Crous, P.W., Rossman, A.Y., Aime, M.C., Allen, W.C., Burgess, T., Groenewald, J.Z. and Castlebury, L.A. (2021). Names of Phytopathogenic Fungi: A Practical Guide. *Phytopathology*. **111**, 1500-1508.

Cui, K. and Shoemaker, S.P. (2018). Public perception of genetically-modified (GM) food: A Nationwide Chinese Consumer Study. *npj Science of Food*. **2**, 10.

Dalhoff, A. (2018). Does the use of antifungal agents in agriculture and food foster polyene resistance development? A reason for concern. *J Glob Antimicrob Resist*. **13**, 40-48.

Darvishi, E., Omidi M., Bushehri A.A., Golshani A. and Smith M.L. (2013). The antifungal eugenol perturbs dual aromatic and branched-chain amino acid permeases in the cytoplasmic membrane of yeast. *PLoS One*. **8**, e76028.

Davies, J., Jones, D.S. and Khorana, H.G. (1966). A further study of misreading of codons induced by streptomycin and neomycin using ribopolynucleotides containing two nucleotides in alternating sequence as templates. *J Mol Biol*. **18**, 48-57.

Davis, B.D. (1987). Mechanism of Bactericidal Action of Aminoglycosides. *Microbiological Reviews*. **51**, 341-350.

Davis, M.P., Sparks, J.S. and Smith, W.L. (2016). Repeated and Widespread Evolution of Bioluminescence in Marine Fishes. *PLoS ONE*. **11**, e0155154.

Delarue, M. (1995). Aminoacyl-tRNA synthetases. *Curr Opin Struct Biol*. **5**, 48-55.

Denning, D.W. (2002). Echinocandins: a new class of antifungal. *J Antimicrob Chemother*. **49**, 889-891.

Dennis, K.E. and Valentine, W.M. (2015). Ziram and Sodium N,N-Dimethyldithiocarbamate Inhibit Ubiquitin Activation through Intracellular Metal Transport and Increased Oxidative Stress in HEK293 Cells. *Chem Res Toxicol*. **28**, 682-690.

Dias, P.J, Teixeira, M.C., Telo, J.P. and Sá-Correia, I. (2010). Insights into the mechanisms of toxicity and tolerance to the agricultural fungicide mancozeb in yeast, as suggested by a chemogenomic approach. *OMICS*. **14**, 211-227.

Dill, G.M. (2005). Glyphosate-resistant crops: history, status and future. *Pest Manag Sci*. **61**, 219-224.

Drawz, S.M. and Bonomo, R.A. (2010). Three decades of beta-lactamase inhibitors. *Clin Microbiol Rev*. **23**, 160-201.

Dock-Bregeon, A., Sankaranarayanan, R., Romby, P., Caillet, J., Springer, M., Rees, B., Francklyn, C.S., Ehresmann, C. and Moras, D. (2000). Transfer RNA-mediated editing in threonyl-tRNA synthetase. The class II solution to the double discrimination problem. *Cell*. **103**, 877-884.

Doern, C.D. (2014). When Does 2 Plus 2 Equal 5? A Review of Antimicrobial Synergy Testing. *J Clin Microbiol*. **52**, 4124-4128.

Dong, J.S., Lau, R., Nielsen, K., Fekete, C.A., Qiu, H.F. and Hinnebusch, A.G. (2004). The essential ATP-binding cassette protein RLI1 functions in translation by promoting preinitiation complex assembly. *J Biol Chem*. **279**, 42157-42168.

Drugbank. https://www.drugbank.ca/drugs/DB00410. Accessed on 22/02/19.

Duncan, K.E. and Howard, R.J. (2000). Cytological analysis of wheat infection by the leaf blotch pathogen *Mycosphaerella graminicola*. *Mycol Res*. **104**, 1074-1082.

Eisler, R. (1998). Copper hazards to fish, wildlife, and invertebrates: A synoptic review. U.S. Geological Survey, Biological Re-sources Division, Biological Science Report USGS/BRD/BSR-1997-0002, Washington, DC. pp 98.

Eriani, G., Delarue, M., Poch, O., Gangloff, J. and Moras, D. (1990). Partition of tRNA synthetases into two classes based on mutually exclusive sets of sequence motifs. *Nature*. **347**, 203-206.

Eriani, G., Cavarelli, J., Martin, F., Ador, L., Rees, B., Thierry, J.C., Gangloff, J. and Moras, D. (1995). The class II aminoacyl-tRNA synthetases and their active site: evolutionary conservation of an ATP binding site. *J Mol Evol*. **40**, 499-508.

van Esse, H.P., Reuber, T.L. and van der Does, D. (2019). Genetic modification to improve disease resistance in crops. *New Phytol*. **225**, 70-86.

Estep, L.K., Torriani, S.F.F., Zala, M., Anderson, N.P., Flowers, M.D., McDonald, B.A., Mundt, C.C. and Brunner, P.C. (2014). Emergence and early evolution of fungicide resistance in North American populations of *Zymoseptoria tritici*. *Plant Pathol*. **64**, 961-971.

European Union (2020). Commission Implementing Regulation (EU) 2020/2087 of 14 December 2020.

Fang., J. and Beattie, D.S. (2003). External alternative NADH dehydrogenase of *Saccharomyces cerevisiae*: a potential source of superoxide. *Free Radic Biol Med*. **34**, 478-488.

Fato, R., Bergamini, C., Bortolus, M., Maniero, A.L., Leoni, S., Ohnishi, T. and Lenaz, G. (2009). Differential effects of mitochondrial Complex I inhibitors on production of reactive oxygen species. *Biochim Biophys Acta*. **1787**, 384-392.

Favorova, O.O. (1984). [Superspecificity of aminoacyl-tRNA-synthases]. *Mol Biol (Mosk)*. **18**, 205-226.

Fersht, A.R. and Kaethner, M.M. (1976). Enzyme hyperspecificity. Rejection of threonine by the valyl-tRNA synthetase by misacylation and hydrolytic editing. *Biochemistry*. **15**, 3342-3346.

Figuccia, S., Degiorgi, A., Berti, C.C., Baruffini, E., Dallabona, C. and Goffrini, P. (2021). Mitochondrial Aminoacyl-tRNA Synthetase and Disease: The Yeast Contribution for Functional Analysis of Novel Variants *Int J Mol Sci*. **22**, 4524.

Figueroa, M., Hammond-Kosack, K.E. and Solomon, P.S. (2018). A review of wheat diseases—a field perspective. *Mol Plant Pathol*. **19**, 1523-1536.

Fischer, P.W., Giroux, A. and L'Abbé, M.R. (1981). The effect of dietary zinc on intestinal copper absorption. *Am J Clin Nutr*. **34**, 1670-1675.

Fisher, M.C., Henk, D.A., Briggs, C.J., Brownstein, J.S., Madoff, L.C., McCraw, S.L. and Gurr, S.J. (2012). Emerging fungal threats to animal, plant and ecosystem health. *Nature*. **484**, 186-194.

Flobak, A., Niederdorfer, B., Nakstad, V.T., Thommesen, L., Klinkenberg, G. and Lægreid, A. (2019). A high-throughput drug combination screen of targeted small molecule inhibitors in cancer cell lines. *Sci Data*. **6**, 237.

Fones, H. and Gurr, S (2015). The impact of Septoria tritici Blotch disease on wheat: An EU perspective. *Fungal Genet Biol*. **79**, 3-7.

Forslund, K., Schreiber, F., Thanintorn, N. and Sonnhammer, E.L.L. (2011). OrthoDisease: tracking disease gene orthologs across 100 species. *Brief Bioinform*. **12**, 463-473.

Foster, A.W., Dainty, S.J., Patterson, C.J., Pohl, E., Blackburn, H., Wilson, C., Hess, C.R., Rutherford, J.C., Quaranta L., Corran, A. and Robinson, N.J. (2014). A chemical potentiator of copper-accumulation used to investigate the iron-regulons of *Saccharomyces cerevisiae*. *Mol Microbiol*. **93**, 317-330.

Fraga, H., Fernandes, D., Novotny, J., Fontes, R., Joaquim, C.G., and da Silva, E. (2003). Firefly Luciferase Produces Hydrogen Peroxide as a Coproduct in Dehydroluciferyl Adenylate Formation. *ChemBioChem*. **7**, 929-935.

Friedrich, T., Steinmüller, K. and Weiss, H. (1995). The proton-pumping respiratory complex I of bacteria and mitochondria and its homologue in chloroplasts. *FEBS Lett*. **367**, 107-111.

Fouché, G., Rosati, D., Venet, C., Josserand, H., Latorse, M., Debieu, D. and Fillinger, S. (2022). LC-MS/MS-Based Fungicide Accumulation Assay to Demonstrate Efflux Activity in the Wheat Pathogen *Zymoseptoria tritici*. *Microorganisms*. **10**, 1494.

Fu, Y., Chen, N., Wang, Z., Luo, S., Ding, Y. and Lu, B. (2021). Degradation of lipid droplets by chimeric autophagy-tethering compounds. *Cell Res*. **31**, 965-979.

Fukai, S., Nureki, O., Sekine, S., Shimada, A., Tao, J., Vassylyev, D.G. and Yokoyama, S. (2000). Structural Basis for Double-Sieve Discrimination of L-Valine from L-Isoleucine and L-Threonine by the Complex of tRNAVal and Valyl-tRNA Synthetase. *Cell*. **103**, 793-803.

Fungicide Resistance Action Committee. (2022). https://www.frac.info/frac-teams/working-groups/ap-fungicides/information.

Fungicide Resistance Action Committee. (2022). https://www.frac.info/frac-teams/working-groups/qol-fungicides/information.

Fungicide Resistance Action Committee. (2022). https://www.frac.info/frac-teams/expert-fora/benzimidazoles/information.

Garside, M. (2019). Global fungicide market revenue 2016-2024. *Statista* (online).

Garza, N.M., Griffin, A.T., Zulkifli, M., Qiu, C., Kaplan, C.D. and Gohil, V.M. (2021). A genome-wide copper-sensitized screen identifies novel regulators of mitochondrial cytochrome c oxidase activity. *J Biol Chem*. **296**, 100485.

Gaur, R.K. (2014). Amino acid frequency distribution among eukaryotic proteins. *IIOABJ*. **5**, 6-11.

Gessler, C., Pertot, I. and Perazzolli, M. (2011). *Plasmopara viticola*: A review of knowledge on downy mildew of grapevine and effective disease management. *Phytopathol Mediterr*. **50**, 3-44.

Giegé, R, Sissler, M. and Florentz, C. (1998). Universal rules and idiosyncratic features in tRNA identity. *Nucleic Acids Res*. **26**, 5017-5035.

Giegé, R. and Springer, M. (2016). Aminoacyl-tRNA Synthetases in the Bacterial World. *EcoSal Plus*. **7**. doi: 10.1128/ecosalplus.ESP-0002-2016.

Grant, C.M., MacIver, F.H. and Dawes, I.W. (1996). Glutathione is an essential metabolite required for resistance to oxidative stress in the yeast *Saccharomyces cerevisiae*. *Curr Genet*. **29**, 511-515.

Green, L.S., Bullard, J.M., Ribble, W., Dean, F., Ayers, D.F., Ochsner, U.A., Janjic, N. and Jarvis, T.C. (2009). Inhibition of Methionyl-tRNA Synthetase by REP8839 and Effects of Resistance Mutations on Enzyme Activity. *Antimicrob Agents Chemother*. **53**, 86-94.

Gomes, A.C., Kordala, A.J., Strack, R., Wang, X., Geslain, R., Delaney, K., Clark, W.C., Keenan, R. and Pan, T. (2016). A dual fluorescent reporter for the investigation of methionine mistranslation in live cells. *RNA*. **22**, 467-476.

Gómez-Navarro, N., Peiró-Chova, L., Rodriguez-Navarro, S., Polaina, J. and Estruch, F. (2013). Rtp1p Is a Karyopherin-Like Protein Required for RNA Polymerase II Biogenesis. *Mol Cell Biol*. **33**, 1756-1767.

Goodwin, S. B., M'barek, S. B., Dhillon, B., Wittenberg, A. H., Crane, C. F., Hane, J. K., Foster, A. J., Van der Lee, T. A., Grimwood, J., Aerts, A., Antoniw, J., Bailey, A., Bluhm, B., Bowler, J., Bristow, J., van der Burgt, A., Canto-Canché, B., Churchill, A. C., Conde-Ferràez, L., Cools, H. J., Coutinho, P.M., Csukai, M., Dehal, P., De Wit, P., Donzelli, B., van de Geest, H.C., van Ham, R.C.H.J., Hammond-Kosack, K.E., Henrissat, B., Kilian, A., Kobayashi, A.K., Koopmann, E., Kourmpetis, Y., Kuzniar, A., Lindquist, E., Lombard, V., Maliepaard, C., Martins, N., Mehrabi, R., Nap, J.P.H., Pomomarenko, A., Rudd, J.J., Salamov, A., Schmutz, J., Schouten, H.J., Shapiro, H., Stergiopoulos, I., Torriani, S.F.F., Tu, de Vries, R.P., Waalwijk, C., Ware, S.B., Wiebenga, A., Zwiers, L., Oliver, R.P., Grigoriev, I.V. and Kema, G.H.J. (2011). Finished Genome of the Fungal Wheat Pathogen *Mycosphaerella graminicola* Reveals Dispensome Structure, Chromosome Plasticity, and Stealth Pathogenesis. *PLoS Genet*. **7**, e1002070.

Gottwald, E.M., Duss, M., Bugarski, M., Haenni, D., Schuh, C.D., Landau, E.M. and Hall, A.M. (2018). The targeted anti-oxidant MitoQ causes mitochondrial swelling and depolarization in kidney tissue. *Physiol Rep*. **6**, e13667.

Gyulkhandanyan, A.V., Feeney, C.J. and Pennefather, P.S. (2003). Modulation of mitochondrial membrane potential and reactive oxygen species production by copper in astrocytes. *J Neurochem*. **87**, 448-460.

Hartley, C. (1921). Damping-off in forest nurseries. *US Dept Agr Bul*. **934**, 99.

Hartman M.C., Josephson K., Lin C.W. and Szostak J.W. (2007). An expanded set of amino acid analogs for the ribosomal translation of unnatural peptides. *PLoS One*. **2**, e972.

Harvey, H.J., Hendry, A.C., Archer, D.B. and Avery, S.V. (2023). Evaluating the potential of natural product combinations with sorbic acid for improving preservative action against food-spoilage yeasts. *Fungal Biology*. **127**, 1218-1223.

Hawkins, N.J. and Fraaije, B.A. (2016). Predicting Resistance by Mutagenesis: Lessons from 45 Years of MBC Resistance. *Front Microbiol*. **7**, 1814.

Hawksworth, D.L and Lücking, R. (2017). Fungal diversity revisited: 2.2 to 3.8 million species. *Microbiol*. Spectr. **5**.

He., L., Kulesskiy, E., Saarela, J., Turunen, L., Wennerberg, K., Aittokllio, T. and Tang, J. (2018). Methods for High-throughput Drug Combination Screening and Synergy Scoring. *Methods Mol Biol*. **1711**, 351-398.

Hellin, P., Duvivier, M., Heick, T.M., Fraaije, B.A., Bataille, C., Clinckemaillie, A., Legrève, A., Jørgensen, L.N., Andersson, B., Samils, B., Rodemann, B., Berg, G., Hutton, F., Garnault, M., El Jarroudi, M., Couleaud, G. and Kildea, S. (2021). Spatio-temporal distribution of DMI and SDHI fungicide resistance of *Zymoseptoria tritici* throughout Europe based on frequencies of key target-site alterations. *Pest Manag Sci*. **77**, 5576-5588.

Helsel, M.E. and Franz, K.J. (2015). Pharmacological activity of metal binding agents that alter copper bioavailability. *Dalton Trans*. **44**, 8760-8770.

Hegreness, M., Shoresh, N., Damian, D., Hartl, D. and Kishony, R. (2008). Accelerated evolution of resistance in multidrug environments. *Proc Natl Acad Sci USA*. **105**, 13997-13981.

Herbert, C., Dujardin, G., Labouesse, M. and Slonimski, P. (1998). Divergence the mitochondrial leucyl tRNA synthetase genes in the two closely related yeasts *Saccharomyces cerevisiae* and S. douglasii: A paradigm of incipient evolution. *Mol Gen Genet*. **213**, 297–309.

Hobbelen, P.H.F., Paveley, N.D. and van den Bosch, F. (2014). The Emergence of Resistance to Fungicides. *PLoS ONE*. **9**, e91910.

Holland, S., Lodwig E., Sideri, T., Reader, T., Clarke, I., Gkargkas, K., Hoyle, D., Delneri, D., Oliver, S.G. and Avery, S.V. (2007). Application of the comprehensive set of heterozygous yeast deletion mutants to elucidate the molecular basis of cellular chromium toxicity. *Genome Biology*. **8**, R268.

Holland, S.L., Ghosh, E. and Avery, S.V. (2010). Chromate-induced sulfur starvation and mRNA mistranslation in yeast are linked in a common mechanism of Cr toxicity. *Toxicol In Vitro*. **24**, 1764-1767.

Holland, S.L. and Avery, S.V. (2011). Chromate toxicity and the role of sulfur. *Metallomics*. **3**, 1119-1123.

Hollomon, D.W. (2015). Fungicide Resistance: Facing the Challenge. *Plant Protect Sci*. **51**, 170-176.

Holman, K.M., Wu, J., Ling, J. and Simonović, M. (2016). The crystal structure of yeast mitochondrial ThrRS in complex with the canonical threonine tRNA. *Nucleic Acids Res*. **44**, 1428-1439.

Hood, M.I. and Skaar, E.P. (2012). Nutritional immunity: transition metals at the pathogen-host interface. *Nat Rev Microbiol*. **10**, 525-537.

Horâk, J. (1997). Yeast nutrient transporters. *Biochim Biophys Acta*. **1331**, 41-79. Pathogenic mechanisms and control strategies of *Botrytis cinerea* causing post-harvest decay in fruits and vegetables. *Food Quality and Safety*. **2**, 111-119.

Hua, L., Yong, C., Zhanquan, Z., Boqiang, L., Guozheng, Q. and Shiping, T. (2018).

Huang, Y., Hung, Y., Hsu, S., Huang, Y. and Hwang, D. (2008). Application of electrolyzed water in the food industry. *Food Control*. **19**, 329-345.

Hunsaker, E.W. and Franz, K.J. (2019). Emerging Opportunities To Manipulate Metal Trafficking for Therapeutic Benefit. *Inorg Chem*. **58**, 13528-13545.

Hurdle, J.G., O'Neill, A.J. and Chopra, I. (2005). Prospects for Aminoacyl-tRNA Synthetase Inhibitors as New Antimicrobial Agents. *Antimicrob Agents Chemother*. **49**, 4821-4833.

Ibba, M., Curnow, A.W. and Söll, D. (1997). Aminoacyl-tRNA synthesis: divergent routes to a common goal. *Trends Biochem Sci*. **22**, 39-42.

Ibba, M. and Söll, D. (2000). Aminoacyl-tRNA Synthesis. *Annu Rev Biochem*. **69**, 617-650.

Ibba, M. and Söll, D. (2001). The renaissance of aminoacyl-tRNA synthesis. *EMBO Rep*. **2**, 382-387.

Ianevski, A., Giri, A.K., Gautam, P., Kononov, A., Potdar, S., Saarela, J., Wennerberg, K. and Aittokallio, T. Prediction of drug combination effects with a minimal set of experiments. *Nature Machine Intelligence*. **1**, 568-577.

Innocenti, A., Hall, R.A., Schlicker, C., Mühlschlegel, F.A. and Supuran, C.T. (2009). Carbonic anhydrase inhibitors. Inhibition of the β-class enzymes from the fungal pathogens Candida albicans and Cryptococcus neoformans with aliphatic and aromatic carboxylates. *Bioorganic Med Chem*. **17**, 2654-2657.

Islahudin, F., Khozoie, C., Bates, S., Ting, K.N., Pleass, R.J. and Avery, S.V. (2013). Cell wall perturbation sensitizes fungi to the antimalarial drug chloroquine. *Antimicrob Agents Chemother*. **57**, 3889-3896.

Iwahashi, Y., Hitoshio, A., Tajima, N. and Nakamura, T. (1989). Characterization of NADH Kinase from *Saccharomyces cerevisiae*. *J Biochem*. **105**, 588-593.

von Jagow, G. and Klingenberg, M. (1970). Pathways of Hydrogen in Mitochondria of Saccharomyces carlsbergensis. *Eur J Biochem*. **12**, 583-592.

Jaiser, S.R. and Winston, G.P. (2010). Copper deficiency myelopathy. *J Neurol*. **257**, 869-881.

Jamieson D.J. (1998). Oxidative stress responses of the yeast *Saccharomyces cerevisiae*. *Yeast*. **14**, 1511–1527.

Jastrzebowska, K. and Gabriel, I. (2015). Inhibitors of amino acids biosynthesis as antifungal agents. *Amino Acids*. **47**, 227-249.

Jauniaux, J.C., Urrestarazu, L.A. and Wiame, J.M. (1978). Arginine metabolism in *Saccharomyces cerevisiae*: subcellular localization of the enzymes. *J Bacteriol*. **133**, 1096-1107.

Jawetz, E. and Gunnison, J.B. (1953). Antibiotic synergism and antagonism: an assessment of the problem. *Pharmacol Rev*. **5**, 175-192.

Jeong, J., Kim, J.Y. and Yoon, J. (2006). The Role of Reactive Oxygen Species in the Electrochemical Inactivation of Microorganisms. *Environ Sci Technol*. **40**, 6117-6122.

Jinna, S. and Finch, J. (2015). Spotlight on tavaborole for the treatment of onychomycosis. *Drug Des Devel Ther*. **9**, 6185-6190.

Jo, S., Son, M., Koh, H., Lee, S., Song, I., Kim, Y., Lee, Y., Jeong, K., Kim, W.B., Il, J.P., Song, B.J. and Huhe, T. (2001). Control of Mitochondrial Redox Balance and Cellular Defense against Oxidative Damage by Mitochondrial NADP+-dependent Isocitrate Dehydrogenase. *J Biol Chem*. **276**, 16168-16176.

Johnson, G.F. (1935). The early history of copper fungicides. *Agric Hist*. **9**, 67-79.

Johnson M.D., MacDougall, C., Ostrosky-Zeichner, L., Perfect, J.R. and Rex, J.H. (2004). Combination Antifungal Therapy. *Antimicrob Agents Chemother*. **48**, 693-715.

Joseph-Horne, T., Hollomon, D.W. and Wood, P.M. (2001). Fungal respiration: a fusion of standard and alternative components. *Biochim Biophys Acta*. **1504**, 179-195.

Kägi, J.H. (1991). Overview of metallothionein. *Methods Enzymol*. **205**, 613-626.

Karlsson, I., Friberg, H., Steinberg, C. and Persson, P. (2014). Fungicide Effects on Fungal Community Composition in the Wheat Phyllosphere. *PLoS ONE*. **9**, e111786.

Karthika, C. and Muraleedharan, N.N. (2009). Contribution of leaf growth on the disappearance of fungicides used on tea under south Indian agroclimatic conditions. *J Zhejian Univ Sci B*. **10**, 422-426.

Kelso, G.F., Porteous, C.M., Coulter, C.V., Hughes, G., Porteous, W.K., Ledgerwood, E.C., Smith, R.A.J. and Murphy, M.P. (2001). Selective Targeting of a Redox-active Ubiquinone to Mitochondria within Cells. *J Biol Chem*. **276**, 4588-4596.

Kema, G.H.J., Yu, D., Rijkenberg, F.H.J., Shaw, M.W. and Baayen, R.P. (1996). Histology of the pathogenesis of *Mycosphaerella graminicola* in wheat. *Phytopathology*. **87**, 777-786.

Keon, J., Antoniw, J., Carzaniga, R., Deller, S., Ward, L., Baker, J.M., Beale, M.H., Hammond-Kosack, K. and Rudd, J.J. (2007). Transcriptional Adaptation of *Mycosphaerella graminicola* to Programmed Cell Death (PCD) of Its Susceptible Wheat Host. *The American Phytopathological Society*. **20**, 178-193.

Keyer, K. and Imlay, J.A. (1996). Superoxide accelerates DNA damage by elevating free-iron levels. *Proc Natl Acad Sci U S A*. **93**, 13635-13640.

Khozoie C., Pleass R.J. and Avery S.V. (2009). The antimalarial drug quinine disrupts Tat2p-mediated tryptophan transport and causes tryptophan starvation. *J Biol Chem*. **284**, 17968–17974.

Kim, G., Sikder, H. and Singh, K.K. (2002). A colony color method identifies the vulnerability of mitochondria to oxidative damage. *Mutagenesis*. **17**, 375-381.

Kim, B.E., Nevitt, T. and Thiele, D.J. (2008). Mechanisms for copper acquisition, distribution and regulation. *Nat Chem Biol*. **4**, 176-185.

Kim, S., Park, C., Chun, H., Lee, D., Choi, J., Lee, H., Cho, S., Park, S., Choi, S., Choi, J. and Yoo, J. (2016). Pilot Screening to Determine Antimicrobial Synergies in a Multidrug-Resistant Bacterial Strain Library. *Microb Drug Resist*. **22**, 372-378.

Kispal, G., Sipos, K., Lange, H., Fekete, Z., Bedekovics, T., Janáky, T., Bassler, J., Netz, D.J.A., Balk, J., Rotte, C. and Lill, R. (2005). Biogenesis of cytosolic ribosomes requires the essential iron–sulphur protein Rli1p and mitochondria. *EMBO*. **24**, 589-598.

Krick, W., Schnedler, N., Burckhardt, G. and Burckhardt, B.C. (2009). Ability of sat-1 to transport sulfate, bicarbonate, or oxalate under physiological conditions. *Am J Physiol Renal Physiol*. **297**, F145-F154.

Kruppa, M., Moir, R.D., Kolodrubetz, D. and Willis, I.M. (2001). Nhp6, an HMG1 Protein, Functions in SNR6 Transcription by RNA Polymerase III in *S. cerevisiae*. *Mol Cell*. **7**, 309-318.

Koc, A., Gasch, A.P., Rutherford, J.C., Kim, H.W., and Gladyshev, V.N. (2004). Methionine sulfoxide reductase regulation of yeast lifespan reveals reactive oxygen species-dependent and -independent components of aging. *PNAS*. **101**, 7999-8004.

Kokina, A., Kibilds, J. and Liepins, J. (2014). Adenine auxotrophy – be aware: some effects of adenine auxotrophy in Saccharomyces cerevisiae strain W303-1A. *FEMS Yeast Research*. **14**, 697-707.

Kosuge, T. and Hishino, T. (1999). The α-aminoadipate pathway for lysine biosynthesis is widely distributed among Thermus strains. *Journal of Bioscience and Bioengineering*. **88**, 672-675.

Kovacs, M., Geltinger, F., Verwanger, T., Weiss, R., Richter, K. and Rinnerthaler, M. (2021). Lipid Droplets Protect Aging Mitochondria and Thus Promote Lifespan in Yeast Cells. *Front Cell Dev Biol*. **9**, 774985.

Kukat, A., Kukat, C., Brocher, J., Schäfer, I., Krohne, G., Trounce, I.A., Villani, G. and Seibel, P. (2008). Generation of ρ^0 cells utilizing a mitochondrially targeted restriction endonuclease and comparative analyses. *Nucleic Acids Res*. **36**, e44.

Kuplińska, A. and Rząd, K. (2021). Molecular targets for antifungals in amino acid and protein biosynthetic pathways. *Amino acids*. **53**, 961-991.

Kushwaha, V. and Capalash, N. (2022). Aminoacyl-tRNA synthetase (AARS) as an attractive drug target in neglected tropical trypanosomatid diseases-Leishmaniasis, Human African Trypanosomiasis and Chagas disease. *Mol Biochem Parasitol*. **251**, 111510.

Kuzmin, E., VanderSluis, B., Wang, W., Tan, G., Deshpande, R., Chen, Y., Usaj, M., Balint, A., Usaj, M.M., van Leeuwen, J., Koch, E.N., Pons, C., Dagilis, A.J., Pryszlak, M., Wang, J.Z.Y., Hanchard, J., Riggi., Xu, K., Heydari, H., San Luis, B., Shuteriqi, E., Zhu, H., van Dyk, N., Sharifpoor, S., Costanzo, M., Loewith, R., Caudy, A., Bolnick, D., Brown, G.W., Andrews, B.J., Boone, C. and Myers, C.L. (2018). Systematic Analysis of Complex Genetic Interactions. *Science*. **360**, eaao1729.

Kwon, N.H., Fox, P.L. and Kim, S. (2019). Aminoacyl-tRNA synthetases as therapeutic targets. *Nat Rev Drug Discov*. **18**, 629-650.

Lamb, J.Y. and Davis, M.P. (2020). Salamanders and other amphibians are aglow with biofluorescence. *Sci Rep*. **10**, 2821.

La Torre, A., Iovino, V. and Caradonia, F. (2018). Copper in plant protection: current situation and prospects. *Phytopathol Mediterr*. **57**, 201-236.

Lee, N., Bertholet, S., Debrabant, A., Muller, J., Duncan, R. and Nakhasi, H.L. (2002). Programmed cell death in the unicellular protozoan parasite *Leishmania*. *Cell Death & Differentiation*. **9**, 53-64.

Lee, J.Y., Kim, D.G., Kim, B., Yang, W.S., Hong, J., Kang, T., Oh, Y.S., Kim, K.R., Han, B.W., Hwang, B.J., Kang, B.S., Kang, M., Kim, M., Kwon, N.H. and Kim, S. (2014). Promiscuous methionyl-tRNA synthetase mediates adaptive mistranslation to protect cells against oxidative stress. *J Cell Sci*. **127**, 4234-4245.

Leroux, P., Fritz, R., Debieu, D., Albertini, C., Lanen, C., Bach, J, Gredt, M. and Chapeland, F. (2002). Mechanisms of resistance to fungicides in field strains of *Botrytis cinerea*. *Pest Manag Sci*. **58**, 876-878.

Letscher-Bru, V. and Herbrecht, R. (2003). Caspofungin: the first representative of a new antifungal class. *J Antimicrob Chemother*. **51**, 513-521.

Leung, C., Chan, D.S., Ma, V.P., Ma, D. (2013). DNA-binding small molecules as inhibitors of transcription factors. *Med Res Rev*. **33**, 823-846.

Levine, R.L., Mosoni, L., Berlett, B.S. and Stadtman, E.R. (1996). Methionine residues as endogenous antioxidants in proteins. *Proc Natl Acad Sci USA*. **223**, 271-281.

Lewis, C.A., Parker, S.J., Fiske, B.P., McCloskey, D., Gui, D.Y., Green, C.R., Vokes, N.I., Feist, A.M., Vander Heiden, M.G. and Metallo, C.M. (2014). Tracing compartmentalized NADPH metabolism in the cytosol and mitochondria of mammalian cells. *Mol Cell*. **55**, 253-263.

Li, Y. and Trush. M.A. (1998). Diphenyleneiodonium, an NAD(P)H oxidase inhibitor, also potently inhibits mitochondrial reactive oxygen species production. *Biochem Biophys Res Commun*. **253**, 295-299.

Li, L., Palencia, A., Lukk, T. and Boniecki, M.T. (2013). Leucyl-tRNA synthetase editing domain functions as a molecular rheostat to control codon ambiguity in Mycoplasma pathogens. *PNAS*. **110**, 3817-3822.

Li, X., Qin, G., Yang, G., Chen, L. and Xie, L. (2016). Biomolecular Network-Based Synergistic Drug Combination Discovery. *Biomed Res Int*. doi: 10.1155/2016/8518945.

Lincecum, T.L., Tukalo, M., Yaremchuk, A., Mursinna, R.S., Williams, A.M., Sproat, B.S., Van Den Eynde, W., Link, A., Van Calenbergh, S., Grotli, M., Martinis, S.A. and Cusack, S. (2003). Structural and Mechanistic Basis of Pre- and Posttransfer Editing by Leucyl-tRNA Synthetase. *Molecular Cell*. **11**, 951-963.

Ling, J., Peterson, K.M., Simonović, I. and Simonović, M. (2012). Yeast mitochondrial threonyl-tRNA synthetase recognizes tRNA isoacceptors by distinct mechanisms and promotes CUN codon reassignment. *PNAS*. **109**, 3281-3286.

Lippard, S.J. (1999). Free Copper Ions in the Cell? *Science*. **284**, 748-749.

Liochecv, S.I. and Fridovich, I. (1999). Superoxide and iron: partners in crime. *IUBMB Life*. **48**, 157-161.

Liu, Y., Fiskum, G. and Schubert, D. (2002). Generation of reactive oxygen species by the mitochondrial electron transport chain. *J Neurochem*. **80**, 780-787.

Liu, C.T., Tomsho, J.W. and Benkovic, S.J. (2014). The unique chemistry of benzoxaboroles: Current and emerging applications in biotechnology and therapeutic treatments. *Bioorganic & Medicinal Chemistry*. **22**, 4462-4473.

Loughran, G., Chou, M., Ivanov, I.P., Jungreis, I., Kellis, M., Kiran, A.M., Baranov, P.V. and Atkins, J.F. (2014). Evidence of efficient stop codon readthrough in four mammalian genes. *Nucleic Acids Research*. **42**, 8928-8938.

Lucas, J.A., Hawkins, N.J. and Fraaije, B.A. (2015). The evolution of fungicide resistance. *Adv Appl Microbiol*. **90**, 29-92.

Lue, S.W. and Kelley, S.O. (2005). An aminoacyl-tRNA synthetase with a defunct editing site. *Biochemistry*. **44**, 3010-3016.

Lum, P.Y., Armour, C.D., Stepaniants, S.B., Cavet, G., Wolf, M.K., Butler, J.S., Hinshaw, J.C., Garnier, P., Prestwich, G.D., Leonardson, A., Garrett-Engele, P., Rush, C.M., Bard, M., Schimmack, G., Phillips, J.W., Roberts, C.J., Shoemaker, D.D. (2004). Discovering modes of action for therapeutic compounds using a genome-wide screen of yeast heterozygotes. *Cell*. **116**, 121-137.

Luo, Y., Henle, E.S. and Linn, S. (1996). Oxidative Damage to DNA Constituents by Iron-mediated Fenton Reactions. *J Biol Chem*. **271**, 21177-21186.

Lushchak, V.I. (2012). Glutathione Homeostasis and Functions: Potential Targets for Medical Interventions. *J Amino Acids*. **2012**, 736837.

Lynch, K.M., Zannini, E., Guo, J., Axel, C., Arendt, E.K., Kildea, S. and Coffey, A. (2016). Control of *Zymoseptoria tritici* cause of septoria tritici blotch of wheat using antifungal *Lactobacillus* strains. *J Appl Microbiol*. **121**, 485-494.

Ma, B. and Uddin, W. (2009). Fitness and Competitive Ability of an Azoxystrobin-Resistant G143A Mutant of Magnaporthe oryzae from Perennial Ryegrass. *Plant Dis*. **93**, 1044-1049.

Macomber, L. and Imlay, J.A. (2009). The iron-sulfur clusters of dehydratases are primary intracellular targets of copper toxicity. *Proc Natl Acad Sci USA.* **106**, 8344-8349.

Mamba, A.M., Mishra, A.K., Mamba, B.B., Njobeh, P.B., Dutton, M.F. and Fosso-Kankeu, E. (2010). Spectral, thermal and in vitro antimicrobial studies of

cyclohexylamine-N-dithiocarbamate transition metal complexes. S*pectrochim Acta Part A Mol Biomol Spectrosc*. **77**, 579-587.

Manoussakis, G., Bolos, C., Ecateriniadou, L. and Sarris, C. (1987). Synthesis, characterization and anti-bacterial studies of mixed-liand complexes of dithiocarbamato-thiocyanato and iron(III), nickel(II), copper(II) and zinc(II). *Eur j Med Chem*. **22**, 421-425.

Mansoury, M., Hamed, M., Karmustaji, R., Hannan, F.A. and Safrany, S.T. (2021). The edge effect: A global problem. The trouble with culturing cells in 96-well plates. *Biochem Biophys Rep*. **26**, 100987.

Marco, G.M. and Stall, R.E. (1983). Control of bacterial spot of pepper initiated by strains of *Xanthomonas campestris* pv. *vesicatoria* that differ in sensitivity to copper. *Plant Disease*. **67**, 779–781.

Margue, C., Philippidou, D., Kozar, I., Cesi, G., Felten, P., Kulms, D., Letellier, E., Haan, C. and Kreis, S. (2019). Kinase inhibitor library screening identifies synergistic drug combinations effective in sensitive and resistant melanoma cells. *J Exp Clin Cancer Res*. **38**, 56.

Markovich, D. (2001). Physiological Roles and Regulation of Mammalian Sulfate Transporters. *Physiol Rev*. **81**, 1499-1533.

Martho, K.F.C., de Melo, A.T., Takahashi, J.P.F., Guerra, J.M., Santos, D.C.dS., Purisco, S.U., Melhem, M.dS.C., Fazioli, R.dA., Phanord, C., Sartorelli, P., Vallim, M.A. and Pascon, R.C. (2016). Amino Acid Permeases and Virulence in *Cryptococcus neoformans*. *PLoS ONE*. **11**, e0163919.

Martins, D. and English, A.M. (2014). Catalase activity is stimulated by H2O2 in rich culture medium and is required for H2O2 resistance and adaptation in yeast. *Redox Biology*. **2**, 308-313.

Martin, F., Barends, S. and Eriani, G. (2004). Single amino acid changes in AspRS reveal alternative routes for expanding its tRNA repertoire in vivo. *Nucleic Acids Res*. **32**, 4081-4089.

Maslanka, R., Zadrag-Tecza, R., and Kwolek-Mirek, M. (2020). Linkage between Carbon Metabolism, Redox Status and Cellular Physiology in the Yeast *Saccharomyces cerevisiae* Devoid of *SOD1* or *SOD2* Gene. *Genes (Basel)*. **11**, 780.

Massart, C., Giusti, N., Beauwens, R., Dumont, J.E., Miot, F. and Sande, J.V. (2014). Diphenyleneiodonium, an inhibitor of NOXes and DUOXes, is also an iodide-specific transporter. *FEBS Open Bio*. **4**, 55-59.

Masner, P., Muster, P., and Schmid, J. (1994). Possible methionine biosynthesis inhibition by pyrimidinamine fungicides. *Pestic Sci*. **42**, 163-166.

Matthews, J.C., Hori, K. and Cormier, M.J. (1977). Substrate and Substrate Analogue Binding Properties of *Renilla* Luciferase. *Biochemistry*. **16**, 5217-5220.

McCarthy, M.W., Kontoyiannis, D.P., Cornely, O.A., Perfet, J.R. and Walsh, T.J. (2017). Novel Agents and Drug Targets to Meet the Challenges of Resistant Fungi. *The Journal of Infectious Diseases*. **216**, S474-S483.

McCarthy, M.W. and Walsh, T.J. (2018). Amino Acid Metabolism and Transport Mechanisms as Potential Antifungal Targets. *Int J Mol Sci*. **19**, 909.

McClain, W.H. (1993). Rules that Govern tRNA Identity in Protein Synthesis. *J Mol Biol*. **234**, 257-280.

McFarland, M.R., Keller, C.D., Childers, B.M., Adeniyi, S.A., Corrigal, H., Raguin, A., Romano, M.C. and Stansfield, I. (2020). *Nucleic Acids Res*. **48**, 3071-3088.

McNabb, D.S., Reed, R. and Marciniaka R.A. (2005). Dual Luciferase Assay System for Rapid Assessment of Gene Expression in Saccharomyces cerevisiae. *Eukaryot Cell*. **4**, 1539-1549.

McPhetres, J., Rutjens, B.T., Weinstein, N. and Brisson, J.A. (2019). Modifying attitudes about modified foods: Increased knowledge leads to more positive attitudes. *Journal of Environmental Psychology*. **64**, 21-29.

Mehta, G.D., Ball, D.A., Eriksson, P.R., Chereji, R.V., Clark, D.J., McNally, J.G., Karpova, T.S. (2018), Single-molecule analysis reveals linked cycles of RSC chromatin remodeling and Ace1p transcription factor binding in yeast. *Mol Cell*. **72,** 875-887.

Meletiadis, J., Pournaras, S., Roilides, E. and Walsh, T.J. (2009). Defining Fractional Inhibitory Concentration Index Cutoffs for Additive Interactions Based on Self-Drug Additive Combinations, Monte Carlo Simulation Analysis, and In Vitro-In Vivo Correlation Data for Antifungal Drug Combinations against Aspergillus fumigatus. *Antimicrob Agents Chemother*. **54**, 602-609.

Mendoza, H., Perlin, M.H. and Schirawski, J. (2020). Mitochondrial Inheritance in Phytopathogenic Fungi—Everything Is Known, or Is It? *Int J Mol Sci*. **21**, 3883.

Menzler-Hokkanen, I. (2006). "Socioeconomic significance of biological control," in *An ecological and societal approach to biological control* (Dordrecht: Springer), 13–25.

Millardet, A. (1881). Notes sur les vignes américaines et opuscules divers sur le même sujet. *Féret & Fils, Bordeaux*.

Miyagi, H., Kawai, S. and Murata, K. (2009). Two sources of mitochondrial NADPH in the yeast *Saccharomyces cerevisiae*. *J Biol Chem*. **284**, 7553-7560.

Mohammadi, S., Saberidokht, B., Subramaniam, S. and Grama, A. (2015). Scope and limitations of yeast as a model organism for studying human tissue-specific pathways. *BMC Systems Biology*. **9**, 96.

Mohler, K., and Ibba, M. (2017). Translational fidelity and mistranslation in the cellular response to stress. *Nat Microbiol*. **2**, 17117.

Moras, D. (2010). Proofreading in translation: Dynamics of the double-sieve model. *Proc Natl Acad Sci U S A*. **107**. 21949-21950.

Moreno-Martinez, E., Vallières, C., Holland, S.L. and Avery, S.V. (2015). Novel, Synergistic Antifungal Combinations that Target Translation Fidelity. *Sci Rep*. **5**, 16700.

Mortimer, R.K. (2000). Evolution and Variation of the Yeast (*Saccharomyces*) Genome. *Genome Res*. **10**, 409-409.

Morton, V. and Staub, T. (2008). A Short History of Fungicides. *The American Phytopathological Society*. https://web.archive.org/web/20160416202111/http://www.apsnet.org/publications/apsnetfeatures/Pages/Fungicides.aspx.

Mosbach, A., Edel, D., Farmer, A.D., Widdison, S., Barchietto, T., Dietrich, R.A., Corran, A. and Scalliet, G. (2017). Anilinopyrimidine Resistance in *Botrytis cinerea* Is Linked to Mitochondrial Function. *Front Microbiol*. **8**, 2361.

Mukhopadhyay, R., Shi, J. and Rosen, B.P. (2000). Purification and Characterization of Acr2p, the *Saccharomyces cerevisiae* Arsenate Reductase. *J Biol Chem*. **275**, 21149-21157.

Murray, G.M. and Brennan, J.P. (2009). Estimating disease losses to the Australian wheat industry. *Australas. Plant Pathol*. **38**, 558-570.

Musiime, O., Tenywa, M.M., Majaliwa, M.J.G., Lufafa, A., Namfumba, D., Wasige, J., Woomer, P.L. and Kyondha, M. (2005). Constraints to rice production in Bugiri district. *Afr Crop Scie Conf Proc*. **7**, 1495-1499.

Nayak, S.U., McLeod Griffliss, J., Blumer, J., O'Riordan, M.A., Gray, W., McKenzie, R., Jurao, R.A., An, Amanda, T., Le, M., Bell, S.J., Ochsner, U.A., Jarvis, T.C., Janjic, N., and Zenilman, J.M. (2017). Safety, Tolerability, Systemic Exposure, and Metabolism of CRS3123, a Methionyl-tRNA Synthetase Inhibitor Developed for Treatment of Clostridium difficile, in a Phase 1 Study. *Antimicrobial Agents and Chemotherapy*. **61**, e02760-16.

Negri, S., Lovato, A., Boscaini, F., Salvetti, E., Torriani, S., Commisso, M., Danzi, R., Ugliano, M., Polverari, A., Tornielli, G.B. and Guzzo, F. (2017). The Induction of Noble Rot (*Botrytis cinerea*) Infection during Postharvest Withering Changes the Metabolome of Grapevine Berries (*Vitis vinifera* L., cv. Garganega). *Front Plant Sci*. **8**, 1002.

Nemat Alla, M.M., Badawi, A.M., Hassan, N.M., El-Bastawisy, Z.M. and Badran, E.G. (2008). Effect of metribuzin, butachlor and chlorimuron-ethyl on amino acid and protein formation in wheat and maize seedlings. *Pestic Biochem Physiol*. **90**, 8-18.

Netzer, N., Goodenbour, J.M., David, A., Dittmar, K.A., Jones, R.B., Schneider, J.R., Boone, D., Eves, E.M., Rosner, M.R., Gibbs, J.S., Embry, A., Dolan, B., Das S., Hickman, H.D., Berglund, P., Bennink, J.R., Yewdell, J.W., and Pan, T. (2009). Innate immune and chemically triggered oxidative stress modifies translational fidelity. *Nature*. **462**, 522-526.

Newman, T.E. and Derbyshire, M.C. (2020). The Evolutionary and Molecular Features of Broad Host-Range Necrotrophy in Plant Pathogenic Fungi. *Front Plant Sci*. **11**, 591733.

Nikiforov, A., Dölle, C., Niere, M. and Ziegler, M. (2011). Pathways and subcellular compartmentation of NAD biosynthesis in human cells: from entry of extracellular precursors to mitochondrial NAD generation. *J Biol Chem*. **286**, 21767-21778.

Nuhu, F., Gordon, A., Sturmey, R., Seymour, A. and Bhandari, S. (2020). Measurement of Glutathione as a Tool for Oxidative Stress Studies by High Performance Liquid Chromatography. *Molecules*. **25**, 4196.

Nunes, E.A., Manieri, T.M., Matias, A.C., Bertuchi, F.R., da Silva, D.A., Lago, L., Sato, R.H. and Cerchiaro, G. (2018). Protective effects of neocuproine copper chelator against oxidative damage in NSC34 cells. *Mutat Res*. **836**, 62-71.

Ochsner, U.A., Sun, X., Jarvis, T., Critchley I. and Janjic, N. (2007). Aminoacyl-tRNA synthetases: essential and still promising targets for new anti-infective agents. *Expert Opin Investig Drugs*. **16**, 573-93.

Odds, F.C. (2003). Synergy, antagonism, and what the chequerboard puts between them. *J Antimicrob Chemother*. **52**, 1.

Ogilvie, A., Wiebauer, K. and Kersten, W. (1975). Inhibition of leucyl-transfer ribonucleic acid synthetasymol. *Biochem J*. **152**, 511-515.

Ogilvie, A., Wiebauer, K. and Kersten, W. (1975). Stringent Control of Ribonucleic Acid Synthesis in Bacillus subtilis Treated with Granaticin. *Biochem J*. **152**, 517-522.

Ogur, M., St. John, R. and Nagai, S. (1957). Tetrazolium Overlay Technique for Population Studies of Respiration Deficiency in Yeast. *Science*. **125**, 928-929.

Ohtake, H., Cervantes, C. and Silver, S. (1987). Decreased chromate uptake in *Pseudomonas fluorescens* carrying a chromate resistance plasmid. *J Bacteriol*. **169**, 3853-3556.

Oliver, R.P. and Hewitt, H.G. (2014). Fungicides in crop protection (2nd ed.). Wallingford, UK: CABI.

Oliveri, V. (2020). Biomedical applications of copper ionophores. *Coordin Chem Rev*. **422**.

Omrane, S., Sghyer, H., Audéon, C., Lanen, C., Duplaix, C., Walker, A. and Fillinger, S. (2015). Fungicide efflux and the MgMFS1 transporter contribute to the multidrug resistance phenotype in *Zymoseptoria tritici* field isolates. *Environ Microbiol*. **17**, 2805-2823.

Omrane, S., Audéon, C., Ignace, A., Duplaix, C., Aouini, L., Kema, G., Walker A. and Fillinger, S. (2017). Plasticity of the MFS1 Promoter Leads to Multidrug Resistance in the Wheat Pathogen *Zymoseptoria tritici*. *mSphere*. **2**, e00393-17.

Onwudiwe, D.C. and Ajibade, P.A. (2012). Thermal Studies of Zn(II), Cd(II) and Hg(II) Complexes of Some N-Alkyl-N-Phenyl-Dithiocarbamates. *Int J Mol Sci*. **13**, 9502-9513.

Oomori T., Oka T., Inuta T. and Arata Y. (2000). The efficiency of disinfection of acidic electrolyzed water in the presence of organic materials. *Anal Sci*. **16**, 365-369.

Outten, C.E. and Culotta, V.C. (2003). A novel NADH kinase is the mitochondrial source of NADPH in *Saccharomyces cerevisiae*. *EMBO J*. **22**, 2015-2024.

Oyedotun, K.S. and Lemire, B.D. (2004). The quaternary structure of the Saccharomyces cerevisiae succinate dehydrogenase. Homology modeling, cofactor docking, and molecular dynamics simulation studies. *J Biol Chem*. **279**, 9424-9431.

Padmanabhan, S.Y. (1973). The great Bengal famine. *Annu Rev Phytopathol*. **11**, 11-26.

Pain, J., Balamurali, M.M., Dancis, A. and Pain, D. (2010). Mitochondrial NADH kinase, Pos5p, is required for efficient iron-sulfur cluster biogenesis in *Saccharomyces cerevisiae*. *J Biol Chem*. **285**, 39409-39424.

Pal, D.S., Mondal, D.K. and Datta, R. (2015). Identification of metal dithiocarbamates as a novel class of antileishmanial agents. *Antimicrob Agents Chemother*. **59**, 2144-2152.

Palmieri, D., Ianiri, G., Del Grosso, C., Barone, G., De Curtis, F., Castoria, R. and Lima, G. (2022). Advances and Perspectives in the Use of Biocontrol Agents against Fungal Plant Diseases. *Horticulturae*. **8**, 577.

Pang, Y.L.J., Poruir, K. and Martinis, S.A. (2014). tRNA synthetase: tRNA Aminoacylation and beyond. *Wiley Interdiscip Rev RNA*. **5**, 461-480.

Parenti, M.A., Hatfield, S.M. and Leyden, J.J. (1987). Mupirocin: a topical antibiotic with a unique structure and mechanism of action. *Clin Pharm*. **6**, 761-770.

Parker, J., Johnston, T.C. and Borgia, P.T. (1980). Mistranslation in cells infected with the bacteriophage MS2: direct evidence of Lys for Asn substitution. *Mol Gen Genet*. **180**, 275-281.

Pathak, V.N. (1997). Postharvest fruit pathology: present status and future possibilities. *Indian Phytopath*. **50**, 161–185.

Pena, M.M., Koch, K.A. and Thiele, D.J. Dynamic regulation of copper uptake and detoxification genes in *Saccharomyces cerevisiae*. *Mol Cell Biol*. **18**, 2514-2523.

Pereira, Y., Lagnielm G., Godat, E., Baudouin-Cornu, P., Junot, C, and Labarre, J. (2008). Chromate causes sulfur starvation in yeast. *Toxicol Sci*. **106**, 400-412.

Perrone, G.G.f, Tan, S.X., Dawes, I.W. (2008). Reactive oxygen species and yeast apoptosis. *Biochim Biophys Acta*. **1783**, 1354-1368.

Phinney, J.T. and Bruland, K.W. (1997). Trace metal exchange in solution by the fungicides ziram and maneb (dithiocarbamates) and subsequent uptake of lipophilic organic zinc, copper and lead complexes into phytoplankton cells. *Environmental Toxicology and Chemistry*. **16**, 2046-2053.

Pittman, D., Webb, J.M., Roshanmanesh, A. and Coker, L.E. (1959). Evidence for the Genetic Control of Photoreactivation. *Genetics*. **45**, 1023-1037.

Plotz, P.H. and Davis, B.D. (1962). Synergism between streptomycin and penicillin: a proposed mechanism. *Science*. **135**, 1067-1068.

Pokrzywinski, K.L. , Biel T.G., Kryndushkin D. and Rao V. A. (2016). Therapeutic targeting of the mitochondria initiates excessive superoxide production and mitochondrial depolarization causing decreased mtDNA integrity. *PLoS ONE*. **11**:e0168283.

http://www.prestwickchemical.com/libraries-screening-lib-pcl.html.

Pufahl, R.A., Singer, C.P., Peariso, K.L., Lin, S, -J., Schmidt, P.J., Fahrni, C.J., Culotta, V.C., Penner-Hahn, J.E. and O'Halloran, T.V. (1997). Metal Ion Chaperone Function of the Soluble Cu(I) Receptor Atx1. *Science*. **278**, 853-856.

Radisky, D. and Kaplan, J. (1999). Regulation of Transition Metal Transport across the Yeast Plasma Membrane. *J Biol Chem*. **274**, 4481-4484.

Rae, T.D., Schmidt, P.J., Pufahl, R.A., Culotta, V.C. and O'Halloran, T.V. (1999). Undetectable intracellular free copper: the requirement of a copper chaperone for superoxide dismutase. *Science* **284**, 805-808.

Rajendran, V., Kalita, P., Shukla H., Kumar, A. and Tripathi, T. (2018). Aminoacyl-tRNA synthetases: Structure, function, and drug discovery. *Int J Biol Macromol*. **111**, 400-414.

Rancati, G., Moffat, J., Typas, A. and Pavelka, N (2018). Emerging and evolving concepts in gene essentiality. *Nat. Rev. Genet.* 19, 34–49.

Ramón-García, S., Ng, C., Anderson, H., Chao, J.D., Zheng, X., Pfeifer, T. and Av-Gay, Y. (2011). *American Society for Microbiology*. **55**, 3861-3869.

Reeder, N.L., Kaplan, J., Xu, J., Youngguist, R.S., Wallace, J., Hu, P., Juhlin, K.D., Schwartz, J.R., Grant, R.A., Fieno, A., Nemeth, S., Reichling, T., Tiesman, J.P., Mills, T., Steinke, M., Wang, S.L., Saunders, C.W. (2011). Zinc Pyrithione Inhibits Yeast Growth through Copper Influx and Inactivation of Iron-Sulfur Proteins. *Antimicrob Agents Chemother*. **55**, 5753-5760.

Regenberg, B., Düring-Olsen, L., Kielland-Brandt, M.C. and Holmberg, S. (1999). Substrate specificity and gene expression of the amino-acid permeases in *Saccharomyces cerevisiae*. *Curr Genet*. **36**, 317-328.

Reiner, C.K., Kada, G. and Gruber, H.J. (2002). Quick measurement of protein sulfhydryls with Ellman's reagent and with 4,4'-dithiodipyridine. *Anal Bioanal Chem*. **373**, 266-276.

Reis, J., Massari, M., Marchese, S., Ceccon, M., Aalbers, F.S., Corana, F., Velente, S., Mai, A., Magnani, F. and Mattevi, A. (2020). A closer look into NADPH oxidase inhibitors: Validation and insight into their mechanism of action. *Redox Biology*. **32**, 101466.

Rich, R.R., Mischis, L.A., Purton, S. and Wiskich, J.T. (2001). The sites of interaction of triphenyltetrazolium chloride with mitochondrial respiratory chains. *FEMS Microbiol Lett*. **202**, 181-187.

Riganti, C., Gazzano, E., Polimeni, M., Costamagna, C., Bosia, A. and Ghigo D. (2004). Diphenyleneiodonium Inhibits the Cell Redox Metabolism and Induces Oxidative Stress. J Biol Chem. **279**, 47726-47731.

Rock, F.L., Mao, W., Yaremchuk, A., Tukalo, M., Crépin, T., Zhou, H., Zhang, Y.K., Hernandez, V., Akama, T., Baker, S.J., Plattner, J.J., Shapiro, L., Martinis, S.A., Benkovic, S.J., Cusack, S. and Alley, M.R. (2007). An antifungal agent inhibits an aminoacyl-tRNA synthetase by trapping tRNA in the editing site. *Science*. **316**, 1759-1761.

Rupp, S., Weber, R.W.S., Rieger, D., Detzel, P. and Hahn, M. (2016). Spread of *Botrytis cinerea* Strains with Multiple Fungicide Resistance in German Horticulture. *Front Microbiol*. **7**, 2075.

Saha, S., Chakrabaty, P.K. and Banerjee, K. (2022). Producing Crops without Mancozeb? Perspectives on Recent Regulatory Dilemmas and Ways Out. *Agri Sci & Tech*. **2**, 272-275.

Saito, S., Michailidies, T.J. and Xiao, C.L. (2016). Generation of Reactive Oxygen Species via NOXa Is Important for Development and Pathogenicity of *Mycosphaerella graminicola*. *Plant Dis*. **100**, 2087-2093.

Salam, S., Iqbal, Z., Khan, A.A. and Mahmood, R. (2021). Oral administration of thiram inhibits brush border membrane enzymes, oxidizes proteins and thiols, impairs redox system and causes histological changes in rat intestine: A dose dependent study. *Pestic Biochem Physiol*. **164**, 14-25.

Salas-Marco, J. and Bedwell, D.M. (2005). Discrimination between defects in elongation fidelity and termination efficiency provides mechanistic insights into translational readthrough. *J Mol Biol*. **348**, 801-815.

Sánchez-Vallet, A., McDonald, M.C., Solomon, P.S. and McDonald, B.A. (2015). Is *Zymoseptoria tritici* a hemibiotroph? *Fungal Genetics and Biology*. **79**, 29-32.

Sangamwar, A.T., Deshpande, U.D. and Pekamwar, S.S. (2008). Antifungals: Need to Search for a New Molecular Target. *Indian J Pharm Sci*. **70**, 423-430.

Savary, S., Ficke, A., Aubertot, J. and Hollier, C. (2012). Crop losses due to diseases and their implications for global food production losses and food security. *Food Sec*. **4**, 519-537.

Scalliet, G., Bowler, J., Luksch, T., Kirchhofer-Allan, L., Steinhauer, D., Ward, K., Niklaus, M., Verras, A., Csukai, M., Daina, A. and Fonné-Pfister, R. (2012). Mutagenesis and Functional Studies with Succinate Dehydrogenase Inhibitors in the Wheat Pathogen *Mycosphaerella graminicola*. *PLoS One*. **7**, e35429.

Schimmel, P. (2011). Mistranslation and its control by tRNA synthetases. *Philos Trans R Soc Lond B Biol Sci*. **366**, 2965-2971.

Schimmel, P. (2018). The emerging complexity of the tRNA world: mammalian tRNAs beyond protein synthesis.

Schmidt, E. and Schimmel, P. (1994). Mutational isolation of a sieve for editing in a transfer RNA synthetase. *Science*. **264**, 265-267.

Schöbel, F., Jacobsen, I.D. and Brock, M. (2010). Evaluation of Lysine Biosynthesis as an Antifungal Drug Target: Biochemical Characterization of *Aspergillus fumigatus* Homocitrate Synthase and Virulence Studies. *Eukaryot Cell*. **9**, 878-893.

Schubart, R. (2000). Dithiocarbamic Acid and Derivatives. *Ullmann's Encyclopedia of Industrial Chemistry*. Weinheim: Wiley-VC.

Schwartz, M.H. and Pan, T. (2018). tRNA misacylation with methionine in the mouse gut microbiome in situ. *Microb Ecol*. **74**, 10-14.

Segal, A.W. (2008). The function of the NADPH oxidase of phagocytes and its relationship to other NOXs in plants, invertebrates, and mammals. *Int J Biochem Cell Biol*. **40**, 604-18.

Shanmuganathan, A., Avery, S.V., Willetts, S.A., Houghton and J.E. (2004). Copper-induced oxidative stress in Saccharomyces cerevisiae targets enzymes of the glycolytic pathway. *FEBS Letters*. **556**. 253-259.

Sharma, P., Yan, F., Doronina, V.A., Escuin-Ordinas, H., Ryan, M.D. and Brown, J.D. (2012). 2A peptides provide distinct solutions to driving stop-carry on translational recoding. *Nucelic Acids Res*. **40**, 3143-3151.

Sharma, N. and Sharma, D. (2015). An upcoming drug for onychomycosis: Tavaborole. *J Pharmacol Pharmacother*. **6**, 236-239.

Sheehan, D.J., Hitchcock, C.A. and Sibley, C.M. (1999). Current and Emerging Azole Antifunal Agents. *Clin Microbiol Rev*. **12**, 40-79.

Sherf, B.A. and Navarro, S.L. (1996). Dual-LuciferaseTM Reporter Assay: An Advanced Co-Reporter Technology Integrating Firefly and Renilla Luciferase Assays. *Promega Notes Mageine*. **57**, 2.

Shetty, N.P., Mehrabi, R., Lütken, H., Haldrup, A., Kema, G.H.J., Collinge, D.B. and Jørgensen, H.J.L. (2007). Role of hydrogen peroxide during the interaction between the hemibiotrophic fungal pathogen *Septoria tritici* and wheat. *New Phytologist*. **174**, 637-647.

Shi, F., Li, X., Bai, Y., Li, L., Pu, M., Liu, L. and Lei, M. (2021). Mechanism of the Zinc Dithiocarbamate-Activated Rubber Vulcanization Process: A Density Functional Theory Study. *ACS Appl Polym Mater*. **3**, 5188-5196.

Sholberg, P.L., Bedford, K.E., Haag, P. and Randall, P. (2001). Survey of *Erwinia amylovora* isolates from British Columbia for resistance to bactericides and virulence on apple. *Canadian Journal of Plant Pathology*. **23**, 60-67.

Sideri, T.C., Willetts, S.A. and Avery, S.V. (2009). Methionine sulphoxide reductases protect iron-sulphur clusters from oxidative inactivation in yeast. *Microbiology (Reading)*. **155**, 612-623.

Sidhu, Y.S., Cairns, T.C., Chaudhari, Y.K., Usher, J., Talbot, N.J., Studholme, D.J., Csukai, M. and Haynes, K. (2015). Exploitation of sulfonylurea resistance marker and non-homologous end joining mutants for functional analysis in *Zymoseptoria tritici*. *Fungal Genet Biol*. **79**, 102-109.

Sierotzki, H. and Gisi, W.U. (2000). Point Mutation in Cytochrome b Gene Conferring Resistance to Strobilurin Fungicides in Erysiphe graminis f. sp. tritici Field Isolates. *Pest Biochem Physiol*. **68**, 107-122.

Silao, F.G.S. and Ljungdahl, P.O. (2021). Amino Acid Sensing and Assimilation by the Fungal Pathogen Candida albicans in the Human Host. *Pathogens*. **11**, 5.

Singh, A., Tiwari, A., Bajpai, J. and Bajpai, A.K. (2018). Polymer-Based Antimicrobial Coatings as Potential Biomaterials: From Action to Application. *Handbook of Antimicrobial Coatings*, edited by A. Tiwari (Elsevier), p. 27-61.

Sissler, M., Pütz, J., Fasiolo, F. and Florentz, C. Mitochondrial Aminoacyl-tRNA Synthetases. In: Madame Curie Bioscience Database [Internet]. Austin (TX): Landes Bioscience; 2000-2013. Available from: https://www.ncbi.nlm.nih.gov/books/NBK6033/.

Sly, W.S. (1995). Human carbonic anhydrases and carbonic anhydrase deficiencies. *Annu Rev Biochem*. **64**, 375-401.

Sorensen, M.A. (2001). Charging levels of four tRNA species in *Escherichia coli* Rel(+) and Rel(-) strains during amino acid starvation: a simple model for the effect of ppGpp on translational accuracy. *J Mol Biol*. **307**, 785-798.

Souri, Z., Karimi, N. and Ahmad, P. (2021). The effect of NADPH oxidase inhibitor diphenyleneiodonium (DPI) and glutathione (GSH) on Isatis cappadocica, under Arsenic (As) toxicity. *Int J Phytoremediation*. **23**, 945-957.

Spencer, E.Y. (1982). Guide to the Chemicals Used in Crop Protection. 7th ed. Publication 1093. Research Institute, Agriculture Canada, Ottawa, Canada: Information Canada, p. 591.

Stapleton, P., Wu, P.J., King, A., Shanon, K., French, G. and Phillips, I. (1995). Incidence and mechanisms of resistance to the combination of amoxicillin and clavulanic acid in Escherichia coli. *Antimicrob Agents Chemother*. **39**, 2478-2483.

Steingrube, V.A., Wallace, R.J., Brown, B.A., Pant, Y., Zeluff, B., Steele, L.C. and Zhang, Y. (1991). Acquired resistance of *Nocardia brasiliensis* to clavulanic acid related to a change in beta-lactamase following therapy with amoxicillin-clavulanic acid. *Antimicrob Agents Chemother*. **35**, 524-528.

Stirling M. and Stirling G. (1997). "Disease Management: Biological Control" in *Plant Pathogens and Plant Diseases*. Eds. Brown J., Ogle H., 427-439.

Strand, M.K., Stuart, G.R., Longley, M.J., Graziewicz, M.A., Dominick, O.C. and Copeland, W.C. (2003). POS5 Gene of *Saccharomyces cerevisiae* Encodes a Mitochondrial NADH Kinase Required for Stability of Mitochondrial DNA. *Eukaryot Cell*. **2**, 809-820.

Strange, R.D. and Scott, P.R. (2005). Plant Disease: A Threat to Global Food Security. *Annu Rev Phytopathol*. **43**, 83-116.

Stefanini, I., Di Paola, M., Liti, G., Marranci, A., Sebastiani, F., Casalone, E. and Cavalieri, D. (2022). Resistance to Arsenite and Arsenate in *Saccharomyces cerevisiae* Arises through the Subtelomeric Expansion of a Cluster of Yeast Genes. *Int J Environ Res Public Health*. **19**, 8119.

Steinberg, G. (2015). Cell biology of *Zymoseptoria tritici*: Pathogen cell organization and wheat infection. *Fungal Genet Biol*. **79**, 17-23.

Struck, C. (2015). Amino acid uptake in rust fungi. *Front Plant Sci*. **6**, 40.

Stuehr, D.J., Fasehun, O.A., Kwon, N.S., Gross, S.S., Gonzalez, J.A., Levi, R. and Nathan, C.F. (1991). Inhibition of macrophage and endothelial cell nitric oxide synthase by diphenyleneiodonium and its analogs. *FASEB J*. **5**, 98-103.

Suzuki-Karasaki, M., Ochiai, T. and Suzuki-Karasaki, Y (2014). Crosstalk between mitochondrial ROS and depolarization in the potentiation of TRAIL-induced apoptosis in human tumor cells. *Int J Oncol*. **44**, 616-628.

Syngenta. Listed fungicides: https://www.syngenta.co.uk/products/search/crop-protection/type/fungicide-376. Accessed on 18/05/2020.

Takemoto, D., Tanaka, A. and Scott, B. (2007). NADPH oxidases in fungi: diverse roles of reactive oxygen species in fungal cellular differentiation. *Fungal Genet Biol*. **44**, 1065-1076.

Talbot, N.J. (2015). Taming a wild beast: Developing molecular tools and new methods to understand the biology of *Zymoseptoria tritici*. *Fungal Genet Biol*. **79**, 193-195.

Tallarida, R.J. (2011). Quantitative methods for assessing drug synergism. *Genes Cancer*. **11**, 1003-1008.

Tamm, L., Thuerig, B., Apostolov, S., Blogg, H., Borgo, E., Corneo, P.E., Fittje, de Palma, M., Donko, A., Experton, C., Marín, É.A., Pérez, Á.M., Pertot, I., Rasmussen, A., Steinshamm, H., Vetemaa, A., Willer, H. and Herforth-Rahmé. (2022). Use of Copper-Based Fungicides in Organic Agriculture in Twelve European Countries. *Agronomy*. **12**, 673.

Tan, G., Yang, J., Li, T., Zhao, J., Sun, S., Li, X., Lin, C., Li, J., Zhou, H. and Lyu, J. (2017). Anaerobic copper toxicity and iron-sulfur cluster biogenesis in *Escherichia coli*. *Appl Environ Microbiol.* **83**, e00867-17.

Tanaka, A., Christensen, M.J., Takemoto, D., Park, P. and Scott, B. (2006). Reactive Oxygen Species Play a Role in Regulating a Fungus–Perennial Ryegrass Mutualistic Interaction. *Plant Cell*. **18**, 1052-1066.

Tardito, S., Bassanetti, I., Bignardi, C., Elviri, L., Tegoni, M., Mucchino, C., Bussolati, O., Franchi-Gazzola, R. and Marchiò, L. (2011). Copper Binding Agents Acting as Copper Ionophores Lead to Caspase Inhibition and Paraptotic Cell Death in Human Cancer Cells. *J Am Chem Soc*. **133**, 6235-6242.

Tarrago, L., Kaya. A., Weerapana, E., Marino, S.M. and Gladyshev, V.N. (2012). Methionine Sulfoxide Reductases Preferentially Reduce Unfolded Oxidized Proteins and Protect Cells from Oxidative Protein Unfolding. *J Biol Chem*. **287**, 24448-24459.

Taylor, M.J. and Richardson, T. (1980). Antioxidant activity of skim milk–Effect of heat and resultant sulfhydryl-groups. *J Dairy Sci*. **63**, 1783-1795.

Thambugala, K.M., Daranagama, D.A., Phillips, A.J.L., Kannangara, S.D. and Promputtha, I. (2020). Fungi vs. Fungi in Biocontrol: An Overview of Fungal Antagonists Applied Against Fungal Plant Pathogens. *Front Cell Infect Microbiol*. **10**, 604923.

Tsvetkov, P., Coy, S., Petrova, B., Dreishpoon, M., Verma, A., Abdusamad, M., Rossen, J., Joesch-Cohen, L., Humeidi, R., Spangler, R.D., Eaton, J.K., Frenkel, E., Kocak, M., Corsello, S.M., Lutsenko, S., Kanarek, N., Santagata, S., Golub, T.R. (2022). Copper induces cell death by targeting lipoylated TCA cycle proteins. *Science*. **375**, 1254-1261.

Tyres, M., and Wright, G.D. (2019). Drug combinations: a strategy to extend the life of antibiotics in the 21st century. *Nature Reviews Microbiology*. **17**, 141-155.

Ugolini, S. and Bruschi, C.V. (1996). The red/white colony color assay in the yeast *Saccharomyces cerevisiae*: epistatic growth advantage of white ade8-18, ade2 cells over red ade2 cells. *Curr Genet*. **30**, 485-492.

UIPP (2002) Annual Report. Paris, France: Union des Industries de la Protection des Plantes. Genescope. *Botrytis cinerea* Estimated losses to vineyards in France. Annual Report.

United Nations, 2019 (global population).

Vallières, C. and Avery, S. (2017). Metal-Based Combinations That Target Protein Synthesis by Fungi. *Adv Microb Physiol*. **70**, 105-121.

Vallières, C., Holland, H.L. and Avery, S.V. (2017). Mitochondrial Ferredoxin Determines Vulnerability of Cells to Copper Excess. *Cell Chem Biol*. **24**, 1228-1237.

Vallières, C., Raulo, R., Dickinson, M. and Avery, S.V. (2018). Novel Combinations of Agents Targeting Translation That Synergistically Inhibit Fungal Pathogens. *Front Microbiol*. **9**, 2355.

Verma, S., Shakaya, V.P.S. and Idnurm, A. (2018). Exploring and exploiting the connection between mitochondria and the virulence of human pathogenic fungi. *Virulence*. **9**, 426-446.

Vogel, H.J. (1996). Escherichia coli and Salmonella: cellular and molecular biology (2nd ed), ASM Press, Washington, DC (1996). pp. 1025-1034.

Vondenhoff, G.H. and Van Aerschot, A. (2011). Aminoacyl-tRNA synthetase inhibitors as potential antibiotics. *Eur J Med Chem*. **46**, 5227-5236.

Wachnowsky, C. and Cowan, J.A. (2017). In Vitro Studies of Cellular Iron-Sulfur Cluster Biosynthesis, Trafficking, and Transport. *Methods Enzymol*. **595**, 55-82.

Wagener, J. and Loiko, V. (2017). Recent Insights into the Paradoxical Effect of Echinocandins. *J Fungi (Basel)*. **4**, 5.

Waggoner, D.J., Bartnikas, T.B. and Gitlin, J.D. (1999). The role of copper in neurodegenerative disease. *Neurobiol Dis*. **6**, 221-230.

Walker, C.H. (2009). Factors determining the toxicity of organic pollutants to animals and plants. Organic Pollutants: An Ecotoxicological Perspective (2nd ed.), CRC Press, London (2009). pp. 17–66.

Wang, Y. and Chiang, E.I. (2012). Low-Dose Methotrexate Inhibits Methionine S-Adenosyltransferase *In Vitro* and *In Vivo*. *Mol Med*. **18**, 423-432.

Wang, Y., Branicky, R., Noë, A. and Hekimi, S. (2018). Superoxide dismutases: Dual roles in controlling ROS damage and regulating ROS signaling. *J Cell Biol*. **217**, 1915-1928.

Wani, S.H. (2010). Inducing fungus-resistance into plants through biotechnology. *Notul Sci Biol*. **2**, 14-21.

Watanabe, K. (2010). Unique features of animal mitochondrial translation systems. The non-universal genetic code, unusual features of the translational apparatus and their relevance to human mitochondrial diseases. *Proc Jpn Acad Ser B Phys Biol Sci*. **86**, 11–39.

Weissbach H., Etienne, F., Hoshi, T., Heinemann, S.H., Lowther, W.T., Matthews, B., St John ,G., Nathan, C. and Brot, N. (2002) Peptide methionine sulfoxide reductase: structure, mechanism of action and biological function. *Arch Biochem Biophys*. **397**, 172–178.

Whale, A.J., King, M., Hull, R.M., Krueger, F. and Houseley, J. (2022). Stimulation of adaptive gene amplification by origin firing under replication fork constraint. *Nucleic Acids Res*. **50**, 915-936.

White, C. and Gadd, G.M. (1986). Uptake and cellular distribution of copper, cobalt and cadmium in strains of *Saccharomyces cerevisiae* cultured on elevated concentrations of these metals. *FEMS Microbiology Ecology*. **38**, 277-283.

Wiese, R.A. (1987). Compendium of wheat diseases (2nd ed.). American Phytopathological Society, St Paul, Minnesota. pp. 43-45.

Wiltrout, E., Goodenbour, J.M., Fréchin, M., and Pan, T. (2012). Misacylation of tRNA with methionine in *Saccharomyces cerevisiae*. *Nucleic Acids Res*. **40**, 10494-10506.

Winterbourne, C.C. (2014). The challenges of using fluorescent probes to detect and quantify specific reactive oxygen species in living cells. *Biochim Biophys Acta*. **1840**, 730-738.

Winzeler, E.A., Shoemaker, D.D., Astromoff, A., Liang, H., Anderson, K., Andre, B., Bangham, R., Benito, R., Boeke, J.D., Bussey, H., Chu, A.M., Connelly, C., Davis, K., Dietrich, F., Dow, S.W., El Bakkoury, M., Foury, F., Friend, S.H., Gentalen, E., Giaever, G., Hegemann, J.H., Jones, T., Laub, M., Liao, H., Liebundguth, N., Lockhart, D.J., Lucau-Danila, A., Lussier, M., M'Rabet, N., Menard, P., Mittmann, M., Pai, C., Rebischung, C., Revuelta, J.L., Riles, L., Roberts, C.J., Ross-MacDonald, P., Scherens, B., Snyder, M., Sookhai-Mahadeo, S., Storms, R.K., Véronneau, S., Voet, M., Volckaert, G., Ward, T.R., Wysocki, R., Yen, G.S., Yu, K., Zimmerman, K., Philippsen, P., Johnston, M. and Davis, R.W. (1999). Functional characterization of the S. cerevisiae genome by gene deletion and parallel analysis. *Science*. **285**, 901-906.

Wipf, D., Ludewig, U., Tegeder, M., Rentsch, D., Koch, W. and Frommer, W.G. (2002). Conservation of amino acid transporters in fungi, plants and animals. *Trends in Biochemical Sciences*. **27**, 139-147.

Woese, C.R., Olsen, G., Ibba, M., Söll, D. (2000). Aminoacyl-tRNA synthetases, the genetic code, and the evolutionary process. *Microbiol Mol Biol Rev*. **64**, 202-236.

Wohlgemuth, F., Gomes, R.L., Singleton, I., Rawson, F.J. and Avery, S.V. (2020). Top-Down Characterization of an Antimicrobial Sanitizer, Leading From Quenchers of Efficacy to Mode of Action. *Front Microbiol*. **11**, 575157.

Wolf, Y.I., Aravind, L., Grishin, N.V. and Koonin, E.V. (1999). Evolution of aminoacyl-tRNA synthetases--analysis of unique domain architectures and phylogenetic trees reveals a complex history of horizontal gene transfer events. *Genome Res*. **9**, 689-710.

Wong, H.E., Huang, C.J. and Zhang, Z. (2018). Amino Acid Misincorporation Propensities Revealed through Systematic Amino Acid Starvation. *Biochemistry*. **57**, 6767-6779.

World Health Organisation. 2013. WHO Model List of Essential Medicines. World Health Organisation. Available < http://www.who.int/medicines/publications/essentialmedicines/18th_EML.pdf >.

Xu, F.F. and Imlay, J.A. (2012). Silver(I), mercury(II), cadmium(II), and zinc(II) target exposed enzymic iron-sulfur clusters when they toxify *Escherichia coli*. *Appl Environ Microbiol*. **78**, 3618-3621.

Xu, R. and Li, Q.Q. (2008). Protocol: Streamline cloning of genes into binary vectors in Agrobacterium via the Gateway TOPO vector system. *Plant Methods*. **4**.

Yamamoto, T., Miyazaki, K. and Eguchi, T. (2007). Substrate specificity analysis and inhibitor design of homoisocitrate dehydrogenase. *Bioorg Med Chem*. **15**, 1346-1355.

Yamamoto, T. and Eguchi, T. (2008). Thiahomoisocitrate: a highly potent inhibitor of homoisocitrate dehydrogenase involved in the α-aminoadipate pathway. *Bioorg Med Chem.* **16**, 3372-3376.

Yang, F., Li, W. and Jørgensen, H.J.L. (2013). Transcriptional Reprogramming of Wheat and the Hemibiotrophic Pathogen Septoria tritici during Two Phases of the Compatible Interaction. *PLoS ONE*. **8**, e81606.

Yang, M., Jaaks, P., Dry, J., Garnett, M., Menden, M.P. and Saez-Rodriguez, J. (2020). Stratification and prediction of drug synergy based on target functional similarity. *npj Syst Biol Appl*. **6**, 16.

Yeh, P.J., Hegreness, M.J., Aiden, A.P. and Kishony, R. (2009). Drug interactions and the evolution of antibiotic resistance. *Nat Rev Microbiol*. **7**, 460-466.

Yildiz, F.H., Davies, J.P. and Grossman, A.R. (1994). Characterization of Sulfate Transport in *Chlamydomonas reinhardtii* during Sulfur-Limited and Sulfur-Sufficient Growth. *Plant Physiol*. **104**, 981-987.

Yoshimi, A., Kojima, K., Takano, Y. and Tanaka, C. (2005). Group III histidine kinase is a positive regulator of Hog1-type mitogen-activated protein kinase in filamentous fungi. *Eukaryot Cell*. **4**, 1820-1828.

Yoo, S., Noh, K., Shin, M., Park, J., Lee, K., Nam, H. and Lee, D. (2018). In silico profiling of systemic effects of drugs to predict unexpected interactions. *Sci Rep*. **8**, 1612.

Zanchin, N.I.T. and Goldfarb, D.S. (1999). Nip7p Interacts with Nop8p, an Essential Nucleolar Protein Required for 60S Ribosome Biogenesis, and the Exosome Subunit Rrp43p. *Mol Cell Biol*. **19**, 1518-1525.

Zhan, J., Pettway, R.E. and McDonald, B.A. (2003). The global genetic structure of the wheat pathogen Mycosphaerella graminicola is characterized by high nuclear diversity, low mitochondrial diversity, regular recombination, and gene flow. *Fungal Genet Biol*. **38**, 287-297.

Zhang, Z. and Ren, Q. (2015). Why are essential genes essential? - The essentiality of Saccharomyces genes. *Microb Cell*. **2**, 280-287.

Zhao, X., Iskar, M., Zeller, G., Kuhm, M., van Noort, V. and Bork, P. (2011). Prediction of Drug Combinations by Integrating Molecular and Pharmacological Data. *PLoS Comput Biol*. **7**, e1002323.

Zhao, W, An, J., Hu, Y., Li, A., Zhang, S., Zhang, B., Zhang, Z., Luo, X., Bian, Q., Ma., Y., Ding, Y., Wang, R. and Liu, Y. (2022). Tavaborole-Induced Inhibition of the Aminoacyl-tRNA Biosynthesis Pathway against *Botrytis cinerea* Contributes to Disease Control and Fruit Quality Preservation. *J Agric Food Chem*. **70**, 12297-12309.

Zheng, W., Sun, W., and Simeonov, A. Drug repurposing screens and synergistic drug-combinations for infectious diseases. *Br J Pharmocol*. **175**, 181-191.

Zhu, B. and Chevion, M. (2000). Copper-mediated toxicity of 2,4,5-trichlorophenol: biphasic effect of the copper(I)-specific chelator neocuproine. *Arch Biochem Biophys*. **380**, 267-273.

Zorov, D.B., Juhaszova, M. and Sollott, S.J. (2014). Mitochondrial Reactive Oxygen Species (ROS) and ROS-Induced ROS Release. *Physiol Rev*. **94**, 909-950.

Zyrina, A.N., Smirnova, E.A., Markova, O.V., Severin, F.F. and Knorre, D.A. (2016). Mitochondrial Superoxide Dismutase and Yap1p Act as a Signaling Module Contributing to Ethanol Tolerance of the Yeast *Saccharomyces cerevisiae*. *Appl Environ Microbiol*. **83**, e02759-16.